In silico guided metabolic engineering of *Aspergillus niger* for sustainable organic acid production

Daniel John Upton

PhD

University of York

Biology

September 2017

Abstract

The filamentous fungus *Aspergillus niger* is a common mould, and has risen to worldwide impact through industrial fermentation that is the chief source of the world's citric acid. As well as the high market value chemical citric acid, *A. niger* fermentation supplies an array of enzymes of biotechnological importance. Industrial fermentation processes continue to be dependent on sucrose-based feed-stocks, and rising energy costs and tightening resources are prompting a shift to more sustainable methods. *A. niger* fermentation is also a promising platform for the sustainable production of many chemicals that could help solve coming world challenges. *A. niger* has within it the metabolic potential to achieve these goals, but these can only be realised with more efficient strain development techniques. This project built on the recent systems biology studies of *A. niger* to create *in silico* tools that guide rational engineering strategies. A dynamic metabolic model, relevant to the industrial setting of batch fermentation, of *A. niger* organic acid production was developed and shown to accurately capture physiological characteristics. An empirical characterisation of organic acid fermentation by the wild-type ATCC1015 strain was used to inform the model, and revealed new findings. The onset of citric acid production coincided with a shift to phosphate-limited growth, caused by a rapid phosphate uptake and storage of phosphate as polyphosphate. The role of polyphosphate in organic acid fermentation has not previously been described. The dynamic model was probed by the engineering of seven targets. To better inform further engineering, the genome-scale metabolic network of *A. niger* was updated and made specific to the ATCC1015 strain, the parent of citric acid producing strains. Finally, a genetic algorithm was developed for *in silico* evolution of *A. niger* organic acid production, and applied to suggest strategies for optimising the production of different organic acids.

Table of Contents

Abstract……2

Table of Contents……...3

List of Tables……..……..7

List of Figures……..……..10

List of Accompanying Material……..…..16

Acknowledgements…….....19

Author's Declaration……..……22

Chapter 1: Introduction……...23

1.1. Rise of the *Aspergilli*……..……..23

1.2. Industrial applications of *Aspergillus niger*……..……24

1.2.1. Citric acid production……...24

1.2.2. Gluconic acid production……..….26

1.2.3. Enzyme production……..26

1.2.4. Biotransformations……...27

1.2.5. Bioremediation……..……..28

1.3. Metabolic potential of *Aspergillus niger*……....29

1.3.1. Platform for production of value-added chemicals……..…..29

1.3.2. Ability to use multiple feed-stocks…….31

1.3.3. Sustainability of fermentation methods……..…….36

1.4. Strain development of *Aspergillus niger*……..…….36

1.4.1. Traditional techniques of strain development……..36

1.4.2. Targeted engineering strategies……38

1.4.3. Computational techniques to guide rational engineering…..48

1.5. Mechanistic understanding of citric acid fermentation……50

1.5.1. Conditions required for citric acid fermentation…….....50

1.5.2. Physiological characteristics of citric acid fermentation…….54

1.5.3. Discoveries into mechanisms underlying citric acid production……...56

1.6. Modelling of citric acid fermentation……..……72
1.6.1. Early models of citric acid fermentation……...72
1.6.2. Genome-scale metabolic modelling……..…74
1.6.3. Dynamic flux balance analysis……..……...78
1.7. Aims of this Thesis……..…….80

Chapter 2: Characterising *Aspergillus niger* ATCC1015 organic acid fermentation……..……81

2.1. Introduction……..81
2.1.1. Aims of this Chapter……..…..83
2.2. Methods……..……84
2.2.1. Time-course shake flask experiments……..……84
2.2.2. Biomass dry weight analysis……..……86
2.2.3. Metabolite analysis……..……86
2.2.4. Polyphosphate analysis……..…91
2.3. Results……94
2.3.1. Citric acid fermentation with glucose as substrate…….....94
2.3.2. Effect of phosphate on citric acid fermentation……..….96
2.3.3. Polyphosphate levels during citric acid fermentation……100
2.3.4. Effect of carbon source on citric acid fermentation……..…102
2.3.5. Effect of initial pH on organic acid fermentation……...114
2.4. Discussion……116

Chapter 3: Dynamic modelling of *Aspergillus niger* organic acid fermentation……121

3.1. Introduction……....121
3.1.1. Aims of this Chapter……..121
3.2. Publication……..……122
3.3. Summary……164

Chapter 4: Engineering of *Aspergillus niger*……165

4.1. Introduction……..165
4.1.1. Aims of this Chapter……..167
4.2. Methods……168

4.2.1. Molecular biology techniques……..168
4.2.2. Polyethylene glycol-mediated protoplast transformation of *Aspergillus niger*……172
4.2.3. Creation of ATCC1015 *pyrG* negative strain……....175
4.2.4. Targeted gene deletion……176
4.2.5. Application of Tet-on expression system……...178
4.2.6. Antisense RNA-mediated knock-down……....182
4.3. Results……188
4.3.1. Knock-outs of the genes encoding oxaloacetate hydrolase and glucose oxidase……188
4.3.2. Constitutive over-expression of a low-affinity glucose transporter……193
4.3.3. Expression of cytosolic citrate synthase……200
4.3.4. Expression of mutated truncated 6-phosphofructo-1-kinase 207
4.3.5. Knock-down of exopolyphosphatase……213
4.3.6. Knock-down of a phosphate transporter……220
4.4. Discussion……225

Chapter 5: Construction of the ATCC1015-specific metabolic model iDU1757……233

5.1. Introduction……233
5.1.1. Aims of this Chapter……234
5.2. Methods……235
5.2.1. Assembly of ATCC1015-specific gene-protein-reaction associations……235
5.2.2. Evidence-based verification of new metabolic reactions……236
5.3. Results……237
5.3.1. Assembly of ATCC1015-specific gene-protein-reaction associations……237
5.3.2. Evidence-based verification of new metabolic reactions and construction of iDU1757……241
5.3.3. Changes in iDU1757 to reactions from iHL1210……252
5.3.4. New substrates in iDU1757……256

5.3.5. Input/output fluxes in iDU1757……257
5.4. Discussion……263

Chapter 6: *In silico* evolution of organic acid production as predictive tool for engineering……264

6.1. Introduction……264
6.1.1. Aims of this Chapter……268
6.2. Methods……269
6.2.1. Designing of genetic algorithm for *in silico* evolution……269
6.2.2. Data analysis of *in silico* evolution output for target prediction……281
6.3. Results……282
6.3.1. *In silico* evolution of citric acid production on glucose……..282
6.3.2. *In silico* evolution of citric acid production on xylose…..…..287
6.3.3. *In silico* evolution of succinic acid production on glucose....292
6.3.4. *In silico* evolution of succinic acid production on xylose.....298
6.3.5. *In silico* evolution of lactic acid production on glucose…….303
6.3.6. *In silico* evolution of malic acid production on glucose…….308
6.3.7. *In silico* evolution of acetic acid production on glucose.....313
6.3.8. *In silico* evolution of gluconic acid production on glucose...318
6.4. Discussion……336

Chapter 7: Final Discussion……...344

Abbreviations……363

References……365

List of Tables

Table 1.1. Feed-stocks used in *Aspergillus niger* citric acid fermentation.....32

Table 1.2. Selectable marker genes used in transformation of *Aspergillus niger*……..41

Table 1.3. Promoters used in *Aspergillus niger* expression studies……...43

Table 2.1. Media composition for fermentation experiments……...85

Table 1. Parameters fitted to our empirical data. (Chapter 3 – publication)…….132

Table 2. Parameters set to empirical values from the literature. (Chapter 3 – publication)…….……...133

Table S1. Biomass equation parameters altered to fit empirical data. (Chapter 3 – publication)……..……..…….136

Table S2. Putative phosphate transporters in ATCC 1015. Top BLASTP hits with phosphate transporters in SwissProt database are given. (Chapter 3 – publication)……..……..141

Table 4.1. Putative phosphate transporters in the ATCC1015 strain……...183

Table 4.2. Primers used in this work……..……184

Table 5.1. iHL1210 reactions for which no hits were found in version 4.0 of the ATCC1015 genome annotation……239

Table 5.2. New reactions in iDU1757 and corresponding literature evidence.....242

Table 5.3. New transport reactions in iDU1757……...246

Table 5.4. New input/output reactions in iDU1757……..246

Table 5.5. New compounds in iDU1757……249

Table 5.6. Reaction species corrections made to reactions from iHL1210.....253

Table 5.7. Compartmentalisation corrections made to reactions from iHL1210……..254

Table 5.8. New carbon sources in iDU1757……..…256

Table 5.9. New nitrogen sources in iDU1757……...256

Table 5.10. New phosphate sources in iDU1757……257

Table 5.11. Input/output fluxes in iDU1757……..258

Table 5.12. Biomass composition in iDU1757……258

Table 6.1. Fluxes used to calculate estimates of target acid yield and time of substrate depletion for fitness evaluation……..272

Table 6.2. Example solution from evolution of citric acid production on glucose……...285

Table 6.3. Example solution from evolution of citric acid production on xylose……..290

Table 6.4. Example solution from evolution of succinic acid production on glucose……296

Table 6.5. Example solution from evolution of succinic acid production on xylose……..…301

Table 6.6. Example solution from evolution of lactic acid production on glucose……306

Table 6.7. Example solution from evolution of malic acid production on glucose……311

Table 6.8. Example solution from evolution of acetic acid production on glucose……316

Table 6.9. Example solution from evolution of gluconic acid production on glucose……321

Table 6.10. Index numbers of mutations and corresponding reactions and mutation effects……323

Table 7.1. Inhibitors of metabolic processes……361

List of Figures

Figure 1.1. Schematic diagram of RNA interference pathway…….47

Figure 1.2. Schematic overview of metabolic and transport reactions relevant to *A. niger* organic acid production……...71

Figure 2.1. Citric acid fermentation with glucose as substrate……95

Figure 2.2. Response of citric acid fermentation to varying phosphate…….97

Figure 2.3. Response of citric acid fermentation to excessive phosphate….99

Figure 2.4. Polyphosphate levels during citric acid fermentation…..……101

Figure 2.5. Response of citric acid fermentation to change in substrate to xylose……..……103

Figure 2.6. Response of citric acid fermentation to glucose/xylose mixture……..……..105

Figure 2.7. Response of citric acid fermentation to change in substrate to arabinose……107

Figure 2.8. Response of citric acid fermentation to change in substrate to glycerol……109

Figure 2.9. Response of citric acid fermentation to change in substrate to sucrose……...111

Figure 2.10. Response of citric acid fermentation to change in substrate to cellobiose……113

Figure 2.11. Organic acid fermentation at initial pH 7…….115

Figure 1. Citric acid production commences upon a biphasic growth switch. (Chapter 3 – publication)……..…126

Figure 2. Comparing empirical and *in silico* data in response to varying phosphate. (Chapter 3 – publication)……...128

Figure 3. Simulating citric acid fermentation by dynamic flux balance analysis. (Chapter 3 – publication)……..…...130

Figure 4. Comparing empirical and *in silico* data in response to different carbon sources. (Chapter 3 – publication)……..…..138

Figure 5. Change in polyphosphate levels during citric acid fermentation. (Chapter 3 – publication)……..…139

Figure S1. Phylogenetic tree of putative phosphate transporters in ATCC 1015. (Chapter 3 – publication)…….……142

Figure 6. Comparing empirical and in silico data in response to Δ*oah* and Δ*gox* knockouts. (Chapter 3 – publication)……..….145

Figure 4.1. Confirmation of oxalate-negative phenotype in Δ*oah* strains…189

Figure 4.2. Confirmation of gluconate-negative phenotype in Δ*gox* strains……190

Figure 4.3. Fermentative effects of *oah* and *gox* knock-outs on citric acid production……..192

Figure 4.4. Dynamic modelling of citric acid fermentation with constitutive low-affinity glucose transport……..194

Figure 4.5. Fermentative effects of over-expression of a low-affinity glucose transporter in the GLU 1 strain with empty vector as negative control…....195

Figure 4.6. Fermentative effects of over-expression of a low-affinity glucose transporter in the GLU 2 strain with empty vector as negative control.…...196

Figure 4.7. Fermentative effects of over-expression of a low-affinity glucose transporter in the GLU 1 strain with no inducer as negative control……..…198

Figure 4.8. Fermentative effects of over-expression of a low-affinity glucose transporter in the GLU 2 strain with no inducer as negative control…..……199

Figure 4.9. Dynamic modelling of citric acid fermentation with constrained mitochondrial citrate export and addition of cytosolic citrate synthase……201

Figure 4.10. Fermentative effects of expression of cytosolic citrate synthase in the CIT 1 strain with empty vector as negative control……...202

Figure 4.11. Fermentative effects of expression of cytosolic citrate synthase in the CIT 2 strain with empty vector as negative control……..…….203

Figure 4.12. Fermentative effects of expression of cytosolic citrate synthase in the CIT 1 strain with no inducer as negative control…….……..205

Figure 4.13. Fermentative effects of expression of cytosolic citrate synthase in the CIT 2 strain with no inducer as negative control…….……..206

Figure 4.14. Fermentative effects of expression of mtPFK1 in the mtPFK1 1 strain with empty vector as negative control……....208

Figure 4.15. Fermentative effects of expression of mtPFK1 in the mtPFK1 2 strain with empty vector as negative control…….……...209

Figure 4.16. Fermentative effects of expression of mtPFK1 in the mtPFK1 1 strain with no inducer as negative control…….……211

Figure 4.17. Fermentative effects of expression of mtPFK1 in the mtPFK1 2 strain with no inducer as negative control…….……212

Figure 4.18. Dynamic modelling of citric acid fermentation with exopolyphosphatase knock-down (PPX KD)……214

Figure 4.19. Fermentative effects of PPX knock-down in the PPX KD 1 strain with empty vector as negative control……...215

Figure 4.20. Fermentative effects of PPX knock-down in the PPX KD 2 strain with empty vector as negative control……..216

Figure 4.21. Fermentative effects of PPX knock-down in the PPX KD 1 strain with no inducer as negative control…….……..218

Figure 4.22. Fermentative effects of PPX knock-down in the PPX KD 2 strain with no inducer as negative control…….…..219

Figure 4.23. Dynamic modelling of citric acid fermentation with constrained phosphate uptake……221

Figure 4.24. Fermentative effects of PHO1 knock-down in the PHO1 KD 1 strain with empty vector as negative control…….222

Figure 4.25. Fermentative effects of PHO1 knock-down in the PHO1 KD 2 strain with empty vector as negative control……...223

Figure 4.26. Growth phenotype of PHO1 KD 2 strain with and without Dox……..224

Figure 5.1. Schematic of annotation process used to map ATCC1015 genes to KEGG reactions……238

Figure 6.1. Schematic of genetic algorithm used for *in silico* evolution of organic acid production……269

Figure 6.2. Dynamic modelling of organic acid fermentation as basis of fitness evaluation……..271

Figure 6.3. Schematic of procedure used to determine scale parameter of Laplace function……280

Figure 6.4. Increase in highest population fitness over generations with evolutionary pressure towards citric acid production on glucose……..283

Figure 6.5. Evolution plot showing the site and frequency of mutations from 10 independent runs with evolutionary pressure towards citric acid production on glucose……..284

Figure 6.6. Dynamic modelling of organic acid fermentation comparing the wild-type with a solution from *in silico* evolution towards citric acid production on glucose……..286

Figure 6.7. Increase in highest population fitness over generations with evolutionary pressure towards citric acid production on xylose……288

Figure 6.8. Evolution plot showing the site and frequency of mutations from 10 independent runs with evolutionary pressure towards citric acid production on xylose…….289

Figure 6.9. Dynamic modelling of organic acid fermentation comparing the wild-type with a solution from *in silico* evolution towards citric acid production on xylose……291

Figure 6.10. Increase in highest population fitness over generations with evolutionary pressure towards succinic acid production on glucose……293

Figure 6.11. Increase in highest population fitness up to 100,000 generations with evolutionary pressure towards succinic acid production on glucose…294

Figure 6.12. Evolution plot showing the site and frequency of mutations from 10 independent runs with evolutionary pressure towards succinic acid production on glucose……..295

Figure 6.13. Dynamic modelling of organic acid fermentation comparing the wild-type with a solution from *in silico* evolution towards succinic acid production on glucose……..297

Figure 6.14. Increase in highest population fitness over generations with evolutionary pressure towards succinic acid production on xylose……..299

Figure 6.15. Evolution plot showing the site and frequency of mutations from 10 independent runs with evolutionary pressure towards succinic acid production on xylose…….300

Figure 6.16. Dynamic modelling of organic acid fermentation comparing the wild-type with a solution from *in silico* evolution towards succinic acid production on xylose…….302

Figure 6.17. Increase in highest population fitness over generations with evolutionary pressure towards lactic acid production on glucose…….304

Figure 6.18. Evolution plot showing the site and frequency of mutations from 10 independent runs with evolutionary pressure towards lactic acid production on glucose……..305

Figure 6.19. Dynamic modelling of organic acid fermentation comparing the wild-type with a solution from *in silico* evolution towards lactic acid production on glucose……..307

Figure 6.20. Increase in highest population fitness over generations with evolutionary pressure towards malic acid production on glucose…….309

Figure 6.21. Evolution plot showing the site and frequency of mutations from 10 independent runs with evolutionary pressure towards malic acid production on glucose……..310

Figure 6.22. Dynamic modelling of organic acid fermentation comparing the wild-type with a solution from *in silico* evolution towards malic acid production on glucose……..312

Figure 6.23. Increase in highest population fitness over generations with evolutionary pressure towards acetic acid production on glucose…….314

Figure 6.24. Evolution plot showing the site and frequency of mutations from 10 independent runs with evolutionary pressure towards acetic acid production on glucose……..315

Figure 6.25. Dynamic modelling of organic acid fermentation comparing the wild-type with a solution from *in silico* evolution towards acetic acid production on glucose……..317

Figure 6.26. Increase in highest population fitness over generations with evolutionary pressure towards gluconic acid production on glucose…….319

Figure 6.27. Evolution plot showing the site and frequency of mutations from 10 independent runs with evolutionary pressure towards gluconic acid production on glucose……..320

Figure 6.28. Dynamic modelling of organic acid fermentation comparing the wild-type with a solution from *in silico* evolution towards gluconic acid production on glucose……..322

Figure 6.29. Flux diagram illustrating re-distribution of flux in evolved succinic acid producer compared to wild-type…….339

Figure 7.1. Schematic overview of metabolic and transport reactions relevant to *A. niger* organic acid production highlighting contributions from this work……346

List of Accompanying Material

This section serves as an index of the accompanying material provided with this thesis. This material is composed of files provided electronically that were used to run the dynamic modelling and *in silico* evolution.

File name	**Function**
fba.java	Java code that runs the FBA.
FBAreader.java	Java code that reads in metabolic network from a given spreadsheet.
trade.java	Java code that runs the dFBA.
iMA871.Acids.xls	Spreadsheet of the adapted iMA871 model used in this work.
iDU1757.xls	Spreadsheet of the iDU1757 model.
Compound_dictionary.xls	Dictionary of the compound codes used in the metabolic models.
manageEvolve.py	Python code used to manage *in silico* evolution by successively calling evolveBatch.java until maximum generations reached.
evolveBatch.java	Java code that performs 500 generation batch of *in silico* evolution. Called by manageEvolve.py.
solve.java	Java code required by evolveBatch.java to evaluate fitness.
computeMaxFlux.java	Java code required by evolveBatch.java to compute the maximum flux of a given reaction.

File name	Function
maxLowerFlux.dat	DAT file required by evolveBatch.java to calculate scale parameter of Laplace function.
maxUpperFlux.dat	DAT file required by evolveBatch.java to calculate scale parameter of Laplace function.
maxLowerFlux_Xyl.dat	DAT file required by evolveBatch.java to calculate scale parameter of Laplace function when evolving on xylose.
maxUpperFlux_Xyl.dat	DAT file required by evolveBatch.java to calculate scale parameter of Laplace function when evolving on xylose.
analyseEvolutionOutput.py	Python code that analyses the evolution output. Creates files of fitness vs. generations, target frequencies, and raw solutions.
analyseEvolutionSolutions.py	Python code that analyses and filters solutions from *in silico* evolution. Creates file of filtered solutions.
analyseSolution.py	Python code used to inspect a solution and produce flux output files by calling solve1.java.
solve1.java	Java code called by analyseSolution.py to evaluate given solution and produce flux output file.
wild_type_bounds.txt	TXT file required by analyseSolution.py and callMutantTrade.py. Gives the wild-type flux bounds of the reactions.

File name	Function
callMutantTrade.py	Python code that calls tradeMutant.java to run dynamic modelling of a chosen solution.
tradeMutant.java	Java code that runs dFBA for a given solution from *in silico* evolution. Called by callMutantTrade.py.
EvolutionSolutions	Directory containing solution files for each of the *in silico* evolution goals. Each file contains the solutions from 10 replicate runs, filtered and ranked. These files were used to produce the evolution plots.

Acknowledgements

I would like to take this as an opportunity to express gratitude to all those who have helped this PhD experience come into being. The four years have been a tremendous and enjoyable journey. The constant pursuit of awareness and the relentless inquisition of Nature's intelligent workings is an uplifting endeavour.

I would first like to thank my undergraduate supervisors, Jennifer Potts and Seishi Shimizu, who motivated and guided me to undertake a PhD. It was certainly the right step. I am very grateful to my PhD supervisors, Jamie Wood and Simon McQueen-Mason, for trusting and accepting me to take on this PhD project. Without their constant presence and gentle direction throughout the four years, I am sure I could have got lost in the whirlpools of research. I have happy memories of our many meetings, and they really helped to make this a joyful and successful ride. I would also like to thank my Thesis Advisory Panel, Gavin Thomas and Maggie Smith, for reviewing my progress and giving me valuable feed-back. They helped give me confidence that I was on the right track, and gave me many useful directions.

I would especially like to thank the BBSRC for their generous funding and management of the Doctoral Training Partnership. As well as covering my living, research, and tuition expenses, they have provided valuable training.

I would like to thank the Biorenewables Development Centre and Citration Technology Ltd for getting me started on this project. I am thankful to all the researchers who came before me, who laid down the bed of research from which this project sprang. I am very grateful to the Centre for Novel Agricultural Products at the Biology Department, where I carried out most of the research for the four years. They provide a friendly and caring atmosphere, and it has been a pleasure to work there. I owe gratitude to the many workers there, for their kind nature and constant willingness to provide

assistance when needed. I am thankful to many others across the Biology Department for their help and guidance.

I would like to thank the other PhD students in my cohort. It really helps when you know there are others in the same boat. Our friendly encounters were uplifting and helped us to not feel alone, especially in the final write-up. Together we do not sink. I am grateful to the Biology student support staff and the Graduate office for taking good care of us and not letting us run astray.

The University of York is home to a thriving population of ducks and geese. I am thankful to the ducks for generating a friendly atmosphere across the campus. Although the greylag geese frequently hissed and flew at me, they helped shape my experience and maintain my vigilance, and for that I am grateful. I would like to offer thanks to all the wildlife across campus, and the many joyful sightings they gave me as I walked back and forth. The kingfishers, the oystercatchers, the goosanders, the pochards, the grebes, the cormorants, the woodpeckers, the treecreepers, the tawny owls, and the bullfinches. All of you. It really helps to be nested in such a natural environment. Special thanks to the robin, that continued singing to me its autumnal song as the PhD drew to an end.

I would like to thank the place where I have been living for the four years, and the many housemates who have shared with me this ideal home. I am grateful to my landlady, who has always been friendly and reliable. It really helps to have peaceful and easy-going living conditions as one pursues a demanding PhD project. Special thanks to my array of houseplants, who have come to share my room with me during the final year. The Areca palms, the Spider plants, the Snake plants, and the Dragon trees. They helped to purify the air in my room, for which I am grateful.

I would especially like to thank my family, my parents and brothers, and wider family. They have maintained a constant interest in my research activities, and continued to wish me well. They provided a fresh outlet for me

to share in my research experiences, the many successes and failures as one pursues the quest. My brother continues to think I have spent the four years trying to make orange juice from mushrooms. He once wrapped up a mushroom as a gift, which he bought singly from a supermarket. I have not yet been able to make orange juice from it, but I shall keep trying. He pretends he has written a book all about the subject I have been studying, which provides all the answers. Unfortunately, this mysterious book has been difficult to find, as there exist no physical or electronic copies. Maybe in another world.

I could go on in these acknowledgements *ad infinitum*, for life is a universal web where we each feed into one another's experiences, either in a known or unknown manner. Just as a stone thrown into a pool propagates many ripples to distant shores, each action does the same, in both space and time. I am sure I owe gratitude to many I am unaware of, whose actions have helped shape this experience. Words are incapable of expressing sufficient acknowledgement, and I hope that the vibrations emanating from my heart shall do the deed. My thanks to all, and I hope in return my actions positively feed into others' experiences.

Author’s Declaration

I declare that the work in this thesis is original and that I am its sole author. No part of this work has been presented previously for an award at any university. References are given for all sources.

The work in chapter 3 is presented as a publication (Upton *et al*, 2017) with a few alterations.

Chapter 1: Introduction

1.1 Rise of the *Aspergilli*

The *Aspergilli* are a group of filamentous fungi that were first documented in 1729 in Micheli's *Nova Plantarum Genera* (Micheli, 1729). The genus *Aspergillus* was named after the aspergillum, an instrument used to sprinkle holy water. On microscopic examination, Micheli observed a shape that resembled the aspergillum. This was the conidiophore, a structure characteristic of the *Aspergilli* that contains a long filament leading to a sporulating head. A more thorough description of the *Aspergilli* was not formulated until 1945 (Thom and Raper, 1945), which identified 14 distinct groups including the key sections Nigri, Nidulantes, Fumigati, and Flavi. To date, over 300 *Aspergillus* species have been reported (Samson *et al*, 2014), among which *A. niger*, *A. nidulans*, and *A. fumigatus* are the most widely studied. Key characteristics are asexual reproduction, a haploid genome, multinucleate cells, colour formation, and production of organic acids and secondary metabolites. The *Aspergilli* display a tolerance to a wide range of conditions, including temperature (10-50°C), pH (2-11), salinity (0-34%), and water activity (0.6-1) (Meyer *et al*, 2011a).

The *Aspergilli* have risen to worldwide impact, present in wide-ranging habitats, and with societal, economic, biotechnological, and medical importance. Species such as *A. fumigatus* have roles in pathogenesis, responsible for the group of diseases known as aspergillosis, which usually affect the respiratory system (Dagenais and Keller, 2009). Some species, particularly *A. flavus*, are implicated in food spoilage and the production of feed-contaminating mycotoxins, such as aflatoxin and ochratoxin (Amaike and Keller, 2011). The species *A. nidulans* provides an important model organism for genetic and molecular cell biology (David *et al*, 2008). Despite causing economic damage and medical problems, the *Aspergilli* have been a source of value, with *A. niger* and *A. oryzae* being important players. *A. oryzae* is established in the food industry, used in Chinese and Japanese

cuisine in the production of soy sauce, soybean paste, and rice-based wine and vinegar (Machida *et al*, 2008). *A. oryzae* also has broad application in industrial enzyme production, including amylases, lipases, pectinases, limoninases, and proteases (Singh *et al*, 2016). Most notable is *A. niger*, which has grown significantly in biotechnological importance over recent decades, with widespread usage in the production of citric acid and enzymes (Pel *et al*, 2007).

With rising importance, advances in knowledge of the *Aspergilli* on a systems biology level have been made in recent years. The genomes of over 350 *Aspergillus* species are soon to be sequenced, with 25 already released and 150 soon to be published (Brandl and Andersen, 2017). There have been over 30 transcriptomic studies, and more than 20 platforms exist for investigating the *Aspergilli* on a transcriptomic level (Andersen and Nielsen, 2009a). Studies on a proteomic and metabolomic level have also been carried out (Andersen and Nielsen, 2009a). Availability of genomic information has enabled construction of five genome-scale metabolic models covering different *Aspergillus* species (*A. nidulans*, *A. niger*, *A. oryzae*, and *A. terreus*) (Andersen *et al*, 2008; Lu *et al*, 2017; Liu *et al*, 2013; Vongsangknak *et al*, 2008; David *et al*, 2008).

1.2 Industrial applications of *Aspergillus niger*

A. niger has become an established industrial organism, and now has a suite of applications. These shall be the focus of this section, to build an awareness of the current standing of *A. niger* in industry.

1.2.1 Citric acid production

Citric acid is a high value commodity chemical, with an annual production of 2 million tonnes a year in 2010 and a rising global demand (F.O. Licht Renewable Chemicals, 2011; IHS, 2015). The properties of citric acid as an acidulant, preservative, flavour enhancer and chelating agent make it suited

to a wide range of applications. Its primary usage is in food and beverages, accounting for 75% of its demand. It is also used in cleaning agents and pharmaceuticals (IHS, 2015).

Commercial production of citric acid began around 1826 in England from imported Italian lemons by John and Edmond Sturge. Industrial-scale citric acid production from lemon juice established during the 19th century, and became monopolised by the Italian citrus industry. Citric acid was produced from lemon juice until 1919 (Kristiansen *et al*, 2014). Manufacture of citric acid from lemons involved extraction of lemon juice which contained around 4% citric acid, followed by precipitation by addition of lime and calcium carbonate. The calcium citrate precipitate was decomposed by addition of sulphuric acid (Wilson, 1921). Chemical synthesis was also achieved from glycerol (Grimoux and Adams, 1880), from dichloroacetone (Kristiansen *et al*, 2014), and by other synthetic routes, however, proved uncompetitive. Citric acid production by fermentation processes was first demonstrated by Wehmer in 1893 using *Penicillium* (Wehmer, 1893). In 1917, Currie established the conditions required for citric acid fermentation by *A. niger* (Currie, 1917). Subsequently, the first industrial processes using *A. niger* fermentation began in 1919 in Belgium, and later in 1923 in the United States by the pharmaceutical company Pfizer. Currently, *A. niger* fermentation is the chief source of citric acid, with citric acid plants operating in Europe, Asia, Africa, and America. Citric acid fermentation by *A. niger* is one of the most efficient biotechnological processes (Baker, 2006). Industrial production by this route is dependent on sucrose-based feedstocks, principally maize starch, sugarcane molasses, and sugarbeet molasses (Dhillon *et al*, 2013a). Other feedstocks, including hydrocarbons, were used in citric acid production by yeast fermentation during the 1960s and 1970s (Mattey, 1999), but with rising oil prices are no longer economical.

Industrial processes of *A. niger* citric acid fermentation were initially dependent on surface culture methods. These achieved a citric acid yield of 70-80% in a fermentation cycle lasting one to two weeks. Despite simple technology and without the need for high investment, these methods were

labour intensive and are rarely used in industry today (Max *et al*, 2010). Submerged culture is now commonly used, as batch or fed-batch fermentation, in bioreactors with a capacity exceeding 100,000 litres and up to 1 million litres. Cultures are inoculated from pre-formed mycelia with a pellet morphology (pellets less than 1 mm in diameter) grown from spores in 24 hours. The fermenters used are made from stainless steel for protection from corrosion by the acidic conditions. The citric acid yield is 70-90% from 16% sugar and is achieved in a fermentation cycle lasting one week (Max *et al*, 2010).

1.2.2 Gluconic acid production

In addition to citric acid, *A. niger* is used by industry in the production of gluconic acid. Over 60,000 tonnes of gluconic acid are produced a year for a range of applications (Ramachandran *et al*, 2006). These are mainly in the food industry, and include meat processing, flavouring and leavening agents, and cheese and tofu production. Due to its valuable chelating properties, gluconic acid is used in cleaning products and in the textile industry. Gluconic acid is also used as an additive in cement and in pharmaceuticals. The industrial process of gluconic acid production by *A. niger* uses fed-batch fermentation with submerged cultures. The pH is held at 6-6.5 by addition of sodium hydroxide, since gluconic acid is produced by pH-sensitive extracellular glucose oxidase. The process achieves a very high productivity, around 15 g L^{-1} h^{-1}, using glucose as substrate (Ramachandran *et al*, 2006).

1.2.3 Enzyme production

As well as organic acid production, enzyme production has become a core industrial application of *A. niger*. Strains of *A. niger* have been developed for production of a multitude of enzymes that have biotechnological value, including cellulases, hemicellulases, proteases, glucoamylases, invertases, lipases, glucose oxidases, tannases, phytases, pectinases, catalases, and naringinases (Pel *et al*, 2007). These enzymes are typically used in the food

and beverage, animal feed, textiles and pulp-and-paper industries. The natural occurrence of these enzymes in saprophytic *A. niger* and its remarkable protein secretion ability are reasons for its employment in this sector. Enzyme-producing strains originate from the CBS 513.88 strain (Pel *et al*, 2007), and in common with citric acid producing strains have been optimised over many years for their role. In particular, protease-deficient strains have been developed, targeting native protease expression that is a key obstacle in this application of *A. niger* (Punt *et al*, 2008). This problem is highlighted by the presence of almost 200 genes in *A. niger* involved in proteolytic degradation (Pel *et al*, 2007). Strategies targeting individual proteases may therefore be ineffective. The challenge is more applicable to heterologous protein production as homologous proteins are less prone to proteolysis (van den Hombergh *et al*, 1997). One study disrupted the *pepA* gene in *A. niger*, which encodes aspergillopepsin A (Mattern *et al*, 1992). The result was a drop in extracellular protease activity of 80 to 85%. A further study characterised and disrupted the protease regulator PrtT, which resulted in very low protease activity (Punt *et al*, 2008).

1.2.4 Biotransformations

In addition to its key roles in industrial organic acid and enzyme production, *A. niger* has been shown to mediate a very large number of biotransformations of biotechnological importance (Parshikov *et al*, 2015a; Parshikov and Sutherland, 2014). These are particularly relevant to the pharmaceutical industry. *A. niger* is able to biotransform aromatic and aliphatic organic compounds, as well as terpenoids, steroids and flavonoids. The reactions involved are wide-ranging, and include hydroxylation, oxidation, reduction, carbonylation, sulphation, demethylation, dechlorination, epoxide hydrolysis, ring cleavage, and conjugation. The specificity and very high stereoselectivity of the reactions make them advantageous over chemical synthesis. Examples include the hydroxylation of L-tyrosine to L-dopa for the treatment of Parkinson's disease, the conversion of ferulic acid to vanillic acid for the production of the flavouring compound vanillin, the

degradation of a number of toxic compounds and pollutants, and the production of fragrances and pesticides (Parshikov *et al*, 2015a; Parshikov and Sutherland, 2014).

1.2.5 Bioremediation

The ability of *A. niger* to perform biotransformations has placed it in the spotlight of bioremediation applications, exploiting its ability to degrade numerous toxins and pollutants. *A. niger* has also been shown to accumulate radionuclides (Song *et al*, 2016) and a number of metals such as chromium, copper, arsenic, lead, and zinc (Holda *et al*, 2011; Kartal *et al*, 2004; Jianlong *et al*, 2001; Price *et al*, 2001). The applicability of *A. niger* in treatment of a range of wastewaters has been demonstrated (Price *et al*, 2001; Holda *et al*, 2011; Jianlong *et al*, 2001; Mahmoid *et al*, 2017). In addition to metal removal, *A. niger* can bioremediate red azo dye from textile wastewater (Mahmoud *et al*, 2017).

1.3 Metabolic potential of *Aspergillus niger*

Although significant value has already been drawn from *A. niger* in its various industrial uses, it has a reservoir of metabolic potential that is yet to be realised. The key aspects of this shall be explored in this section.

1.3.1 Platform for production of value-added chemicals

The availability of genomic information has highlighted the biosynthetic potential of *A. niger*. In particular, around 80 secondary metabolite gene clusters have been identified in *A. niger* (Inglis *et al*, 2013). This is a source of potential value, as secondary metabolites have important therapeutic and pharmaceutical properties. Over 70% of these gene clusters encode silent biosynthetic pathways, involved in the formation of polyketides and non-ribosomal peptides (Fisch *et al*, 2009). A silent biosynthetic pathway is usually inactive, and only switched on in response to certain environmental conditions. It was shown that the transcriptional suppression of around 50 of these gene clusters can be reversed by the addition of epigenome-modifying agents (Fisch *et al*, 2009). One such cluster, the *yan* cluster, has been well characterised, and contains 10 genes shown to be responsible for the production of a range of yanuthones (Holm *et al*, 2014; Petersen *et al*, 2015). One of these, yanuthone D, is a complex meroterpenoid derived from the polyketide 6-methylsalicylic acid, and has important antibiotic properties. Other yanuthones produced by this gene cluster also display antimicrobial activities. Another cluster, the *aza* cluster, ordinarily silent, was activated by over-expression of its corresponding transcriptional activator, *azaR* (Zabala *et al*, 2012). As a result, 13 genes of the cluster were expressed, and a new group of compounds, named azanigerones, were produced. The azanigerones belong to the azaphilone family of compounds, which are structurally diverse and exhibit a range of biological activities, including antimicrobial, anti-inflammatory, and anti-cancer. This same strategy was applied to another silent gene cluster, named *pyn* (Awakawa *et al*, 2013). Over-expression of the associated transcriptional activator, *pynR*, led to the

expression of five genes of the cluster and production of a new pyranonigrin compound, pyranonigrin E, that may be involved in the scavenging of superoxide radicals.

In addition to activating silent gene clusters to produce new valuable compounds, it has been demonstrated that gene deletion strategies can be applied to alter the metabolite production profile, shifting flux to a metabolite of interest. This is an extra means of releasing the metabolic potential of *A. niger*. In this example, the gene encoding cytosolic ATP citrate lyase was deleted, which changed the profile of organic acids produced (Meijer *et al*, 2009a). Succinic acid production, the original target, increased 3-fold, however, the yield was still very low (0.25 g/L). Acetic acid, not normally detected, was produced at high yield. This example illustrates that *A. niger* can be genetically manipulated to serve as a production platform of numerous chemicals.

The potential of *A. niger* is further expanded by its ability to act as a host of foreign genes encoding new metabolic activities, that when introduced lead to the production of new metabolites in this established industrial platform. This has recently been achieved for the production of L-lactic acid and itaconic acid, two chemicals of industrial value. *A. niger* was engineered to produce L-lactic acid by expression of a mouse lactate dehydrogenase gene, and gave a yield of 7.7 g/L from 60 g/L glucose (Dave and Punekar, 2015). The production of itaconic acid naturally occurs in *A. terreus*, and the responsible gene cluster was transferred to *A. niger* in combination with a cytosolic citrate synthase gene, resulting in a yield of 26.2 g/L itaconic acid from 100 g/L glucose (Hossain *et al*, 2016).

1.3.2 Ability to use multiple feed-stocks

The saprophytic nature of *A. niger* gives it the ability to grow on an extensive array of substrates. It is reported that around 70 carbon sources and 30 nitrogen sources support the growth of *A. niger* (Lu *et al*, 2017), and it is probable that this represents only a fraction of its total potential. The degradative ability of *A. niger* is a contributive factor towards its industrial value. This is well illustrated in Table 1.1, which gives the various feed-stocks that have been shown to be applicable to *A. niger* citric acid fermentation. These feed-stocks are typically waste streams from agricultural and industrial processes, and their disposal is problematic both environmentally and economically. Although considered as waste, these feed-stocks have significant carbon content, usually in the form of sugars or sugar polymers. By employing the saprotrophic ability of *A. niger*, value can be drawn from these underused resource streams.

Table 1.1. Feed-stocks used in *Aspergillus niger* citric acid fermentation

Feed-stock	Citric acid produced	Citric acid produced (% carbon source consumed)	Fermentation method	Additives	Reference
Pineapple waste	194 g/kg DW	74%	Solid-state	Methanol (3%)	Tran *et al*, 1998
Cassava waste	35 g/kg DW	70%	Solid-state	Methanol	Bindumole *et al*, 2005
Oil palm empty fruit bunches	370 g/kg DW	-	Solid-state	Methanol (2%), sucrose (6.4%)	Bari *et al*, 2010
Palm oil mill effluent	5 g/L	-	Submerged	Wheat flour (4%), glucose (4%)	Alam *et al*, 2008
Milk factory waste water	16.5 g/L	-	Immobilised	None	Lee *et al*, 2006
Corn husks	259 g/kg DW	-	Submerged	Methanol (3%), enzyme cocktail (Rapidase Pomaliq)	Hang and Woodams, 2000
Corn distillers grain	-	25%	Solid-state	None	Xie and West, 2006
Corn stover hydrolysate	100 g/L	94%	Submerged	None	Zhou *et al*, 2017
Corn waste	-	32%	Solid-state	Methanol (2%)	Kuforiji *et al*, 2010
Acasia arabica pod	24 g/L	-	Submerged	None	Patagundi and Kaliwal, 2008

Feed-stock	**Citric acid produced**	**Citric acid produced (% carbon source consumed)**	**Fermentation method**	**Additives**	**Reference**
Dalbergia sissoo pod	12 g/L	-	Submerged	None	Patagundi and Kaliwal, 2008
Parkia biglobosa pod	7 g/L	-	Submerged	None	Patagundi and Kaliwal, 2008
Peltophorum pterocarpum pod	9 g/L	-	Submerged	None	Patagundi and Kaliwal, 2008
Mixed fruit waste	-	47%	Solid-state	Methanol (4%)	Kumar *et al*, 2003
Maosmi waste	-	50%	Solid-state	Methanol (4%), sucrose (21.6 g per 100 g dry solid)	Kumar *et al*, 2003
Apple pomace	364 g/kg DW	-	Solid-state	Methanol (3%)	Dhillon *et al*, 2013a
Brewer's spent grain	59 g/kg DW	-	Solid-state	None	Dhillon *et al*, 2013a
Citrus waste	12 g/kg DW	-	Solid-state	None	Dhillon *et al*, 2013a
Apple pomace sludge	40 g/L	-	Submerged	Methanol (3%)	Dhillon *et al*, 2013b
Sugarcane bagasse	132 g/kg DW	96%	Solid-state	Methanol (4%), sugarcane molasses (to give 14% sugar)	Khosravi-Darani and Zoghi, 2008
Carob pod	-	51%	Surface	Methanol (4%)	Roukas, 1998

Feed-stock	**Citric acid produced**	**Citric acid produced (% carbon source consumed)**	**Fermentation method**	**Additives**	**Reference**
Orange press liquor	30 g/kg substrate	73%	Submerged	Methanol (4%)	Aravantinos-Zafiris *et al*, 1994
Orange peel autohydrolysate	9 g/L	53%	Submerged	Methanol (4%)	Rivas *et al*, 2008
Orange peel	640 g/kg DW	-	Solid-state	Methanol (3.5%), molasses (to give 14% sugar)	Hamdy, 2013
Orange peel	193 g/kg DW	38%	Solid-state	None	Torrado *et al*, 2011
Carrot processing waste	-	36%	Solid-state	-	Garg and Hang, 1995
Biodiesel by-products (tung cake and 20% glycerol)	350 g/kg DW	-	Solid-state	None	Schneider *et al*, 2014
Rice straw	50 g/kg DW	-	Solid-state	Molasses (14%)	Ali *et al*, 2012
Banana extract	45 g/L	41%	Submerged	None	Sassi *et al*, 1991
Coffee husk	150 g/kg DW	82%	Solid-state	None	Shankaranand and Lonsane, 1994

Feed-stock	**Citric acid produced**	**Citric acid produced (% carbon source consumed)**	**Fermentation method**	**Additives**	**Reference**
Date waste	98 g/L	63%	Submerged	Methanol (3%)	Acourene and Ammouche, 2012
Date pulp	168 g/kg substrate	87%	Solid-state	Methanol (4%)	Assadi and Nikkhah, 2002
Brewery spent liquid	11 g/L	-	Submerged	Methanol (3%)	Dhillon *et al*, 2012
Rapeseed oil	-	115%	Submerged	-	Elimer, 1998
Whey permeate	12 g/L	15%	Submerged	None	Houssain and Ahmed, 1992
Xylan	40 g/L	29%	Semi-solid	None	Kirimura *et al*, 1999a
Cellulose hydrolysate	102 g/L	68%	Semi-solid	None	Watanabe *et al*, 1998
Grape pomace	-	60%	Solid-state	Methanol (3%)	Hang and Woodams, 1985

Feed-stocks are often supplemented with mineral solutions of varying and optimised proportions, and this information is available in the reference and not given in the additives column. Unless indicated otherwise, the amount of citric acid produced is either given as grams per kilogram of feed-stock dry weight (g/kg DW), or grams per litre of culture (g/L). A hyphen indicates that the information could not be found.

1.3.3 Sustainability of fermentation methods

With rising costs in energy and tightening resources, industry is seeking more sustainable and cost-competitive fermentation processes. Citric acid production is still dependent on increasingly expensive sucrose-based feed-stocks, and has a growing demand (Dhillon *et al*, 2013a). Therefore, the need to shift to more sustainable and lower cost feed-stocks has attracted significant study (Dhillon *et al*, 2013a). The potential of a large number of agro-industrial waste streams for *A. niger* citric acid fermentation has been demonstrated (Table 1.1). These rely on strain optimisation to be suitable for industry. Consequently, the ability to quickly and efficiently develop new strains to maximise citric acid yield from a given feed-stock is paramount in today's fast-moving business climate.

1.4 Strain development of *Aspergillus niger*

Harnessing the potential of the rich metabolism of *A. niger* is dependent on strain development techniques. Current industrial applications employ *A. niger* strains that took many decades of development. To establish new applications and improve existing ones, more efficient and directed strategies of strain development are needed. In this section, the different approaches to strain development in *A. niger* shall be examined.

1.4.1 Traditional techniques of strain development

Before the advent of recombinant DNA technology, strain development was reliant on random mutagenesis coupled with screening procedures to identify desirable phenotypes. In organisms that undergo sexual reproduction, breeding could be applied, however, the asexuality of *A. niger* prevents such techniques. The genetic instability of *A. niger* gives rise to spontaneous mutants over multiple rounds of propagation, and can be used as a source of new strains without the need for mutagenising agents. To achieve higher mutation rates and increased frequency of desirable mutations, many

mutagenesis techniques exist that use either irradiation or chemical mutagens. Among these are ultraviolet (UV), X-ray, gamma and microwave-irradiation, ethyl methane sulphonate, acridine orange, nitrosoguanidine, nitrous acid, and ethidium bromide, all of which have been applied in *A. niger* strain development (Lofty *et al*, 2007; Hu *et al*, 2014; Liu *et al*, 2003; Awan *et al*, 2011; Yongquan, 2001; Markwell *et al*, 1989; Javed *et al*, 2011). Of these, UV-induced mutagenesis is the most common. The traditional techniques in industry frequently used a nitrous acid pre-treatment, followed by UV-irradiation (personal communication with Citration Technology Ltd). Nitrous acid facilitated depigmentation of spore suspensions, making UV more effective. The strength of mutagenising agents was such that a 5% survival rate was achieved.

The use of mutagenesis methods to induce random mutations is coupled with labourious screening procedures to identify chance mutations that give a desirable phenotype. The underlying mutations are often unknown, and the resultant mutant strains may be less genetically stable. The traditional screening techniques in industry used primary and secondary screens. The primary screen was based on a bilayer agar plate system, with a base layer containing calcium carbonate (personal communication with Citration Technology Ltd). The use of calcium carbonate enabled visualisation of acid production, which caused a clear zone surrounding the colony. The ratio of acid zone to colony diameter was used as an indicator of desirable phenotypes. An alternative primary screen was based on a multiwell plate system (personal communication with Citration Technology Ltd). Each well contained liquid medium inoculated with spores, which grew on the surface, and the underlying medium was tested for differences in metabolite production. Mutant strains that showed a desirable phenotype in primary screening were isolated and tested in shake flask culture as the secondary screen, and if successful were further tested at 10 to 15 litre bioreactor scale (personal communication with Citration Technology Ltd).

1.4.2 Targeted engineering strategies

Traditional methods of *A. niger* strain development were time-consuming, and with advances in recombinant DNA technology, targeted engineering strategies are now possible. The earliest efforts to genetically engineer *A. niger* were reported in 1985 (Buxton *et al*, 1985), however, were met with a very low transformation efficiency. In subsequent years, some improvements have been made in the ability to manipulate the genome of *A. niger*. In this section, the current engineering tool-kit is explored.

Genetic engineering requires the entry of DNA into cells, mediated by transformation. The cell walls of fungi provide a barrier, and filamentous fungi in general are more problematic, due to a more complex and less easily permeabilised cell wall (Rivera *et al*, 2014). The most popular transformation techniques for filamentous fungi rely on enzymatic treatment to produce protoplasts. In the presence of polyethylene glycol and calcium chloride, DNA uptake is achieved. Transformed protoplasts then require a regeneration phase on osmotically-stabilised medium. Although the production of viable protoplasts as well as inefficiencies in protoplast regeneration can present difficulties, the technique has been commonly applied to engineering of *A. niger*. Other methods that have been used include electroporation, and more recently, shock wave treatment. While electroporation has most often been used with protoplasts, germinated conidia were successfully transformed by electroporation in *A. niger* (Ozeki *et al*, 1994). This is promising, and the technique proved faster than conventional methods dependent on protoplasts, but the transformation efficiency was very low. The development of shock wave-mediated techniques has allowed very fast and efficient transformation of *A. niger*, and can be used with spores (Magaña-Ortíz *et al*, 2013). Transformation frequency was improved by three orders of magnitude compared to standard methods. Although this is a notable advance, the required equipment and expertise are beyond the scope of many laboratories.

One of the challenges of *A. niger* transformation is the very low frequency of homologous recombination (HR). Plasmid DNA is most frequently integrated

at random sites by non-homologous end joining (NHEJ) (Meyer, 2008). Therefore, targeting to particular loci is troublesome, and the variable positional effects of random integration can affect target gene expression and give unpredictable results. Integration by HR in *A. niger* requires large flanking regions of homology, over 1 kb in length, which can achieve a HR frequency of 20% (Meyer *et al*, 2007). This obstacle was partly overcome via disruption of the NHEJ pathway in *A. niger*, by deletion of the *kusA* gene (Meyer *et al*, 2007). The resultant Δ*kusA* strain had HR frequencies of 90% when 0.5 kb regions of homology were used, however, HR frequency was dramatically decreased with reduced length of homologous regions (Meyer *et al*, 2007). The downside of this solution is decreased genetic stability of NHEJ-deficient strains. An alternative approach is the use of autonomously replicating plasmids (ARPs). Naturally occurring plasmids are not typically found in filamentous fungi, and therefore the discovery of autonomously replicating sequences (ARSs) has been difficult. Despite this, a 6 kb ARS named AMA1 was isolated from *Aspergillus nidulans*, which functioned in *A. niger* (Gems *et al*, 1991). Plasmids containing the AMA1 sequence transform at much higher frequencies, about 100 times greater than integrative vectors. The plasmids have been shown to be maintained freely without genomic integration, and with a copy number of 10-30 per haploid genome (Gems *et al*, 1991). The benefit of using ARPs, aside from the increased transformation efficiency, is that they give more reliable results, which are not prone to positional effects of genomic integration. ARPs can be used in gene expression studies, but not in targeted gene insertion or deletion. An attempt was made to use plasmids carrying AMA1 in this project, however, mitotic instability proved problematic, and caused a significantly reduced growth rate of transformant strains in fermentation experiments. It was shown previously that the plasmid is lost from 65% of progeny (Gems *et al*, 1991). Aside from mitotic instability of ARPs, other disadvantages are increased variation in expression levels due to varying copy number of the plasmid. It is therefore more difficult to achieve a desired and predictable expression level.

Key to a transformation system is a selectable marker gene, which enables selection of strains carrying the DNA of interest by growth on selective medium. Selectable marker genes enable growth in the absence of a particular nutrient (prototrophy), or in the presence of a particular compound (resistance). The first selectable marker gene to be used in transformation of *A. niger* was the *argB* gene from *A. nidulans*, which allows growth in the absence of arginine (Buxton *et al*, 1985). A number of different marker genes have now been used for *A. niger* transformation (Table 1.2). The most commonly used is the gene encoding orotidine-5'-phosphate decarboxylase, known as *pyrG*. To use this marker gene, one needs an auxotrophic mutant strain (*pyrG*-negative) that requires uridine for growth. Transformants with the *pyrG*-positive phenotype are selected by growth in the absence of uridine. The advantage of the *pyrG* selectable marker gene is its counter-selectability. The *pyrG*-negative phenotype can be selected by resistance to 5-fluoro-orotic acid (5-FOA). This facilitates isolation of uridine auxotrophs, and recycling of the marker gene.

Table 1.2. Selectable marker genes used in transformation of *Aspergillus niger.*

Selectable marker name	Function	Selection	Counter-selection	Reference
argB	ornithine transcarbamylase	Growth in the absence of arginine	None	Buxton *et al*, 1985
hph	hygromycin B phosphotransferase	Resistance to hygromycin	None	Dai *et al*, 2013
niaD	nitrate reductase	Growth with nitrate as sole nitrogen source	Resistance to chlorate	Campbell *et al*, 1989
ble	bleomycin resistance	Resistance to bleomycin	None	Arentshorst *et al*, 2015
bar	bialaphos resistance	Resistance to bialaphos	None	Li and Yan, 2014
amdS	acetamidase	Growth with acetamide as sole nitrogen source	Resistance to fluoro-acetamide	Kelly and Hynes, 1985
oliC	oligomycin resistance	Resistance to oligomycin	None	Ward *et al*, 1988
pyrG	orotidine-5'-phosphate decarboxylase	Growth in the absence of uridine	Resistance to 5-fluoro-orotic acid	Van Hartingsveldt *et al*, 1987
hisB	histidine biosynthesis	Growth in the absence of histidine	None	Fiedler *et al*, 2017

Genetic engineering is often associated with expression of a gene of interest, either knocking-in a new activity or knocking-up an existing one. The choice of a suitable promoter is required. A range of promoters have now been characterised and applied in *A. niger* expression studies (Table 1.3). Among these are constitutive promoters and inducible promoters. The most commonly used are the strong constitutive glyceraldehyde-3-phosphate dehydrogenase promoter (P*gpdA*) and the inducible glucoamylase promoter (P*glaA*). Inducible promoters are important engineering tools, allowing different levels of expression to be tested, and providing a more reliable negative control by the absence of inducer. The *glaA* promoter has been subjected to extensive studies to define its expression conditions (Ganzlin and Rinas, 2008). It is most readily induced by maltose, and also has activity in the presence of starch and maltodextrins. It is repressed by xylose, through the action of the carbon catabolite repressor CreA. It has a complex relationship with glucose, induced at low concentrations while repressed at high concentrations. The metabolic dependency of this promoter and its complex expression patterns make it a poor choice for studies probing the metabolic effects of targeted gene expression, such as those in this thesis. Furthermore, P*glaA* is not a tight promoter, having low levels of expression in the absence of inducer. To establish a more powerful tool for expression studies, researchers developed a metabolically-independent and tunable expression system for *A. niger*, that is silent under non-induced conditions (Meyer *et al*, 2011a). The system is based on the tetracycline resistance operon (Tet) of *Escherichia coli*. In the absence of tetracycline, the repressor protein TetR binds to the operator sequence (*tetO*) of Tet, preventing transcription. In the presence of tetracycline, TetR dissociates from *tetO*, enabling transcription. The Tet system from *E. coli* was adapted to function in *A. niger*, and with increased sensitivity to the tetracycline derivative doxycycline (Dox). The modified system is tight and achieves dose-dependent expression levels, with a rapid response to addition of Dox.

Table 1.3. Promoters used in *Aspergillus niger* expression studies.

Promoter name	**Source**	**Expression conditions**	**Reference**
P*glaA*	glucoamylase	presence of maltose, starch or maltodextrin; absence of xylose	Ganzlin and Rinas, 2008
P*inuE*	exo-inulinase	presence of sucrose; absence of glucose	Kwon *et al*, 2011
P*catR*	catalase	presence of hydrogen peroxide or calcium carbonate	Sharma *et al*, 2012b
P*sucA*	β-fructo-furanosidase	presence of sucrose	Roth and Dersch, 2010
P*bphA*	benzoate *p*-hydroxylase	presence of benzoate	Antunes *et al*, 2016
P*gpdA*	glyceraldehyde-3-phosphate dehydrogenase	Constitutive	Hellmuth *et al*, 1995
P*citA*	citrate synthase	Constitutive	Dave and Punekar, 2011
P*adhA*	alcohol dehydrogenase	Constitutive	Saunders *et al*, 1989
P*pki*	pyruvate kinase	Constitutive	Kusters-van Someren *et al*, 1992
P*mbfA*	multiprotein bridging factor	Constitutive	Blumhoff *et al*, 2013
P*coxA*	cytochrome c oxidase	Constitutive	Blumhoff *et al*, 2013
P*srpB*	nucleolar protein	Constitutive	Blumhoff *et al*, 2013

Promoter name	**Source**	**Expression conditions**	**Reference**
P*tvdA*	transport vesicle docking protein	Constitutive	Blumhoff *et al*, 2013
P*mdhA*	malate dehydrogenase	Constitutive	Blumhoff *et al*, 2013
P*manB*	alpha-1,6-mannase	Constitutive	Blumhoff *et al*, 2013

An important component of an engineering tool-kit is the ability to delete target genes, to generate knock-out strains. Gene deletion is frequently applied in metabolic engineering to block competing metabolic fluxes, and investigate metabolic pathways. For many years, gene deletion tools for *A. niger* have been limited. The first reports of *A. niger* gene deletion appeared around the year 2000, when a gene homologous to protein disulphide isomerase, *prpA,* was deleted (Wang and Ward, 2000). The strategy employed was based on transformation with a linear DNA fragment, which contained the *pyrG* selectable marker gene flanked by *prpA* flanking regions. The method is dependent on homologous recombination, inefficient in *A. niger*. As DNA most frequently integrates at random sites, gene deletion does not occur in the majority of transformants. Therefore, PCR screening of transformants is required to identify knock-out strains. A further limitation of this strategy is that only single deletions can be made, unless a strain is available with several auxotrophies each complemented by a different marker gene. Despite its limitations, it was not until recently that improved techniques became available. A gene deletion system was developed that enables more efficient creation of knock-out strains, and through recycling of the marker gene, can be used to delete multiple genes (Delmas *et al*, 2014). The system exploits the counter-selective *pyrG* marker gene. A plasmid carrying the *pyrG* gene and 1.5 kb flanking regions of the target gene is transformed into a *pyrG*-negative strain. Integration of the plasmid by recombination based on homology of the flanking regions leads to unstable plasmid integration, whereas integration at random sites is stable. The transformants that undergo plasmid excision due to unstable integration either lose the target gene (deletion) or revert to the wild-type. In both cases, the *pyrG* gene is lost, allowing recycling of the marker gene. To remove the selective pressure on retaining the plasmid, transformants are grown in the presence of uridine. The resulting *pyrG*-negative strains are selected by resistance to 5-fluoro-orotic acid, and screened by PCR to identify knock-out strains, which usually occur at a frequency of 50%.

Although gene knock-out is a useful genetic tool for probing metabolism, it is not always suitable. Some targets are essential to spore germination or growth, resulting in a lethal phenotype if gene deletion is applied. Additionally, constraining metabolic flux, rather than blocking it, may sometimes be the desired outcome. Therefore, the ability to knock-down expression of a target gene is necessary. The tools to accomplish this in *A. niger* are not well developed. The first reported knock-down in *A. niger* was in the year 2000, when researchers expressed antisense RNA targeting complementary mRNA of a protein disulphide isomerase gene, *pdiA* (Ngiam *et al*, 2000). The strategy was successful, and lowered PDIA activity by 50%. Antisense RNA-mediated downregulation is an established technique, but with little application in *A. niger*. A plasmid is constructed to express antisense RNA, which binds to target mRNA and disrupts translation. The expression level of antisense RNA determines the extent of knock-down. Alternative methods for downregulation of target gene expression rely on RNA interference (RNAi) (Figure 1.1). Although this tool has been used extensively in other organisms, it was not until 2008 that RNAi was first performed in *A. niger* (Barnes *et al*, 2008). RNAi exploits the cellular machinery. RNA-induced silencing complexes (RISCs) assemble from endoribonucleases and silencing RNAs (siRNA), and mediate the degradation of mRNA that has a complementary sequence to the siRNA (Figure 1.1). siRNA is double-stranded (ds)RNA, about 22 nucleotides in length, and can be synthesised and introduced into the cell. The technique was demonstrated in *A. niger* by addition of siRNA to protoplasts, and using a β-glururonidase (GUS) reporter gene (Barnes *et al*, 2008). GUS activity was reduced by up to 80%, dependent on the siRNA concentration. Despite the success, the knock-down effect was only transient and not stable beyond conidiation. A more stable means of RNAi is the expression of dsRNA from a vector, which has been carried out in *A. niger* (Oliveira *et al*, 2008). The technique was used to knock-down activity of the regulator XlnR, which is involved in activating the transcription of genes associated with breakdown of xylan and cellulose as well as xylose metabolism. Expression levels of *xlnR* were shown to be decreased by up to 75%, which resulted in reduced expression of XlnR-regulated genes, and subsequently lower xylanolytic

activity (Oliveira *et al*, 2008). The knock-down, however, was only observed in 12% of transformant strains and the results were varied. It is clear that the engineering tools to knock-down gene expression in *A. niger* are in need of improvement.

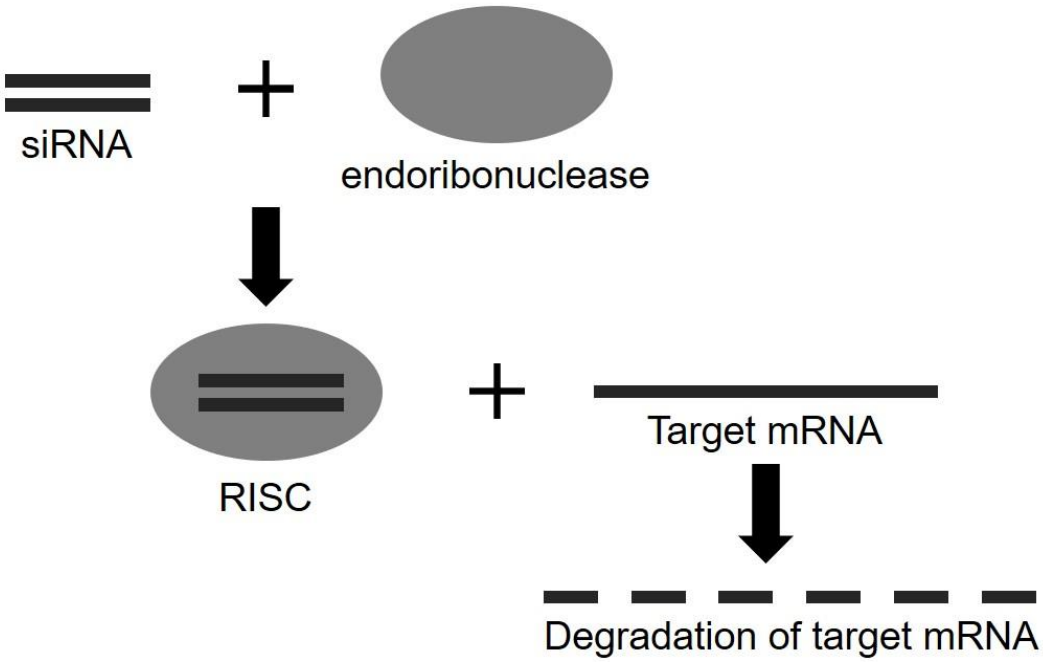

Figure 1.1. Schematic diagram of RNA interference pathway. Double-stranded silencing RNA (siRNA) with a complementary sequence to the target mRNA associates with an endoribonuclease to form an RNA-induced silencing complex (RISC). The RISC mediates the degradation of the target mRNA.

Recent additions to the *A. niger* engineering tool-box include the powerful genome editing system now widely known as CRISPR (clustered regularly interspaced short palindromic repeats)-Cas9 (Nødvig *et al*, 2015). The CRISPR-Cas9 system originates from bacteria, most commonly *Streptococcus pyogenes*, and has been recently adapted to work in filamentous fungi, including *A. niger* (Nødvig *et al*, 2015). The system operates by creating a double strand break at a specific site in target DNA, mediated by RNA-guided Cas9 nuclease. A single guide (sg)-RNA contains a 20-bp targeting sequence. The site-specific DNA break induces DNA repair mechanisms that either cause mutations or insert new DNA at the target site.

The technique was applied in *A. niger* by expression of Cas9 and sgRNA from a self-replicative plasmid containing AMA1. The polyketide synthase gene *albA*, responsible for spore pigmentation, was successfully disrupted (Nødvig *et al*, 2015). Gene editing by CRISPR-Cas9 has subsequently been applied in metabolic engineering of *A. niger* to produce galactaric acid (Kuivanen *et al*, 2016). Six genes were successfully deleted by co-transforming the Cas9 expression vector with two synthetic sgRNAs, each targeted to a specific site to accurately delete the target gene. The technique proved significantly more reliable than conventional methods, with a deletion frequency up to 100%. These are promising steps forward in the ability to accurately and reliably edit the *A. niger* genome.

1.4.3 Computational techniques to guide rational engineering

The ability to apply rational engineering to *A. niger* enables more directed strategies of strain development. The complexity and unpredictability of metabolic engineering may, however, present challenges in making the right choice of targets. Advances in systems biology approaches are paving the way for the deployment of computational techniques to guide rational metabolic engineering strategies. This area of study is the primary focus of the work in this thesis. Computational tools for metabolic engineering depend on metabolic models, and these are described later in this chapter. The complexity of metabolic networks results in a combinatorial explosion when considering engineering strategies. To find optimal solutions requires optimisation algorithms. One of the first computational tools developed for this task was OptKnock, which was able to identify gene deletion strategies for optimising the production of a given byproduct during growth (Burgard *et al*, 2003). The tool used mixed integer linear programming, and was limited to predicting knock-out targets. The ability of OptKnock to predict knock-out strategies was demonstrated in *Escherichia coli*, for the targeted overproduction of succinate, lactate, and 1,3-propanediol, and was in agreement with previously applied engineering strategies, while also finding less intuitive solutions.

Other approaches have employed meta-heuristic algorithms, including the bees algorithm (Choon *et al*, 2014), ant colony optimisation (Chong *et al*, 2014), the bat algorithm (San Chua *et al*, 2015), and a hybrid of the bees and hill climbing algorithms (Choon *et al*, 2015). These were limited to predicting gene deletion strategies, and their applicability was mainly demonstrated for succinate and lactate production in *E. coli.* Other applications were succinate and glycerol production in *Saccharomyces cerevisiae* (Choon *et al*, 2014), and ethanol production in *Bacillus subtilis* and *Clostridium thermocellum* (Choon *et al*, 2015).

Tools have also been developed that use genetic algorithms, drawing parallels with natural evolution. One of the first examples of these was OptGene, which was used to suggest knock-out strategies for increasing production of succinate, glycerol, and vanillin in *S. cerevisiae* (Patil *et al*, 2005). The technique could be applied to a non-linear evolutionary objective function, however, was limited by the need to set a fixed number of gene deletions and was not guaranteed to find the global optimum. This limitation was overcome in a further development, which allowed solutions with a variable number of knock-outs (Rocha *et al*, 2008). The enhanced tool was applied to suggest engineering approaches for production of succinate and lactate in *E. coli* and *S. cerevisiae*. As with previous meta-heuristic algorithms, only gene deletions were considered, reducing the set of possible solutions. More recently, a genetic algorithm based tool was developed that included in its search space targets for knock-up and knock-down, and was applied for the optimisation of succinate and lactate production in *E. coli* (Gonçalves *et al*, 2012). Alternative engineering strategies were found, that were not solely dependent on gene deletion.

Although there has recently been extensive work to construct *in silico* tools to suggest engineering strategies for strain development, these have been limited to a narrow range of target organisms, mainly *E. coli* and *S. cerevisiae*. The work in this thesis describes for the first time a computational tool applicable to optimisation of organic acid production in

A. niger, based on a dynamic model of organic acid fermentation developed in this project. The tool implements a genetic algorithm, and is able to predict engineering strategies that use combinations of knock-out, knock-up, and knock-down, to maximise production of a given acid.

1.5 Mechanistic understanding of citric acid fermentation

The use of rational engineering in strain development requires a mechanistic understanding of the metabolism underpinning fermentation processes. Citric acid fermentation by *A. niger* was first established in 1917, when Currie experimented with different strains under different conditions (Currie, 1917). It was shown that *A. niger* secreted significant amounts of citric acid when grown in a low pH medium with a high sugar concentration. The low pH served to inhibit competing production of the acids oxalic and gluconic. Subsequently, industrial processes developed that exploited the findings to more cheaply manufacture citric acid by *A. niger* fermentation, and optimised strains by mutagenesis. Over the years, many studies were carried out to develop an understanding of the acidogenic behaviour of *A. niger*. These shall be the focus of this section, to build an awareness of the current knowledge forming the basis of targeted engineering. Contributions to this important understanding by the work in this thesis shall be outlined.

1.5.1 Conditions required for citric acid fermentation

Following Currie's work in 1917, many experiments were performed to investigate the response of citric acid fermentation to varying conditions. Findings were conflicting, some suggesting the need for deficiencies of phosphate and trace metals, and others showing citric acid production in the presence of these. It was not until 1948 that a more systematic study gave a clearer picture (Shu and Johnson, 1948). Iron, zinc, and phosphate were shown to play key roles, and were found to be interdependent. Limitation of only one of these was necessary for citric acid production, and each of the constituents was essential for optimal growth. The effects of nitrogen and

magnesium were also examined, and although these showed correlation with growth, their changing concentration had little impact on citric acid production. This suggested that iron, zinc, and phosphate affected citric acid production independently of growth, as growth-limitation via nitrogen or magnesium deficiency failed to achieve the same levels of citric acid yield. The same study investigated the response to changes in manganese concentration, and observed a relationship with phosphate. On increasing manganese, citric acid yield decreased more rapidly in high phosphate media than in low phosphate media. A different study showed that a partial deficiency of any of zinc, iron, copper, manganese, phosphate, magnesium, or potassium induced organic acid production, suggesting a non-specific effect (Chesters and Rolinson, 1951). Very small quantities of zinc, iron, copper, and manganese were shown to be necessary for citric acid production (Tomlinson *et al*, 1950), suggesting a complete absence of any of these metals is detrimental. The sensitivity of citric acid fermentation to manganese is well known, and it was shown that this is less pronounced at higher levels of copper or lower sugar concentrations (Mirminachi *et al*, 2002). Many investigations have been carried out to determine the role of manganese. It was reported that enzymes of the pentose-phosphate pathway exhibit a decreased activity under manganese-deficient conditions, suggesting that a shortage of manganese constrains anabolism, thereby allowing a higher flux to citric acid (Kubicek and Röhr, 1977). In line with this, other studies observed that a deficiency of manganese causes reduced DNA synthesis (Hockertz *et al*, 1987), altered cell wall composition (Kisser *et al*, 1980), lower lipid levels (Orthofer *et al*, 1979), and increased protein degradation (Ma *et al*, 1985). Interestingly, manganese insensitivity was shown at higher initial pH, by a mutant strain that is not dependent on low pH to produce citric acid (Ruijter *et al*, 1999). This indicated that the effect of manganese is pH-dependent.

A key factor in citric acid producing conditions is the substrate and its concentration. It was long established that a high sugar concentration is a necessity. The response to varying sugar concentration was tested, and the results showed that citric acid was only produced above 25 g/L sugar (Xu *et*

al, 1989a). A relationship with growth was also observed, with a 20% drop in growth rate on increasing the sugar concentration from 10 g/L to 140 g/L. Experiments performed using glucostat cultures showed that increases in glucose concentration increased the rate of citric acid production while decreasing the growth rate (Papagianni *et al*, 1999). When *A. niger* was pre-grown at high sugar concentration and transferred to low sugar concentration, citric acid production continued (Xu *et al*, 1989a). This implied that high sugar induced a particular metabolic state, enabling citric acid production. Investigations into the sugar source revealed that sucrose was the most effective, followed by glucose and fructose, and then lactose (Houssain *et al*, 1984). Sucrose was observed to undergo very rapid hydrolysis, completely hydrolysed within the first 30 hours of fermentation. No citric acid was produced with galactose as substrate (Houssain *et al*, 1984). Differences in enzyme activity were observed which may be causative factors of the altered citric acid production or effects. 2-oxoglutarate dehydrogenase activity was high when galactose was used, and undetected on sucrose. When the sugar source was switched from galactose to sucrose, the activities of pyruvate carboxylase and aconitase increased (Houssain *et al*, 1984). A more thorough investigation into the response of citric acid fermentation to different carbon sources was performed (Xu *et al*, 1989a). The highest yields of citric acid were obtained when using sucrose, maltose, mannose, glucose or fructose. Disaccharides were observed to be more effective, which may be due to increased carbon uptake. Citric acid production occurred on other substrates such as sorbitol and xylose. A number of other carbon sources, including cellobiose, arabinose, starch, cellulose, mannitol and glycerol, gave very low yields of citric acid despite good growth. When using mycelia pre-grown at high sucrose concentration, a striking observation was made. Citric acid production was achieved on a number of substrates that otherwise produced very little or none, including cellobiose, arabinose, and glycerol (Xu *et al*, 1989a). This suggested the need for induction of the required metabolic state by high sucrose concentration.

Aeration is known to be important to citric acid fermentation, through its effect on dissolved oxygen and carbon dioxide levels. A study was carried out to investigate the response to different levels of dissolved oxygen (Kubicek *et al*, 1980a). Lowering dissolved oxygen caused a decrease in citric acid production, eventually leading to its absence. Citric acid production stopped upon interrupting aeration, and did not resume when restoring the level of dissolved oxygen, despite a continuation of growth. It was therefore suspected that oxygen played a regulatory role. A correlation with ATP levels was not observed, suggesting the regulatory effect was not mediated by ATP. A separate study also investigated the effect of interrupting the air supply, and observed a dependence of citric acid production on oxygen, however, the previous finding that citric acid production fails to recover after an interrupted oxygen supply could not be reproduced (Dawson *et al*, 1986). The level of carbon dioxide is also affected by aeration, and was shown to be a factor in citric acid production (McIntyre and McNeil, 1997). On increasing dissolved carbon dioxide, the rates of growth and citric acid production decreased. A correlation with morphology was observed, with increased pellet diameter and hyphal length.

It is clear that citric acid producing conditions depend on a number of factors. The picture is further complicated by the observation that in the presence of certain additives citric acid production is increased. One of these is *n*-dodecane, which was shown to act as an oxygen-vector, thereby increasing the level of dissolved oxygen (Jianlong, 2000). Other beneficial additives that have received some attention and which have a less explicable effect are the alcohols methanol and ethanol. The addition of methanol or ethanol was shown to enhance citric acid production, and increased the tolerance to trace metals such as iron, zinc, and manganese (Moyer, 1953). Methanol was found to be more effective than ethanol. The cause of the beneficial effect remains to be elucidated, although it has been suggested that methanol acts by increasing membrane permeability, and thereby facilitating citrate secretion. It may be that alcohols indicate the presence of competing organisms, and the increased citric acid production could be a regulated response to kill off competitors. It is known that methanol is

produced by some species of bacteria when grown on pectin (Schink and Zeikus, 1980), and several species of microorganisms are known to produce ethanol (Lin and Tanaka, 2006). Another additive that has been found to stimulate citric acid production is phytate (Jianlong and Ping, 1998). In the presence of phytate, citric acid production and sugar uptake increased, while growth decreased. A change in enzyme activities was observed, including a decreased NADP-isocitrate dehydrogenase activity and an increased pyruvate carboxylase activity (Jianlong and Ping, 1998). It was thought that phytate acted by modulating the activity of these enzymes, however, the altered activities may simply be effects of increased citric acid production rather than causes. Alternatively, it may be that the metal chelating properties of phytate were responsible.

It is widely regarded that morphology is an important factor in citric acid producing conditions, and this has been the subject of some study (Papagianni and Mattey, 2006; Papagianni *et al*, 1999). Morphological observations are made on microscopic and macroscopic scales, both of which have characteristics associated with citric acid producing mycelia. The micro-morphology is characterised as short, swollen hyphal filaments with swollen tips which aggregate into clumps, while the macro-morphology is characterised as small pellets with a smooth, hard surface. It is known that the desired morphology is influenced by a number of factors including agitation, aeration, pH, substrate concentration, trace metals, and the spore concentration of the inoculum (Papagianni and Mattey, 2006; Papagianni *et al*, 1999).

1.5.2 Physiological characteristics of citric acid fermentation

A number of studies have revealed some of the physiological characteristics of citric acid fermentation. Citric acid production has been observed to coincide with a phase of restricted growth, preceded by a phase of fast growth (Roehr *et al*, 1981). Investigations into biomass composition revealed major differences in citric acid producing conditions (Jernejc *et al*, 1992). Nucleic acid and protein levels were significantly reduced, approximately 2-

fold. A significant decrease in lipid levels was also observed, around 4-fold. A detailed analysis of lipid composition revealed a decrease in phospholipid, with a significantly lower proportion of phosphatidyl-choline and increased proportions of phosphatidyl-ethanolamine and diphosphatidyl-glycerol (Jernejc *et al*, 1989). The ratio of saturated to unsaturated fatty acids was lower, and there was a greater proportion of linolenic acid and reduced proportions of palmitic and stearic acids (Jernejc *et al*, 1989). Other physiological characteristics associated with citric acid fermentation are high cAMP levels (Al Obaidi and Berry, 1980), and a polyol productive phase followed by polyol consumption (Röhr *et al*, 1987). The polyols observed to accumulate during fermentation are glycerol, arabitol, erythritol, and mannitol.

The work presented in this thesis makes a contribution to the physiological picture of citric acid fermentation. The response to phosphate was investigated, and evidence for a phosphate storage mechanism via polyphosphate was obtained. The dynamics of phosphate uptake, storage, and release correlated with the different fermentation phases. This aspect of citric acid fermentation has never previously been reported.

1.5.3 Discoveries into mechanisms underlying citric acid production

The mechanisms underlying the phenomenal citric acid producing ability of *A. niger* have been the focus of extensive research. A comprehensive understanding would be highly valued in the field of synthetic biology, providing the metabolic blueprint of an efficient production organism. This section aims to exhaustively review the research so far, and its mechanistic discoveries. A schematic overview is given in Figure 1.2.

The first step in the metabolic pipeline of citric acid production is carbon uptake. Carbon is usually supplied in the form of sugars, most commonly sucrose or its hydrolysis products glucose and fructose. Crossing biological membranes is no trivial task, and may pose a bottleneck. Therefore, some study has focused on understanding this first step. It is known that sucrose is rapidly hydrolysed by *A. niger* (Houssain *et al*, 1984). The extracellular hydrolysis of sucrose is mediated by a membrane-bound invertase (Papagianni, 2007). The products, glucose and fructose, are then taken up. It was shown that fructose has a significantly lower uptake rate than glucose late in fermentation, due to citrate inhibition (Bizukojc and Ledakowicz, 2004). Glucose uptake has been well characterised. *A. niger* expresses a high-affinity glucose transporter, that is inhibited by citrate (Mischak *et al*, 1984; Torres *et al*, 1996a). At high glucose concentration (15%), a low-affinity glucose transporter is also formed (Torres *et al*, 1996a). The activity of both transporters is reduced at low pH and inhibited by citrate, however, the low-affinity transporter is less sensitive to such conditions (Torres *et al*, 1996a). It has therefore been suggested that the low-affinity transporter is an important player in citric acid producing conditions. Interestingly, in an optimised industrial strain the low-affinity transporter is constitutively expressed at a high level (Yin *et al*, 2017). In this project, the low-affinity transporter was a target to increase the rate of glucose uptake. As well as transport-mediated uptake, glucose can also enter via passive diffusion. Modelling studies suggested that passive diffusion is the main contributor to glucose uptake in citric acid fermentation, following kinetic characterisation of

the various glucose uptake systems (Wayman and Mattey, 2000; Papagianni and Mattey, 2004).

Once glucose and fructose have entered the cell, the next step is phosphorylation by hexokinase. Hexokinase catalyses the first reaction of glycolysis, and is subject to regulation. Characterisation of the enzyme from *A. niger* revealed a 100-fold higher affinity for glucose than for fructose (Steinböck *et al*, 1994). The enzyme is inhibited by ADP and citrate, and is highly expressed during citric acid fermentation (Steinböck *et al*, 1994). Inhibition by citrate was shown to be weak, lowering hexokinase activity by only 10% at 10 mM citrate (Panneman *et al*, 1998). This enables a high flux through this reaction during citric acid producing conditions. A glucokinase was also identified in *A. niger*. The enzyme is inhibited by ADP but not by citrate, and its activity rapidly decreases below pH 7.5 (Panneman *et al*, 1996). Based on kinetic characteristics, it was determined that glucokinase is the main contributor to glucose phosphorylation at pH 7.5, while hexokinase predominates at pH 6.5 (Panneman *et al*, 1998). The importance of glucokinase was illustrated by the increasing expression of this enzyme during citric acid production in a characterised industrial strain (Yin *et al*, 2017). Hexokinase activity was also found to be strongly increased in mutant strains that produce significantly more citric acid (Schreferl-Kunar *et al*, 1989).

One of the regulatory aspects of *A. niger* hexokinase is its inhibition by trehalose-6-phosphate (Arisan-Atac *et al*, 1996a; Panneman *et al*, 1998). Physiological concentrations of trehalose-6-phosphate were shown to strongly inhibit the enzyme (Panneman *et al*, 1998). Therefore, this has attracted some investigation. Trehalose-6-phosphate is produced by trehalose-6-phosphate synthase. Two genes encoding this enzyme in *A. niger* were identified, *tpsA* and *tpsB* (Wolschek and Kubicek, 1997). The *tpsA* gene is constitutively expressed, and is subject to CreA-mediated carbon catabolite repression (Wolschek and Kubicek, 1997). The *tpsB* gene, on the other hand, is only expressed in response to heat shock (Wolschek and Kubicek, 1997). In a *tpsA*-disrupted strain, the onset of citric acid

production was earlier. Although the yield was the same, the time taken to reach it was decreased (Arisan-Atac *et al*, 1996a). The opposite effect was observed upon over-expression of the *tpsA* gene (Arisan-Atac *et al*, 1996a). These findings point to a role of trehalose-6-phosphate synthase in citric acid production, through its regulatory effect over hexokinase. This is further supported by the observation that trehalose levels are high early in fermentation, and decline later as citric acid is produced (Peksel *et al*, 2002). In growth on low glucose, trehalose levels are higher, and citric acid is not produced (Peksel *et al*, 2002).

Glucose-6-phosphate, the product of hexokinase, can either continue down glycolysis or be diverted to the pentose phosphate pathway. Glucose-6-phosphate dehydrogenase catalyses the first reaction of the pentose phosphate pathway. Its activity was shown to decrease during citric acid production (Kirimura *et al*, 1984; Legiša and Mattey, 1988). Another enzyme of the pentose phosphate pathway is 6-phosphogluconate dehydrogenase. A strong inhibition by citrate was determined for this enzyme, which was reversed in the presence of manganese (Legiša and Mattey, 1988). An increasing activity of glycolytic enzymes is characteristic of citric acid production, including fructose-bisphosphate aldolase (Kirimura *et al*, 1984) and 6-phosphofructo-1-kinase (Legiša and Mattey, 1988). Following these findings, it is suggested that a redistribution of flux from the pentose phosphate pathway to glycolysis is a key event in citric acid fermentation.

The second phosphorylation reaction of glycolysis is catalysed by 6-phosphofructo-1-kinase (PFK1). This is typically a tightly controlled step, and therefore a number of studies have been devoted to understanding the role of PFK1 in citric acid production. Early studies focused on characterisation of the regulatory properties of PFK1 from *A. niger*. These revealed the inhibition by intracellular concentrations of citrate, and showed that this is counteracted by ammonium ions, AMP, and phosphate (Habison *et al*, 1979; Habison *et al*, 1983). The intracellular concentrations of AMP and phosphate during citric acid production, however, were shown to be insufficient to counteract the citrate inhibition of PFK1 (Habison *et al*, 1979). In the case of ammonium,

a correlation was observed with the rate of citric acid production (Habison *et al*, 1979). Phosphoenolpyruvate also inhibited PFK1, as well as saturating concentrations of ATP (Habison *et al*, 1983). The effect of AMP and ADP was dependent on the level of fructose-6-phosphate, with activation at low concentrations and inhibition at high concentrations (Habison *et al*, 1983). In the absence of citrate, phosphate had no effect (Habison *et al*, 1983).

The early theory that elevated ammonium circumvents PFK1 citrate inhibition was supported by the effect of impaired protein synthesis. These observations were made in mutant strains or by addition of methanol or cycloheximide. These conditions constrained protein synthesis and significantly increased the intracellular ammonium concentration, as well as citric acid production (Rugsaseel *et al*, 1996). Subsequent research, however, has shed doubt on the theory. Evidence suggests that ammonium combines with fructose-6-phosphate to form glucosamine, in a reaction catalysed by glucosamine-6-phosphate deaminase (Šolar *et al*, 2008). This competes with PFK1 for fructose-6-phosphate. Glucosamine is observed to accumulate rapidly early in citric acid fermentation (Papagianni *et al*, 2005; Šolar *et al*, 2008). The addition of ammonium later in fermentation results in glucosamine formation and a temporary decline in citric acid production (Papagianni *et al*, 2005).

An additional player in PFK1 regulation is fructose-2,6-bisphosphate, which was shown to be stimulating and partially relieved citrate inhibition (Arts *et al*, 1987). A rise in the level of fructose-2,6-bisphosphate was observed in citric acid producing conditions (Kubicek-Pranz *et al*, 1990). The enzyme responsible, 6-phosphofructo-2-kinase (PFK2), was characterised (Harmsen *et al*, 1992). This revealed a weak inhibition by phosphoenolpyruvate, AMP, and citrate, and an absence of regulation by phosphorylation/dephosphorylation mechanisms. The weakly regulated PFK2 enzyme may be one means by which *A. niger* achieves a high glycolytic flux during citric acid production. This is supported by the observation that the level of fructose-2,6-bisphosphate is 2-fold lower in

strains over-expressing PFK1, explaining the null effect on citric acid production in these strains (Ruijter *et al*, 1997).

Another factor in PFK1 regulation is its phosphorylation by a cAMP-dependent protein kinase. It was demonstrated that *A. niger* PFK1 activity is lost after incubation with a phosphatase (Legiša and Benčina, 1994). When inactive PFK1 was isolated from mycelia early in citric acid fermentation, it could be activated by phosphorylation in the presence of cAMP, ATP, magnesium, and a protein kinase isolated from *A. niger* (Legiša and Benčina, 1994). In earlier studies, cAMP was observed to have a stimulatory effect on citric acid production, and it was proposed that this was due to increased glycolytic flux (Wold and Suzuki, 1973). Further evidence for the potential role of cAMP came from the observation that its intracellular concentration increases early in citric acid fermentation (Gradisnik-Grapulin and Legisa, 1997). The effect was not observed at lower sucrose concentrations. Interestingly, the effect was also absent in the presence of light, and it was suggested that this results from photoregulation of phosphodiesterase (Gradisnik-Grapulin and Legisa, 1997). There are conflicting findings regarding cAMP, however. In a separate study, no correlation was found between cAMP levels and citric acid producing conditions (Xu *et al*, 1989b). The intracellular cAMP concentration was unaffected by changes in the sugar source and the level of manganese, although these altered citric acid production (Xu *et al*, 1989b). It was also reported that citric acid production is insensitive to cAMP (Habison *et al*, 1979). Differences in the experimental setup, including culture conditions and the strain, may account for the observed discrepancies.

A more convincing resolution to PFK1 citrate inhibition was delivered by a series of more recent studies (Mesojednik and Legiša, 2005; Mlakar and Legiša, 2006; Capuder *et al*, 2009). PFK1 was observed to undergo a post-translational cleavage, yielding a C-terminal truncated protein. This fragmented protein exhibited PFK1 activity after phosphorylation by cAMP-dependent protein kinase. The truncated PFK1 was absent early in fermentation, and its appearance coincided with a sudden growth shift

(Mesojednik and Legiša, 2005). A detailed kinetic characterisation revealed striking findings. Truncated PFK1 was completely insensitive to citrate inhibition, suggesting the allosteric sites for citrate were lost. The citrate-insensitive PFK1 was more efficient, and activated to a higher level by positive effectors (Mlakar and Legiša, 2006). Fructose-2,6-bisphosphate was found to significantly increase the activity with respect to the native enzyme (Mesojednik and Legiša, 2005; Capuder *et al*, 2009). Engineering was carried out to directly encode the truncated PFK1 from a modified gene (Capuder *et al*, 2009). Site-directed mutagenesis of the phosphorylation site was performed, substituting a threonine residue for glutamate. This resulted in a constitutively active PFK1, insensitive to citrate and without the need for phosphorylation by cAMP-dependent protein kinase. Citric acid production was increased by up to 70% (Capuder *et al*, 2009). In this project, further investigations were made, to see if the effect is reproduced in the ATCC1015 strain.

The importance of PFK1 to citric acid production is highlighted by studies that investigated mutant strains. Heightened activities of PFK1 were observed in mutants that produce more citric acid (Schreferl-Kunar *et al*, 1989). In another mutant strain, PFK1 citrate inhibition was much less pronounced, and citric acid production by this mutant was less sensitive to manganese (Schreferl *et al*, 1986).

The final step of glycolysis is catalysed by pyruvate kinase. In addition to hexokinase and PFK1, pyruvate kinase is often subject to regulation. As this may have implications in citric acid production, the regulatory properties of pyruvate kinase from *A. niger* were characterised (Meixner-Monori *et al*, 1984). The enzyme was activated by fructose-1,6-bisphosphate and monovalent cations. A very high affinity was determined for fructose-1,6-bisphosphate. Activity was slightly augmented by ATP. No significant inhibitory factors were found. The findings suggested no regulatory role of pyruvate kinase in citric acid production. Over-expression of the enzyme had no significant effect (Ruijter *et al*, 1997).

The maintenance of a high glycolytic flux requires an adequate supply of NAD. The NADH produced by glycolysis is ordinarily recycled to NAD by oxidative phosphorylation, coupled with ATP production. Given a high sugar uptake rate under citric acid producing conditions, this would produce a significant amount of ATP, and subsequently limit the production of citric acid. Therefore, an alternative means of NADH recycling is needed that keeps ATP levels low. This mechanistic aspect of citric acid fermentation has attracted considerable attention. It was observed that *A. niger* has two respiratory systems, characterised by their sensitivity to different inhibitors (Zehentgruber *et al*, 1980; Kirimura *et al*, 1987). One of these is composed of cytochromes and is inhibited by cyanide (CN) and antimycin A. The other is unaffected by these, but is disabled in the presence of salicylhydroxamic acid (SHAM). The SHAM-sensitive system decouples NADH recycling from ATP production, and is composed of an alternative oxidase (AOX). Chloramphenicol, a stimulator of SHAM-sensitive respiration, was shown to increase citric acid production (Zehentgruber *et al*, 1980). On the other hand, the addition of SHAM strongly repressed it, with little effect on growth (Zehentgruber *et al*, 1980; Kirimura *et al*, 2000). During citric acid fermentation, respiratory activity was shown to progressively shift from the CN-sensitive system to the SHAM-sensitive system (Kirimura *et al*, 1987). Disruption of oxidative phosphorylation was shown to increase AOX activity (Zehentgruber *et al*, 1980; Kirimura *et al*, 1996; Kirimura *et al*, 2000), and also increased citric acid production without affecting growth or morphology (Kirimura *et al*, 2000; Wang *et al*, 2015). A number of studies have revealed complex I as the key player. In a citric acid producing strain, it was observed that complex I activity is lost at the onset of citric acid production, while AOX activity is increased (Wallrath *et al*, 1991). A further investigation revealed a disruption in the assembly of complex I that leads to its instability (Schmidt *et al*, 1992). A relationship with manganese was also discovered. The addition of manganese prevented loss of complex I activity and stopped citric acid production (Wallrath *et al*, 1992). In another study, the gene encoding the NADH-binding subunit of complex I was disrupted in a non-producing wild-type strain (Prömper *et al*, 1993). The mutant accumulated intracellular citrate to 6.5 times the level of the wild-type, however, was unable to secrete

the over-produced citric acid. This suggested the lack of citrate transport mechanisms, otherwise present in citric acid producing strains. It has been argued that loss of complex I results in increased AOX activity due to differences in NADH-binding affinities. The higher affinity of complex I for NADH allows it to out-compete AOX, and in its absence AOX is able to recycle NADH without producing ATP (Prömper *et al*, 1993). The importance of AOX in citric acid production has made it a target of considerable research. The *A. niger* gene responsible, *aox1*, was identified (Kirimura *et al*, 1999b). A mitochondrial import signal was found (Kirimura *et al*, 1999b), and AOX activity was shown to be localised in mitochondria (Kirimura *et al*, 2000; Kirimura *et al*, 2006). The expression of *aox1* was visually observed in fluorescence experiments (Kirimura *et al*, 2006). A response was observed to addition of antimycin A, with increased *aox1* expression and heightened AOX activity. The expression of *aox1* occurred at different glucose concentrations (Kirimura *et al*, 2006), and was shown to be constitutive, even present in spores (Hattori *et al*, 2008). A transcriptional study revealed a correlation between *aox1* mRNA levels and AOX activity, suggesting regulation of AOX at the transcriptional level (Hattori *et al*, 2009). Only one gene could be found encoding AOX (Hattori *et al*, 2009). In an industrial strain, the gene increased in expression during citric acid fermentation (Yin *et al*, 2017).

There is evidence that ATP-citrate lyase supports AOX in the maintenance of a low ATP level and NADH recycling. Two cytosolic ATP-citrate lyases were found to be up-regulated during citric acid production in an industrial strain (Yin *et al*, 2017). It was proposed that these operated in a futile cycle in conjunction with mitochondrial citrate synthase to consume excess ATP (Yin *et al*, 2017). The reaction catalysed by citrate synthase is exergonic and irreversible. The reverse, catalysed by ATP-citrate lyase, therefore requires ATP hydrolysis (Aoshima, 2007). The energy lost in this futile cycle is via the citrate synthase reaction, which has a free energy change of -37.6 kJ/mol (Guynn *et al*, 1973). ATP-citrate lyase is widely found in eukaryotes, where it is important in the provision of cytosolic acetyl-CoA. It is however found in only a few species of prokaryotes (Gawryluk *et al*, 2015). Another form of

citrate lyase exists only in prokaryotes that is not dependent on ATP hydrolysis and this catalyses the breakdown of citrate to oxaloacetate and acetate (Subramanian and Sivaraman, 1984). When genes encoding subunits of the ATP-citrate lyase were deleted in *A. niger*, a significant drop in citric acid production resulted (Chen *et al*, 2014). Over-expression, on the other hand, increased citric acid production (Chen *et al*, 2014). The findings suggest that ATP-citrate lyase plays an important role, however, there is some evidence on the contrary. In a separate investigation, a pronounced drop in ATP-citrate lyase activity was observed during citric acid fermentation (Jernejc *et al*, 1991).

It is clear that numerous factors are involved in supporting a high glycolytic flux during citric acid fermentation. The final product of this pathway is pyruvate. The mechanism of citric acid formation from this point was first studied in tracer experiments, using 14C-labelled glucose and carbon dioxide (Cleland and Johnson, 1954). These revealed that glucose is split into two C3 molecules (pyruvate), one of which decarboxylates to C2 (acetyl-CoA), while the other carboxylates to C4 (oxaloacetate). Citric acid is then formed by condensation of the C2 and C4 products, and not broken down by the tricarboxylic acid (TCA) cycle. It was shown that the C4 precursor is produced by fixation of carbon dioxide. The findings were supported by later experiments using 13C-labelled glucose, that highlighted the importance of the pyruvate carboxylase reaction in providing most of the oxaloacetate precursor (Peksel *et al*, 2002). Due to its role in citric acid production, further investigations were made to characterise pyruvate carboxylase from *A. niger*. Early research showed that the enzyme contains biotin, is activated by magnesium and potassium ions, and inhibited by sodium and L-aspartate (Bloom and Johnson, 1962; Feir and Suzuki, 1969). Acetyl-CoA was found to have no effect. The location of pyruvate carboxylase was subject to some debate, due to variation between different strains of *A. niger*. The enzyme activity was detected in both the cytosol and mitochondria in five strains tested (Bercovitz *et al*, 1990), however, in two citric acid producing strains the enzyme was only present in mitochondria (Purohit and Ratledge, 1988). Activity of the mitochondrial enzyme required the presence of acetyl-CoA.

This is characteristic of mitochondrial pyruvate carboxylase, unlike the cytosolic version (Purohit and Ratledge, 1988). The location of the enzyme was suggested as an important factor in determining the organic acid produced and its yield (Bercovitz *et al*, 1990). Oxaloacetate is the precursor of both oxalic and citric acid. Oxaloacetate hydrolase (OAH), localised in the cytosol, hydrolyses oxaloacetate producing oxalate and acetate (Kubicek *et al*, 1988). Meanwhile, citrate synthase, localised in the mitochondria, combines oxaloacetate with acetyl-CoA to form citric acid (Ruijter *et al*, 2000). As citrate synthase is directly involved in citric acid formation, the *A. niger* enzyme was characterised (Kubicek and Röhr, 1980b). Only coenzyme A and ATP inhibited the enzyme, while citrate had no effect. Therefore, it was suggested that *A. niger* citrate synthase is weakly regulated. This was supported by the observation that 11-fold over-expression of citrate synthase had no effect on citric acid production, indicating that the step was not limiting (Ruijter *et al*, 2000).

The accumulation of citric acid requires a block in the TCA cycle, to prevent its catabolic breakdown. The enzymes aconitase, isocitrate dehydrogenase, and α-ketoglutarate dehydrogenase have all been targets of investigation, as a disruption of any of these could lead to citric acid accumulation. Several studies showed a decline in aconitase activity during citric acid fermentation (Ramakrishnan *et al*, 1955; Szczodrak, 1981; Agrawal *et al*, 1983), however, others found no significant changes (La Nauze, 1966; Ahmed *et al*, 1972; Kirimura *et al*, 1984; Kubicek and Röhr, 1985). Although it was suspected aconitase may play a role, evidence stacked up against this. In two strains that give different yields of citric acid, the aconitase activity was the same (La Nauze, 1966). When aconitase activity was doubled by a 20-fold increase in iron, citric acid was still produced, with a reduction of just 25% (La Nauze, 1966). Aconitase catalyses a reversible reaction, and the equilibrium was shown to lie in favour of citrate (Kubicek and Röhr, 1985). Aconitase activity was 2-fold higher with isocitrate as the substrate, and during citric acid fermentation intracellular citrate was 10 times higher than isocitrate (Kubicek and Röhr, 1985). These findings suggested that a disruption of aconitase was unnecessary, as a block further down-stream would still cause citric acid

to accumulate. The next step, catalysed by isocitrate dehydrogenase (ICDH), has also been the subject of conflicting observations. A drop in ICDH activity during citric acid fermentation was reported by numerous studies (Ramakrishnan *et al*, 1955; Bowes and Mattey, 1980; Szczodrak, 1981; Agrawal *et al*, 1983; Kirimura *et al*, 1984; Jaklitsch *et al*, 1991), yet others showed no effect (La Nauze, 1966; Ahmed *et al*, 1972). The finding that ICDH from *A. niger* is inhibited by citrate suggested it may become disrupted under citric acid producing conditions (Ramakrishnan *et al*, 1955; Mattey, 1977; Kubicek and Röhr, 1978; Mattey and Bowes, 1978; Meixner-Monori *et al*, 1986). Although physiological citrate concentrations were found to inhibit ICDH, the effect was absent below pH 7.6 (Mattey and Bowes, 1978). It is known that the intracellular pH drops to 6.5 in citric acid fermentation (Legiša and Kidrič, 1989), making ICDH citrate-insensitive. A more detailed characterisation revealed that ICDH requires manganese or magnesium, and that citrate inhibition occurs via chelation of the metal ion cofactor (Meixner-Monori *et al*, 1986). When the manganese level was increased, ICDH activity was significantly higher, and citric acid production was reduced by 75% (Gupta and Sharma, 2002). In a manganese-insensitive mutant strain, ICDH activity and citric acid production were unaffected (Gupta and Sharma, 2002). The effects, however, do not confirm a direct role of ICDH. Manganese has a multiplicity of effects, and the altered ICDH activity may be caused by a shift to non-citric acid producing conditions. In other investigations, a relationship between glycerol accumulation and ICDH activity was proposed, that may trigger the onset of citric acid production (Legiša and Mattey, 1986; Legiša and Kidrič, 1989). Glycerol was observed to accumulate early in citric acid fermentation, up to 100 mM. Its production may be an osmoregulatory mechanism in response to the high sugar concentration. The rise in glycerol peaked at the beginning of citric acid production, followed by a rapid assimilation. A significant inhibition of ICDH by glycerol was observed, around 90% at 100 mM glycerol. In the presence of manganese, the inhibitory effect was absent. Subsequent experiments, however, contradicted the theory (Arisan-Atac and Kubicek, 1996b). *A. niger* was shown to catabolise citrate with or without the presence of glycerol, indicating an active ICDH. Moreover, glycerol had no effect on the activity of

purified ICDH, and only inhibited in crude extracts, suggesting the previous result was an artefact. Until recently, there was no clear evidence that ICDH is a factor in the causation of citric acid over-production. When ICDH was over-expressed in *A. niger*, citric acid production decreased by 20% (Kobayashi *et al*, 2014). This effect was similar to that observed when aconitase activity was doubled (La Nauze, 1966), suggesting the activities of these two enzymes are contributive factors. The minor effects, however, indicate a blockage of the TCA cycle at a different point. The step following ICDH is catalysed by α-ketoglutarate dehydrogenase. There is evidence supporting the argument that disruption of this enzyme is mainly responsible for citric acid accumulation (Kubicek and Röhr, 1978; Meixner-Monori *et al*, 1985). An analysis of the levels of TCA cycle intermediates during citric acid production was suggestive of a block at this step (Kubicek and Röhr, 1978). A characterisation of the regulatory properties of α-ketoglutarate dehydrogenase from *A. niger* showed inhibition by NADH, oxaloacetate, succinate, and *cis*-aconitate (Meixner-Monori *et al*, 1985). It was proposed that high levels of oxaloacetate and NADH early in fermentation cause an inhibition of the enzyme. A subsequent build-up of α-ketoglutarate results in ICDH inhibition (Kubicek and Röhr, 1978; Meixner-Monori *et al*, 1986). As aconitase favours citrate formation (Kubicek and Röhr, 1985), the end result is the accumulation of citric acid. Overall, the evidence suggests that a combined disruption of the three enzymes involved in citrate catabolism leads to citric acid over-production. This was shown to be the case for an industrial strain (Yin *et al*, 2017). An aconitase-encoding gene was mutated, and aconitase, ICDH, and α-ketoglutarate dehydrogenase were all down-regulated at the transcriptional level during citric acid production.

A block in the TCA cycle at α-ketoglutarate dehydrogenase can be bypassed by the gamma-aminobutyric acid (GABA) shunt, which is an alternative pathway for producing succinate from α-ketoglutarate. The GABA shunt was shown to be operative in *A. niger*, and increased in activity during citric acid production (Kumar *et al*, 2000). Furthermore, a transcriptomic analysis of an industrial strain showed an up-regulation of the GABA shunt (Yin *et al*, 2017).

It may be that the pathway is used as a means of supplementing low succinate levels during citric acid fermentation.

Once citric acid accumulates in the mitochondria, a mechanism is needed to transport it to the cytosol for subsequent citrate secretion. In other organisms, it is known that a malate-citrate antiporter exists, which exchanges cytosolic malate for mitochondrial citrate (Kirimura *et al*, 2016). A putative gene encoding this transporter in *A. niger* was identified, and shown to be transcribed throughout citric acid fermentation (Kirimura *et al*, 2016). To investigate further, the gene was disrupted, and this resulted in a small decrease in citric acid production early in fermentation (Kirimura *et al*, 2016). This suggested the presence of other genes responsible for mitochondrial citrate export, and it is reported that a number of putative organic acid transporter genes are transcribed in *A. niger* (Kirimura *et al*, 2016). As the export of mitochondrial citrate may be a limiting step, an engineering effort was made to increase the cytosolic malate concentration (De Jongh and Nielsen, 2008). Genes encoding malate dehydrogenase and fumarase were over-expressed and targeted to the cytosol, individually and together. These enzymes are involved in malate production. In all cases, citric acid production was increased. A fumarate reductase gene was also over-expressed, to irreversibly convert fumarate to succinate. This also increased citric acid production, suggesting that cytosolic succinate may be able to substitute for malate in citrate antiport (De Jongh and Nielsen, 2008). Although the observed effects may not be specifically due to increased mitochondrial citrate export, the findings provide some evidence that this step acts as a bottleneck. In this project, a different approach was taken to investigate this. An attempt was made to express cytosolic citrate synthase, to bypass the mitochondrial citrate transport step.

The final step of the citric acid producing metabolic pipeline is citrate secretion. Researchers have frequently observed an intracellular citrate accumulation without a corresponding rise in the level of extracellular citric acid (Legiša and Kidrič, 1989; Prömper *et al*, 1993). Although clearly important, there have been relatively few studies to elucidate this final step. It

was demonstrated that citrate transport in *A. niger* is bidirectional, with citric acid taken up even as citric acid is produced (Kontopidis *et al*, 1995). It was later shown that both citrate import and export occur via an active proton symport mechanism, with highest activity at low extracellular pH (Netik *et al*, 1997). A possible relationship with manganese was also observed. Citrate uptake required manganese, whereas in the presence of manganese citrate export did not occur (Netik *et al*, 1997). The sensitivity of citrate export to manganese is, however, questionable. In a mutant strain that does not produce oxalic or gluconic acid, citrate secretion occurred regardless of the manganese concentration at a pH of 5 (Ruijter *et al*, 1999). The transporter responsible for citrate secretion was very recently identified (GenBank accession number EHA22412) (Odoni *et al*, 2018). Expression of this transporter in *S. cerevisiae* led to citrate secretion. On the other hand, its knock-out in *A. niger* abolished citric acid production (Odoni *et al*, 2018). The identified transporter could be a valuable over-expression target for increasing citric acid production in engineered strains.

Decades of research have tried to unravel the acidogenic behaviour of *A. niger*, and there is yet to be a clear mechanistic picture. Across numerous studies, different strains and conditions have been used, and these variations may partly account for conflicting findings. It is possible that among the wild-type citric acid producing strains, different mechanisms of acidogenesis have evolved, and in response to different conditions. The leading cause of organic acid production by *A. niger* is yet to be fully understood. In recent years, evidence has gathered to suggest the behaviour is a deliberate response to the environment, rather than uncontrolled overflow metabolism. An investigation was performed to analyse the transcriptional response to different ambient pH values (Andersen *et al*, 2009b). This was based on the observation that *A. niger* produces different organic acids under different conditions. The expression of a number of genes relevant to organic acid production responded in a coordinated manner to changes in ambient pH. In total, the expression profiles of 109 genes showed a direct correlation with pH. This enabled the identification of putative pH-dependent *cis*-acting regulatory motifs, as well as a number of

putative pH-responsive transcription factors. In *A. nidulans*, the Pal/PacC pH-signalling pathway has been characterised, and candidate genes encoding all components of this pathway were identified in *A. niger* (Andersen *et al*, 2009b). Following this transcriptomic study, a pH-responsive transcription factor was knocked out (Poulsen *et al*, 2012). Oxalic acid production increased significantly, and the expression of 241 genes was altered. In another investigation, a non-acidifying mutant strain of *A. niger* was studied, and the phenotype was traced to a mutation in the *laeA* gene (Niu *et al*, 2016). LaeA is a nuclear protein with methyltransferase activity, and acts as a global regulator of secondary metabolism (Niu *et al*, 2016). Further research showed that deletion of the *laeA* gene in *A. niger* eliminates citric acid production, while over-expression leads to a 40% increase in citric acid production (Niu *et al*, 2016). From these findings, it is clear that the acidogenic behaviour of *A. niger* is under transcriptional control. A full mechanistic understanding of citric acid fermentation therefore needs to encompass the underlying changes in the transcriptome and the roles of transcription factors, as well as changes in the metabolome. This is highlighted by the transcriptome analysis of an industrial strain, which showed dynamic expression of nearly 500 genes at various time-points during citric acid fermentation (Yin *et al*, 2017). Given that the behaviour may be a regulated response, it poses the question of what has driven the evolution of this acidogenic trait. It may be a means of mobilising limiting phosphate and trace metals, which explains the absence of citric acid production when all these are abundant. It may also be a competition strategy, to acidify the environment and kill off rival microorganisms. An additional benefit is that the acidified environment may help degrade plant biomass, which the saprotrophic *A. niger* thrives on.

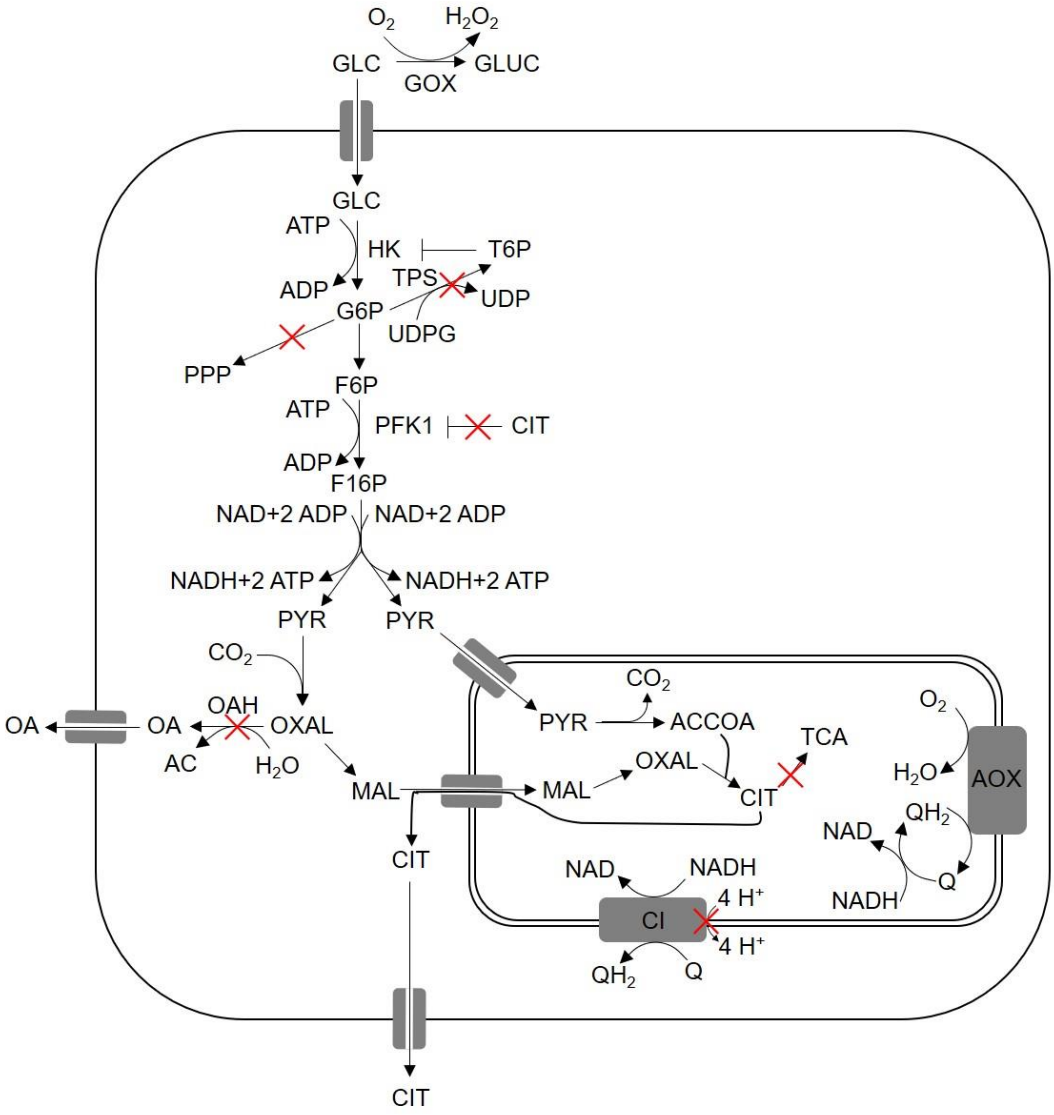

Figure 1.2. Schematic overview of metabolic and transport reactions relevant to *A. niger* organic acid production. The intracellular compartment reflects the mitochondria. Red crosses indicate reactions that when disrupted lead to improvements in citric acid production. Abbreviations are as follows: GLC, glucose; GLUC, gluconic acid; GOX, glucose oxidase; HK, hexokinase; G6P, glucose-6-phosphate; T6P, trehalose-6-phosphate; UDPG, UDP-glucose; TPS, trehalose-6-phosphate synthase; PPP, pentose phosphate pathway; F6P, fructose-6-phosphate; F16P, fructose-1,6-bisphosphate; PFK1, 6-phosphofructo-1-kinase; CIT, citric acid; PYR, pyruvate; OXAL, oxaloacetate; OA, oxalic acid; OAH, oxaloacetate hydrolase; AC, acetic acid; MAL, malic acid; ACCOA, acetyl-CoA; TCA, tricarboxylic acid cycle; CI, complex I; AOX, alternative oxidase; Q, ubiquinone; QH2, ubiquinol.

1.6 Modelling of citric acid fermentation

Advances in understanding of the physiological characteristics and mechanisms of *A. niger* fermentation processes informs modelling, paving the way for process optimisation and *in silico* guided metabolic engineering strategies. Efforts to model citric acid fermentation shall be the focus of this section, and the contributions of the work in this thesis shall be outlined.

1.6.1 Early models of citric acid fermentation

Early modelling efforts were focused on capturing the kinetics of growth and citric acid production to inform process control and optimisation (Roehr *et al*, 1981). Based on empirical data, it was observed that fermentation occurred in two main phases. The first phase was characterised by high growth and low citric acid production, while the second phase was characterised by low growth and high citric acid production. By obtaining higher resolution data, with data-points at 2 hour intervals, the phases were further divided. These phases were attributed to germination, hyphal growth, pellet growth, restricted growth, a transitional period, and idiophase growth. Different mathematical models were applied to capture the growth curve in each phase. Citric acid production was observed to be divided into the same phases, but with a lag. The same models used for growth captured the kinetics of citric acid production. Although this modelling attempt reflected the kinetics of citric acid fermentation, it did not take into account the underlying metabolic changes.

A model was later developed that took into account the main metabolic pathways and the energy requirements for growth and maintenance processes (Krzystek *et al*, 1996). Metabolic pathways were summarised by 10 stoichiometric equations, and an elemental biomass composition was used. This simplified metabolic model was used to calculate maximum yields of citric acid and biomass per gram of sucrose, which were 0.9 g and 0.18 g respectively.

A more detailed model was developed that included the reactions of carbohydrate metabolism (Torres *et al*, 1996b). An S-system model was implemented based on biochemical systems theory. The reactions of glycolysis were represented as well as pyruvate carboxylase, malate dehydrogenase and fumarase. Linear programming was applied to give optimum solutions of steady-state flux. Kinetic parameters and metabolite concentrations were obtained from empirical data at a time-point during the citric acid producing phase. The model was applied to predict changes required to optimise citric acid yield, and suggested the need to simultaneously modulate the activities of at least seven enzymes. This early modelling effort was still very simplified, not taking into account biomass production, maintenance processes, and omitting a large number of metabolic reactions. The metabolic network was subsequently extended, in an expanded and updated model (Alvarez-Vasquez *et al*, 2000). The new model included all major metabolic and transport reactions relevant to citric acid metabolism, such as glycolysis, the TCA cycle, anaplerotic pyruvate carboxylase, and cytosolic and mitochondrial transport processes. Available empirical data on metabolite concentrations, enzyme activities, fluxes, and kinetic parameters were applied to the model. The new model suggested the need to over-express 13 enzyme and transport processes, and found that glycolytic reactions and transport steps are most significant.

The disadvantage of the S-system model is its complexity and dependency on a large number of kinetic parameters, that need to be drawn from extensive empirical data from multiple sources. The use of stoichiometric modelling circumvents the need for kinetic parameters, and can be applied to metabolic flux analysis under the assumption that metabolite concentrations remain at a steady-state. The first stoichiometric model of *A. niger* was developed in 2003, and included 284 metabolites, 268 metabolic reactions, and 67 transport reactions (David *et al*, 2003). The metabolic network was a comprehensive coverage of the central carbon metabolism of *A. niger*, and was compartmentalised into cytosolic, mitochondrial, glyoxysomal and extracellular compartments. An equation for biomass production was

included, taking into account the main cellular components such as protein, nucleic acids, carbohydrates, lipids, and polyols. This was a step-forward from the elemental biomass composition used in previous models, however, was based on data of the cellular biomass composition of *A. oryzae*. The energy requirements for biomass production and maintenance processes were also included, based on experimentally determined energetic parameters. The model was applied to calculate flux distributions with an objective of biomass production, to give predictions of growth rate and metabolite output in response to different environmental and genetic conditions. Although the model provided a better representation of metabolism, it could only be applied to make static predictions, and therefore was not useful for dynamic modelling of citric acid fermentation.

The early models so far described did not reflect the morphological structure of citric acid producing mycelia. It is known that morphology is an important factor in citric acid fermentation. An attempt to capture the effects of morphological changes was made by the development of a morphologically structured model for *A. niger* citric acid fermentation (Bizukojc and Ledakowicz, 2003). This model represented the hyphae as four zones, based on microscopic analysis of hyphae stained with an agent that changes colour based on respiratory activity. Each zone was classified based on physiological and morphological characteristics, and assigned different metabolic functions in line with experimental data. The model included 10 ordinary differential equations, describing changes in biomass, zone fractions, and extracellular components. The predictions of the model agreed well with experimental data on citric acid fermentation.

1.6.2 Genome-scale metabolic modelling

Advances in genome sequencing technologies and annotation tools over recent years have opened the way for metabolic network constructions on a genome-scale. These comprehensively capture the metabolism of an organism, and provide a bridge between the genome and the metabolome, significantly aiding in metabolic engineering efforts. Metabolic networks are

applied in stoichiometric modelling, to build genome-scale metabolic models (GSMMs). The advantage of stoichiometric models is that they do not rely on kinetic parameters, that are difficult to source. Using the mathematical method of flux balance analysis (Orth *et al*, 2010), they are able to make predictions of metabolic flux distributions under different conditions, assuming that the metabolite concentrations remain at a steady-state. The heart of a stoichiometric model is a stoichiometric matrix ($\boldsymbol{S}$), that mathematically represents the metabolic network. Each row represents a metabolite, and each column represents a reaction. The entries in the matrix are the stoichiometric coefficients, which are negative for the reactants and positive for the products. The vector $\boldsymbol{v}$ represents the flux of all reactions, and the vector $\boldsymbol{x}$ represents the concentrations of all metabolites. As the metabolite concentrations are assumed constant, it follows that

$$\boldsymbol{S}.\boldsymbol{v} = \mathbf{0}$$

This gives a system of mass balance equations, and as the number of reactions exceeds the number of metabolites, there is no unique solution. The set of solutions is given by the solution space, which can be narrowed by imposing constraints on the lower and upper bounds of $\boldsymbol{v}$. To obtain a single solution requires an objective function, which maximises or minimises the flux of a given set of reactions. The vector $\boldsymbol{c}$ gives the weights, which indicate the contributions of each reaction to the objective. Most commonly, the objective is the flux maximisation of a single reaction, and therefore $\boldsymbol{c}$ is a vector of zeroes with a one at the reaction of interest, usually biomass production (growth). The objective function is given as

$$\boldsymbol{Z} = \boldsymbol{c}^{\boldsymbol{T}}.\boldsymbol{v}$$

and the optimisation is solved by linear programming.

To date, at least 165 genome-scale metabolic models have been produced, spanning a wide range of organisms. The first genome-scale metabolic

network of *A. niger* was published in 2007 (Sun *et al*, 2007), following the genome sequencing and annotation of the enzyme-producing CBS 513.88 strain (Pel *et al*, 2007). The network was based on the annotation of CBS 513.88, as well as genomic information of the ATCC 9029 strain, and included 2443 reactions and 2349 metabolites. Construction of this network was achieved by using automated techniques and based on sequence information. The network was not manually curated to reflect literature evidence, and was not compartmentalised. The network also included a large number of reactions disconnected from central metabolism. A more substantial effort was made in construction of the *A. niger* GSMM iMA871, released in 2008 (Andersen *et al*, 2008). The metabolic network included 2240 reactions and 1045 metabolites. The reactions were associated with 871 open-reading frames (ORFs), based on the CBS 513.88 genome annotation. Manual curation was applied in the construction process, and reactions were added to the network based on literature evidence from 371 articles. To establish connectivity of the network, some reactions were added based on gap-filling and inference. The network was compartmentalised into extracellular, cytosolic, and mitochondrial compartments. The metabolic model incorporated energetic parameters, including non-growth associated maintenance (NGAM) set to 1.9 mmol ATP gDW^{-1} h^{-1}, and growth-associated maintenance (GAM) set to 61 mmol ATP gDW^{-1}. The equation for biomass was more extensive than in a previous stoichiometric model of *A. niger* (David *et al*, 2003), and was based on empirical data of *A. niger* biomass composition, however, was not specific to citric acid producing conditions. iMA871 includes 115 carbon sources and 23 nitrogen sources. Among the carbon sources, 49 are known and 66 are hypothetical. 16 of the nitrogen sources are reported in the literature. Although iMA871 was primarily based on the CBS 513.88 genome annotation, gene-protein-reaction (GPR) associations were also included for the ATCC1015 strain. The ATCC1015 genome was first sequenced in 2006 by the Joint Genome Institute (JGI) (Baker, 2006). The ATCC1015 GPR associations were mapped from CBS 513.88. Therefore, it can not be said that iMA871 truly reflects the ATCC1015 genome, as ATCC1015 genes without a match in CBS 513.88 would not be included.

The iMA871 model was subsequently expanded to provide predictions on organic acid production (Andersen *et al*, 2009b). The objective function was set to proton production, based on the hypothesis that *A. niger* is evolutionarily optimised to efficiently acidify the environment in response to the ambient pH. Acid-dissociation reactions were added to the model for seven acids (oxalic, citric, gluconic, malic, lactic, acetic, and succinic). These reactions gave the number of protons released by a particular acid at a particular ambient pH value, based on acid-dissociation constants. The model was used to give static predictions on organic acid production in response to extracellular pH. The model predicted oxalic acid production in a broad pH range, followed by citric at low pH. Citric acid was only produced at low pH when oxalic was disallowed, suggesting an unknown factor not captured by the model. Physiologically, oxalic acid production is absent at low pH. Although the production of gluconic acid is observed in *A. niger* organic acid fermentations, it was not predicted by the model. This suggested that gluconic acid production is an inefficient means of acidification, and therefore uncoupled from the proton production response. Instead, gluconic acid may be produced as a means of quickly sequestering glucose. The modelling predictions gave further evidence to the hypothesis that *A. niger* deliberately produces organic acids to efficiently acidify its surroundings.

Very recently, a new GSMM of *A. niger*, iHL1210, was published (Lu *et al*, 2017). In the updated GSMM, the number of unique reactions increased from 1380 to 1764, and the number of unique metabolites from 775 to 902. The number of unique ORFs increased from 871 to 1210. The improved GPR associations corresponded to the CBS 513.88 strain. The iHL1210 model included the peroxisome compartment, absent in iMA871. The biomass equation was also expanded, providing greater coverage of the *A. niger* biomass composition. Cofactors were included, and the intracellular metabolite pool was expanded to include free amino acids. In terms of energetic parameters, the value for GAM was the same as iMA871, and the value for NGAM was changed to 3.73 mmol ATP gDW^{-1} h^{-1}. It was found that

reactions in iMA871 had mass and charge imbalances, and these were corrected in iHL1210. The new model was validated with reference to a range of physiological data, including 13C metabolic flux analysis and transcriptomics.

Since previous *A. niger* GSMMs were based on the genome annotation of the enzyme-producing CBS 513.88 strain, the work in this thesis aimed to construct an ATCC1015-specific GSMM of *A. niger*. The new model, iDU1757, is more relevant to studies on organic acid production. The GPR associations are more exhaustive and specific to ATCC1015, and therefore more reliably inform targeted engineering strategies. The iDU1757 model incorporates the proton production response that was previously added to iMA871 (Andersen *et al*, 2009b). In addition, it is an updated model, and includes new reactions based on literature evidence. These add new carbon and nitrogen sources to the model. In previous GSMMs of *A. niger*, the biomass equation did not reflect citric acid producing conditions. Biomass parameters were determined based on generic empirical data of *A. niger* biomass composition. The biomass equation in iDU1757 is modified in line with empirical data from organic acid fermentation. The refined model gives more accurate growth predictions under the conditions routinely used in these fermentations.

1.6.3 Dynamic flux balance analysis

Previous stoichiometric metabolic modelling of *A. niger* used FBA that is limited to static predictions. Although these have value, *A. niger* fermentation is a dynamic process, particularly in the industrial setting where batch or fed-batch cultivations are used. To capture the dynamic fermentative behaviour, dynamic modelling is required. FBA can be expanded to dynamic FBA (dFBA), as was demonstrated in modelling of the diauxic growth of *E. coli* (Mahadevan *et al*, 2002). Kinetic information can be incorporated into dFBA, to describe changes in flux constraints in response to a changing environment. This approach enables the model to capture dynamic physiological characteristics, and to give time-course simulations of

fermentation. In this project, dFBA was employed for the first time in dynamic modelling of *A. niger* organic acid fermentation. A setup was designed to reflect observed physiological behaviour, and the dynamic model was calibrated and validated with reference to empirical data. The proton production response previously used to give static predictions was modelled in a dynamic manner. Acid-dissociation reactions are dynamic, dependent on the ambient pH. As acids are produced, the ambient pH falls. Therefore, dynamic modelling is especially important in predictions of organic acid production given a changing extracellular pH. The model gave accurate descriptions of organic acid fermentative time series in response to different environmental and genetic backgrounds.

1.7 Aims of this Thesis

The primary goal of this thesis was to develop an *in silico* guided metabolic engineering platform for *A. niger* organic acid fermentation. This was driven by the known potential of the industrial organism *A. niger*, and the need to switch to more efficient strain development techniques to realise this potential. The project began by establishing experimental procedures to obtain high quality empirical data on *A. niger* organic acid fermentative time series. The output of this was used to design, calibrate, and validate a dynamic model, with the aim of capturing observed physiological behaviour in computer simulations. The developed model was used as a predictive platform to suggest targets for engineering. The *A. niger* engineering tool-kit was explored, and procedures were established for use in this project. These enabled the creation of strains with targeted changes in gene expression. Engineered strains were characterised in fermentation experiments to test model predictions and make further refinements. The next aim was to update the *A. niger* metabolic network and its gene-protein-reaction associations, and to make these specific to the parent citric acid producing ATCC1015 strain. The final aim was to design and develop an *in silico* evolution algorithm, to predict combinations of targets that optimise productivity of a given organic acid.

Chapter 2: Characterising *Aspergillus niger* ATCC1015 organic acid fermentation

2.1 Introduction

Organic acid fermentation by *A. niger* has been the subject of much scientific and industrial study. The variable experimental conditions across different studies – the strain used, the media composition, and the fermentation setup – make it difficult to draw comparisons and cause conflicting observations. It was necessary to establish a uniform empirical system in this project as a source of accurate and reliable data for calibrating and testing models. The system was also applied to further develop an understanding of the physiological characteristics of *A. niger* fermentation in response to varying conditions, and to characterise engineered strains.

The work in this chapter was centred on the ATCC1015 strain, as this is the naturally evolved parent citric acid producing strain for which the genome is sequenced. The use of systems biology tools to predict targets for engineering is dependent on genomic information, and so it was important to develop a model based on empirical data obtained using the sequenced ATCC1015 strain. It is known that significant genetic variation occurs between different strains of *A. niger* (Andersen *et al*, 2011), and therefore it is bad practice to assume that data from one strain can be applied to a model based on another. An additional reason for using the ATCC1015 strain in this work is that industrial citric acid producing strains were developed from this strain over many decades of mutagenesis procedures. The drive behind the development of computational techniques is initiated by the goal to replace these time-consuming methods with *in silico* guided rational engineering. To demonstrate the power of these newly emerging strategies and draw comparisons with traditional methods, it is necessary to use the same starting point.

A system was developed in this work to obtain empirical time-course fermentation data from shake flask cultures. Experiments using submerged cultures are performed in shake flasks or small-scale bioreactors. Although the use of bioreactors is more closely related to an industrial setting, the cost and expertise required limit the experimental scope. Therefore, shake flasks were used, which allowed testing of multiple conditions in parallel and with sufficient biological replication. An efficient experimental system was established that avoided the need for destructive sampling, while providing high quality data. This allowed fermentation of the same cultures to be monitored over time, minimising experimental error and variation in data obtained.

Despite extensive study into the characteristics of *A. niger* organic acid fermentation and the conditions required, there remains debate about the cause of the acidogenic behaviour. Some researchers have argued the need for phosphate-limiting conditions, while others have reported citric acid production with excess phosphate and limiting trace metals (Shu and Johnson, 1948). Manganese deficiency is regarded as a necessity (Kubicek and Röhr, 1977; Mirminachi *et al*, 2002), however, its effect is absent in mutant strains grown at higher initial pH (Ruijter *et al*, 1999). The timing of citric acid production is established (Roehr *et al*, 1981), but the triggering events are poorly described. The work performed in this chapter was mainly aimed at acquiring a better understanding of the role of phosphate in citric acid fermentation, and also looked at the effect of varying carbon uptake rate by changing the substrate used. The effect of initial pH was also examined, and the roles of oxalic and gluconic acid production were explored. Time series of changes in external phosphate concentration were obtained, characterising phosphate uptake and also revealing phosphate release in response to certain conditions. Phosphate storage by *A. niger* was also investigated. The work revealed new findings, more accurately describing the physiological characteristics of organic acid fermentation that laid the foundation for designing a dynamic model.

2.1.1 Aims of this Chapter

The work described in this chapter aimed to develop an empirical system for obtaining high quality data on organic acid fermentative time series, and to gain a deeper understanding of the physiological characteristics of *A. niger* fermentation in response to varying conditions.

2.2 Methods

2.2.1 Time-course shake flask experiments

Fermentative time series were obtained from shake flask experiments. The parent citric acid producing ATCC1015 strain was used, unless indicated otherwise. The ATCC1015 strain was obtained from American Type Culture Collection (ATCC; LGC Standards). 250 ml DeLong neck baffled shake flasks (Bellco Glass Inc.) were used with a working volume of 30 ml. Before use, flasks were siliconized with 2% (v/v) dimethyldichlorosilane. Cultures were grown in the following medium (personal communication with Citration Technology Ltd), unless described otherwise: glucose (160 g/L; 888 mM) (Fisher Scientific), urea (3.6 g/L; 59.9 mM), $(NH_4)_2SO_4$ (0.52 g/L; 3.94 mM), K_2HPO_4 (0.5 g/L; 2.9 mM), $CaCO_3$ (0.03125 g/L; 0.31223 mM), $MgSO_4.7H_2O$ (0.275 g/L; 1.116 mM), $ZnSO_4.7H_2O$ (0.00225 g/L; 0.00782 mM), $FeSO_4.7H_2O$ (0.0095 g/L; 0.0342 mM), $CuSO_4.5H_2O$ (0.0117 g/L; 0.0469 mM), $MnCl_2.(H_2O)_4$ (0.0000108 g/L; 0.0000546 mM), citric acid monohydrate (3.3 g/L; 15.7 mM), and Tween 80 (0.0094%) (Table 2.1). The concentration of manganese in the medium was determined as 7 ppb by ion-coupled plasma mass spectrometry (ICP-MS) (Biorenewables Development Centre). For experiments using alternative carbon sources, glucose was substituted for either D-xylose (160 g/L; 1066 mM) (Acros Organics), L-arabinose (160 g/L; 1066 mM) (Acros Organics), glycerol (160 g/L; 1737 mM) (Fisher Scientific), sucrose (160 g/L; 467 mM) (Fisher Scientific), or cellobiose (160 g/L; 467 mM) (Sigma). The medium was sterilised by autoclaving at 121°C for 15 minutes. The pH of the medium was adjusted to 2.0 after autoclaving by addition of sterile 2 M H_2SO_4. For experiments starting at pH 7, the pH of the medium was confirmed to be 7 after autoclaving and did not need to be adjusted. Glucose was prepared separately and filter sterilised (0.22 µm). Cultures were inoculated with 1×10^6 spores/ml, by adding 1 ml 3×10^7 spores/ml to 30 ml medium. Spores were harvested from potato dextrose agar (PDA) slants incubated at 37°C for 2 days, by gently shaking in 2 ml saline Tween (0.1% Tween 80, 9 g/L NaCl). Spores were washed three

times in saline Tween, and counted using an Improved Neubauer haemocytometer (Hawksley). Freeze-dried spores or spores frozen on Microbank™ beads (Pro-Lab Diagnostics) were used to inoculate PDA slants. Cultures were incubated at 30°C with shaking at 250 rpm. 500 µl samples were taken at 24 hour intervals for measurements of biomass dry weight and external metabolites, and added to 1.5 ml Eppendorf tubes. Samples were taken using a 1.25 ml sterile pipette tip with the tapered end cut off. Cultures were manually shaken while taking samples to ensure homogeneity. Samples were centrifuged at 9000×g for 5 minutes in a microfuge. 105 µl culture supernatant was transferred to a 1.5 ml Eppendorf tube. After vortexing, 5 µl of this was transferred to another tube and diluted 1:200 in dH_2O. Sample dilutions were vortexed, and all samples of culture supernatant were frozen at −20°C.

Table 2.1. Media composition for fermentation experiments.

Component	**Concentration (g/L)**	**Concentration (mM)**
Glucose	160	888
Urea	3.6	59.9
$(NH_4)_2SO_4$	0.52	3.94
K_2HPO_4	0.5	2.9
$CaCO_3$	0.03125	0.31223
$MgSO_4.7H_2O$	0.275	1.116
$ZnSO_4.7H_2O$	0.00225	0.00782
$FeSO_4.7H_2O$	0.0095	0.0342
$CuSO_4.5H_2O$	0.0117	0.0469
$MnCl_2.(H_2O)_4$	0.0000108	0.0000546
citric acid monohydrate	3.3	15.7
Tween 80	0.0094% (v/v)	-

2.2.2 Biomass dry weight analysis

Biomass dry weight was determined by washing biomass in dH_2O, and drying at 70°C with weighing at 24 hour intervals until constant weight. All weighing was performed on a Mettler AE 163 balance (Mettler Toledo) with accuracy to 0.00001 g. 500 µl samples were collected in pre-dried, pre-weighed 1.5 ml Eppendorf tubes, as previously described (section 2.2.1). Tubes were pre-dried at 70°C with lids open for 24 hours. Biomass was washed by adding 1 ml dH_2O, centrifuging at 9000×g for 5 minutes in a microfuge and then removing the supernatant. The wash step was repeated four times, which was sufficient to ensure complete removal of dissolved matter. Biomass dry weight was calculated by subtracting the empty weight. This gave a value per 500 µl, and was multiplied by 2000 to give a value per litre.

The method gave accurate and precise data if the culture morphology was filamentous or pelleted (small pellets < 1 mm diameter).

2.2.3 Metabolite analysis

Sample dilutions of culture supernatant stored at −20°C were thawed, and vortexed prior to metabolite analysis. Various commercial assay kits were used to measure metabolites of interest, as described below.

2.2.3.1 D-Glucose assay

Glucose was measured by the glucose oxidase-peroxidase method (specific for D-glucose) using an enzymatic assay kit (K-GLUC, Megazyme), with reference to the manufacturer's instructions. The assay works as follows: Glucose oxidase catalyses the reaction of D-glucose with oxygen and water to form D-gluconate and hydrogen peroxide. Peroxidase catalyses the reaction of hydrogen peroxide with *p*-hydroxybenzoic acid and 4-aminoantipyrine to form quinoneimine dye. The quinoneimine dye is measured spectrophotomically. The assay was performed in a 96-well optical

plate. 150 µl glucose determination reagent (GOPOD reagent) was added to wells. 5 µl 1:200 sample dilution was then added. The reaction was incubated at 37°C for 20 minutes. Absorbance was measured at 492 nm using a Sunrise™ plate reader (Tecan). Glucose concentration was calculated with reference to standards.

2.2.3.2 Phosphate assay

Phosphate was measured by the malachite green-ammonium molybdate method using an assay kit (ab65622, Abcam), with reference to the manufacturer's instructions. The assay works as follows: Malachite green and ammonium molybdate form a chromogenic complex with phosphate which is measured spectrophotomically. The assay was performed in a 96-well optical plate. 85 µl 1:200 sample dilution was added to wells. 15 µl phosphate reagent was then added. The reaction was incubated at room temperature for 30 minutes. Absorbance was measured at 650 nm using a Sunrise™ plate reader (Tecan). Phosphate concentration was calculated with reference to a standard curve.

2.2.3.3 Citric acid assay

Citric acid was measured by the citrate lyase method (specific for citric acid) using an assay kit (K-CITR, Megazyme), with reference to the manufacturer's instructions. The assay works as follows: Citrate lyase converts citrate into oxaloacetate and acetate. L-malate dehydrogenase converts oxaloacetate and NADH into L-malate and NAD. NADH consumption is measured by the decrease in absorbance at 340 nm. As oxaloacetate is converted to pyruvate in the presence of oxaloacetate decarboxylase, D-lactate dehydrogenase is also included in the assay to convert pyruvate and NADH into D-lactate and NAD. The assay was performed in a 96-well optical plate. A master mix was prepared containing 71 µl dH_2O, 25 µl solution 1 (buffer), 10 µl solution 2 (NADH) and 1 µl suspension 3 (L-malate dehydrogenase/D-lactate dehydrogenase) per well. 107 µl master mix was added to wells. 10 µl 1:200 sample dilution was then

added. Absorbance was measured at 340 nm using a BMG Polarstar plate reader (BMG Labtech). After addition of 20 µl 1:20 dilution suspension 4 (citrate lyase), the reaction was incubated at room temperature for 20 minutes. The absorbance at 340 nm was measured again at the end of the reaction, and the citric acid concentration was calculated by the decrease in absorbance with reference to standards.

2.2.3.4 Oxalic acid assay

Oxalic acid was measured by the oxalate oxidase method (specific for oxalic acid) using an assay kit (Oxalate-100, Libios), with reference to the manufacturer's instructions. The assay works as follows: Oxalate oxidase catalyses the reaction of oxalate with oxygen to form hydrogen peroxide and carbon dioxide. In the presence of peroxidase, hydrogen peroxide reacts with 3-(dimethylamino)-benzoic acid (DMAB) and 3-methyl-2-benzothiazolinone hydrazine (MBTH) to form a coloured compound which is measured spectrophotomically. The assay was performed in a 96-well optical plate. A master mix was prepared containing 50 µl reagent 1 (DMAB) and 50 µl reagent 2 (MBTH) per well. 100 µl master mix was added to wells. 5 µl 1:50 sample dilution was then added. 10 µl reagent 3 (oxalate oxidase/peroxidase) was added last. The reaction was incubated at room temperature for 10 minutes. Absorbance was measured at 595 nm using a Sunrise™ plate reader (Tecan). Oxalic acid concentration was calculated with reference to standards.

2.2.3.5 D-Gluconic acid assay

Gluconic acid was measured by the gluconate kinase method (specific for D-gluconic acid) using an assay kit (K-GATE, Megazyme), with reference to the manufacturer's instructions. The assay works as follows: Gluconate kinase catalyses the reaction of D-gluconate with ATP to form D-gluconate-6-phosphate and ADP. 6-phosphogluconate dehydrogenase converts D-gluconate-6-phosphate and NADP to ribulose-5-phosphate, NADPH and carbon dioxide. The formation of NADPH is measured by the increase in

absorbance at 340 nm. The assay was performed in a 96-well optical plate. A master mix was prepared containing 81 µl dH_2O, 10 µl solution 1 (buffer), 10 µl solution 2 (NADP/ATP) and 1 µl suspension 3 (6-phosphogluconate dehydrogenase) per well. 102 µl master mix was added to wells. 5 µl 1:200 sample dilution was then added. Absorbance was measured at 340 nm using a BMG Polarstar plate reader (BMG Labtech). After addition of 20 µl 1:20 dilution suspension 4 (gluconate kinase), the reaction was incubated at room temperature for 10 minutes. The absorbance at 340 nm was measured again at the end of the reaction, and the gluconic acid concentration was calculated by the increase in absorbance with reference to standards.

2.2.3.6 D-Xylose assay

Xylose was measured by the xylose dehydrogenase method (specific for D-xylose) using an assay kit (K-XYLOSE, Megazyme), with reference to the manufacturer's instructions. The assay works as follows: Xylose mutarotase converts α-D-xylose to β-D-xylose. β-xylose dehydrogenase converts β-D-xylose and NAD to D-xylonic acid and NADH. The formation of NADH is measured by the increase in absorbance at 340 nm. As D-glucose interferes with β-xylose dehydrogenase, hexokinase and ATP are also included in the assay to convert D-glucose into D-glucose-6-phosphate. The assay was performed in a 96-well optical plate. A master mix was prepared containing 77.5 µl dH_2O, 20 µl solution 1 (buffer), 20 µl solution 2 (NAD/ATP) and 1 µl suspension 3 (hexokinase) per well. 118.5 µl master mix was added to wells. 5 µl 1:200 sample dilution was then added. Absorbance was measured at 340 nm using a BMG Polarstar plate reader (BMG Labtech). After addition of 25 µl 1:10 dilution solution 4 (β-xylose dehydrogenase/xylose mutarotase), the reaction was incubated at room temperature for 10 minutes. The absorbance at 340 nm was measured again at the end of the reaction, and the xylose concentration was calculated by the increase in absorbance with reference to standards.

2.2.3.7 L-Arabinose assay

Arabinose was measured by the galactose dehydrogenase method (specific for L-arabinose and D-galactose) using an assay kit (K-ARGA, Megazyme), with reference to the manufacturer's instructions. The assay works as follows: Galactose mutarotase converts α-L-arabinose to β-L-arabinose. β-galactose dehydrogenase converts β-L-arabinose and NAD to L-arabinonic acid and NADH. The formation of NADH is measured by the increase in absorbance at 340 nm. The assay was performed in a 96-well optical plate. A master mix was prepared containing 81 µl dH_2O, 10 µl solution 1 (buffer), and 5 µl solution 2 (NAD) per well. 96 µl master mix was added to wells. 5 µl 1:200 sample dilution was then added. Absorbance was measured at 340 nm using a BMG Polarstar plate reader (BMG Labtech). After addition of 20 µl 1:20 dilution suspension 3 (β-galactose dehydrogenase/galactose mutarotase), the reaction was incubated at room temperature for 10 minutes. The absorbance at 340 nm was measured again at the end of the reaction, and the arabinose concentration was calculated by the increase in absorbance with reference to standards.

2.2.3.8 Glycerol assay

Glycerol was measured by the glycerokinase method (specific for glycerol) using an assay kit (K-GCROLGK, Megazyme), with reference to the manufacturer's instructions. The assay works as follows: Glycerokinase converts glycerol and ATP to L-glycerol-3-phosphate and ADP. ADP-glucokinase converts ADP and D-glucose to glucose-6-phosphate and AMP. Glucose-6-phosphate dehydrogenase converts glucose-6-phosphate and NAD to 6-phosphogluconate and NADH. The formation of NADH is measured by the increase in absorbance at 340 nm. The assay was performed in a 96-well optical plate. A master mix was prepared containing 56 µl dH_2O, 10 µl solution 1 (buffer), 10 µl solution 2 (NAD/ATP/D-glucose) and 1 µl suspension 3 (ADP-glucokinase/glucose-6-phosphate dehydrogenase) per well. 77 µl master mix was added to wells. 5 µl 1:500 sample dilution was then added. Absorbance was measured at 340 nm using

a BMG Polarstar plate reader (BMG Labtech). After addition of 20 µl 1:20 dilution suspension 4 (glycerokinase), the reaction was incubated at room temperature for 10 minutes. The absorbance at 340 nm was measured again at the end of the reaction, and the glycerol concentration was calculated by the increase in absorbance with reference to standards.

2.2.3.9 Cellobiose assay

Cellobiose was determined by measurement of glucose before and after hydrolysis with β-glucosidase. Hydrolysis reactions were performed in a volume of 10 µl, and contained 5 µl 1:200 sample dilution, 4 µl 0.1 M sodium acetate buffer (pH 4), and 1 µl β-glucosidase (E-BGLUC, Megazyme). The reactions were incubated at 37°C for 20 minutes. The 10 µl hydrolysis reactions were used directly in the glucose assay. Glucose was measured as previously described (see Methods section 2.2.3.1). The concentration of cellobiose (g/L) was calculated by subtracting the glucose concentration (g/L) in non-hydrolysed sample from the glucose concentration (g/L) in hydrolysed sample, and multiplying by 0.95. The multiplication factor was determined from the molecular weights of cellobiose and glucose. Values were normalised with reference to standards.

2.2.4 Polyphosphate analysis

The polyphosphate content of biomass samples from shake flask cultures was determined with reference to a previously reported method (Nishi, 1961).

Mycelia were harvested from 30 ml culture (one flask) per sample. To obtain sufficient biomass, one-day-old cultures required the pooling of four flasks, giving 120 ml culture per sample. Mycelia were harvested by filtration through a double layer of Miracloth (Calbiochem), and washed in 300 ml ice-cold 100 mM Tris.HCl (pH 7), followed by 600 ml ice-cold dH_2O. Washed mycelia were transferred to 15 ml Falcon tubes, flash frozen in liquid nitrogen, freeze dried, and stored at −80ºC. Freeze dried mycelia were

weighed out in 2 ml vials, approximately 50 mg per vial, using a Mettler AE 163 balance (Mettler Toledo). The exact amount of biomass added to each vial was recorded. Biomass was ground using the TissueLyser II (QIAGEN) at 30 Hz for 90 seconds three times. Each vial contained 2 beads. Powdered mycelia were lysed by incubation in 10% (w/v) lysing enzymes (from *Trichoderma harzianum*; Sigma) for 3 hours. The residue (containing polyphosphate, phospholipid, DNA and RNA) was retained and the supernatant (containing orthophosphate, sugar-phosphate and nucleotides) was discarded. To remove phospholipid content from the residue, samples were incubated successively in 100% ethanol, ethanol-ether (3:1), and methanol-chloroform (1:1), each for one hour. The supernatants (containing phospholipid) were discarded, and the residue (containing polyphosphate, DNA and RNA) was retained. To extract polyphosphate from the residue, samples were incubated three times in 600 µl 7.5 mM sodium tetraborate buffer (pH 9.0). The supernatants (containing polyphosphate) were retained and the remaining residue (containing DNA and RNA) was discarded. The polyphosphate extractions were pooled to give a volume of 1.8 ml, which was equally split between two new vials. The polyphosphate fractions were dried in a Savant SPD131DDA SpeedVac Concentrator (Thermo Fisher Scientific). All incubation steps were done at 30°C in a volume of 2 ml per vial, with shaking at 30 rpm, unless described otherwise. Samples were centrifuged between incubation steps at 13,000 rpm for 10 minutes at 4°C in a microfuge.

Polyphosphate was determined by measuring free phosphate with and without acid hydrolysis, using the previously described phosphate assay (see section 2.2.3.2). From each sample, one fraction was used in acid hydrolysis, and the other fraction was re-dissolved in 2 ml dH_2O. Acid hydrolysis was performed by boiling at 100°C in 2 ml 0.5 M H_2SO_4 for 3 hours. To determine if the hydrolysis reaction was complete, free phosphate was measured at 30 minute intervals during hydrolysis. The phosphate content of polyphosphate was calculated from the increase in phosphate with acid hydrolysis. The amount per gram biomass dry weight was calculated knowing the amount of biomass added to the vial. This was multiplied by the biomass dry weight

(g/L) of the corresponding culture, to determine the phosphate content of polyphosphate as grams per litre of culture.

2.3 Results

2.3.1 Citric acid fermentation with glucose as substrate

To characterise citric acid fermentation by the ATCC1015 strain with glucose as substrate, a fermentation experiment was performed at initial pH 2. The experiment was started at pH 2 to prevent production of oxalic and gluconic acid. These competing acids were not detected in the culture at any time-point under these conditions. Time series were obtained for biomass, phosphate, citric acid, and glucose (Figure 2.1).

Biomass data revealed a biphasic growth behaviour, with a growth shift occurring at day 3. Citric acid production commenced after day 2, and was synchronous with the second growth phase. Up to 60 g/L (312 mM) citric acid was produced. Glucose was consumed by day 6, after which production of biomass and citric acid ceased.

To further investigate the growth behaviour and potential cause of the growth shift, data on phosphate depletion were obtained. These revealed a rapid phosphate uptake, with phosphate depleted by day 2. This finding suggested that exhaustion of phosphate may trigger the growth shift, and production of citric acid. The continuation of growth in the absence of external phosphate revealed a phosphate storage mechanism, and a switch in phosphate source from external to internal stored phosphate. From these findings, a switch to a phosphate-limited growth phase was hypothesised in this work.

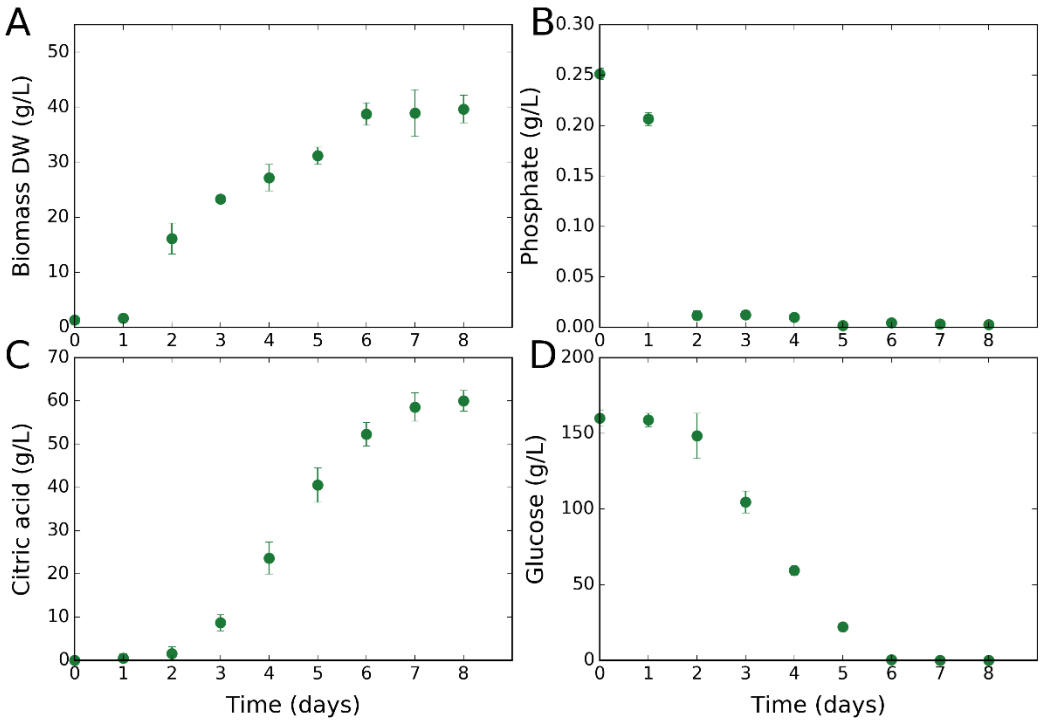

Figure 2.1. Citric acid fermentation with glucose as substrate. The ATCC1015 strain was characterised in a time-course fermentation experiment at initial pH 2 with glucose as substrate. Each data-point is the mean average of four biological replicates and error bars represent standard deviation. Citric acid data are normalised to reflect the amount produced (subtracting the zero-point – some citric acid was initially present in the media). **(A)** Change in biomass dry weight (g/L) over time. **(B)** Change in external phosphate concentration (g/L) over time. **(C)** Change in external citric acid concentration (g/L) over time. **(D)** Change in external glucose concentration (g/L) over time.

2.3.2 Effect of phosphate on citric acid fermentation

To further investigate the hypothesised phosphate-limited growth phase, the initial amount of phosphate was varied. Three different phosphate levels were tested (in g/L: 0.05, 0.09, and 0.17; in mM: 0.53, 0.95, and 1.79), and time series were obtained for biomass, phosphate, citric acid and glucose (Figure 2.2).

Growth rate increased with increasing phosphate, yet phosphate was depleted by day 1 to day 2 in all conditions. Therefore, the effect on growth rate was due to differences in the rate of release of stored phosphate, confirming that growth enters a phosphate-limited phase. In higher phosphate cultures, more phosphate was stored, leading to an increased rate of release of stored phosphate, and a higher growth rate. The initial amount of phosphate determined the growth rate during the phosphate-limited growth phase, and the timing of the growth shift.

Citric acid production was highest in the culture with most phosphate, producing around 50 g/L (260 mM) by day 6. The lower phosphate cultures produced less biomass, and had a slower glucose uptake, explaining the reduced citric acid production. Citric acid was produced after day 2, during phosphate-limited growth.

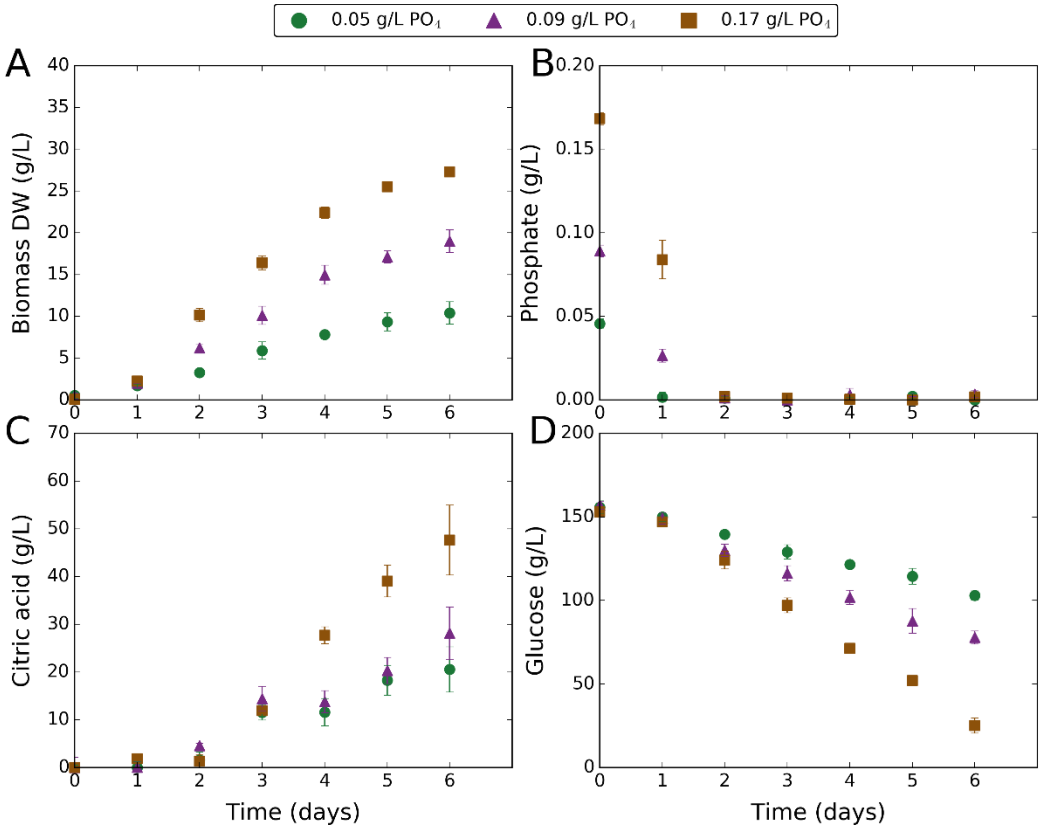

Figure 2.2. Response of citric acid fermentation to varying phosphate. Citric acid fermentation was tested at three different phosphate levels in a time-course fermentation experiment at initial pH 2 with glucose as substrate. Green circles correspond to 0.05 g/L phosphate. Purple triangles correspond to 0.09 g/L phosphate. Brown squares correspond to 0.17 g/L phosphate. Each data-point is the mean average of four biological replicates and error bars represent standard deviation. Citric acid data are normalised to reflect the amount produced (subtracting the zero-point – some citric acid was initially present in the media). **(A)** Change in biomass dry weight (g/L) over time. **(B)** Change in external phosphate concentration (g/L) over time. **(C)** Change in external citric acid concentration (g/L) over time. **(D)** Change in external glucose concentration (g/L) over time.

From the findings so far, it was expected that provision of excessive phosphate would prevent occurrence of phosphate-limited growth. The observed synchrony of citric acid production with phosphate-limited growth suggested a possible causal link. Therefore, it was predicted that citric acid would not be produced in the absence of phosphate-limited growth under conditions of excessive phosphate. To test this hypothesis, a fermentation experiment was performed at a very high phosphate level (4.5 g/L; 47.38 mM), generating time series for biomass, phosphate, citric acid, and glucose (Figure 2.3).

A significant drop in growth rate was observed at day 3, despite the presence of excessive phosphate. Citric acid production commenced at the point of this growth shift, and up to 50 g/L was produced by day 6. Although this appeared to negate the hypothesis, it was observed that phosphate uptake stopped between day 3 and 4. This seemed to coincide with the growth shift, suggesting a switch to phosphate-limited growth. It is suspected that phosphate storage reached a saturation point, causing phosphate uptake to stop in order to prevent deleterious accumulation of free intracellular phosphate. Growth subsequently became phosphate-limited, constrained by a very slow rate of release of stored phosphate. By day 5, growth stopped, yet citric acid production continued, showing that citric acid can be produced in the absence of growth.

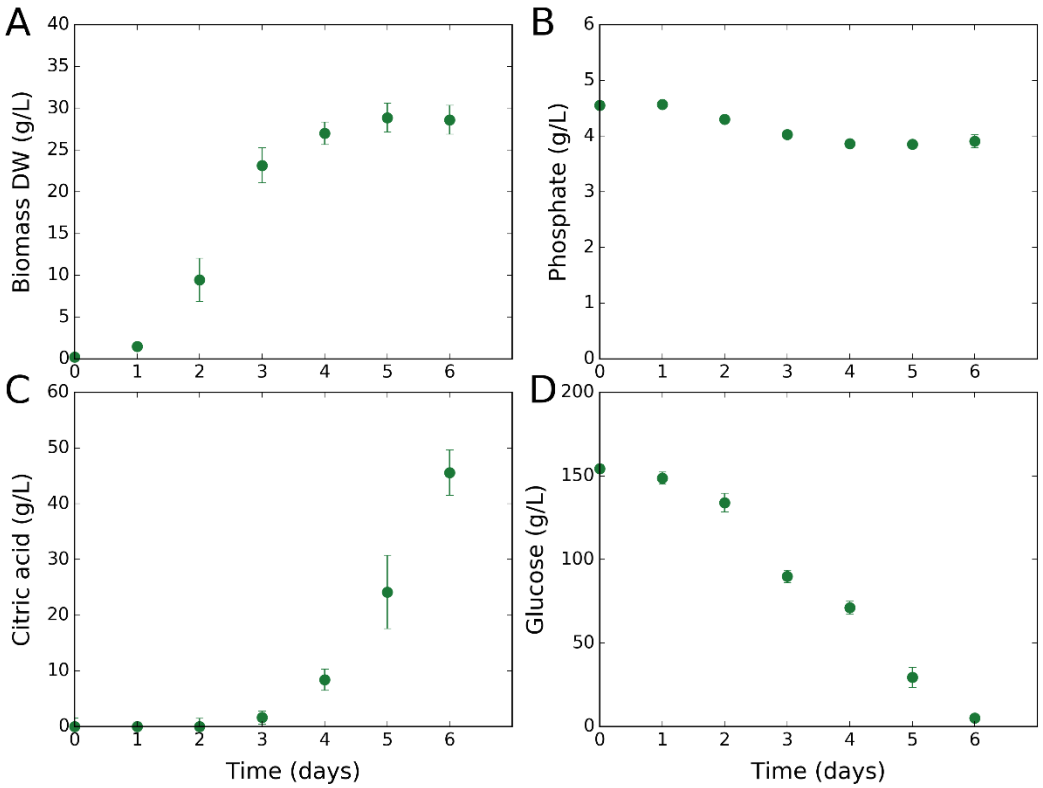

Figure 2.3. Response of citric acid fermentation to excessive phosphate. Citric acid fermentation was tested at a very high phosphate level (4.5 g/L) in a time-course fermentation experiment at initial pH 2 with glucose as substrate. Each data-point is the mean average of four biological replicates and error bars represent standard deviation. Citric acid data are normalised to reflect the amount produced (subtracting the zero-point – some citric acid was initially present in the media). **(A)** Change in biomass dry weight (g/L) over time. **(B)** Change in external phosphate concentration (g/L) over time. **(C)** Change in external citric acid concentration (g/L) over time. **(D)** Change in external glucose concentration (g/L) over time.

2.3.3 Polyphosphate levels during citric acid fermentation

It has been observed in this work that *A. niger* has a rapid phosphate uptake, and thereafter grows in the absence of external phosphate at a lower growth rate. Therefore, a phosphate storage mechanism must exist. It was hypothesised that this occurred via polyphosphate, following previous findings that reported the presence of polyphosphate in *A. niger* (Nishi, 1961). To confirm this hypothesis, biomass samples were taken at time-points during citric acid fermentation, and polyphosphate was extracted and quantified (see Methods section 2.2.4). The phosphate content of polyphosphate extractions was calculated, and a time series generated showing the change in polyphosphate levels during citric acid fermentation (Figure 2.4).

The level of polyphosphate was observed to rise early in fermentation, peaking at day 2 at the point of external phosphate depletion. Polyphosphate levels then dropped at a decreasing rate during phosphate-limited growth and citric acid production. These findings confirmed polyphosphate as the means of phosphate storage. The results gave a qualitative description of the changing polyphosphate levels, but were quantitatively underestimated. The amount of phosphate supplied in the medium was about 0.25 g/L (2.63 mM), yet the phosphate content of polyphosphate was only about 0.03 g/L (0.32 mM) at the highest level. The discrepancy may be due to incomplete extraction of the polyphosphate from biomass.

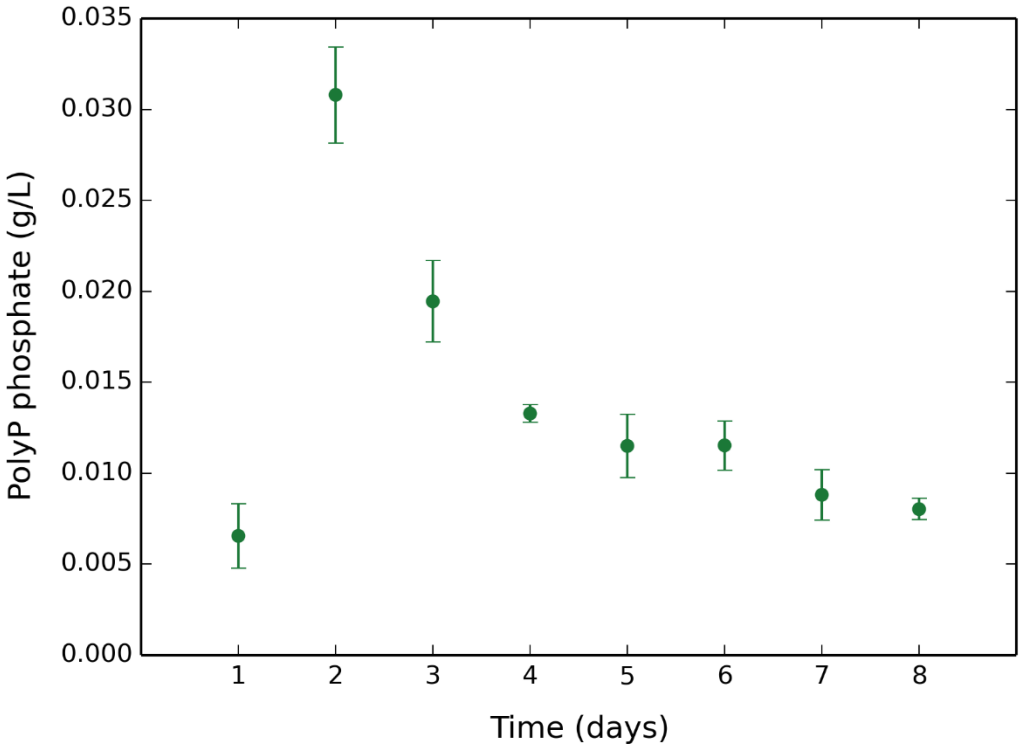

Figure 2.4. Polyphosphate levels during citric acid fermentation. Polyphosphate was extracted from biomass samples and quantified. The phosphate content of polyphosphate as grams per litre of culture was calculated. Each data-point is the mean average of three biological replicates and error bars represent standard deviation.

2.3.4 Effect of carbon source on citric acid fermentation

To investigate whether the physiological characteristics of citric acid fermentation on glucose occur with other substrates, a number of fermentation experiments were performed in this work to determine the fermentative response to different carbon sources. The same concentration of carbon source was used in each experiment (160 g/L).

The pentose sugars D-xylose and L-arabinose were chosen as they are abundant in the hemicellulose fraction of plant biomass, and known to be metabolised by *A. niger*.

When xylose was applied as substrate, the same behaviour was observed as for glucose, with no differences in growth or carbon source and phosphate uptake (Figure 2.5). The timing of citric acid production was also the same, commencing after phosphate depletion and synchronous with phosphate-limited growth. Although xylose uptake was similar to glucose, the citric acid produced was approximately 2-fold less in cultures grown on xylose. This suggests an additional limiting factor when xylose is used as substrate, and may result from metabolic constraints or observed morphological differences. Xylose cultures were more viscous and more abundant in pellets, which were smaller. The effect on aeration by the increased viscosity may account for differences in citric acid production.

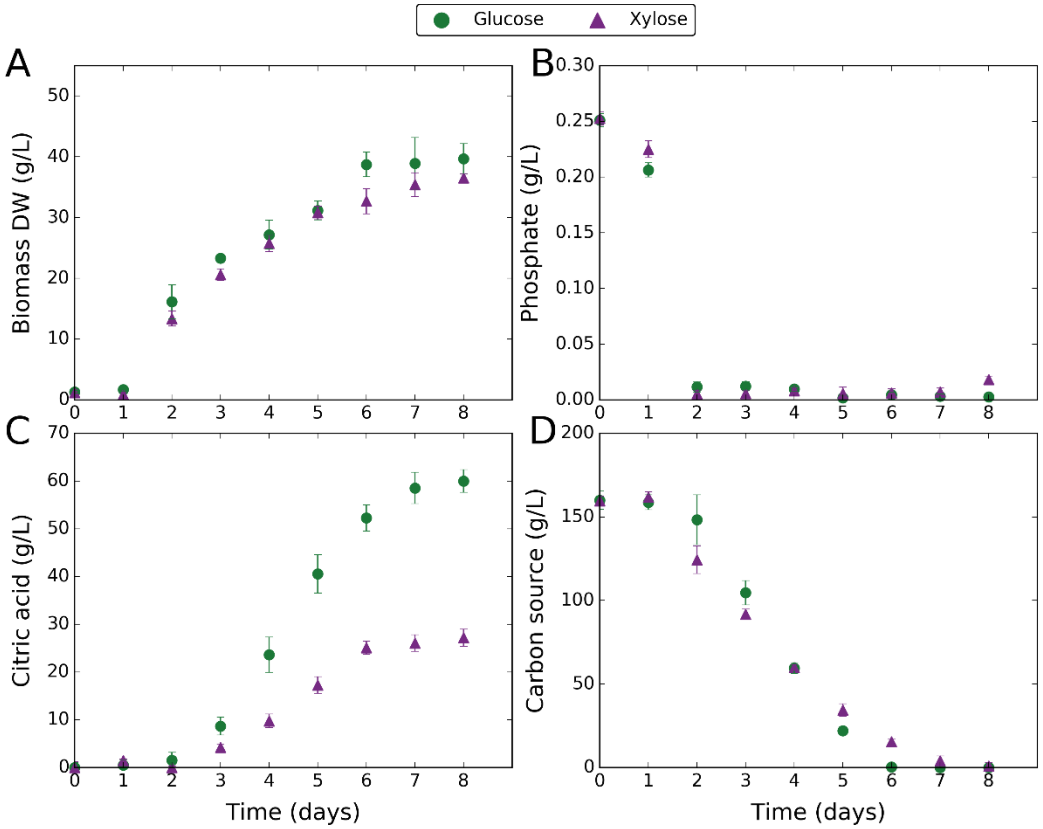

Figure 2.5. Response of citric acid fermentation to change in substrate to xylose. The effect on citric acid fermentation of changing substrate from glucose to xylose was determined in a time-course fermentation experiment. Green circles correspond to glucose as substrate. Purple triangles correspond to xylose as substrate. Each data-point is the mean average of four biological replicates and error bars represent standard deviation. Citric acid data are normalised to reflect the amount produced (subtracting the zero-point – some citric acid was initially present in the media). **(A)** Change in biomass dry weight (g/L) over time. **(B)** Change in external phosphate concentration (g/L) over time. **(C)** Change in external citric acid concentration (g/L) over time. **(D)** Change in external carbon source concentration (g/L) over time.

Fermentation on xylose was further probed in a mixed carbon source experiment, with a 1:1 mixture of glucose and xylose (Figure 2.6). In comparison to glucose as sole substrate, no differences were seen up to day 4, at which point glucose became depleted. Total carbon uptake was slightly higher until day 4, due to the combined uptake of glucose and xylose. This, however, did not lead to any increases in growth or citric acid production. Xylose was still utilised despite the presence of glucose, but at an uptake rate approximately 2-fold lower than with xylose alone. It is suspected that the decreased xylose uptake, which did not begin until after day 2, was caused by the presence of glucose. Beyond day 4, carbon uptake decreased, as did citric acid production. The final yield of citric acid was 80% of that achieved with glucose as the sole carbon source, but higher than with xylose alone. The morphological effects previously observed in xylose cultures did not occur in mixed glucose/xylose cultures.

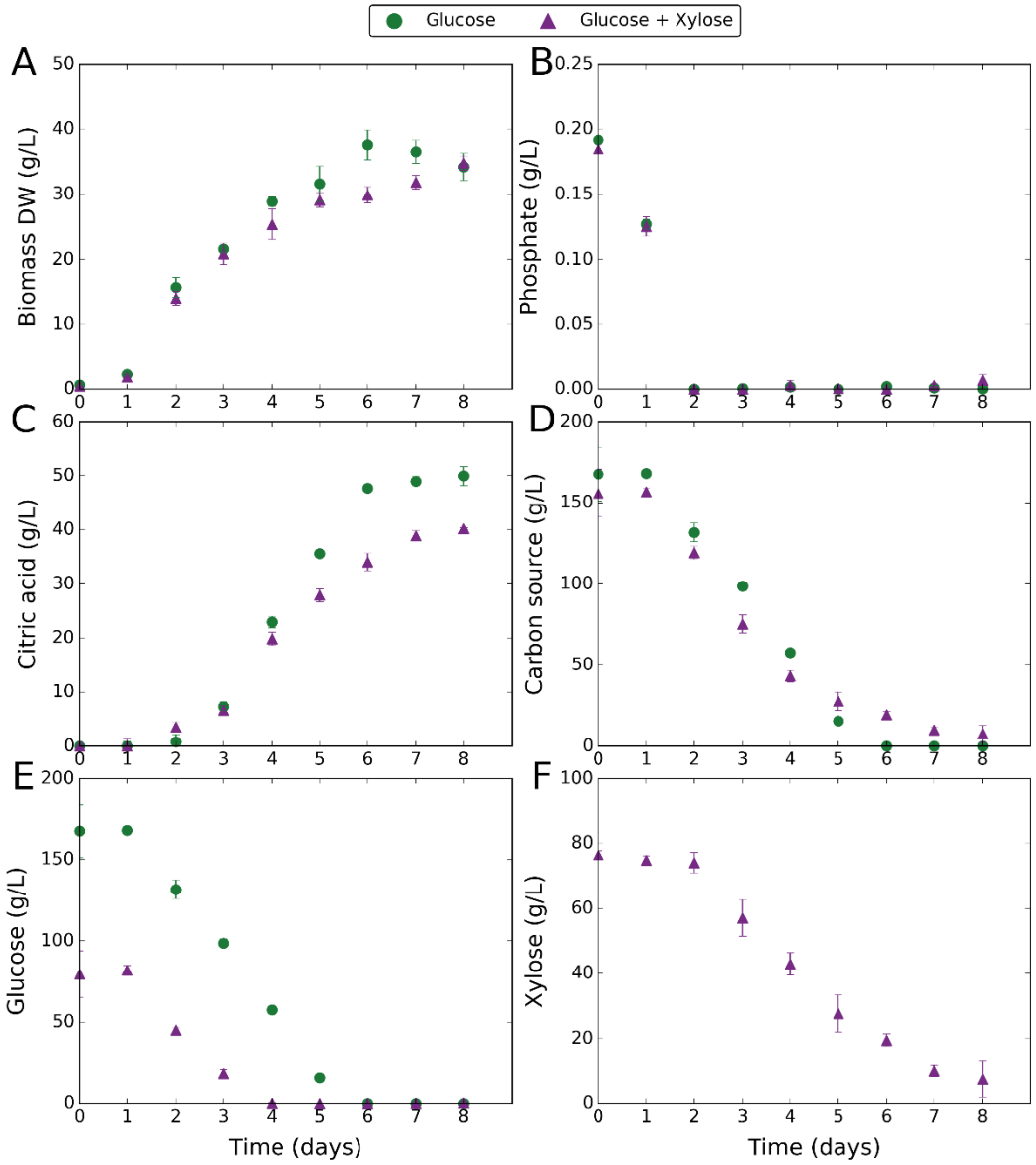

Figure 2.6. Response of citric acid fermentation to glucose/xylose mixture. The effect on citric acid fermentation of changing substrate from glucose to a 1:1 glucose/xylose mixture was determined in a time-course fermentation experiment. Green circles correspond to glucose as substrate. Purple triangles correspond to glucose/xylose as substrate. Each data-point is the mean average of four biological replicates and error bars represent standard deviation. Citric acid data are normalised to reflect the amount produced (subtracting the zero-point – some citric acid was initially present in the media). **(A)** Change in biomass dry weight (g/L) over time. **(B)** Change in external phosphate concentration (g/L) over time. **(C)** Change in external citric acid concentration (g/L) over time. **(D)** Change in external carbon source concentration (g/L) over time. **(E)** Change in external glucose concentration (g/L) over time. **(F)** Change in external xylose concentration (g/L) over time.

When arabinose was applied as substrate, some significant differences were observed (Figure 2.7). Growth was significantly reduced, and no citric acid was produced. The uptake of phosphate also appeared to be slowed down, not depleted until after day 2. These effects resulted from a very slow arabinose uptake, relative to glucose. It is suspected that growth was consistently limited by the rate of carbon uptake, and therefore citric acid was not produced as phosphate-limited growth did not occur. It is known that L-arabinose does not trigger germination of *A. niger* (Hayer *et al*, 2013), but in this experiment germination did occur. This is likely due to contamination of the source of L-arabinose (>99% purity) by traces of other sugars that do trigger germination, such as D-glucose.

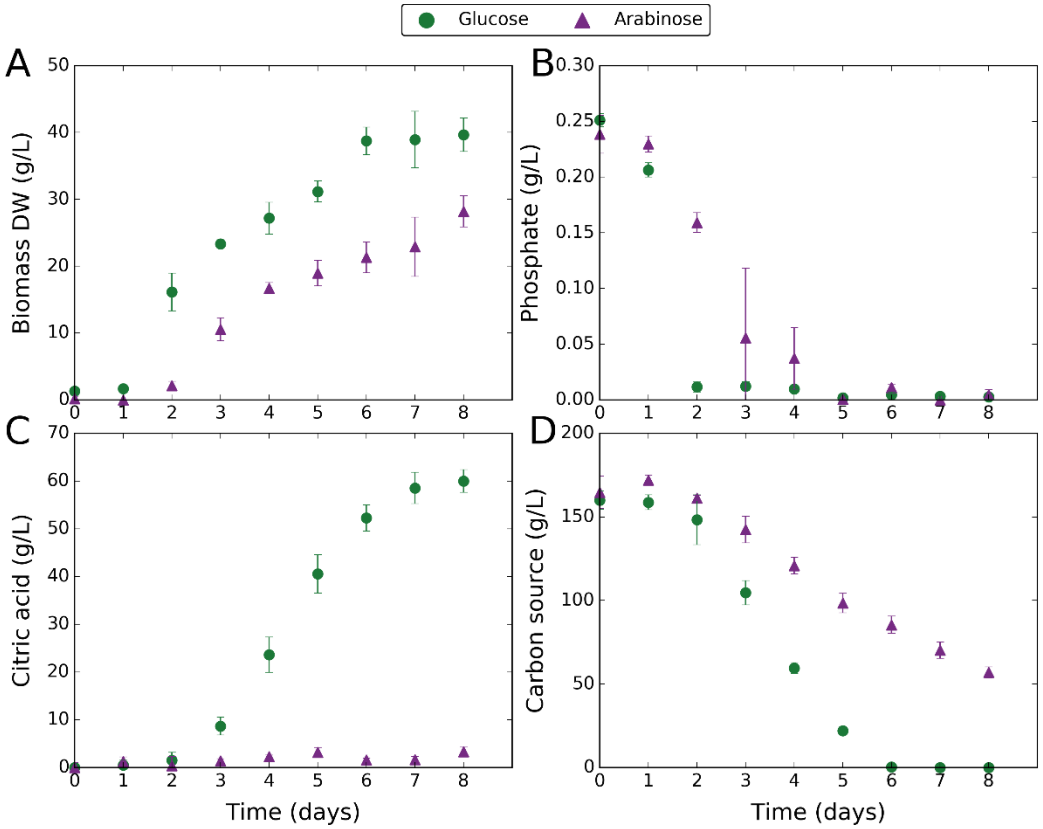

Figure 2.7. Response of citric acid fermentation to change in substrate to arabinose. The effect on citric acid fermentation of changing substrate from glucose to arabinose was determined in a time-course fermentation experiment. Green circles correspond to glucose as substrate. Purple triangles correspond to arabinose as substrate. Each data-point is the mean average of four biological replicates and error bars represent standard deviation. Citric acid data are normalised to reflect the amount produced (subtracting the zero-point – some citric acid was initially present in the media). **(A)** Change in biomass dry weight (g/L) over time. **(B)** Change in external phosphate concentration (g/L) over time. **(C)** Change in external citric acid concentration (g/L) over time. **(D)** Change in external carbon source concentration (g/L) over time.

As well as the pentose sugars xylose and arabinose, the polyol glycerol was tested as a substrate and the fermentative behaviour determined. Glycerol was chosen because it is a by-product of biodiesel production, and has growing biotechnological interest. The response to glycerol as carbon source was similar to arabinose, resulting from a very slow glycerol uptake relative to glucose (Figure 2.8). Glycerol cultures had reduced growth and produced no citric acid. Phosphate uptake was also slower, not depleted until day 3. As with arabinose, it is suspected that growth was persistently limited by the carbon uptake rate. Therefore, phosphate-limited growth was absent, which explains why citric acid production did not occur.

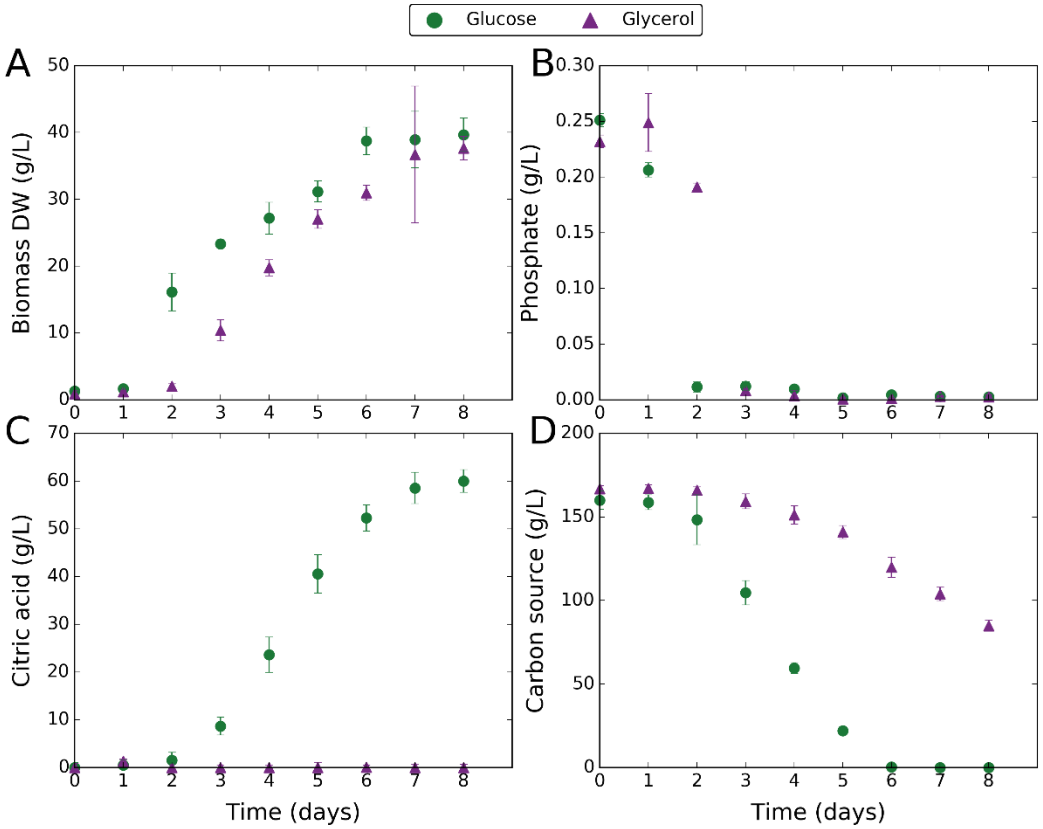

Figure 2.8. Response of citric acid fermentation to change in substrate to glycerol. The effect on citric acid fermentation of changing substrate from glucose to glycerol was determined in a time-course fermentation experiment. Green circles correspond to glucose as substrate. Purple triangles correspond to glycerol as substrate. Each data-point is the mean average of four biological replicates and error bars represent standard deviation. Citric acid data are normalised to reflect the amount produced (subtracting the zero-point – some citric acid was initially present in the media). **(A)** Change in biomass dry weight (g/L) over time. **(B)** Change in external phosphate concentration (g/L) over time. **(C)** Change in external citric acid concentration (g/L) over time. **(D)** Change in external carbon source concentration (g/L) over time.

To see whether fermentative performance is different on substrates other than monosaccharides, fermentation experiments were conducted on the disaccharides sucrose and cellobiose. Industrial citric acid production typically relies on sucrose-based feedstocks, and so it was important to test sucrose in the experimental system used in this work. Cellobiose was chosen based on knowledge that fungi possess the ability to take up cellobiose directly without the need for extracellular hydrolysis, potentially allowing a more efficient carbon uptake. The presence of cellobiose in resource streams from lignocellulosic plant biomass also made it worth exploring as a substrate for fermentation.

When sucrose was used as the carbon source, growth was similar to glucose cultures, however, citric acid yield was reduced at least 2-fold (Figure 2.9). Phosphate was depleted by day 2, and the timing of citric acid production was the same. Differences in citric acid production were not observed until after day 4, when sucrose cultures stopped producing citric acid. A possible cause for this was discovered on examination of the glucose data. Glucose appeared in the supernatant of sucrose cultures, about 40 g/L (222 mM) by day 1. This indicated a rapid extracellular sucrose hydrolysis, with a loss of at least 50% of the sucrose in only the first day. No further increases in glucose concentration were observed beyond day 1, and the glucose was consumed by day 5, coinciding with the end of citric acid production. Although data on sucrose consumption were not obtained, these findings suggest that the sucrose cultures were exhausted of carbon by day 5, due to a faster carbon uptake rate. Despite this, the rate of citric acid production was not increased, suggesting a limiting factor other than carbon uptake. This resulted in a lower citric acid yield, as carbon uptake was excessive, and the excess carbon was lost to other processes.

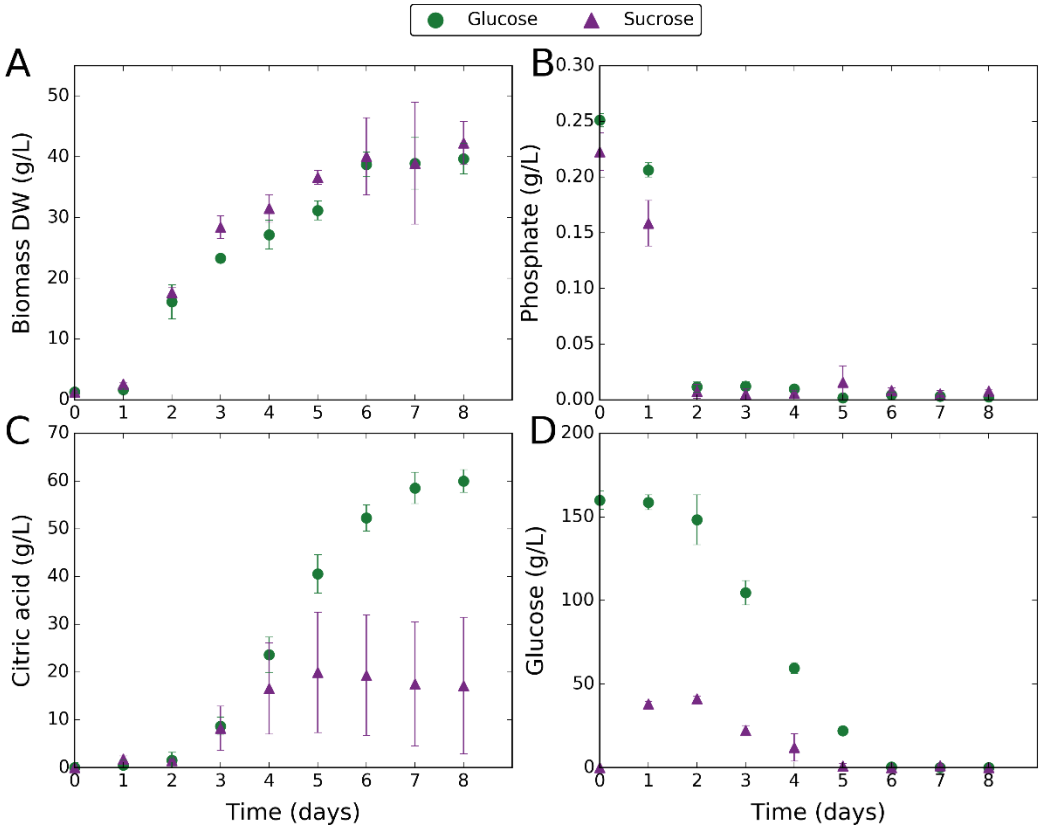

Figure 2.9. Response of citric acid fermentation to change in substrate to sucrose. The effect on citric acid fermentation of changing substrate from glucose to sucrose was determined in a time-course fermentation experiment. Green circles correspond to glucose as substrate. Purple triangles correspond to sucrose as substrate. Each data-point is the mean average of four biological replicates and error bars represent standard deviation. Citric acid data are normalised to reflect the amount produced (subtracting the zero-point – some citric acid was initially present in the media). **(A)** Change in biomass dry weight (g/L) over time. **(B)** Change in external phosphate concentration (g/L) over time. **(C)** Change in external citric acid concentration (g/L) over time. **(D)** Change in external glucose concentration (g/L) over time.

When fermentation was performed with cellobiose as the substrate, no differences were observed until after day 3 in comparison with glucose (Figure 2.10). No glucose appeared in the supernatant of cellobiose cultures, indicating that cellobiose was taken up directly and hydrolysed intracellularly. Data on cellobiose consumption showed a similar uptake rate to glucose until day 3, during which time biomass production was the same. Beyond day 3, no cellobiose was consumed, and growth stopped. No citric acid was produced, despite depletion of phosphate by day 2, and a similar carbon uptake rate to day 3. There is no clear cause for its absence between day 2 and 3 when glucose cultures started producing citric acid, and it is unsurprising that citric acid production was not observed after day 3. The termination of cellobiose uptake is unexplained.

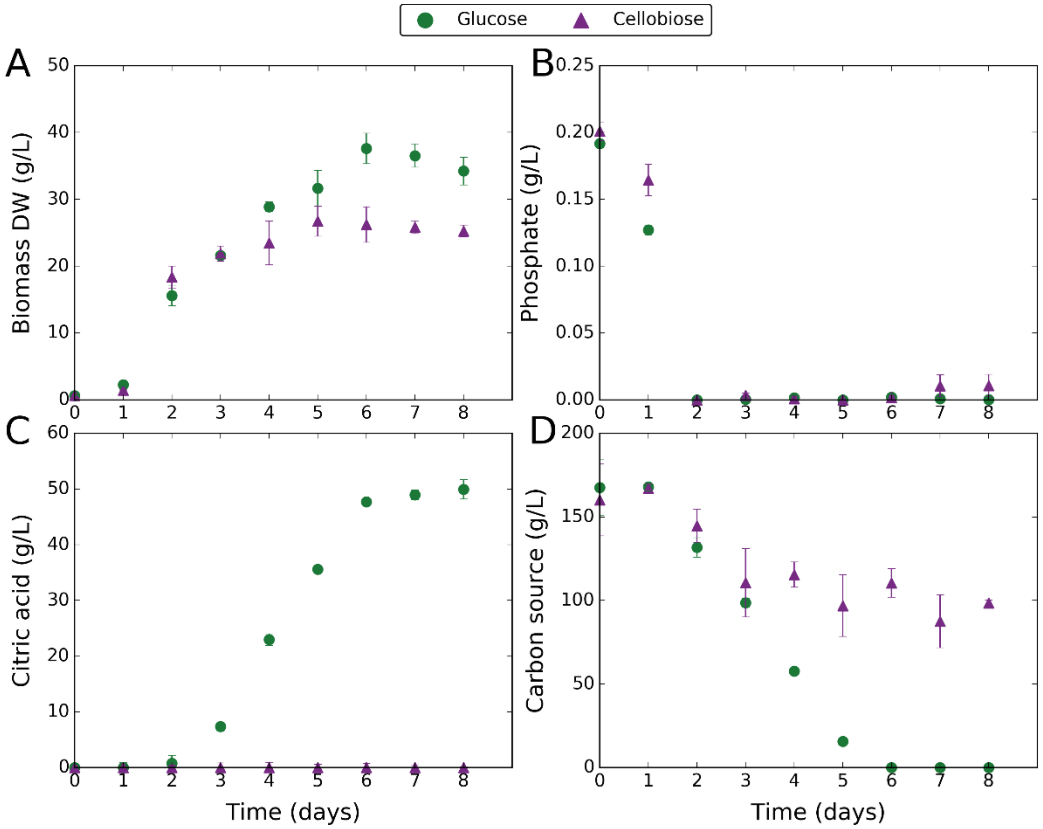

Figure 2.10. Response of citric acid fermentation to change in substrate to cellobiose. The effect on citric acid fermentation of changing substrate from glucose to cellobiose was determined in a time-course fermentation experiment. Green circles correspond to glucose as substrate. Purple triangles correspond to cellobiose as substrate. Each data-point is the mean average of four biological replicates and error bars represent standard deviation. Citric acid data are normalised to reflect the amount produced (subtracting the zero-point – some citric acid was initially present in the media). **(A)** Change in biomass dry weight (g/L) over time. **(B)** Change in external phosphate concentration (g/L) over time. **(C)** Change in external citric acid concentration (g/L) over time. **(D)** Change in external carbon source concentration (g/L) over time.

2.3.5 Effect of initial pH on organic acid fermentation

It has been previously discussed in this chapter that citric acid production depends on a low initial pH (around 2), to prevent the competing production of the acids oxalic and gluconic. Many fermentation experiments in this work were therefore started at pH 2. To investigate whether the physiological characteristics observed in these experiments also occurred at higher initial pH, a fermentation experiment was performed at initial pH 7. Time series were obtained for citric acid, oxalic acid, gluconic acid, and phosphate (Figure 2.11).

A rapid phosphate uptake was observed, as in experiments starting at pH 2, with phosphate depleted by day 2. This was followed by the synchronous production of oxalic and citric acid, which began at day 3 to 4. The timing suggests that both acids are produced during phosphate-limited growth, however, biomass data were not obtained in this experiment to further support this. Although citric acid was produced, the amounts were very low compared to experiments at initial pH 2.

While citric and oxalic acid were produced later in fermentation, gluconic acid was produced early on, peaking at day 3. Gluconic acid production stopped at day 3, reaching between 10 and 15 g/L (51 and 76 mM). These findings suggest gluconic acid is produced independently of citric and oxalic. Gluconic acid is known to be produced by extracellular glucose oxidase (Mischak *et al*, 1985), and may be a means of quickly sequestering glucose. The inactivity of glucose oxidase at low pH causes gluconic acid production to stop once the ambient pH has fallen to around 2.

Cultures at initial pH 7 were morphologically different to those at pH 2, with increased and more variable pellet size (around 2-3 mm in diameter). The larger pellet size prevented measurements of biomass in these cultures without destructive sampling. The morphological effects may explain the increased variance seen in data from experiments at pH 7. Differences in pellet size may affect aerobicity and transport processes.

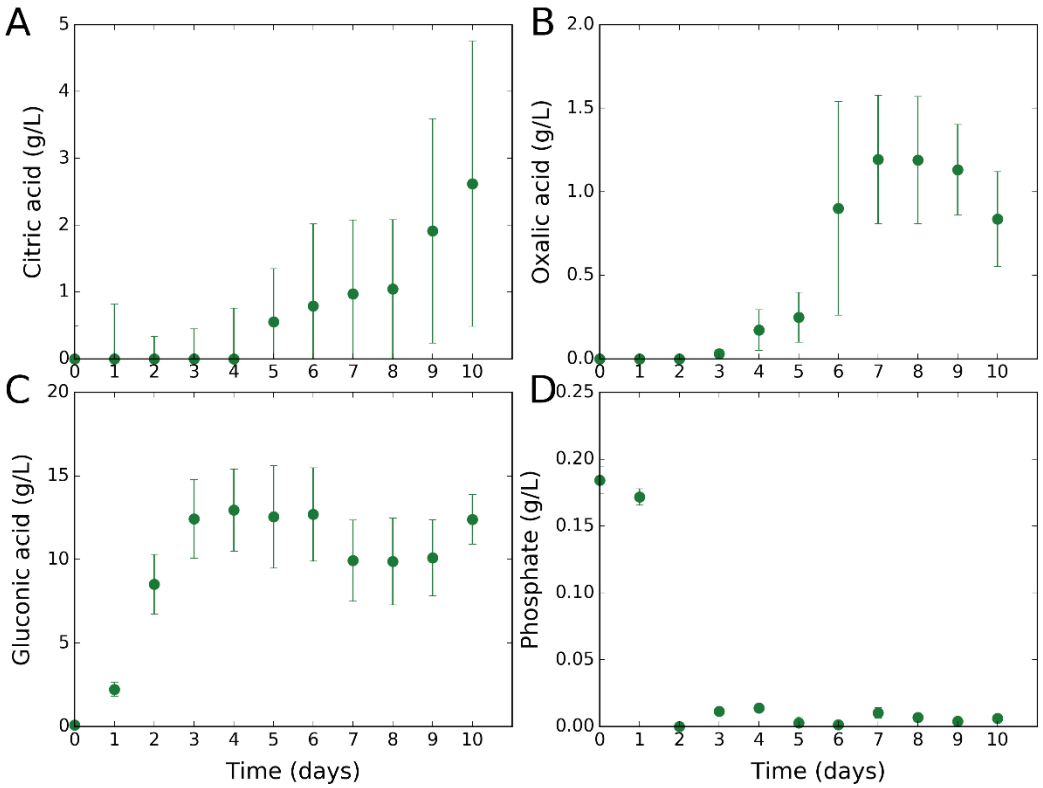

Figure 2.11. Organic acid fermentation at initial pH 7. Organic acid fermentation at initial pH 7 was characterised in a time-course fermentation experiment with glucose as substrate. Each data-point is the mean average of four biological replicates and error bars represent standard deviation. Citric acid data are normalised to reflect the amount produced (subtracting the zero-point – some citric acid was initially present in the media). **(A)** Change in external citric acid concentration (g/L) over time. **(B)** Change in external oxalic acid concentration (g/L) over time. **(C)** Change in external gluconic acid concentration (g/L) over time. **(D)** Change in external phosphate concentration (g/L) over time.

2.4 Discussion

The work performed in this chapter was driven by the need to establish a uniform empirical system to inform modelling. The system was applied to deepen understanding of the physiological characteristics of *A. niger* organic acid fermentation, as a prerequisite to design a dynamic model. The wild-type citric acid producing ATCC1015 strain was the subject of investigation. Therefore, the observations reported in this chapter relate to a naturally evolved strain. An understanding of the natural acidogenic behaviour is critical to guide rational engineering strategies.

It is well established in the literature that *A. niger* citric acid fermentation is biphasic (Roehr *et al*, 1981). The first phase is characterised by rapid growth and minimal or no citric acid production, while the second phase is characterised by restricted growth and increased citric acid production. The trigger of this phase shift, however, is less well understood. In this work, original observations were reproduced, and the underlying events explored. Phosphate uptake was monitored, and the response to different levels of phosphate was investigated. The phase shift was observed to coincide with depletion of external phosphate, suggesting a switch to phosphate-limited growth. More phosphate was taken up early in fermentation than needed to support growth, and thereafter growth continued in the absence of phosphate. This clearly revealed a phosphate storage mechanism. During the second phase, the restricted growth rate correlated with the initial amount of phosphate. When more phosphate was stored, the growth rate was higher. This gave strong evidence that the phase shift was triggered by a switch to phosphate-limited growth. Although sufficient phosphate was available in storage to support growth, *A. niger* constrained its rate of release. The result was self-imposed phosphate-limited growth. In other observations, it was confirmed that *A. niger* is able to rapidly release the stored phosphate and does so in response to certain conditions. These include a temporary halt in aeration or exhaustion of the carbon source. This indicated an energy function of the stored phosphate, which may explain its

regulated release. Due to the impact of these findings, further investigations were made. It was hypothesised that the phosphate was stored as polyphosphate. Polyphosphate has been previously observed in *A. niger* (Nishi, 1961; Hesse *et al*, 2002). Polyphosphate is simply a polymer of phosphate. Its formation is catalysed by polyphosphate kinase (PPK), in reactions that hydrolyse ATP (Zhang *et al*, 2002). PPK can also catalyse the reverse reaction when ADP levels are high, forming ATP (Zhang *et al*, 2002). Polyphosphate therefore stores energy as well as phosphate, and so it seemed plausible that it was the mediator of the phosphate storage mechanism. Another enzyme, exopolyphosphatase (PPX) hydrolyses polyphosphate releasing phosphate (Gerasimaitė and Mayer, 2017). A new hypothesis is that the actions of PPK and PPX serve to dissipate ATP, through the continuous making and breaking of polyphosphate. This would help to maintain a low ATP level, important to citric acid production. It should be noted that although PPK has been identified in several species of bacteria and is highly conserved (Zhang *et al*, 2002), it is rarely found in eukaryotes. It was identified in the yeast *Candida humicola* with homology to bacterial PPK, but efforts to reveal its activity in *Saccharomyces cerevisiae* have failed (McGrath *et al*, 2005). No putative PPK exists in *S. cerevisiae* (McGrath *et al*, 2005), and likewise for *A. niger*. It is now known that polyphosphate is formed by the vacuolar transporter chaperone complex in *S. cerevisiae*, that also uses ATP (Gerasimaitė and Mayer, 2017). It may be that the same mechanism exists in *A. niger*. If so, an alternative mechanism of producing ATP from polyphosphate hydrolysis is needed, that is independent of PPK. An analysis of polyphosphate levels during citric acid fermentation confirmed that phosphate storage occurs via polyphosphate. The level of polyphosphate increased early in fermentation, peaking at the point of external phosphate depletion. This was followed by a decrease, which correlated with biomass production during the phosphate-limited growth phase. It appears that the rate of polyphosphate hydrolysis determines the growth rate, and consequently the rate of citric acid production. It is probable that this is regulated by the intracellular ATP concentration, explaining the rapid polyphosphate hydrolysis under energy limiting conditions. Further investigation is needed to elucidate the exact mechanistic detail.

The work described in this chapter mainly used glucose as the substrate for fermentation. To investigate the effect of substrate on citric acid fermentation, experiments were also carried out with other carbon sources. It was important to extend the physiological characterisation to substrates that are more applicable to sustainable biorefinery processes. The carbon uptake rate is a key factor in citric acid production, as demonstrated by previous studies (Torres *et al*, 1994). One means of exploring this is by using different carbon sources that have different uptake rates. When xylose was tested, the uptake rate was the same as for glucose and the same physiological characteristics were observed. Citric acid production, however, was reduced by a factor of two. It was suspected that a difference in morphology and culture viscosity was responsible. Decreased citric acid production on xylose with comparison to glucose was also seen in previous research (Xu *et al*, 1989a). As xylose is an abundant pentose sugar in the hemicellulose fraction of waste plant biomass, it was promising to see an assimilation as efficient as glucose. Since sustainable fermentation processes typically use feed-stocks that contain a mixture of sugars, it was necessary to test the fermentative performance of xylose in the presence of glucose. Although xylose was still consumed, its uptake rate was lowered two-fold with respect to xylose alone. It is suspected that this effect was caused by carbon catabolite repression. It is known that carbon catabolite repression occurs in *A. niger* and is mediated by CreA (de Vries *et al*, 1999). In this experiment, an increase in total carbon uptake was observed until glucose exhaustion, due to the combined uptake of two different sugars. This did not correlate with an increase in citric acid production, however. This suggests another bottleneck must be overcome first, before improvements can be made by enhancing carbon uptake. Once xylose was the only sugar left, a drop in carbon uptake was observed. At the same time, the rate of citric acid production decreased. Therefore, carbon uptake became the limiting factor later in fermentation, whereas a different factor was limiting earlier in fermentation. These findings were reproduced and became more pronounced when sucrose was applied as substrate. A very rapid extracellular sucrose hydrolysis was observed, consistent with previous

studies (Houssain *et al*, 1984). This enabled a faster carbon uptake. Citric acid production stopped at day 5, suggesting exhaustion of the carbon source at this point. Despite significantly increased carbon uptake early in fermentation, citric acid production was unaffected. Meanwhile, biomass production was slightly higher. The final yield of citric acid was at least two-fold lower than with glucose alone, as the excessive carbon uptake early on was lost to other processes such as growth. This suggests a delicate balance between growth and citric acid output that determines the productivity and yield. On the one hand, growth is needed to create the machinery for citric acid production, and on the other, growth competes with citric acid production for a common substrate. Sucrose is usually regarded as the preferred substrate for citric acid fermentation (Houssain *et al*, 1984), and industrial processes use sucrose-based feed-stocks (Dhillon *et al*, 2013a). This is not consistent with the observations in this work, which showed glucose to be superior when the ATCC1015 strain is used. The strain used may account for the discrepancy. Other strains may be able to handle the increased carbon uptake, due to absence of a limitation at another step in the citric acid production pipeline. In these cases, sucrose becomes the superior substrate, as the higher flux of carbon is able to pass through to output of citric acid. In addition to xylose and sucrose, other carbon sources were tested including arabinose, glycerol and cellobiose. These were chosen due to their relevance in sustainable fermentation processes. Like xylose, arabinose and cellobiose are present in lignocellulosic resource streams. Glycerol is a by-product of biodiesel production. No citric acid was produced on these substrates, due to a very slow rate of carbon uptake. This is an important observation, as it illustrates the need to consider the transport step when engineering strains for optimal citric acid production on different feed-stocks. Previous studies also showed no citric acid production when using arabinose, cellobiose, or glycerol as carbon source (Xu *et al*, 1989a).

The majority of the work in this chapter was focused on citric acid fermentation at a starting pH of 2. The low pH was needed to prevent the competing production of oxalic and gluconic acid, which occur at higher pH (Ruijter *et al*, 1999). With observations from many experiments, a picture of

the physiological characteristics of citric acid fermentation developed. To further expand this picture, organic acid fermentation was characterised at an initial pH of 7. It was observed that oxalic acid production behaved similarly to citric. This suggests that the two acids are produced as part of the same response. It was predicted that production of these acids is the most efficient means of acidification (Andersen *et al*, 2009b). This suggests that the excess carbon available in phosphate-limited growth is channelled into proton production, resulting in the formation of oxalic and citric acid. This explains the synchronicity of the production of these acids with phosphate-limited growth. While a relationship was observed between oxalic and citric acid production, gluconic acid behaved very differently. Gluconic acid was only produced early in fermentation, and not during phosphate-limited growth. It is known that gluconic acid is formed by extracellular glucose oxidase (Mischak *et al*, 1985). This enzyme is inactive at low pH (Wilson and Turner, 1992), which explains the decline in gluconic acid production as pH drops. Gluconic acid production was not predicted as an efficient means of acidification (Andersen *et al*, 2009b), which suggests its formation occurs independently of oxalic and citric. Instead, it may be a strategy to quickly sequester glucose in a form less accessible to other organisms. *A. niger* is able to catabolise gluconic acid, and does so later in fermentation once preferred carbon sources are used up (Andersen *et al*, 2009b).

Chapter 3: Dynamic modelling of *Aspergillus niger* organic acid fermentation

3.1 Introduction

In this chapter, a dynamic model of *A. niger* organic acid fermentation developed in this work is described. This work is presented as a publication (Upton *et al*, 2017) with a few alterations. This dynamic model builds on previous modelling work, and is informed by empirical observations of *A. niger* organic acid fermentation. The dynamic model accurately captures physiological characteristics, and is demonstrated as a predictive platform for metabolic engineering.

3.1.1 Aims of this Chapter

The work described in this chapter aimed to develop a dynamic model of *A. niger* organic acid fermentation that accurately captures physiological characteristics and can be applied as a predictive platform for engineering.

3.2 Publication

Title: An accurate description of *Aspergillus niger* organic acid batch fermentation through dynamic metabolic modelling

Authors: Daniel J. Upton, Simon J. McQueen-Mason, A. Jamie Wood

Abstract

Background

Aspergillus niger fermentation has provided the chief source of industrial citric acid for over 50 years. Traditional strain development of this organism was achieved through random mutagenesis, but advances in genomics have enabled development of genome-scale metabolic modelling that can be used to make predictive improvements in fermentation performance. The parent citric acid producing strain of *A. niger*, ATCC 1015, has been described previously by a genome-scale metabolic model that encapsulates its response to ambient pH. Here, we report the development of a novel double optimisation modelling approach that generates time-dependent citric acid fermentation using dynamic flux balance analysis.

Results

The output from this model shows a good match with empirical fermentation data. Our studies suggest that citric acid production commences upon a switch to phosphate-limited growth and this is validated by fitting to empirical data, which confirms the biphasic growth behaviour and the role of phosphate storage as polyphosphate.

Conclusions

The calibrated time-course model reflects observed metabolic events and generates reliable *in silico* data for industrially relevant fermentative time series, and for the behaviour of engineered strains suggesting that our approach can be used as a powerful tool for predictive metabolic engineering.

Keywords: *Aspergillus niger;* citric acid; dFBA; metabolic modelling; polyphosphate

Background

Due to its natural ability to secrete organic acids and proteins, the filamentous fungus *Aspergillus niger* is an established organism for the industrial production of citric acid and enzymes. *A. niger* is metabolically highly versatile, a feature that has made it useful for a wide range of biotechnological biotransformations [1]. *A. niger* also produces a wide range of secondary metabolites, with over 100 reported to date [2]. *A. niger* is a saprotroph and its natural habitat is soil, although it can be found in wide-ranging habitats, such as rotting fruit, plant debris, and indoor environments. This fast-growing fungus is both acid- and thermo-tolerant, able to grow in the pH range 1.4-9.8 and in the temperature range 6-47ºC [3]. This versatility and its ease of culture has helped it become an established industrial organism. Its haploid genome is around 35 Mb in size with 8 chromosomes which contain about 12,000 genes, 57% of which have functional assignments [4]. *Aspergilli* are an important and diverse group, which in addition to *A. niger,* include well-studied species such as the model genetic organism *A. nidulans*, the pathogen *A. fumigatus* and the domesticated *A. oryzae*. Full genome sequences are currently available for 18 species of the *Aspergilli* group [5] and some of these have been subject to extensive systems biology studies [6].

With global production of 2 million tonnes a year, citric acid is an industrial chemical with many applications [7]. Its main use is in the food and drinks industry, but is also used in cleaning agents, pharmaceuticals, animal feed, and metal cleaning [8]. Industries using *A. niger* fermentation are dependent on sucrose-based feedstocks, but with rising costs and increasing concerns over food security, a switch to more sustainable and lower cost feedstocks is desirable [9]. *A. niger* can assimilate a wide range of carbon sources, and

therefore has great potential for exploiting underused resource streams such as pentose sugars from lignocellulose.

The best industrial strains are capable of producing over 70% of the theoretical yield of citric acid [10]. Such strains have been developed over many decades by time-consuming random mutagenesis. The genotype of resulting strains remains unknown, and random mutagenesis can lead to genetic instability of developed strains. Rational engineering of *A. niger* is now feasible, particularly with advances in genomics over recent years that have paved the way for genome-scale metabolic modelling [5, 11]. Industrially, *A. niger* is utilised via large-scale batch fermentations rather than continuous culture methods, typically in reactors in excess of 100,000 litres [12]. In order for genome-scale models to accurately capture the behaviour of these cultures, techniques which model the batch growth, rather than simple chemostat-like cultures, are required.

The genome of the parent citric acid producing strain of *A. niger*, ATCC 1015, has been sequenced [4]. This enabled development of the genome-scale metabolic model for *A. niger*, *i*MA871, which reflects ATCC 1015 metabolism [13]. The model was further developed to reflect the well-known behaviour of *A. niger* to acidify its surroundings in response to ambient pH [14]. This was achieved by incorporating acid-dissociation reactions for seven organic acids reportedly secreted by *A. niger*. Each reaction gives the number of protons released by a particular acid as a function of ambient pH. Citric acid production was modelled statically using flux balance analysis (FBA). The objective function was either set to proton production at a fixed growth rate or proton production was incorporated into the biomass equation. The nature of organic acid production in response to ambient pH is, however, a dynamic one, with acid-dissociation reactions changing as protons are produced.

In this article, we further develop the *A. niger* metabolic model to take into account the dynamic nature of organic acid production. By designing a novel modelling approach that employs dynamic flux balance analysis (dFBA), we

demonstrate a model that gives time-course fermentative series of citric acid production. We validate the new model by fitting to empirical data from ATCC 1015 citric acid fermentations, and demonstrate how the resultant time-course calibrated model can be used as a powerful platform for metabolic engineering of *A. niger*.

Results

Citric acid fermentation occurs as part of a biphasic growth response

To investigate citric acid production by the parent citric acid producing ATCC 1015 strain, empirical time course data were obtained from fermentation performed in shake flasks. Biomass and citric acid production were monitored with samples taken at 24 hour time-points. Biphasic growth behaviour was observed, with a drop in growth rate at day 3 (Fig 1A). Citric acid production commenced at day 3, coinciding with the biphasic growth shift (Fig 1B). 60 g/L citric acid was produced.

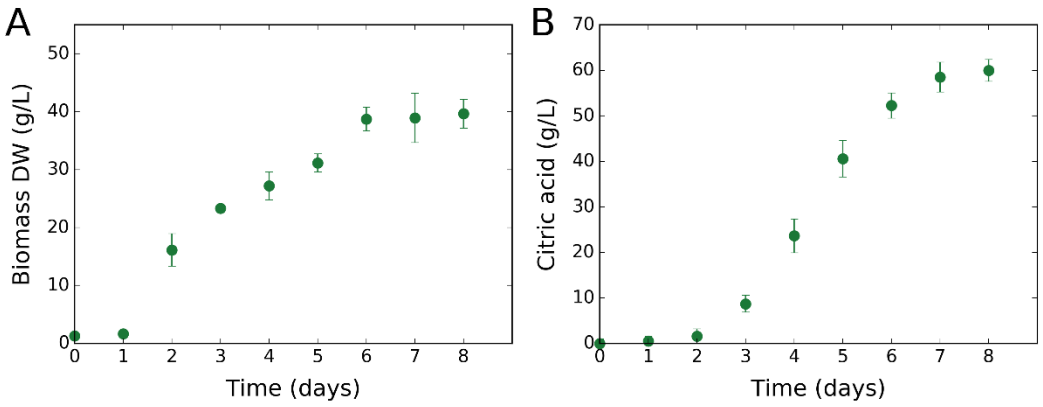

Figure 1. Citric acid production commences upon a biphasic growth switch. Empirical data plotted is the mean average of 4 biological replicates and error bars represent standard deviation. Citric acid data are normalised to reflect the amount produced (subtracting the zero-point – some citric acid was initially present in the media). **A)** Change in biomass dry weight (g/L) over time. **B)** Change in external citric acid concentration (g/L) over time.

In order to better understand the basis of this growth behaviour we developed a dynamic flux balance analysis (dFBA) model based on the previously published FBA model [13, 14]. To validate the model and further investigate the biphasic growth behaviour, empirical data were obtained for citric acid fermentation under a range of phosphate levels (0.05, 0.09 and 0.17 g/L). Samples of the cultures were taken every 24 hours to produce a time-course of biomass dry weight, phosphate depletion, citric acid production, and glucose consumption (Fig 2). Phosphate was rapidly taken up and depleted by day 2 (Fig 2B), yet growth continued (Fig 2A). Phosphate was therefore clearly stored internally to enable growth during absence of external phosphate. Biphasic growth was observed, with growth becoming phosphate-limited. The biphasic growth shift was synchronous with depletion of external phosphate. The phosphate-limited growth rate was a function of the initial phosphate concentration, with increased growth rate at higher phosphate. The timing of citric acid production was observed to coincide with the onset of phosphate-limited growth and external phosphate depletion (Fig 2C). Up to 50 g/L citric acid was produced, with the culture at 0.17 g/L phosphate producing the most. Glucose uptake was relatively slow for the lower phosphate cultures and a limiting factor in citric acid production (Fig 2D).

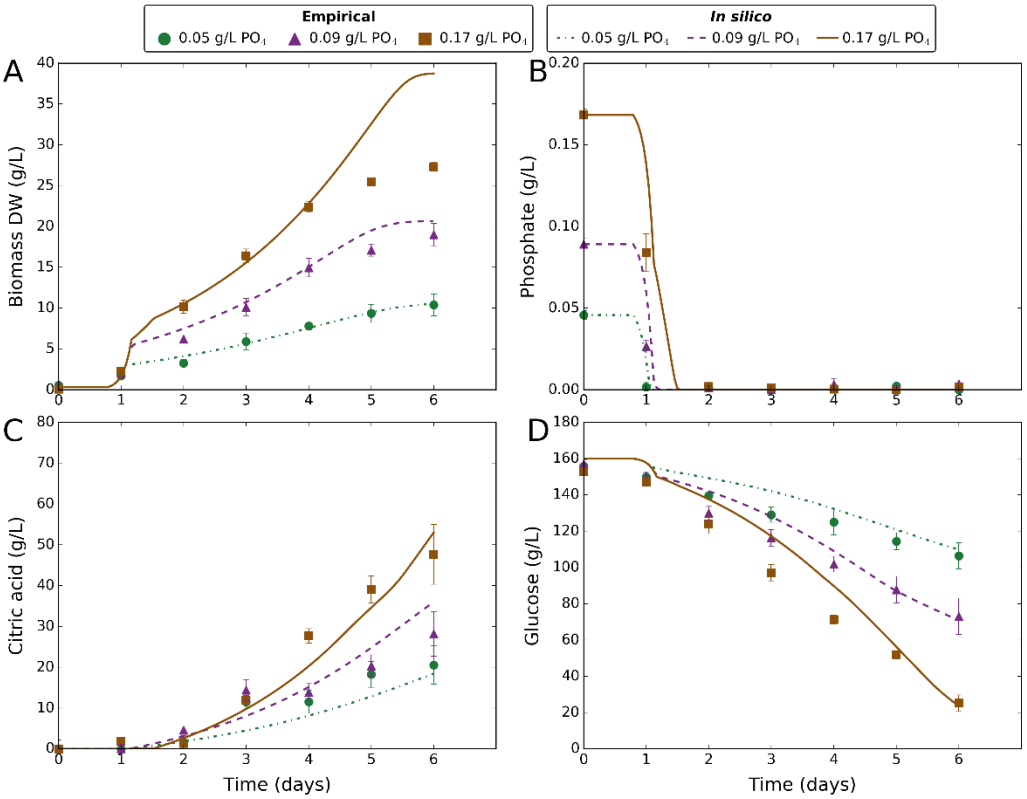

Figure 2. Comparing empirical and *in silico* data in response to varying phosphate. Markers represent empirical data and lines represent *in silico* data. Green circles and dashed-dotted lines correspond to 0.05 g/L phosphate. Purple triangles and dashed lines correspond to 0.09 g/L phosphate. Brown squares and solid lines correspond to 0.17 g/L phosphate. Empirical data plotted is the mean average of 4 biological replicates and error bars represent standard deviation. Citric acid data are normalised to reflect the amount produced (subtracting the zero-point – some citric acid was initially present in the media). *In silico* data-points are one per minute. **A)** Change in biomass dry weight (g/L) over time. **B)** Change in external phosphate concentration (g/L) over time. **C)** Change in external citric acid concentration (g/L) over time. **D)** Change in external glucose concentration (g/L) over time.

From these observations, we hypothesised that the biphasic growth shift is caused by a switch to phosphate-limited growth, resulting in citric acid production. This hypothesis was motivated by examination of our data, existing knowledge of *A. niger* [10] and also the ecological evidence that organic acids are released extracellularly in order to facilitate the mobilisation of phosphate, especially in soil [15]. We decided to examine the plausibility of this hypothesis using dFBA modelling.

Simulating citric acid fermentation by dynamic flux balance analysis

To create time-course simulations comparable to the citric acid fermentation empirical data, dynamic flux balance analysis (dFBA) was used with the *i*MA871 metabolic model [13]. Citric acid production was modelled by incorporating kinetic acid-dissociation reactions into the dFBA schema for the organic acids in *i*MA871 and setting the objective to proton production. This explicit inclusion leads to an acid hierarchy [14], which suggested that citric acid production was the most efficient means of acidification with oxalic acid production switched off.

In the standard setting for the metabolic model citric acid secretion is included as a part of the external constraints during growth [13]; however, this is not supported by our observations. Therefore, a novel modelling approach was designed to simulate the biphasic growth behaviour with citric acid production commencing upon a biphasic growth shift coupled to phosphate intake. To achieve this, a double optimisation dFBA setup was designed (Fig 3). The objective is first set to biomass production, with the maximised growth rate then used in the second optimisation. The second objective is dependent on the growth-limiting condition of the first optimisation. The decision process uses a boolean expression. If the flux of the external phosphate uptake reaction is lower than its flux constraint, the second objective is set to phosphate storage to store excess phosphate not used for growth. Otherwise, the flux of this reaction is equal to its flux constraint and the second objective is set to proton production to make use of the carbon not used for growth (phosphate-limited growth).

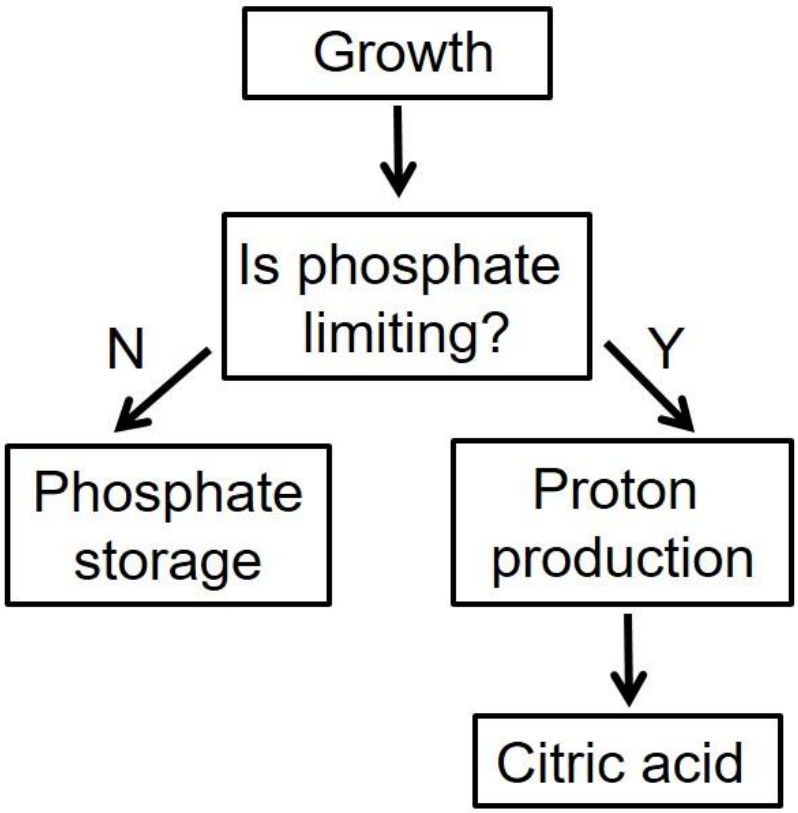

Figure 3. Simulating citric acid fermentation by dynamic flux balance analysis. A schematic showing the decision process implemented in the dFBA model.

The dynamic modelling approach, dFBA, therefore includes a number of metabolite pools that are tracked outside of the FBA, including external glucose, external phosphate, external pH, organic acids as well as the hypothesised stored phosphate. These metabolite pools are linked to the FBA simulations at each step via first order differential equations describing transport processes. These differential equations are solved at each time-step to provide flux constraints for the FBA optimisations occurring in a tandem fashion and assuming the metabolic system remains at a steady-state despite the small changes in the external constraints. All equations used are detailed in the methods, but are essentially either linear diffusion or Michaelis-Menten transport equations across the membrane as described below and mathematically in the methods section. Literature sources were used to parameterise the model wherever available as described below.

Following previous studies [16, 17], glucose uptake was modelled as the sum of passive diffusion and facilitated diffusion, using empirical values from the literature [16, 17] for all transport-mediated kinetic parameters (Table 2). The calculated parameter for passive diffusion overestimated glucose uptake, and therefore was fitted to empirical data (Table 1). Transport-mediated glucose uptake in *A. niger* is inhibited by low pH and non-competitively inhibited by external citrate [17], and this was therefore included in the modelled glucose uptake. *A. niger* has both low- and high-affinity glucose transport systems [17], both of which were included in the model. The low-affinity system is reported only active above 150 g/L glucose, [17] and so this system was only included in the model at high glucose (>150 g/L).

Phosphate uptake and release of stored phosphate were modelled according to Michaelis-Menten kinetics. As no characterised phosphate transporters could be found for *A. niger* in the literature, kinetic parameters were fitted to empirical data on phosphate uptake (Table 1).

Table 1. Parameters fitted to our empirical data.

Parameter	Description	Value
$v_{Pe,max}$ (mmol gDW^{-1} h^{-1})	External phosphate maximum input rate[a]	0.08
K_{Pe} (mM)	External phosphate Michaelis constant	0.0333
$v_{P,max}$ (mmol gDW^{-1} h^{-1})	Internal phosphate maximum input rate	0.0008
K_P (mM)	Internal phosphate Michaelis constant	0.0833
v_{G1} (mmol gDW^{-1} h^{-1})	External glucose passive uptake rate	0.00031419 × [GLC][b]
v_{X1} (mmol gDW^{-1} h^{-1})	External xylose passive uptake rate	0.00033 × [XYL][c]
$v_{X2,max}$ (mmol gDW^{-1} h^{-1})	External xylose high-affinity transport maximum rate	0.2
K_{X2} (mM)	External xylose high-affinity transport Michaelis constant	3.33
$v_{X3,max}$ (mmol gDW^{-1} h^{-1})	External xylose low-affinity transport maximum rate	2.5
K_{X3} (mM)	External xylose low-affinity transport Michaelis constant	3.33
[GOX] (mg gDW^{-1})	Concentration of external glucose oxidase enzyme	0.1
v_{CIT} (mmol gDW^{-1} h^{-1})	Citric acid output rate constraint[d]	0.12
v_{OXAL} (mmol gDW^{-1} h^{-1})	Oxalic acid output rate constraint	0.01

[a]External phosphate input rate changed 8 hours after the dFBA start time to 0.015 mmol gDW^{-1} h^{-1} if initial pH 2 or 0.004 mmol gDW^{-1} h^{-1} if initial pH 7. [b][GLC] is concentration of external glucose in mM. [c][XYL] is concentration of external xylose in mM. [d]Citric acid output rate constraint changed to 0.016 mmol gDW^{-1} h^{-1} if initial pH above 2.

Table 2. Parameters set to empirical values from the literature.

Parameter	Description	Value	References
$v_{G2,max}$ (mmol gDW^{-1} h^{-1})	External glucose high-affinity transport maximum rate	0.186	[16, 17]
K_{G2} (mM)	External glucose high-affinity transport Michaelis constant	0.26	[16, 17]
K_{i2} (mM)	External glucose high-affinity transport citrate inhibition constant	933	[16, 17]
$v_{G3,max}$ (mmol gDW^{-1} h^{-1})	External glucose low-affinity transport maximum rate	2.706	[16, 17]
K_{G3} (mM)	External glucose low-affinity transport Michaelis constant	3.67	[16, 17]
K_{i3} (mM)	External glucose low-affinity transport citrate inhibition constant	233.21	[16, 17]
$v_{GOX,max}$ (mmol gDW^{-1} h^{-1})	Glucose oxidase (GOX) maximum reaction rate	27.48 × [GOX][a]	[26]
K_{GOX} (mM)	Glucose oxidase (GOX) Michaelis constant	33	[26, 27]

[a][GOX] is concentration of external glucose oxidase enzyme in mg gDW^{-1} and was fitted to empirical data (Table 1).

Fitting of model parameters to empirical data and model validation

The empirical data obtained from the experiment varying phosphate were used to fit model parameters and validate the model. A total of eight parameters were fitted to a data-set containing 84 data-points. As each data-point was in quadruplicate with very low error margins, we decided to use the data-set for both model training and validation. The trained model was later applied to independent data-sets (Fig 4), which gave further validation. Using the trained model, citric acid fermentation was simulated for each of the phosphate levels tested, and model predictions plotted alongside empirical data (Fig 2). The modelled biphasic growth behaviour gave good fits to empirical data, with external phosphate depletion being the trigger that results in phosphate-limited growth and citric acid production. All the model outputs showed a strong qualitative comparison to the empirical data with unfitted parameters taken directly from the literature. Notably the modelled glucose uptake fitted empirical data closely (Fig 2D) with unadjusted literature values for transport-mediated uptake rate and affinity.

However, a number of adjustments were required for the model to fit the empirical data more closely. In particular, the model underestimated biomass production during phosphate-limited growth, suggesting a lower phosphate demand not reflected in the *i*MA871 biomass equation. These contrasting observations in the different areas of growth suggest that the biomass equation for the *i*MA871 model represents an average biomass composition over different growth conditions and that therefore the biomass equation needs to be altered. Differences in biomass composition in different growth conditions have previously been reported in *Escherichia coli* [18]. To reflect citric acid producing conditions, two new fitted parameters were added to the model, the nucleic acid and phospholipid components of the biomass equation (Supplementary Table S1). The ratios between the different components of each, and the total mass of the biomass components were kept constant. Change in mass was balanced by adjustment of the glycerol component, which has been reported to increase during citric acid producing conditions [19]. The additional parameters increase the complexity of the

model, and the likelihood of overfitting. Therefore, Akaike Information Criterion (AIC) [20] was used to measure the quality of fit and assess improvement in the model (Table 4) (see Methods).

Table S1. Biomass equation parameters altered to fit empirical data.

Compound	**Before fitting (mmol gDW^{-1} h^{-1})**	**After fitting (mmol gDW^{-1} h^{-1})**
AMP	-0.01402222	-0.0046740733
GMP	-0.01688834	-0.0056294467
CMP	-0.01402222	-0.0046740733
UMP	-0.01117424	-0.0037247467
DAMP	-0.00193736	-0.0006457867
DCMP	-0.00201544	-0.0006718133
DTMP	-0.00193736	-0.0006457867
DGMP	-0.00201544	-0.0006718133
PC	-0.015312	-0.005104
PS	-0.000359	-0.0001196667
PE	-0.034807	-0.0116023333
GL	-0.46	-0.9030928715
ADP	71.60986992	71.5025795733
PI	71.60986992	71.5025795733
ATP	-71.60986992	-71.5025735267
H2O	-69.08036756	-69.0511151733

Our model initially overestimated citric acid production. This may be due to the many internal constraints imposed on the internal metabolism by the intracellular accumulation of, or simply high throughputs of citrate that are not accounted for by the steady-state methodology of flux balance analysis. For example, the citrate sensitivity of 6-phosphofructo-1-kinase is a target of attempts to increase citrate production [21] and the rates of mitochondrial citrate export [22] and citrate secretion may be limiting. To reflect these constraints a limit to the citric acid output rate, v_{CIT}, was added and fitted as a parameter to more closely reflect empirical data (Table 1). Carbon uptake was decreased slightly as a result of the constraint on citric acid output, but still gave close fits to empirical data. The new model was assessed by calculating the AIC (see Methods), which showed a significant improvement (Table 4).

Citric acid production on other carbon sources

To further investigate the biphasic growth behaviour, we tested citric acid fermentation using D-xylose as a substrate at an initial concentration of 160 g/L. The same biphasic growth shift coupled citric acid response was seen with xylose (Fig 4) as seen with glucose. We applied our model, with previously fitted parameters unchanged. The empirical data from this experiment was not used in previous model training, and served to provide further validation with glucose as substrate and at a different phosphate level. The uptake rate of xylose was modelled similarly to glucose as the sum of passive and facilitated diffusion. The kinetic parameters for xylose uptake were fitted to our empirical data (Table 1). Close fits were achieved for biomass production and carbon source consumption, demonstrating the wide applicability of the dynamic model. Citric acid production was overestimated by the model, which may suggest a further limiting factor with xylose as the carbon source. The constraint applied to citric acid output rate, v_{CIT}, was the same as for glucose (Table 1). The discrepancy may be due to differing morphology as we observed decreased biomass pellet sizes and higher viscosity in cultures grown on xylose.

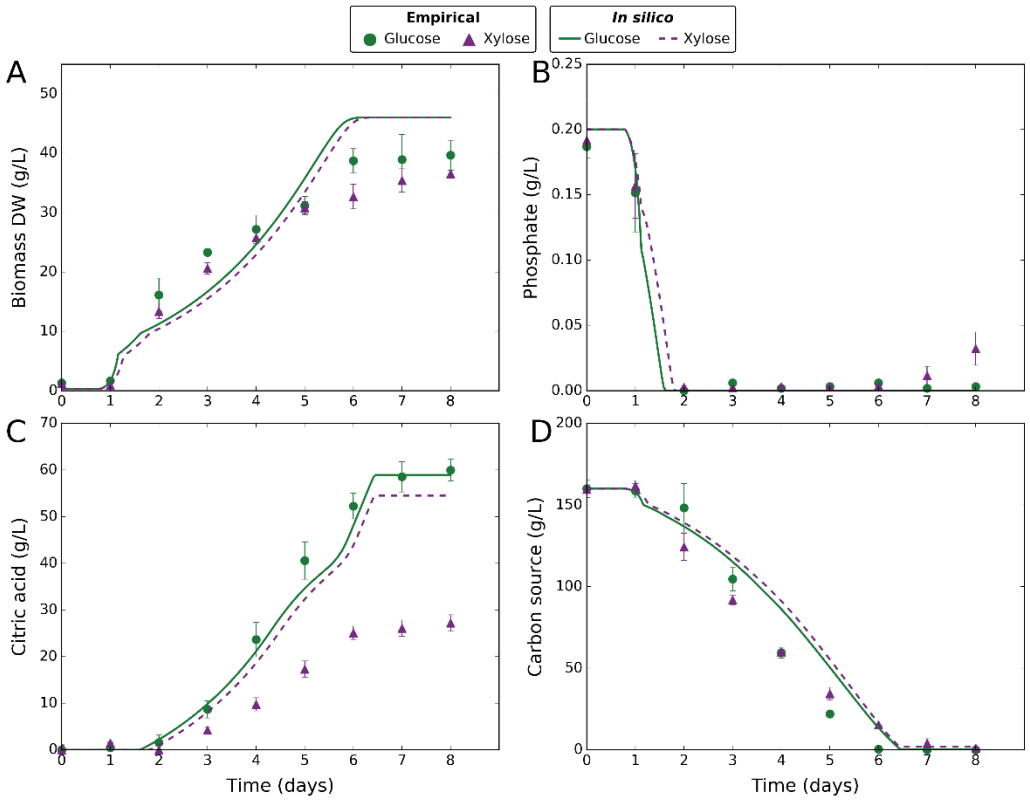

Figure 4. Comparing empirical and *in silico* data in response to different carbon sources. Markers represent empirical data and lines represent *in silico* data. Green circles and solid lines correspond to glucose. Purple triangles and dashed lines correspond to xylose. Empirical data plotted is the mean average of 4 biological replicates and error bars represent standard deviation. Citric acid data are normalised to reflect the amount produced (subtracting the zero-point – some citric acid was initially present in the media). *In silico* data-points are one per minute. **A)** Change in biomass dry weight (g/L) over time. **B)** Change in external phosphate concentration (g/L) over time. **C)** Change in external citric acid concentration (g/L) over time. **D)** Change in external carbon source concentration (g/L) over time.

Investigating the role of phosphate during citric acid fermentation

As growth on glucose continued beyond external phosphate depletion (Fig 2B), it became clear that *A. niger* has a phosphate storage mechanism, possibly via accumulation of polyphosphate as previously reported [23]. To investigate this, polyphosphate was extracted from biomass grown under citric acid producing conditions and quantified. Polyphosphate levels were observed to rise early on in fermentation, peaking at day 2 at the point of external phosphate depletion (Fig 5). Polyphosphate levels dropped rapidly from day 2 to day 4, with a more gradual decrease later in fermentation coinciding with phosphate-limited growth and citric acid production.

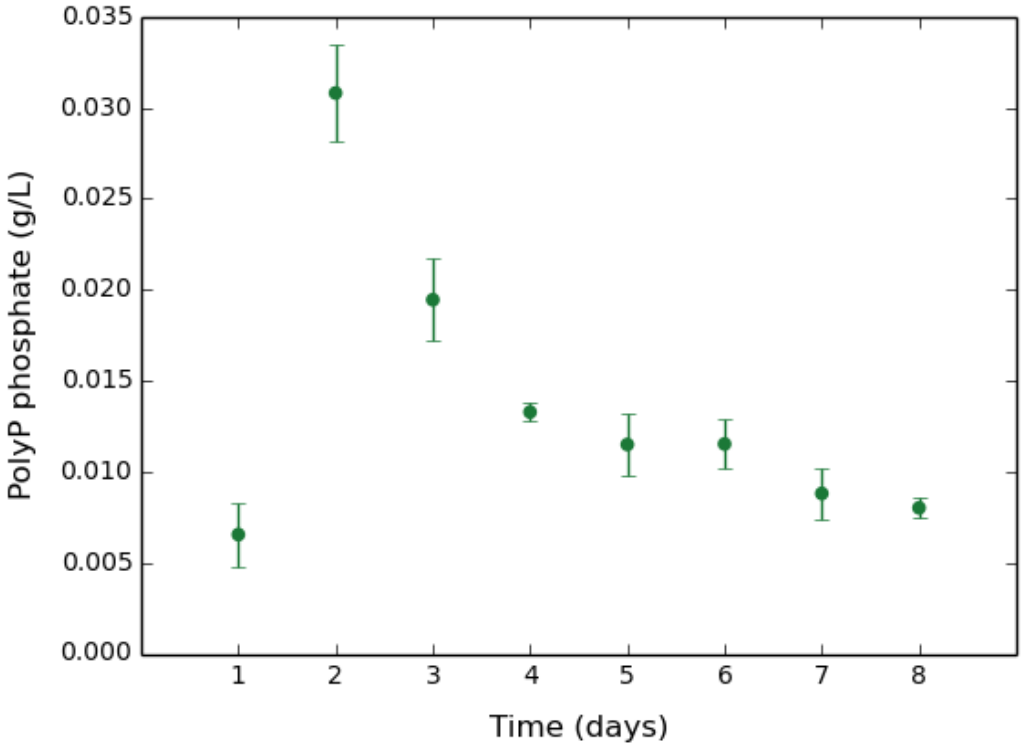

Figure 5. Change in polyphosphate levels during citric acid fermentation. Empirical data plotted is the mean average of 3 biological replicates and error bars represent standard deviation.

To further investigate the importance of phosphate, we searched for the genes encoding phosphate transporters in *A. niger* ATCC 1015. A total of 8 putative genes were found (based on similarity to known transporters), suggesting *A. niger* has evolved a range of phosphate uptake mechanisms as adaptation to different environmental conditions (Supplementary Table S2). It may be that only a subset of these genes encode phosphate transporters while others encode phosphate sensors. One of the genes (accession number EHA22558) has clear homologues in other species (Fig S1), but none of these have been characterised or parameterised at the level of protein activity. The other gene annotations are more speculative so may not encode phosphate transporters [24].

Table S2. Putative phosphate transporters in ATCC 1015. Top BLASTP hits with phosphate transporters in SwissProt database are given.

ATCC 1015 locus tag	GenBank accession	Top BLASTP hit (SwissProt)	Transporter family (of SwissProt hit)	Identity (%)	E-value
ASPNIDRAFT_173247	EHA22558	P15710.1	Inorganic phosphate transporter family	37	4e-130
ASPNIDRAFT_190334	EHA20653	P25297.2	Major facilitator superfamily	34	2e-90
ASPNIDRAFT_121846	EHA27663	Q7RVX9.2	Major facilitator superfamily	61	0.0
ASPNIDRAFT_52154	EHA22720	O42885.2	Major facilitator superfamily	29	2e-42
ASPNIDRAFT_42307	EHA25335	Q9S735.1	Major facilitator superfamily	27	6e-12
ASPNIDRAFT_175394	EHA23128	Q8H074.1	Major facilitator superfamily	25	2e-26
ASPNIDRAFT_206238	EHA26306	P27514.2	Divalent anion:Na^+ symporter family	41	0.0
ASPNIDRAFT_35379	EHA27197	Q8H074.1	Major facilitator superfamily	24	2e-22

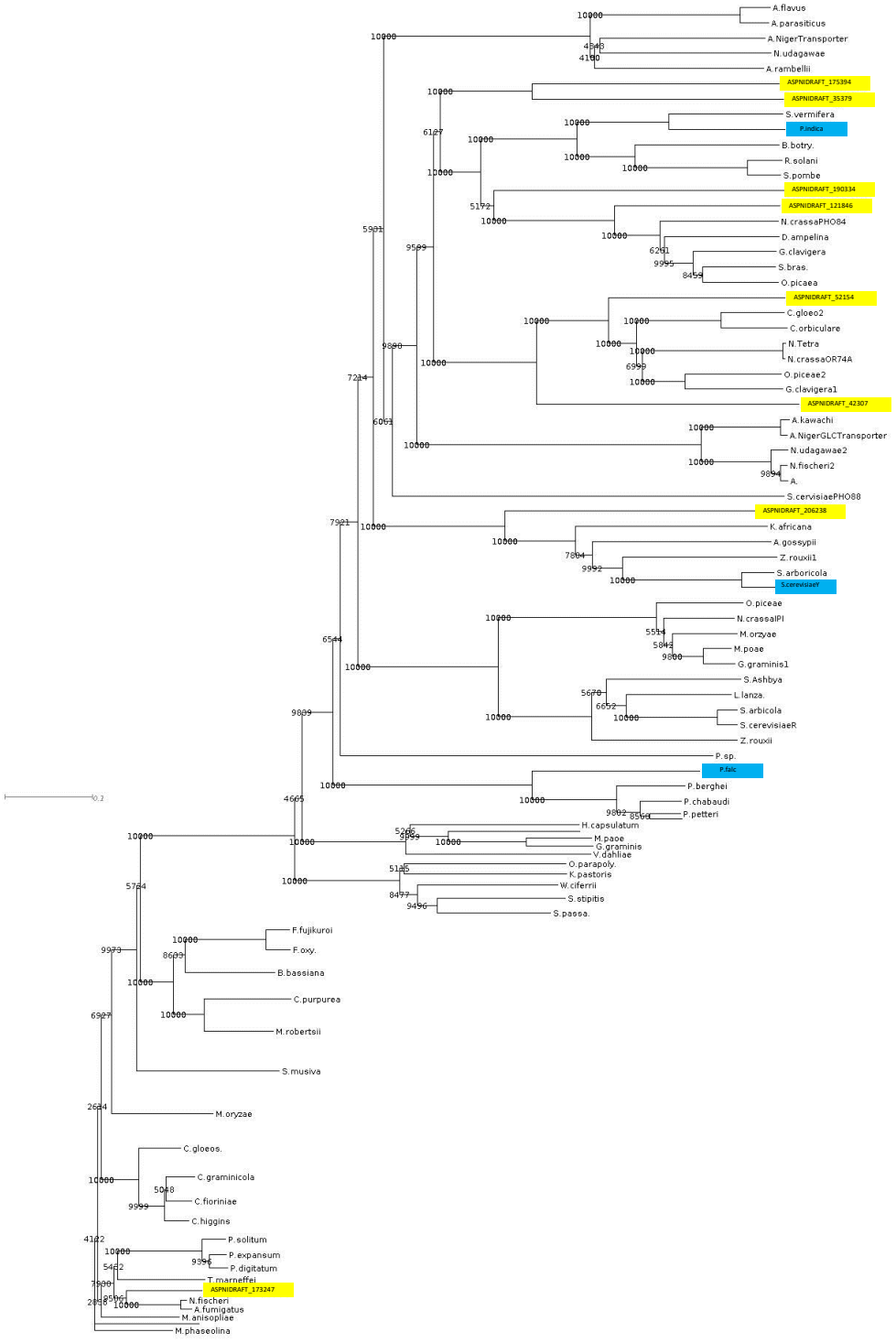

Figure S1. Phylogenetic tree of putative phosphate transporters in ATCC 1015. A phylogenetic tree was constructed from a library of around 100 phosphate transporters. MUSCLE was used for the sequence alignment, and CLUSTAL was used to assemble the tree. The putative ATCC 1015 phosphate transporters are highlighted in yellow, and experimentally characterised phosphate transporters are highlighted in blue.

The dFBA model provides a platform for predictive metabolic engineering

A prediction of the model is that oxalic acid production is the most efficient means of acidification at initial pH 7, followed by citric acid. It is well known that *A. niger* predominantly secretes oxalic and gluconic acid at higher initial pH and that by imposing a low initial pH during fermentation, production of these competing organic acids is prevented and citric acid production is increased [14]. Our model suggests that by switching off oxalic acid production by deletion of oxaloacetate hydrolase (*oah*), citric acid will solely be produced. The model does not predict gluconic acid production suggesting this may be decoupled from proton production and is instead a means of quickly sequestering glucose, through the action of extracellular glucose oxidase, early in fermentation [14].

To investigate this phenomenon, we engineered the ATCC 1015 strain by targeted gene deletion strategies to knockout *oah* and the gene encoding glucose oxidase (*gox*) responsible for gluconic acid production. We created two single knockouts (Δ*oah* and Δ*gox*) and a double knockout (Δ*oah* Δ*gox*), and characterised citric acid fermentation by these knockout strains at initial pH 7 with comparison to the ATCC 1015 Δ*pyrG* negative control strain (Fig 6). The oxalate and gluconate negative phenotypes were confirmed (Fig 6). Citric acid yield was significantly increased in the Δ*oah* strain with a further marginal improvement in Δ*oah* Δ*gox*. This was not the case for the Δ*gox* strain suggesting gluconic acid production occurs independently of proton production without impacting citric acid fermentation. Gluconic acid was produced early in fermentation while oxalic and citric acid production occurred later. The synchronicity of oxalic and citric acid production suggests they are part of the same proton production response. In this experiment, the Mn^{2+} concentration was increased to 1000 ppb. Citric acid production usually requires Mn^{2+}-deficient media, though was previously reported insensitive to Mn^{2+} in an *oah* and *gox* double negative mutant strain at pH 5 [25]. The presence of Mn^{2+} did not prevent citric acid production at initial pH 7, suggesting that its effect is limited to low pH conditions.

We applied our dFBA model to the Δ*oah* and Δ*gox* knockouts at initial pH 7, which gave close fits for oxalic and gluconic production. The differences in predicted citric acid production between the knockout strains showed a qualitative fit with empirical data (Fig 6). However, constraints on oxalic and citric acid output rates, v_{OXAL} and v_{CIT} respectively (Table 1), were required to achieve the close fits. The constraint on citric acid output rate, v_{CIT}, was different to that applied at initial pH 2. This may be due to morphological differences as we observed increased biomass pellet sizes when *A. niger* was grown at higher initial pH. The impact of differing morphology on transport processes and on anaerobicity within pellets requires further investigation. The widely reported absence of oxalic acid production below pH 2 [10, 25] was implemented in the model to reflect empirical data. To simulate gluconic acid production, the flux of the extracellular GOX and gluconic acid dissociation reactions were forced dependent on GOX kinetic parameters and the ambient pH. The kinetic parameters V_{max} and K_M of GOX (Table 2) were taken from the literature [26, 27]. The concentration of GOX per gram biomass dry weight is unknown for these experimental conditions so was fitted to empirical data (Table 1). The proportion of active GOX was based on empirical data of GOX activity at varying pH [28].

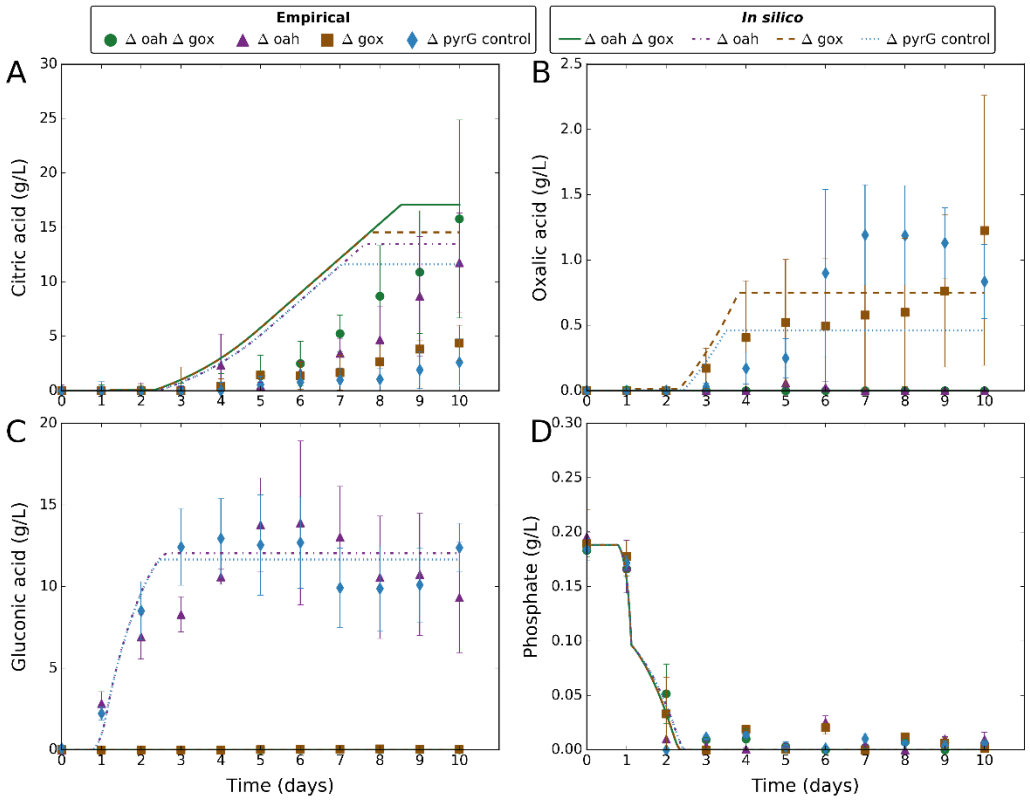

Figure 6. Comparing empirical and *in silico* data in response to Δ*oah* and Δ*gox* knockouts at initial pH 7. Markers represent empirical data and lines represent *in silico* data. Green circles and solid lines correspond to Δ*oah* Δ*gox*. Purple triangles and dashed-dotted lines correspond to Δ*oah*. Brown squares and dashed lines correspond to Δ*gox*. Blue diamonds and dotted lines correspond to Δ*pyrG* control. Empirical data plotted is the mean average of 4 biological replicates and error bars represent standard deviation. Citric acid data are normalised to reflect the amount produced (subtracting the zero-point – some citric acid was initially present in the media). *In silico* data-points are one per minute. **A)** Change in external citric acid concentration (g/L) over time. **B)** Change in external oxalic acid concentration (g/L) over time. **C)** Change in external gluconic acid concentration (g/L) over time. **D)** Change in external phosphate concentration (g/L) over time.

Discussion

We have developed a novel dynamic model of *A. niger* citric acid fermentation that employs dFBA, to give time-course simulations of batch fermentation relevant to the industrial and experimental modes of *A. niger* fermentation. Our physiologically motivated double optimisation approach is a novel use of dFBA. Previous work incorporated proton production into the *i*MA871 metabolic model and used FBA in a static manner to give predictions on organic acid production [13, 14] at fixed values of pH. Since acid dissociation reactions are dependent on the dynamic ambient pH, the application of dFBA with the dynamic tracking of pH enables more accurate predictions on organic acid production. The dynamic model was also expanded to include alternative feedstocks. Xylose was chosen as it is a pentose sugar abundant in hemicellulose in plant biomass and readily metabolised by *A. niger*. This new dynamic model is therefore a valuable addition to the *A. niger* metabolic modelling toolbox and a powerful demonstration of the promise of dFBA for applications in industrial biotechnology.

We tested the ability of the model to predict the impact of genetic modifications on organic acid fermentation at higher initial pH. We deleted genes encoding oxaloacetate acetylhydrolase (*oah*) and glucose oxidase (*gox*) to eliminate oxalic and gluconic production respectively. Deletion of *oah* significantly increased citric acid production, and this was also observed in model predictions, though less pronounced. This suggests that the presence of oxalic acid in the cytosol in the *oah* positive strains may have negating effects on citric acid production not reflected by the model. It is expected that cytosolic organic acid accumulation may occur as a result of constrained transport, which is likely to have regulatory effects on organic acid production as a safeguard mechanism.

A. niger has been an industrial workhorse for decades and is essential to the world's citric acid production. This is achieved through batch or fed-batch fermentation and the new model enables simulation of the dynamic process for the first time. The underlying causes of the naturally evolved property of organic acid production are still unclear. It was previously reported through static FBA predictions [14] that this may be driven by the biological objective of proton production. In line with empirical findings, oxalic acid production was revealed as the most efficient means of proton production at wide ranging pH with citric acid second at low pH. We have now shown this in a dynamic manner with variable external pH taken into account. Empirical data revealed that oxalic and citric acid production are synchronous upon a switch to phosphate-limited growth. This suggests they are coupled and part of the same proton production response. This is further supported by the significant increase in citric acid production in Δ*oah*.

The role of phosphate is striking as organic acid secretion has been reported in *A. niger* and other organisms as a phosphate mobilisation strategy [15, 29, 30]. The observed phosphate-limited growth results from the ability of *A. niger* to rapidly take up phosphate and store it as polyphosphate. The constraint on polyphosphate hydrolysis then limits growth, enabling flux of carbon to organic acid production. While *A. niger* has sufficient stored phosphate for growth, it does not use it and keeps it reserved. This behaviour may be due to the energy storage value of polyphosphate. We have observed a release of phosphate late in fermentation upon carbon depletion, which suggests *A. niger* is capable of rapid polyphosphate hydrolysis as a means to create ATP when other energy sources are limiting. The control mechanisms that exist in *A. niger* to regulate polyphosphate hydrolysis and their relation to organic acid production warrant further investigation.

Our modelling approach has further demonstrated the potential of dFBA; the augmentation of static steady state FBA by dynamic transport processes and time varying pools of metabolites. It has also revealed some fundamental issues with the application of these techniques to real applications. The

objective function – the biomass equation – is fundamental to FBA and is typically constructed with evidence from mass spectrometry. Our work suggests that this function is strongly dependent on the fermentation context and may even be variable over the growth process. Biologically this is highly plausible, but dramatically increases the complexity of model implementation and fitting. In addition, it is clear that important regulatory constraints on the metabolic process, in this case citrate accumulation, need to be included. In this manner, we have created an augmented dFBA model in a potentially grey area between a complete kinetic model and the genetically based simplicity of an FBA model. Further work is required to fully understand validity of such models.

Conclusions

Our findings reveal a naturally evolved behaviour that has been exploited by industry for decades to produce citric acid. Our work, encapsulated in a dynamic model, further elucidates the causative factors in organic acid fermentation by *A. niger* exploited by industrial processes. The model provides a means to further probe this behaviour and accurately explore the effects of genetic changes on organic acid fermentation in a dynamic manner. This new addition to the *A. niger* systems biology toolbox paves the way for metabolic engineering efforts to create new strains capable of enhanced citric acid production on low-cost feedstocks.

Methods

Shake flask experiments

Citric acid fermentation experiments were performed in 250 ml DeLong neck baffled shake flasks (Bellco Glass Inc.; Vineland, NJ, USA) with 30 ml medium. Flasks were siliconized with 2% (v/v) dimethyldichlorosilane. Cultures were incubated at 30ºC with shaking at 250 rpm. The following medium was used: glucose (160 g/L), urea (3.6 g/L), $(NH_4)_2SO_4$ (0.52 g/L), K_2HPO_4 (0.5 g/L), $CaCO_3$ (0.03125 g/L), $MgSO_4.7H_2O$ (0.275 g/L), $ZnSO_4.7H_2O$ (0.00225 g/L), $FeSO_4.7H_2O$ (0.0095 g/L), $CuSO_4.5H_2O$ (0.0117 g/L), $MnCl_2.(H_2O)_4$ (0.0000108 g/L), citric acid monohydrate (3.3 g/L), Tween 80 (0.0094%). The Mn^{2+} concentration was confirmed as 7 ppb by ICP-MS (Biorenewables Development Centre, York, UK). The medium was autoclaved (121ºC 15 minutes) excluding glucose which was filter sterilised (0.22 µm). The pH of the medium was adjusted after autoclaving by addition of sterile 2 M H_2SO_4. The medium included 10 mM uridine in experiments using *pyrG* negative strains. The medium was inoculated with 1×10^6 spores/ml. Spores were harvested from potato dextrose agar slants incubated for 2 days at 37ºC. 2 ml saline Tween (0.1% Tween 80, 9 g/L NaCl) was added per slant and shaken to disperse spores. Spores were washed 3 times in saline Tween. 500 µl samples of cultures were taken every 24 hours for determination of biomass, metabolites and phosphate. Samples were collected in pre-dried, pre-weighed 1.5 ml Eppendorf tubes and centrifuged at 9000 g for 5 minutes. The supernatant was retained for metabolite analysis and phosphate determination and stored at -20ºC.

Biomass dry weight determination

Mycelia were washed 4 times in 1 ml dH_2O and centrifuged at 9000 g for 5 minutes. Biomass was dried at 70ºC to constant weight. Biomass dry weight was determined by subtracting weight of the pre-dried 1.5 ml Eppendorf tube.

Metabolite analysis

Enzymatic assay kits were used to determine the level of metabolites. Glucose, citric acid, xylose, glycerol and gluconic acid were determined using Megazyme assay kits (K-GLUC, K-CITR, K-XYLOSE, K-GCROLGK, and K-GATE respectively) (Megazyme International Ireland Ltd., Wicklow, Ireland). Oxalic acid was determined using the LIBIOS oxalate assay kit (Oxalate-100; LIBIOS, France).

Phosphate determination

Phosphate was determined by the ammonium molybdate method, using an assay kit (ab65622; Abcam, Cambridge, UK).

Polyphosphate extraction and quantification

Mycelia were grown up in shake flasks using the same method as previously described. Mycelia were harvested at 8 time-points (days 1 to 8) in triplicate. To obtain sufficient biomass, one flask was harvested per sample. Day 1 samples required the pooling of 4 flasks per replicate. Mycelia were harvested using a double layer of Miracloth (Calbiochem) and washed in 300 ml ice-cold 100 mM Tris.HCl pH 7 followed by 600 ml ice-cold dH_2O. Washed mycelia were transferred to 15 ml Falcon tubes, flash frozen in liquid nitrogen, freeze dried, and stored at -80ºC. Freeze dried mycelia were weighed out in 2 ml vials, approximately 50 mg per vial. Biomass was ground using the TissueLyser II (QIAGEN; Crawley, UK) at 30 Hz for 90 seconds 3 times. Each vial contained 2 beads. Powdered mycelia were lysed by adding 2 ml 10% (w/v) lysing enzymes from *Trichoderma harzianum* (Sigma, Dorset, UK) and incubating at 30ºC with shaking for 3 hours. Samples were centrifuged and supernatant discarded. Polyphosphate was extracted following a previously described protocol [23]. All centrifuge steps were done at 13,000 rpm for 10 minutes at 4ºC and all shaking was done at 30 rpm. The polyphosphate fraction was dried in a Savant SPD131DDA SpeedVac

Concentrator (Thermo Fisher Scientific). Polyphosphate was quantified by measuring free phosphate before and after acid hydrolysis using the previously described phosphate determination method. Acid hydrolysis was performed by adding 2 ml 0.5 M H_2SO_4 to the dry pellet and boiling at 100ºC for 3 hours.

Dynamic modelling of organic acid fermentation

Modelling was performed using the *i*MA871 metabolic model [13] as the model for the flux balance analysis. During this project, a more complete model of *A. niger* metabolism was published [31] but as this retains the core of *i*MA871 and is not specific to ATCC 1015 we have not adopted this model. The FBA calculations were performed using bespoke Java code which implements the GLPK toolkit (GNU). dFBA routines were written directly into the Java code with the differential equations solved by simple time-stepping (Euler method) with small values for the time-step. The ODEs (ordinary differential equations) were solved according to

$$C_{n+1} = C_n + t f_n B_n, \quad (1)$$

where C_{n+1} is the mmol of compound at time-point n+1, C_n is the mmol of compound at time-point n, t is the time-step (1/60 h), f_n is the flux (mmol gDW^{-1} h^{-1}) at time-point n, and B_n is the biomass (gDW) at time-point n. The flux constraints at time-point n+1 were calculated by the following kinetic equations. External phosphate input (PIe<==>) was constrained according to

$$v_{Pe} = \frac{v_{Pe,max} P_e}{K_{Pe} + P_e}, \quad (2)$$

where v_{Pe} is the external phosphate uptake rate (mmol gDW^{-1} h^{-1}) and P_e is the external phosphate concentration (mM).

Internal phosphate input (PI<==>) was constrained according to

$$v_P = \frac{v_{P,max} P}{K_P + P}, \tag{3}$$

where v_P is the internal phosphate input rate (mmol gDW^{-1} h^{-1}) and P is the concentration of stored phosphate (mM).

If external glucose was below 150 g/L, external glucose uptake (DGLCe<==>DGLC) was constrained according to

$$v_G = v_{G1} G + \frac{v_{G2,max} G}{K_{G2}\left(1+\frac{C}{K_{i2}}\right)+G\left(1+\frac{C}{K_{i2}}\right)}, \tag{4}$$

where v_G is the external glucose uptake rate (mmol gDW^{-1} h^{-1}), G is the external glucose concentration (mM), and C is the external citrate concentration (mM).

If external glucose was greater than or equal to 150 g/L, external glucose uptake was constrained according to

$$v_G = v_{G1} G + \frac{v_{G2,max} G}{K_{G2}\left(1+\frac{C}{K_{i2}}\right)+G\left(1+\frac{C}{K_{i2}}\right)} + \frac{v_{G3,max} G}{K_{G3}\left(1+\frac{C}{K_{i3}}\right)+G\left(1+\frac{C}{K_{i3}}\right)}, \tag{5}$$

where v_G is the external glucose uptake rate (mmol gDW^{-1} h^{-1}), G is the external glucose concentration (mM), and C is the external citrate concentration (mM).

If external xylose was below 150 g/L, external xylose uptake (XYLe<==>) was constrained according to

$$v_X = v_{X1}X + \frac{v_{X2,max}X}{K_{X2}+X}, \quad (6)$$

where v_X is the external xylose uptake rate (mmol gDW^{-1} h^{-1}), and X is the external xylose concentration (mM).

If external xylose was greater than or equal to 150 g/L, external xylose uptake was constrained according to

$$v_X = v_{X1}X + \frac{v_{X2,max}X}{K_{X2}+X} + \frac{v_{X3,max}X}{K_{X3}+X}, \quad (7)$$

where v_X is the external xylose uptake rate (mmol gDW^{-1} h^{-1}), and X is the external xylose concentration (mM).

The extracellular GOX (glucose oxidase) reaction rate was calculated according to,

$$v_{GOX} = p_{GOX}\frac{v_{GOX,max}G}{K_{GOX}+G}, \quad (8)$$

where v_{GOX} is the GOX reaction rate, p_{GOX} is the proportion of active GOX, and G is the external glucose concentration (mM).

The proportion of active GOX, p_{GOX}, as a function of pH was determined according to,

$$p_{GOX} = -0.102pH^2 + 1.082pH - 1.95 \quad (9)$$

The kinetic parameters were either fitted to our empirical data (Table 1) or set to empirical values from the literature if available (Table 2).

The *i*MA871 model was adapted to include proton production as an objective function and acid-dissociation reactions for seven acids (citric, oxalic, gluconic, acetic, malic, succinic, lactic) but as a function of a dynamic external pH rather than a fixed pH [14]. The acid-dissociation reactions are extracellular and the model assumes that the acids are secreted in the fully associated form and dissociated only in the extracellular environment. This is a simplification of the model. In actuality, the acids exist in a partially dissociated form at the intracellular pH and may be exported in this form together with protons (symport). The number of protons released in each acid-dissociation reaction was calculated at each time-step according to the following equation based on ambient pH and pKa values.

$$H = \frac{K_1(H_e)^{-1} + 2K_1K_2(H_e)^{-2} + 3K_1K_2K_3(H_e)^{-3}}{1 + K_1(H_e)^{-1} + K_1K_2(H_e)^{-2} + K_1K_2K_3(H_e)^{-3}}, \quad (10)$$

where K_1, K_2, and K_3 are constants calculated from pKa values of each acid species (Table 3), and H_e is the external molar concentration of protons that is tracked in the dFBA as a dynamic pool.

An output reaction was added for external protons (Hpe<==>), which was set as the objective when maximising proton production. An explicit phosphate storage reaction was also included in the dFBA. An input reaction for internal phosphate (PI<==>) was added to the metabolic model, and the dynamic pool of internal phosphate was tracked in the dFBA. This new reaction was set as the objective when maximising phosphate storage.

When plotting alongside empirical data, the dFBA start time was taken as the spore germination time, 18 hours after inoculation. The initial biomass dry weight was set to 0.3125 g/L following empirical data.

Table 3. Acid constants for Equation 10.

Acid species	K_1	K_2	K_3
Citric acid	$10^{-3.128}$	$10^{-4.761}$	$10^{-6.396}$
Gluconic acid	$10^{-3.7}$	0	0
Acetic acid	$10^{-4.757}$	0	0
Malic acid	$10^{-3.459}$	$10^{-5.097}$	0
Succinic acid	$10^{-4.207}$	$10^{-5.636}$	0
Lactic acid	$10^{-3.86}$	0	0
Oxalic acid	$10^{-1.252}$	$10^{-4.266}$	0

Model parameterisation

Glucose transport-mediated uptake [16, 17] and glucose oxidase [26, 27] kinetic parameters were calculated from empirical data in the literature (Table 2). The concentration of active GOX enzyme [GOX] was fitted to empirical data (Table 1). The other kinetic parameters in the model were fitted to empirical data via a manual fitting routine (Table 1).

Quality of fit assessment and model selection

Akaike Information Criterion (AIC) [20] was used to measure the quality of fit and assess improvement in the model. The AIC was calculated according to

$$AIC = 2k + nln\left(\frac{RSS}{n}\right), \quad (11)$$

where k is the number of fitted parameters, n is the number of data-points, and RSS is the residual sum of squares.

Table 4. AIC scores for model selection.

Additional parameters	**Number of fitted parameters**	**AIC score**
None	5	438
Nucleic acid component of biomass equation	6	416
Phospholipid component of biomass equation	6	422
Nucleic acid and phospholipid components of biomass equation	7	393
Nucleic acid and phospholipid components of biomass equation, and citric acid output constraint	8	300

Targeted gene deletion of *oah* and *gox*

Targeted gene deletion was performed using a previously reported strategy [32]. As this technique requires a *pyrG* negative strain, the *pyrG* gene first had to be deleted from ATCC 1015. This was achieved using homologous recombination. ATCC 1015 was transformed with linear DNA containing 2 kb up- and 1.5 kb down-stream flanking regions of the *pyrG* gene (accession number EHA25155), kindly given by M Kokolski (University of Nottingham). Polyethylene glycol (PEG)-mediated transformation of protoplasts was used [32]. Successful deletions were selected by resistance to 5-fluoroorotic acid (5-FOA) (Fluorochem; Derbyshire, UK) and uridine auxotrophy, and confirmed by PCR and DNA sequencing using primers external to the gene (pyrG_ex_fw and pyrG_ex_rv). The *oah* and *gox* genes were identified in the ATCC 1015 genome as accession numbers EHA22250 and EHA27180, respectively. 1.5 kb up- and down-stream flanking regions were cloned from ATCC 1015 gDNA using Phusion HF DNA polymerase (Thermo Fisher Scientific), and the following primers: oah_up_fw, oah_up_rv, oah_down_fw, oah_down_rv, gox_up_fw, gox_up_rv, gox_down_fw, gox_down_rv. 15-bp tails (underlined) were added to outermost primers for In-Fusion® HD cloning (Clontech; France) into the pc3 vector between the NotI and SpeI restriction sites. To join up- and down-stream fragments together, overlap extension PCR was used with 30-bp overlapping tails (underlined) added to innermost primers. Overlapping fragments were first annealed as follows: 50 µl reaction containing 200 ng each fragment, 400 µM dNTPs, HF buffer, and 1 U Phusion HF DNA polymerase run on SOE1 programme (94ºC 5 minutes, then 94ºC 30 seconds, 60ºC 90 seconds, 72 ºC 90 seconds 10 times, then 10 ºC forever). The annealed product was then amplified using outermost primers as follows: 100 µl reaction containing 50 µl first reaction, 1 µM each primer, 400 µM dNTPs, HF buffer and 1 U Phusion HF DNA polymerase run on SOE2 programme (94ºC 2 minutes, then 94ºC 30 seconds, 60ºC 30 seconds, 72ºC 90 seconds 35 times, then 72ºC 10 minutes, 10ºC forever). The annealed product was gel purified using the QIAquick gel extraction kit (QIAGEN; Crawley, UK). Transformation was performed using XL10-Gold Ultracompetent cells according to the manufacturer's instructions (Agilent

Technologies; Cheshire, UK). Plasmid was isolated using the Wizard® Plus SV minipreps DNA purification kit (Promega; Southampton, UK). Plasmid integrity was confirmed by DNA sequencing. ATCC 1015 Δ*pyrG* was transformed with the pc3-oah and pc3-gox deletion vectors using the previously reported PEG-mediated protoplast transformation protocol [32]. The gene deletion procedure previously outlined [32] was then followed with minor modifications. 1.5 g/L 5-FOA was used to select for *pyrG* negative colonies with incubation at 37ºC for 3 days. *oah* and *gox* knockouts were identified by PCR screening with primers external and internal to the deletion site (oah_ex_fw, oah_ex_rv, oah_int_fw, oah_int_rv, gox_ex_fw, gox_ev_rv, gox_int_fw, gox_int_rv). Gene deletion was further confirmed by DNA sequencing of the region external to the deletion site. To create the Δ*oah* Δ*gox* double knockout, the deletion procedure for *gox* was applied to ATCC 1015 Δ*pyrG* Δ*oah*.

Table 5. Primers used in this work.

Primer	**Nucleotide sequence (5' to 3')**
pyrG_ex_fw	CTTTGCAGGTGTGGCTGAAC
pyrG_ex_rv	ACAGCAGTGCTTATCTGCGA
oah_up_fw	ACCGCGGTGGCGGCCGCGCTGTGTCCATACCATCAATCC
oah_up_rv	GAATGTTGCAGACAGACAGAAAGCAAAAGAGCAGGCAGTAGTAAGCAAGAAT
oah_down_fw	TCTTTCTTATTCTTGCTTACTACTGCCTGCTCTTTTGCTTTCTGTCTGTCTGC
oah_down_rv	CGGGGGATCCACTAGTTCTCCTCTTCCCCTGCCTTT
gox_up_fw	ACCGCGGTGGCGGCCGCGAGATGGCAATTTCCGCGAC
gox_up_rv	GAATATTCGAGGATTGTGGGAGAGACAGCGCGTGCAAACTCACCACCAAG
gox_down_fw	CTGTCTTGACCTTGGTGGTGAGTTTGCACGCGCTGTCTCTCCCACAATCC
gox_down_rv	CGGGGGATCCACTAGTCTACGCTCATGTCCTGGTCC
oah_ex_fw	TAAGGCTACCCAACCCACCC
oah_ex_rv	GCTTATCTAGGCCCCTGCTG
oah_int_fw	ACCCAACCACACCATCCTTC
oah_int_rv	ACCCAGTTCCCCACTAACAC
gox_ex_fw	CACTATCGCCAAGCAGGGAT
gox_ex_rv	AAGGTCTCGTTGAAGGTGGC
gox_int_fw	AGCAACCAGCCTTTCCTCTC
gox_int_rv	CCCAGTTCCAGCCCTCATTT

References

1. Parshikov IA, Woodling KA, Sutherland JB. Biotransformations of organic compounds mediated by cultures of *Aspergillus niger*. Appl Microbiol Biot. 2015;99:6971-86.

2. Nielsen KF, Mogensen JM, Johansen M, Larsen TO, Frisvad JC. Review of secondary metabolites and mycotoxins from the *Aspergillus niger* group. Anal Bioanal Chem. 2009;395:1225-42.

3. Schuster E, Dunn-Coleman N, Frisvad JC, Van Dijck P. On the safety of *Aspergillus niger*–a review. Appl Microbiol Biot. 2002;59:426-35.

4. Andersen MR, Salazar MP, Schaap PJ, van de Vondervoort PJI, Culley D, Thykaer J, et al. Comparative genomics of citric-acid-producing *Aspergillus niger* ATCC 1015 versus enzyme-producing CBS 513.88. Genome Res. 2011;21:885-897.

5. Cerqueira GC, Arnaud MB, Inglis DO, Skrzypek MS, Binkley G, Simison M, Miyasato SR, Binkley J, Orvis J, Shah P, Wymore F. The *Aspergillus* Genome Database: multispecies curation and incorporation of RNA-Seq data to improve structural gene annotations. Nucleic Acids Res. 2014;42:705-710.

6. Knuf C, Nielsen J. *Aspergilli*: systems biology and industrial applications. Biotechnol J. 2012;7:1147-55.

7. Chinese citric acid industry begins to consolidate. In: Analysis. F.O. Licht Renewable Chemicals. 2011. http://stage.renewablechemicals.agra-net.com/chinese-citric-acid-industry-begins-to-consolidate/. Accessed 6 July 2017.

8. Citric Acid. In: Chemical Economics Handbook. IHS. 2015. https://www.ihs.com/products/citric-acid-chemical-economics-handbook.html. Accessed 6 July 2017.

9. Dhillon GS, Brar SK, Kaur S, Verma M. Screening of agro-industrial wastes for citric acid bioproduction by *Aspergillus niger* NRRL 2001 through solid state fermentation. J Sci Food Agr. 2013;93:1560-1567.

10. Papagianni M. Advances in citric acid fermentation by *Aspergillus niger*: Biochemical aspects, membrane transport and modeling. Biotechnol Adv. 2007;25:244-63.

11. Orth JD, Thiele I, Palsson BØ. What is flux balance analysis? Nat Biotechnol. 2010;28:245-8.

12. Max B, Salgado JM, Rodríguez N, Cortés S, Converti A, Domínguez JM. Biotechnological production of citric acid. Braz J Microbiol. 2010;41:862-75.

13. Andersen MR, Nielsen ML, Nielsen J. Metabolic model integration of the bibliome, genome, metabolome and reactome of *Aspergillus niger*. Mol Syst Biol. 2008;4:178.

14. Andersen MR, Lehmann L, Nielsen J. Systemic analysis of the response of *Aspergillus niger* to ambient pH. Genome Biol. 2009;10:R47.

15. Schneider KD, Van Straaten P, Orduña D, Mira R, Glasauer S, Trevors J, Fallow D, Smith PS. Comparing phosphorus mobilization strategies using *Aspergillus niger* for the mineral dissolution of three phosphate rocks. J Appl Microbiol. 2010;108:366-74.

16. Torres NV, Riol-Cimas JM, Wolschek M, Kubicek CP. Glucose transport by *Aspergillus niger*: the low-affinity carrier is only formed during growth on high glucose concentrations. Appl Microbiol Biot. 1996;44:790-4.

17. Papagianni M, Mattey M. Modeling the mechanisms of glucose transport through the cell membrane of *Aspergillus niger* in submerged citric acid fermentation processes. Biochem Eng J. 2004;20:7-12.

18. Gonzalez JE, Long CP, Antoniewicz MR. Comprehensive analysis of glucose and xylose metabolism in *Escherichia coli* under aerobic and anaerobic conditions by 13 C metabolic flux analysis. Metab Eng. 2017;39:9-18.

19. Legiša M, Kidrič J. Initiation of citric acid accumulation in the early stages of *Aspergillus niger* growth. Appl Microbiol Biot. 1989;31:453-7.

20. Akaike H. Information theory and an extension of the maximum likelihood principle. In: Petrov BN, Csáki F. 2nd International Symposium on Information Theory. Budapest: Akadémiai Kiadó; 1973. p. 267–281.

21. Capuder M, Šolar T, Benčina M, Legiša M. Highly active, citrate inhibition resistant form of *Aspergillus niger* 6-phosphofructo-1-kinase encoded by a modified pfkA gene. J Biotechnol. 2009;144:51-7.

22. De Jongh WA, Nielsen J. Enhanced citrate production through gene insertion in *Aspergillus niger*. Metab Eng. 2008;10:87-96.

23. Nishi A. Role of polyphosphate and phospholipid in germinating spores of *Aspergillus niger*. J Bacteriol. 1961;81:10.

24. Huson DH, Richter DC, Rausch C, Dezulian T, Franz M, Rupp R. Dendroscope: An interactive viewer for large phylogenetic trees. BMC Bioinformatics. 2007;8:1.

25. Ruijter GJ, van de Vondervoort PJ, Visser J. Oxalic acid production by *Aspergillus niger*: an oxalate-non-producing mutant produces citric acid at pH 5 and in the presence of manganese. Microbiology. 1999;145:2569-76.

26. Kalisz HM, Hecht HJ, Schomburg D, Schmid RD. Effects of carbohydrate depletion on the structure, stability and activity of glucose oxidase from *Aspergillus niger*. BBA-Protein Struct M. 1991;1080:138-142.

27. Swoboda BE, Massey V. Purification and properties of the glucose oxidase from *Aspergillus niger*. J Biol Chem. 1965;240:2209-15.

28. Wilson R, Turner APF. Glucose oxidase: an ideal enzyme. Biosens Bioelectron. 1992;7:165-85.

29. Rodríguez H, Fraga R. Phosphate solubilizing bacteria and their role in plant growth promotion. Biotechnol Adv. 1999;17:319-39.

30. Chuang CC, Kuo YL, Chao CC, Chao WL. Solubilization of inorganic phosphates and plant growth promotion by *Aspergillus niger*. Biol Fert Soils. 2007;43:575-584.

31. Lu H, Cao W, Ouyang L, Xia J, Huang M, Chu J, Zhuang Y, Zhang S, Noorman H. Comprehensive reconstruction and *in silico* analysis of *Aspergillus niger* genome-scale metabolic network model that accounts for 1210 ORFs. Biotechnol Bioeng. 2017;114:685-95.

32. Delmas S, Llanos A, Parrou JL, Kokolski M, Pullan ST, Shunburne L, Archer DB. Development of an unmarked gene deletion system for the filamentous fungi *Aspergillus niger* and *Talaromyces versatilis*. Appl Environ Microb. 2014;80:3484-7.

3.3 Summary

In this chapter, a dynamic model of *A. niger* organic acid fermentation was described. This is a significant contribution of this thesis, and the work is presented as a publication (Upton *et al*, 2017) with a few alterations. The dynamic model built on previous modelling work, and was shown to accurately capture physiological characteristics in response to different environmental and genetic conditions. The applicability of the dynamic model as a predictive metabolic engineering platform was demonstrated.

Chapter 4: Engineering of *Aspergillus niger*

4.1 Introduction

In previous chapters of this thesis, a physiological description of *A. niger* organic acid fermentation was given. This was used to design a dynamic model, which was shown to capture the physiological characteristics in computer simulations. The drive behind this work was to establish a predictive platform to suggest targets for rational engineering of *A. niger*, to increase citric acid productivity. The development of new strains by targeted engineering is required to test model predictions and make further refinements. The *A. niger* engineering tool-kit is described in Chapter 1. The work reported in this chapter applied a number of these tools to create new strains. In all cases, the wild-type citric acid producing ATCC1015 strain was used as the starting point.

A gene deletion strategy that enables the creation of multiple knock-out strains (Delmas *et al*, 2014) was used to probe the characteristics of oxalate- and gluconate-negative strains. Oxaloacetate hydrolase (OAH) is the enzyme that produces oxalic acid (Kubicek *et al*, 1988), and the gene encoding this (*oah*) was deleted. Gluconic acid is produced by extracellular glucose oxidase (GOX) (Mischak *et al*, 1985), and the gene responsible (*gox*) was also deleted. Two single knock-outs were created, Δ*oah* and Δ*gox*, as well as a double knock-out, Δ*oah* Δ*gox*. The empirical system developed previously in this project was used to characterise these engineered strains to determine the effect on citric acid production at initial pH 7.

As well as switching off expression, tools for gene over-expression were used. A prediction of the dynamic model was that glucose uptake would be significantly increased if the low-affinity glucose transporter were constitutively active. Constitutive expression of a low-affinity glucose transporter was also observed in an industrial strain (Yin *et al*, 2017). As

glucose uptake is a key factor in citric acid production (Torres *et al*, 1994), a candidate low-affinity glucose transporter gene was constitutively over-expressed. The effect on citric acid fermentation was determined.

In addition to knocking out and knocking up expression of target genes, new metabolic activities were knocked in. These targeted different points of the citric acid producing metabolic pipeline. These targets were informed by the current mechanistic understanding of citric acid fermentation, reviewed in Chapter 1. One of these was the introduction of cytosolic citrate synthase activity, which *A. niger* does not ordinarily have (Jaklitsch *et al*, 1991). It is supposed that mitochondrial citrate export may be a rate-limiting step (De Jongh and Nielsen, 2008). It was hypothesised that the presence of cytosolic citrate synthase would bypass such a constraint, and therefore increase citric acid production. The dynamic model supported this hypothesis. The other target for knock-in was a deregulated 6-phosphofructo-1-kinase (PFK1) gene. The gene is a mutated and truncated version of the native PFK1 gene, that encodes a constitutively active and citrate-insensitive PFK1. This target was chosen based on previous studies reported in the literature (Capuder *et al*, 2009). An increase in citric acid production was previously observed, but in a different strain. As PFK1 is a key regulatory point of glycolysis and high glycolytic flux is crucial to citric acid production, it was important to investigate this in the ATCC1015 strain.

The final engineering tool applied in this work was antisense-RNA mediated knock-down. This was used to down-regulate the expression of an exopolyphosphatase (PPX) gene, and a phosphate transporter (PHO1) gene. The PPX gene was targeted based on modelling predictions. It was hypothesised that knock-down of PPX would decrease the rate of release of stored phosphate, thereby decreasing growth and increasing citric acid production. The dynamic model supported this hypothesis. It was necessary to test this. Likewise, the PHO1 gene was targeted to validate predictions made by the dynamic model. It was suggested that a slower phosphate uptake would delay the onset of phosphate-limited growth and citric acid

production. Knock-down of a phosphate transporter was performed in an attempt to reduce the rate of phosphate uptake and test these predictions.

4.1.1 Aims of this Chapter

The work described in this chapter aimed to develop and apply engineering strategies to create new strains of interest, for characterisation in fermentation experiments and to test model predictions.

4.2 Methods

4.2.1 Molecular biology techniques

4.2.1.1 Polymerase chain reaction (PCR)

PCR was used to clone regions of genomic DNA (gDNA) or plasmid DNA, or to screen transformants. Unless described otherwise, PCR reactions contained 0.2 U Phusion® High-Fidelity DNA polymerase (Thermo Fisher Scientific), 1× HF buffer, 200 µM dNTPs, 50-100 ng template DNA and 0.5 µM primers in a reaction volume of 50 µl. If cloning from plasmid DNA and using the PCR product in vector construction, only 0.2-1 ng template DNA was used in order to minimise background in colony screening of bacterial transformants. The PCR programme was: initial denaturation at 98°C for 2 minutes, then 30 cycles of denaturation at 98°C for 10 seconds, annealing for 30 seconds, and extension at 72°C for 15 seconds/kb, then a final extension step at 72°C for 7 minutes. Annealing temperature depended on the primer pair and was calculated by the NEB Tm Calculator (New England Biolabs; http://tmcalculator.neb.com). Primers were designed using the NCBI Primer-BLAST tool (https://www.ncbi.nlm.nih.gov/tools/primer-blast). Primers were synthesised by Integrated DNA Technologies (IDT).

4.2.1.2 Overlap-extension PCR

Overlap-extension PCR was used to join together DNA fragments. 30-bp overlapping tails were added to the 5’ end of innermost primers. The two overlapping DNA fragments were joined in a 50 µl annealing reaction containing 1 U Phusion HF DNA polymerase (Thermo Fisher Scientific), 200 ng DNA fragments, 400 µM dNTPs, and 1× HF buffer. The annealing programme was: initial denaturation at 94ºC for 5 minutes, then 10 cycles of denaturation at 94ºC for 30 seconds, annealing at 60ºC for 90 seconds, and extension at 72ºC for 90 seconds. The annealed product was amplified in a 100 µl PCR reaction containing 50 µl of the annealing reaction, 1 U Phusion

HF DNA polymerase (Thermo Fisher Scientific), 1 µM outermost primers, 400 µM dNTPs, and 1× HF buffer. The PCR programme was: initial denaturation at 94ºC for 2 minutes, then 35 cycles of denaturation at 94ºC for 30 seconds, annealing at 60ºC for 30 seconds, and extension at 72ºC for 90 seconds, then a final extension step at 72ºC for 10 minutes. The annealed product was gel extracted.

4.2.1.3 Agarose gel electrophoresis

DNA fragments were separated by agarose gel electrophoresis at 100-120 V for 20-50 minutes. Gels consisted of 1% (w/v) agarose in 0.5× Tris-Borate-EDTA (TBE) buffer (45 mM Tris, 45 mM boric acid, 1 mM EDTA) and 0.5 µg/ml ethidium bromide. Samples were mixed with 6× purple gel loading dye (New England Biolabs). The 2-log DNA ladder (New England Biolabs) was used as the molecular weight marker, unless stated otherwise. DNA was visualised by staining with ethidium bromide under UV light using the UVI gel documentation system (UVItec).

4.2.1.4 Purification of PCR products

PCR products were purified using the NucleoSpin® Gel and PCR clean-up kit (Macherey-Nagel), following the manufacturer's instructions. DNA was eluted in 15 µl elution buffer NE.

4.2.1.5 Gel extraction of DNA fragments

Mixtures of DNA fragments were separated by agarose gel electrophoresis with a long running time of 50 minutes. The fragment of interest was visualised by UV light using a UV transilluminator (UVItec) and the band cut out using a scalpel. DNA was extracted from agarose and purified using the NucleoSpin® Gel and PCR clean-up kit (Macherey-Nagel), following the manufacturer's instructions. DNA was eluted in 15 µl elution buffer NE.

4.2.1.6 DNA quantification

DNA concentration was determined using a NanoDrop 1000 spectrophotometer (Thermo Fisher Scientific) with a 1.2 µl sample.

4.2.1.7 In-Fusion® HD cloning

The In-Fusion® HD cloning kit (Clontech) was used to insert DNA fragments into plasmids, following the manufacturer's instructions. 15-bp tails were added to the 5’ end of primers with homology to the plasmid insertion site. The plasmid was linearised by restriction digest at the insertion site. A reaction volume of 5 µl was used containing 1 µl In-Fusion® HD enzyme premix, 30 ng DNA fragment, and 30 ng linearised plasmid. The reaction was incubated at 50°C for 15 minutes. After cooling on ice, 5 µl of the reaction was used in bacterial transformation.

4.2.1.8 Bacterial transformation

Escherichia coli XL10-Gold ultracompetent cells (Agilent Technologies) were used and transformed following the manufacturer’s instructions. 50 µl cells were thawed on ice and gently mixed with plasmid DNA. The cells were incubated on ice for 30 minutes, then heat-shocked at 42°C for 30 seconds, then incubated on ice for 2 minutes. The cells were recovered by addition of 200 µl SOC medium and incubation at 37°C for 1 hour with shaking at 200 rpm. The cells were plated (50 µl per plate) on Luria-Bertani broth (LB) agar containing 50 mg/L carbenicillin. For blue-white screening, 50 µl 2% (w/v) X-Gal (5-bromo-4-chloro-3-indolyl β-D-galactopyranoside) in dimethylformamide and 50 µl 0.1 M isopropyl-β-thiogalactopyranoside (IPTG) were spread on plates prior to inoculation. Plates were incubated at 37°C overnight.

4.2.1.9 Colony screening

To identify transformants containing the desired plasmid DNA, screening of bacterial colonies was performed by PCR of cultures grown from single colonies. Single colonies were picked using a sterile pipette tip and placed in 3 ml LB containing 50 mg/L carbenicillin. In blue-white screening, only white colonies were picked. Bacterial cultures were incubated at 37°C overnight with shaking at 200 rpm. 1 µl of a 1:10 dilution of culture was used as template in a 10 µl PCR reaction. PCR was done as previously described, except that the initial denaturation step was extended to 5 minutes and the annealing time decreased to 10 seconds. Primers were designed to amplify a 0.4-0.6 kb region, using one primer internal to the insert and the other primer external to the insert. The 10 µl PCR reactions were run on agarose gel electrophoresis to identify positive transformants.

4.2.1.10 Storage of bacterial transformants

Glycerol stocks were made for long-term storage of bacterial transformants. 200 µl culture was mixed with 200 µl 50% (v/v) glycerol and stored at −80°C.

4.2.1.11 Preparation of plasmid DNA

Plasmid DNA was prepared from bacterial cultures. 3 ml LB containing 50 mg/L carbenicillin was inoculated with the relevant bacterial transformant. Cultures were incubated at 37°C overnight with shaking at 200 rpm. Plasmid DNA was isolated and purified from bacterial cultures using the Wizard® Plus SV miniprep kit (Promega), following the manufacturer's instructions. Plasmid DNA was eluted in 100 µl nuclease-free water. Plasmid DNA was concentrated by ethanol precipitation. Plasmid DNA was made up to a volume of 500 µl with dH_2O, and mixed with 50 µl 5 M NaCl and 1 ml 100% ethanol in a 1.5 ml Eppendorf tube. After 10 minutes at −80°C, plasmid DNA was centrifuged at full speed for 15 minutes in a microcentrifuge. The supernatant was discarded and the DNA pellet resuspended in 1 ml 70% ethanol, followed by centrifugation at full speed for 5 minutes. The

supernatant was discarded and residual ethanol was evaporated in a Savant™ SpeedVac™ DNA concentrator (Thermo Fisher Scientific). The plasmid DNA pellet was resuspended in 20 µl nuclease-free water.

4.2.1.12 Restriction endonuclease digestion of plasmid DNA

Plasmid DNA was digested by restriction endonucleases as an extra step to confirm plasmid integrity or to create linear plasmid DNA for In-Fusion® HD cloning. Digestion reactions contained 1 µg DNA, 10 U restriction enzymes, and 1× compatible buffer in a reaction volume of 20 µl. Reactions were incubated at 37°C for 1 hour. Linearised plasmid was isolated by gel extraction.

4.2.1.13 DNA sequencing

DNA sequencing was used to confirm plasmid integrity. DNA sequencing was performed by DNA Sequencing and Services (MRC-PPU, University of Dundee, Scotland; https://www.dnaseq.co.uk) using an Applied Biosystems 3730 capillary DNA sequencer (Applied Biosystems). Sequencing primers were designed at intervals of 0.5-1 kb across the insert, and included primers flanking the insert.

4.2.2 Polyethylene glycol-mediated protoplast transformation of *Aspergillus niger*

A. niger was transformed by polyethylene glycol (PEG)-mediated protoplast transformation, with reference to previously described protocols (Delmas *et al*, 2014).

4.2.2.1 Creation of protoplasts

Protoplasts were created by treatment of mycelia with lysing enzymes. Mycelia were grown up in 200 ml *Aspergillus* minimal medium (AMM) (10 g/L glucose, 6 g/L $NaNO_3$, 1 g/L casamino acids, 0.52 g/L KCl, 0.52 g/L

$MgSO_4.7H_2O$, 1.52 g/L KH_2PO4, 0.008 mg/L $Na_2B_4O_7.10H_2O$, 0.16 mg/L $CuSO_4.5H_2O$, 0.2562 mg/L $FeCl_3.6H_2O$, 0.1212 mg/L $MnSO_4.H_2O$, 0.16 mg/L $NaMoO_4.2H_2O$, 0.00285 g/L $ZnSO_4.7H_2O$ [pH 6.5]) for 18 hours at 30°C with shaking at 180 rpm in 1 litre flasks. AMM was supplemented with 10 mM uridine for pyrG negative strains. Cultures were inoculated with 1×10^6 spores/ml. Mycelia were harvested by filtration through a double layer of sterile Miracloth (Calbiochem), and washed with 100 ml ice-cold mycelium wash buffer (0.6 M $MgSO_4.7H_2O$). Mycelia were transferred to a 50 ml Falcon tube and resuspended in 5 ml/g mycelial wet weight ice-cold MM buffer (1.2 M $MgSO_4.7H_2O$, 20 mM MES [pH 5.8]). The mycelial suspension was transferred to a 1 litre flask, and mixed with 100 mg/g mycelial wet weight lysing enzymes (from *Trichoderma harzianum*; Sigma) and 100 mg/g mycelial wet weight bovine serum albumin (BSA). The suspension was incubated at 30°C with shaking at 80 rpm for 30 minutes then 50 rpm for 2-3 hours, until sufficient protoplast formation was observed under the microscope. The suspension was slowly filtered through sterile polyallomer wool, and protoplast suspension collected in 50 ml Falcon tubes (15 ml per tube) on ice. 30 ml ice-cold NM buffer (1 M NaCl, 20 mM MES [pH 5.8]) was added to each tube, and mixed gently by inversion. The protoplast suspensions were centrifuged at 2500 rpm for 10 minutes at 4°C in a benchtop centrifuge. The supernatants were discarded, and each pellet was resuspended in 1 ml ice-cold STC (1.2 M sorbitol, 10 mM Tris, 50 mM $CaCl_2.2H_2O$ [pH 7.5]). The protoplast resuspensions were pooled in a 50 ml Falcon tube, and ice-cold STC was added up to 50 ml, with gentle mixing by inversion. The protoplast suspension was centrifuged at 2000 rpm for 10 minutes at 4°C in a benchtop centrifuge. The supernatant was discarded, and the pellet resuspended in 1 ml ice-cold STC. Protoplasts were counted using an Improved Neubauer haemocytometer (Hawksley), and diluted to 5×10^7/ml in ice-cold STC in sterile 1.5 ml Eppendorf tubes.

4.2.2.2 Storage of protoplasts

Long-term storage of protoplasts was achieved by use of the Mr. Frosty™ freezing container (Nalgene, Thermo Scientific), that has a cooling rate of

−1°C per minute. Previous studies showed that storage of protoplasts at −80°C using the Mr. Frosty™ retained 60% viability (de Bekker *et al*, 2009). 300 µl aliquots of protoplasts (5×10^7/ml) in 1.5 ml Eppendorf tubes were cooled to −80°C in the Mr. Frosty™ and stored at −80°C. Protoplast aliquots were thawed in a 37°C water bath for 90 seconds then kept on ice prior to transformation.

4.2.2.3 Transformation of protoplasts

3 µg plasmid DNA was used per transformation and added to a 15 ml Falcon tube with 10 µl STC prior to mixing with protoplasts. This was done to minimise the osmotic damage to protoplasts on contact with the aqueous plasmid DNA solution. 100 µl protoplast suspension (5×10^7/ml) was added and gently mixed, then incubated at room temperature for 25 minutes. Negative control transformations were performed by using STC in place of plasmid DNA. 200 µl PEG solution (60% (w/v) PEG 4000, 10 mM Tris, 50 mM $CaCl_2.2H_2O$ [pH 7.5]) was added gradually with gentle mixing, following by a further 200 µl and then 850 µl. After 20 minutes incubation at room temperature, ice-cold STC was added up to 10 ml and mixed gently by inversion. Centrifugation was then performed at 2000 rpm for 10 minutes at 4°C in a benchtop centrifuge. The supernatant was discarded and the protoplasts were resuspended in 300 µl STC. 100 µl aliquots of this suspension were plated on sorbitol-AMM (AMM as previously described, containing 1.2 M sorbitol and 1.5% (w/v) agar). Plates were incubated at 30°C, until sporulating transformant colonies were observed.

4.2.2.4 Propagation and purification of transformant colonies

Sporulating transformant colonies were propagated and purified by swabbing spores onto AMM slants (AMM as previously described, containing 1.5% (w/v) agar) using a sterile cotton wool swab. Slants were incubated at 37°C until sporulation. Spores were harvested by swabbing with a sterile cotton

wool swab and suspended in 1 ml saline Tween (0.1% (v/v) Tween 80, 9 g/L NaCl).

4.2.2.5 PCR screening of transformant colonies

To confirm genomic plasmid integration, transformant colonies were screened by PCR using one primer internal to the insert and the other primer external to the insert. The primer pair was designed to amplify a 0.4-0.6 kb region. PCR template was prepared by scraping mycelia with a pipette tip from an AMM slant inoculated with spores of the transformant colony. Mycelia were placed into a 100 µl solution containing 10 mM NaCl, 10 mM Tris-HCl (pH 7.5), 1 mM EDTA and 2 µl 1 M NaOH. The mycelial suspension was boiled at 100°C for 10 minutes and vortexed. 1 µl of this was used as DNA template in a 10 µl PCR reaction.

4.2.2.6 Storage of transformant strains

Long-term stocks of transformant strains were made by use of the Microbank™ bacterial and fungal preservation system (Pro-Lab Diagnostics). 700 µl spore suspension was added per vial and mixed gently by inversion. After 2 minutes incubation, liquid was decanted and vials were stored at −80°C.

4.2.3 Creation of ATCC1015 *pyrG* negative strain

Engineering was performed using the *pyrG* selectable marker gene, therefore required a *pyrG* negative strain. As the engineering work described in this chapter was done on the ATCC1015 strain, a *pyrG* negative strain of ATCC1015 was required and was created by deletion of the *pyrG* gene. This was achieved by homologous recombination. ATCC1015 was transformed with a fragment of linear DNA containing 2 kb up- and 1.5 kb down-stream flanking regions of the *pyrG* gene (GenBank accession number EHA25155), kindly given by M Kokolski (University of Nottingham). PEG-mediated protoplast transformation was used, as previously described. Sorbitol-AMM

was supplemented with 1.6 mM uridine to allow growth of uridine auxotrophic *pyrG* negative transformants. After protoplast regeneration, successful deletions were selected by resistance to 5-fluoroorotic acid (5-FOA) (Fluorochem) and uridine auxotrophy, and confirmed by PCR and DNA sequencing using primers external to the *pyrG* gene (pyrG_ex_fw and pyrG_ex_rv; Table 4.2).

4.2.4 Targeted gene deletion

Targeted gene deletion was performed following previously described procedures (Delmas *et al*, 2014). The ATCC1015 Δ*pyrG* strain was used.

4.2.4.1 Construction of deletion vectors

Deletion vectors were constructed from the pc3 plasmid, kindly given by M Kokolski (University of Nottingham). A 3 kb deletion fragment containing 1.5 kb up- and down-stream flanking regions of the target gene was made by overlap extension PCR. The deletion fragment was inserted into the pc3 plasmid between the NotI and SpeI restriction sites. The size of deletion was between 1 kb and 2 kb. For target genes greater than 2 kb, the deletion region was designed to include the transcription and translation start sites to ensure gene knock-out. The primers pc3_fw and pc3_rv (Table 4.2) were designed flanking the insertion site, and were used in PCR screening of bacterial transformants and in DNA sequencing of deletion constructs.

4.2.4.2 Screening of knock-out strains

It was observed that plasmid excision events occurred without the need for growth on uridine-containing media. Spores from transformant strains propagated on AMM without uridine produced *pyrG* negative colonies, therefore extra growth cycles in the presence of uridine were omitted. 50 µl spore suspensions of transformants were plated on AMM containing 1.6 mM uridine and 1.5 g/L 5-FOA. A filter sterile (0.22 µm) stock solution of 5-FOA was made in dimethylsulphoxide (DMSO) at 100 mg/ml, and stored at 4°C

with protection from light. Uridine and 5-FOA were added to media after autoclaving. The presence of 5-FOA at 1.5 g/L was necessary to prevent growth of *pyrG* positive strains and ensure only *pyrG* negative colonies could form. The spore concentration of inoculum varied and was adjusted to give around 5 colonies per plate. Plates were incubated at 37°C for 3 days, by which time sporulating colonies appeared. The *pyrG* negative colonies were screened by PCR to identify knock-out strains. Spores were carefully picked from colonies using a sterile pipette tip. A potato dextrose agar (PDA) slant containing 10 mM uridine was inoculated with spores picked from one colony. PDA slants were incubated at 37°C for 1 day to grow mycelia for use in PCR screening. Two PCR reactions were done for each colony; one using primers external to the deletion site and one using primers internal to the deletion site. Knock-out strains were identified by a positive external PCR and a negative internal PCR, and these were propagated on PDA slants containing 10 mM uridine. Knock-outs were tested for uridine auxotrophy to confirm purity of the *pyrG* negative phenotype. Knock-outs were confirmed by DNA sequencing of the region flanking the deletion site, using the external primers.

4.2.4.3 Deletion of the gene encoding oxaloacetate hydrolase

The ATCC1015 gene encoding oxaloacetate hydrolase (*oah)* was identified as GenBank accession number EHA22250. No other genes encoding oxaloacetate hydrolase were identified in the ATCC1015 genome. The deletion vector pc3-*oah* was constructed to delete the 1.7 kb *oah* gene, creating the ATCC1015 Δ*pyrG* Δ*oah* strain. The primers oah_up_fw and oah_up_rv were used to clone the up-stream flanking region, and the primers oah_down_fw and oah_down_rv were used to clone the down-stream flanking region. The external primers oah_ex_fw and oah_ex_rv, and the internal primers oah_int_fw and oah_int_rv were used in PCR screening to identify Δ*oah* strains. Gene deletion of *oah* was confirmed in six out of ten *pyrG* negative colonies screened. An additional six primers, oah_seq1-6, were used in DNA sequencing of the pc3-oah vector. Primers are given in Table 4.2.

4.2.4.4 Deletion of the gene encoding glucose oxidase

The ATCC1015 gene encoding glucose oxidase (*gox*) was identified as GenBank accession number EHA27180. Two other genes in the ATCC1015 genome were identified as having putative glucose oxidase function (GenBank accession numbers EHA23687 and EHA25730), however, EHA27180 was chosen as the target for gene deletion due to greater homology to characterised glucose oxidases from *A. niger* (GenBank accession numbers FJ979866, DQ836361, and X16061). The deletion vector pc3-gox was constructed to delete a 1.6 kb region from the 2.8 kb *gox* gene, creating the ATCC1015 Δ*pyrG* Δ*gox* strain. The deletion region was designed to include the promoter, and transcription and translation start sites. The primers gox_up_fw and gox_up_rv were used to clone the up-stream flanking region, and the primers gox_down_fw and gox_down_rv were used to clone the down-stream flanking region. The external primers gox_ex_fw and gox_ex_rv, and the internal primers gox_int_fw and gox_int_rv were used in PCR screening to identify Δ*gox* strains. Gene deletion of *gox* was confirmed in nine out of twenty *pyrG* negative colonies screened. An additional two primers, gox_seq1-2, were used in DNA sequencing of the pc3-gox vector. Primers are given in Table 4.2.

4.2.4.5 Creation of the Δoah Δgox *double knock-out strain*

To create the Δ*oah* Δ*gox* double knock-out, the *gox* gene was deleted from the Δ*oah* strain, following the same procedure used to create the single *gox* knock-out. Gene deletion of *gox* was confirmed in four out of twenty Δ*oah pyrG* negative colonies screened, giving the ATCC1015 Δ*pyrG* Δ*oah* Δ*gox* strain.

4.2.5 Application of Tet-on expression system

The Tet-on expression system was previously developed for gene expression in *A. niger* (Meyer *et al*, 2011b), and was applied in this work for the over-expression of *A. niger* genes and the expression of new metabolic

activities. A new expression vector was constructed in this work from the pc3 and pVG2.2 plasmids, and was designed for targeting to the *pyrG* locus in genomic integration. The new plasmid was named pc3-pyrG-VG2. The pVG2.2 plasmid was obtained from the Fungal Genetics Stock Center (FGSC). Expression vectors were transformed into the ATCC1015 Δ*pyrG* strain. Transformant strains were *pyrG* positive and grown in the absence of uridine to maintain the *pyrG* positive phenotype. Expression was induced by the addition of doxycycline (Dox). Doxycycline hyclate (Sigma) was dissolved in dH_2O at 50 mg/ml to prepare a stock solution. The solution was filter sterilised (0.22 µm) and stored at −20°C with protection from light. Dox was added to media after autoclaving at varying concentrations, between 5 and 50 µg/ml. Negative controls were performed, either by growing the same engineered strain in the absence of Dox or by using a strain transformed with the pc3-pyrG-VG2 empty vector.

4.2.5.1 Construction of the pc3-pyrG-VG2 expression vector

A 3 kb region of homology was inserted into the pc3 plasmid at the NotI restriction site, creating the pc3-pyrG plasmid. The 3 kb insert was cloned from the *pyrG* deletion fragment using the pc3_pyrG_del_fw and pc3_pyrG_del_rv primers (Table 4.2). The insert contained 1.5 kb flanking regions of the *pyrG* deletion site. The tails added to primers for In-Fusion® HD cloning were designed to disrupt the NotI restriction site in the pc3 plasmid, so that the pc3-pyrG plasmid contained a unique NotI restriction site between the two flanking regions. This facilitated insertion of the pVG2.2 plasmid DNA encoding the Tet-on expression system (PgpdA-rtTA-TcgrA-tetO7-Pmin-TrpC) into the pc3-pyrG plasmid at this site. This was achieved using the primers pc3_pyrG_VG2_fw and pc3_pyrG_VG2_rv (Table 4.2). The resulting plasmid was named pc3-pyrG-VG2, and was used as the expression vector in this work. The primers pyrG_del_fw and pc3_rv were used in PCR screening of the pc3-pyrG plasmid, and the primers VG2_fw and pc3_pyrG_col_rv were used in PCR screening of the pc3-pyrG-VG2 plasmid. An additional five primers, VG2_seq1-5, were used in plasmid DNA sequencing. Primers are given in Table 4.2.

4.2.5.2 Over-expression of a glucose transporter

The ATCC1015 gene with GenBank accession number EHA22798 was identified as a putative low-affinity glucose transporter gene, with 79% identity to a low-affinity glucose transporter from *Aspergillus nidulans* (GenBank accession number CAH23705) (Forment *et al*, 2006). The 1.8 kb gene was cloned using the primers GLU_fw and GLU_rv (Table 4.2), and inserted into the pc3-pyrG-VG2 plasmid at the PmeI restriction site, creating the pc3-pyrG-VG2-GLU vector. The primers GLU_col_fw and pc3_pyrG_VG2_col_rv were used in PCR screening, and an additional two primers were used in plasmid DNA sequencing, GLU_seq1-2 (Table 4.2). Two transformant strains were isolated and propagated, and named ATCC1015 Δ*pyrG* GLU 1 and ATCC1015 Δ*pyrG* GLU 2.

4.2.5.3 Expression of cytosolic citrate synthase

The ATCC1015 gene encoding mitochondrial citrate synthase was identified as GenBank accession number EHA28609. Two other citrate synthase genes were identified (GenBank accession numbers EHA26823 and EHA18674), however, EHA28609 was chosen for engineering in this work due to complete homology to two characterised citrate synthases from *A. niger* strains WU-2223L and N400 (GenBank accession numbers BAA09691 and CAB77625, respectively). The mitochondrial import signal and cleavage site were reported for the homologous citrate synthases, as well as putative peroxisomal import signals (Kirimura *et al*, 1999c; Ruijter *et al*, 2000). The 1.7 kb ATCC1015 citrate synthase gene was cloned without the import signals for targeting to the cytosol, using the primers CIT_fw and CIT_rv (Table 4.2). The forward primer included the translation start site and ribosome binding site, and the reverse primer included the translation stop codon. The resulting cytosolic citrate synthase gene was inserted into the pc3-pyrG-VG2 plasmid at the PmeI restriction site, creating the pc3-pyrG-VG2-CIT vector. The primers CIT_col_fw and pc3_pyrG_VG2_col_rv were used in PCR screening, and an additional two primers were used in plasmid DNA sequencing, CIT_seq1-2 (Table 4.2). Two transformant strains were

isolated and propagated, and named ATCC1015 Δ*pyrG* CIT 1 and ATCC1015 Δ*pyrG* CIT 2.

4.2.5.4 Expression of mutated truncated 6-phosphofructo-1-kinase

The ATCC1015 gene encoding 6-phosphofructo-1-kinase (PFK1) was identified as GenBank accession number EHA18863. With reference to previous studies (Capuder *et al*, 2009), a mutated truncated form of PFK1 (mtPFK1) was expressed. Overlap extension PCR was applied to create a truncated form of the PFK1 gene (tPFK1), using the primers PFK1_up_fw, PFK1_up_rv, PFK1_down_fw, and PFK1_down_rv (Table 4.2). The PFK1_down_fw primer included a translation stop codon. The resulting tPFK1 gene was inserted into the pc3 plasmid between the NotI and SpeI restriction sites, creating the pc3-tPFK1 plasmid. To create the mtPFK1 gene, overlap extension PCR was used, with the pc3-tPFK1 plasmid as template DNA. The primers PFK1_up_fw, mtPFK1_up_rv, mtPFK1_down_fw, and PFK1_down_rv were used (Table 4.2). The mtPFK1_down_fw primer was mutagenic, switching the ACC codon for GAG to mutate threonine 89 to glutamate. The mtPFK1 gene was inserted into the pc3 plasmid at the NotI restriction site, creating the pc3-mtPFK1 plasmid. The pc3-tPFK1 and pc3-mtPFK1 plasmids were previously constructed in an attempt to delete the native PFK1 gene, replacing it with either tPFK1 or mtPFK1. As this strategy was unsuccessful, the 1.5 kb mtPFK1 gene was cloned from the pc3-mtPFK1 plasmid using the primers mtPFK1_fw and mtPFK1_rv (Table 4.2), for insertion into the pc3-pyrG-VG2 plasmid at the PmeI restriction site, creating the pc3-pyrG-VG2-mtPFK1 vector. The primers mtPFK1_col_fw and pc3_pyrG_VG2_col_rv were used in PCR screening, and an additional three primers were used in plasmid DNA sequencing, mtPFK1_seq1-3 (Table 4.2). Two transformant strains were isolated and propagated, and named ATCC1015 Δ*pyrG* mtPFK1 1 and ATCC1015 Δ*pyrG* mtPFK1 2.

4.2.6 Antisense RNA-mediated knock-down

To knock-down expression of target genes, antisense RNA was expressed. The pc3-pyrG-VG2 expression vector was used, with approximately 0.5 kb antisense inserts. The antisense RNA was designed to bind to an exonic region of the messenger RNA (mRNA) of the target gene, near to or spanning the translation start site. Expression of antisense RNA was induced by addition of Dox. Negative controls were performed, either by growing the same engineered strain in the absence of Dox or by using a strain transformed with the pc3-pyrG-VG2 empty vector.

4.2.6.1 Knock-down of exopolyphosphatase

A single putative exopolyphosphatase (PPX) gene was found in the ATCC1015 genome (GenBank accession number EHA28530). The putative PPX from ATCC1015 has homology (e-value = 5e-26) to a characterised PPX from *Saccharomyces cerevisiae* (GenBank accession number AAA65933) (Wurst *et al*, 1995). A 0.6 kb antisense region of the ATCC1015 PPX gene was cloned using the primers PPX_KD_fw and PPX_KD_rv (Table 4.2), and inserted into the pc3-pyrG-VG2 plasmid at the PmeI restriction site, creating the pc3-pyrG-VG2-PPX_KD vector. The primers PPX_KD_col_fw and pc3_pyrG_VG2_col_rv were used in PCR screening (Table 4.2). Two transformant strains were isolated and propagated, and named ATCC1015 Δ*pyrG* PPX KD 1 and ATCC1015 Δ*pyrG* PPX KD 2.

4.2.6.2 Knock-down of a phosphate transporter

A total of eight putative phosphate transporter genes were found in the ATCC1015 genome using the NCBI database (Table 4.1). To investigate these, a phylogenetic tree was constructed from a library of around 100 phosphate transporters (Chapter 3 – Figure S1). The eight candidate ATCC1015 transporters were aligned against these using MUSCLE (Edgar, 2004). CLUSTAL was used to assemble the phylogenetic tree (Higgins and Sharp, 1988). Based on the phylogenetic tree, the gene with GenBank

accession number EHA22558 was chosen for engineering in this work. A 0.5 kb antisense region of the putative ATCC1015 phosphate transporter gene was cloned using the primers PHO1_KD_fw and PHO1_KD_rv (Table 4.2), and inserted into the pc3-pyrG-VG2 plasmid at the PmeI restriction site, creating the pc3-pyrG-VG2-PHO1_KD vector. The primers PHO1_KD_col_fw and pc3_pyrG_VG2_col_rv were used in PCR screening (Table 4.2). Two transformant strains were isolated and propagated, and named ATCC1015 Δ*pyrG* PHO1 KD 1 and ATCC1015 Δ*pyrG* PHO1 KD 2.

Table 4.1. Putative phosphate transporters in the ATCC1015 strain.

ATCC 1015 locus tag	GenBank accession	Top BLASTP hit (SwissProt)	Transporter family (of SwissProt hit)	Identity (%)	E-value
ASPNIDRAFT_173247	EHA22558	P15710.1	Inorganic phosphate transporter family	37	4e-130
ASPNIDRAFT_190334	EHA20653	P25297.2	Major facilitator superfamily	34	2e-90
ASPNIDRAFT_121846	EHA27663	Q7RVX9.2	Major facilitator superfamily	61	0.0
ASPNIDRAFT_52154	EHA22720	O42885.2	Major facilitator superfamily	29	2e-42
ASPNIDRAFT_42307	EHA25335	Q9S735.1	Major facilitator superfamily	27	6e-12
ASPNIDRAFT_175394	EHA23128	Q8H074.1	Major facilitator superfamily	25	2e-26
ASPNIDRAFT_206238	EHA26306	P27514.2	Divalent anion:Na^+ symporter family	41	0.0
ASPNIDRAFT_35379	EHA27197	Q8H074.1	Major facilitator superfamily	24	2e-22

Table 4.2. Primers used in this work. Tails added to primers for In-Fusion® HD cloning or overlap extension PCR are underlined.

Primer	**Nucleotide sequence (5' to 3')**
pyrG_ex_fw	CTTTGCAGGTGTGGCTGAAC
pyrG_ex_rv	ACAGCAGTGCTTATCTGCGA
pc3_fw	TACCGCCTTTGAGTGAGCTG
pc3_rv	TTCCATTCGCCATTCAGGCT
oah_up_fw	ACCGCGGTGGCGGCCGCGCTGTGTCCATACCATCAATCC
oah_up_rv	GAATGTTGCAGACAGACAGAAAGCAAAAGAGCAGGCAGTAGTAAGCAAGAAT
oah_down_fw	TCTTTCTTATTCTTGCTTACTACTGCCTGCTCTTTTGCTTTCTGTCTGTCTGC
oah_down_rv	CGGGGGATCCACTAGTTCTCCTCTTCCCCTGCCTTT
oah_ex_fw	TAAGGCTACCCAACCCACCC
oah_ex_rv	GCTTATCTAGGCCCCTGCTG
oah_int_fw	ACCCAACCACACCATCCTTC
oah_int_rv	ACCCAGTTCCCCACTAACAC
oah_seq1	ATTAATCATTCAAGTAGCCACCAA
oah_seq2	GAGGAGACGTACCGGGGC
oah_seq3	TACTGCCTGCTCTTTTGCTTT
oah_seq4	GAATCAGGGGAGAATGAGGG
oah_seq5	GCCAGCTGGATGAGGAATG

Primer	**Nucleotide sequence (5’ to 3’)**
oah_seq6	AGCTGCAGTGCGGACTCT
gox_up_fw	ACCGCGGTGGCGGCCGCGAGATGGCAATTTCCGCGAC
gox_up_rv	GAATATTCGAGGATTGTGGGAGAGACAGCGCGTGCAAACTCACCACCAAG
gox_down_fw	CTGTCTTGACCTTGGTGGTGAGTTTGCACGCGCTGTCTCTCCCACAATCC
gox_down_rv	CGGGGGATCCACTAGTCTACGCTCATGTCCTGGTCC
gox_ex_fw	CACTATCGCCAAGCAGGGAT
gox_ex_rv	AAGGTCTCGTTGAAGGTGGC
gox_int_fw	AGCAACCAGCCTTTCCTCTC
gox_int_rv	CCCAGTTCCAGCCCTCATTT
gox_seq1	GTCTGGGACGAGGACGAAT
gox_seq2	CTACCATGGCGTGGGTACTT
pc3_pyrG_del_fw	ACCGCGGTGGCGGCCGTAAAAGCACGCACGTGTCC
pc3_pyrG_del_rv	AGTTCTAGAGCGGCCAGTATCCAGGCACACGAACC
pc3_pyrG_VG2_fw	ATCAACACCGCGGCCGCAGCGCGCAATTAACCCTCAC
pc3_pyrG_VG2_rv	ATCCTCCTTGCGGCCGCAAGGAACAGTGAGCGACCGA
pyrG_del_fw	GGCAAAGCATACGAAGGATG
VG2_fw	CCGACCGGGATCCACTTAAC
pc3_pyrG_col_rv	CATTGGTCCGTTTCCGCTTC
VG2_seq1	TCCCTGGTAGGCAGCTTTG

Primer	**Nucleotide sequence (5’ to 3’)**
VG2_seq2	GGACAGGCATCATACCCACT
VG2_seq3	TTGATATGCTGCCTGCTGAC
VG2_seq4	GCAAAGTCATAAACGGCGCT
VG2_seq5	TGTTCCTCCAATACGCAGCC
GLU_fw	CAGACATCACCGTTTAAACCGTTGTATGAATCCACCGGC
GLU_rv	CGGCATCTACTGTTTAAACAAAATGAGTTCGCGCGAGTG
GLU_col_fw	CCCCCTTCATCTCTAGCTCC
pc3_pyrG_VG2_col_rv	TACTAGGGTTGCGAGGTCCA
GLU_seq1	GTCTGTCATCCACATCGTCG
GLU_seq2	GTGCAAGCTGTACGGTGTCA
CIT_fw	CAGACATCACCGTTTAAACACATTCGCCATGGCTTCTACCGGCAAGGCCAAGG
CIT_rv	CGGCATCTACTGTTTAAACTTAGAAGGCCTCGGTGCTGTAGG
CIT_col_fw	GCCAGGTCTACAAGATCGCT
CIT_seq1	TGACTGGCGAGATCCCTACCG
CIT_seq2	AGGATGGCAAGGTCGCTCCT
PFK1_up_fw	ACCGCGGTGGCGGCCGCATATCTCCACCGCCAAACCG
PFK1_up_rv	GTCTAGGCGTTTATCGCTGCTTTTTGCTCAATCATAGTGCCGGCACAGAC
PFK1_down_fw	GGTTTCCCCGGTCTGTGCCGGCACTATGATTGAGCAAAAAGCAGCGATAA
PFK1_down_rv	CGGGGGATCCACTAGTAAGCAGCGGGAATGTCTGA

Primer	**Nucleotide sequence (5’ to 3’)**
mtPFK1_up_rv	ACCGGGGCGCTCACGGAACTCCATGCAGCGGGCGGAACCGATCAAGGTAC
mtPFK1_down_fw	TCCCGTGGTGGTACCTTGATCGGTTCCGCCCGCTGCATGGAGTTCCGTGAG
mtPFK1_fw	CAGACATCACCGTTTAAACCCCCCAACAAAAACCATCGC
mtPFK1_rv	CGGCATCTACTGTTTAAACTCTAGGCGTTTATCGCTGCT
mtPFK1_col_fw	ACAAGGTTTGTCGCCACAGT
mtPFK1_seq1	GTCCTCCGTGGCATTGAC
mtPFK1_seq2	AGGATGACATGTGCGCTATC
mtPFK1_seq3	GCTCCTCCCAGAGAACAAGG
PPX_KD_fw	CAGACATCACCGTTTAAACCTACGAGCGAGGTGCATGAT
PPX_KD_rv	CGGCATCTACTGTTTAAACATGCCTCCTTCTGAGCACAG
PPX_KD_col_fw	ACCATGTTTCTTCGTCCGGG
PHO1_KD_fw	CAGACATCACCGTTTAAACGAAGGGGGAACTGTAGACGG
PHO1_KD_rv	CGGCATCTACTGTTTAAACACGATGTGGCCAACTCCTG
PHO1_KD_col_fw	TCTTGATGGTATCCGCCGTG

4.3 Results

4.3.1 Knock-outs of the genes encoding oxaloacetate hydrolase and glucose oxidase

It is established that citric acid producing conditions rely on a low initial pH around 2.0, to prevent the competing production of the organic acids oxalic and gluconic, which occurs at higher initial pH. Oxalic acid is produced by oxaloacetate hydrolase (OAH), and gluconic acid is produced by extracellular glucose oxidase (GOX). To investigate the fermentative effects of these metabolic activities on citric acid production in the ATCC1015 strain, the genes encoding OAH and GOX were targeted for gene deletion in ATCC1015. A previously reported *A. niger* gene deletion strategy (Delmas *et al*, 2014) was applied in this work to create Δ*oah* and Δ*gox* single knock-outs, and a Δ*oah* Δ*gox* double knock-out. The *pyrG* gene was deleted from ATCC1015 to create a *pyrG* negative ATCC1015 strain for use in this engineering work. The resulting ATCC1015 Δ*pyrG* strain was used as a control strain in fermentation experiments characterising the effects of knock-outs.

To confirm an oxalate-negative phenotype, three Δ*oah* single knock-out strains were tested in a fermentation experiment at initial pH 7 (Figure 4.1). Each Δ*oah* strain tested was isolated from a different colony to confirm the phenotype was the result of the *oah* gene deletion event rather than spontaneous mutations. At day 6, the concentration of oxalic acid in the culture supernatant was determined. No oxalic acid could be detected in any of the Δ*oah* cultures, whereas the control strain produced around 1 g/L oxalic acid by day 6. This confirmed the oxalate-negative phenotype of the Δ*oah* strains, resulting from deletion of *oah*.

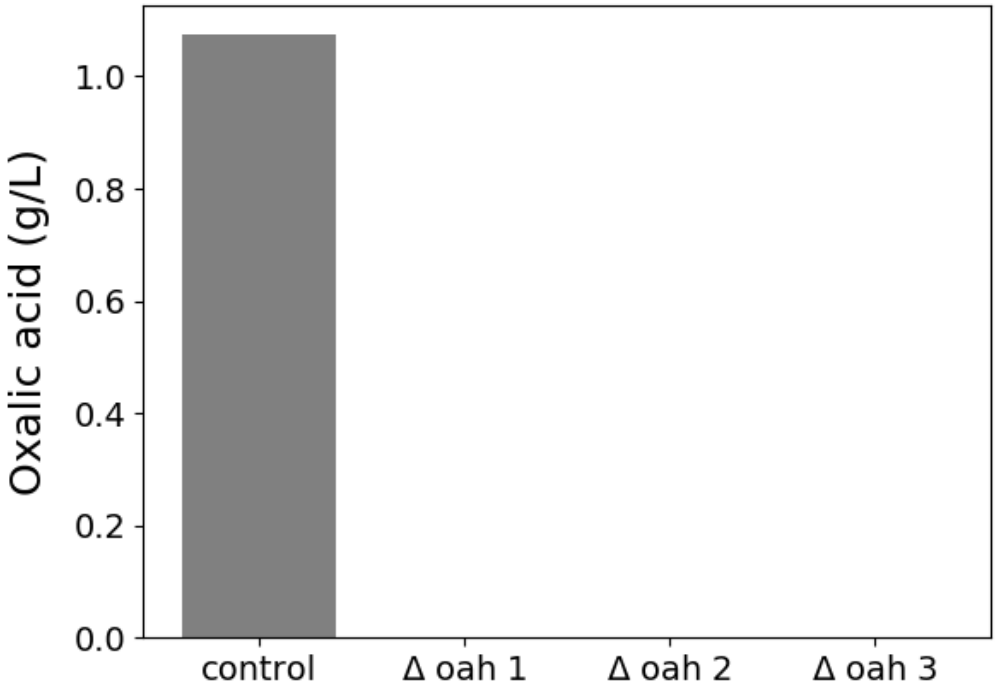

Figure 4.1. Confirmation of oxalate-negative phenotype in Δ*oah* strains. Three Δ*oah* strains were tested in a fermentation experiment at initial pH 7 to confirm the oxalate-negative phenotype. ATCC1015 Δ*pyrG* was used as the control strain. The concentration of oxalic acid (g/L) in culture supernatant at day 6 is shown. One biological replicate was tested for each strain.

To confirm a gluconate-negative phenotype, three Δ*gox* single knock-out strains were tested in a fermentation experiment at initial pH 7 (Figure 4.2). Each Δ*gox* strain tested was isolated from a different colony to confirm the phenotype was the result of the *gox* gene deletion event rather than spontaneous mutations. At day 2, the concentration of gluconic acid in the culture supernatant was determined. No gluconic acid could be detected in any of the Δ*gox* cultures, whereas the control strain produced around 8 g/L gluconic acid by day 2. This confirmed the gluconate-negative phenotype of the Δ*gox* strains, resulting from deletion of *gox*.

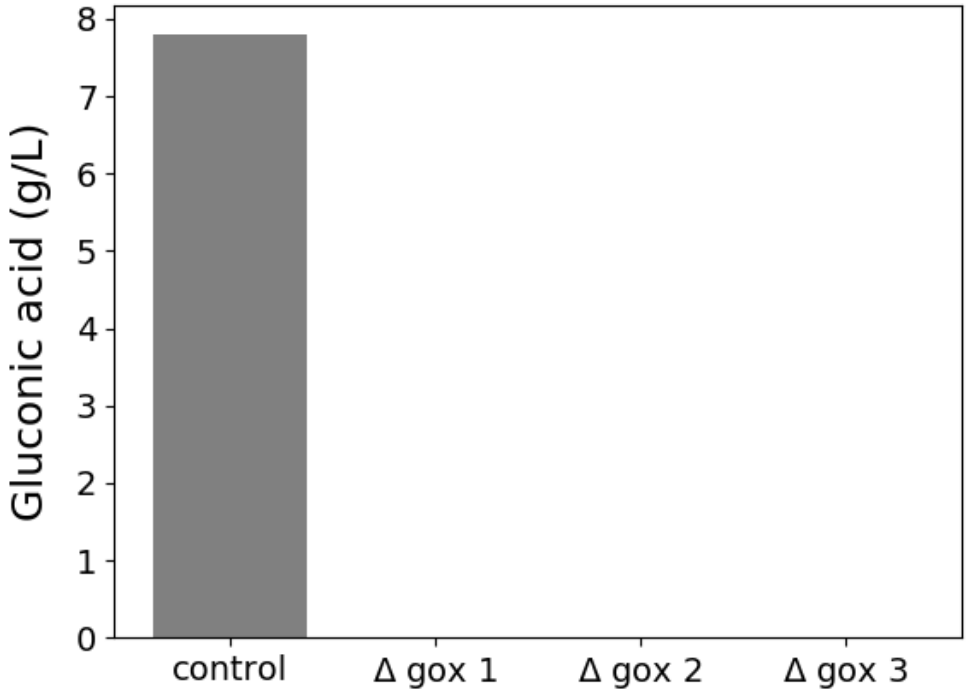

Figure 4.2. Confirmation of gluconate-negative phenotype in Δ*gox* strains. Three Δ*gox* strains were tested in a fermentation experiment at initial pH 7 to confirm the gluconate-negative phenotype. ATCC1015 Δ*pyrG* was used as the control strain. The concentration of gluconic acid (g/L) in culture supernatant at day 2 is shown. One biological replicate was tested for each strain.

To characterise the fermentative effects of *oah* and *gox* knock-outs on citric acid production, a time-course fermentation experiment was performed at initial pH 7. A time series of the organic acids oxalic, gluconic, and citric was obtained for the Δ*oah* and Δ*gox* single knock-outs, and the Δ*oah* Δ*gox* double knock-out (Figure 4.3). Deletion of *oah* significantly increased citric acid production, approximately four-fold. Deletion of *gox*, however, had no significant effect on citric or oxalic acid production. This finding suggests that gluconic acid production occurs independently of citric and oxalic. This is further supported by the different timings observed in the production of organic acids. Citric and oxalic acid production were synchronous, whereas gluconic acid was produced early in fermentation.

Although citric acid production was increased at initial pH 7 by deletion of *oah*, it did not reach the levels observed at initial pH 2 (up to 60 g/L). This may be due to the differing culture morphology. The increased pellet size observed at higher initial pH may affect aerobicity and transport processes, with an impact on citric acid production. The variation was also greater in this experiment compared to experiments starting at pH 2. This may also result from morphological differences, with a more uniform culture morphology at initial pH 2 producing less variable data.

The concentration of manganese was increased to 1000 ppb in this experiment, following previous studies that reported manganese-insensitive citric acid production at pH 5 in a mutant strain lacking GOX and OAH (Ruijter *et al*, 1999). The findings in this work are consistent with previous findings, showing that citric acid production is not reliant on manganese-deficient media at higher initial pH. The morphology was also unaffected by the increased manganese concentration, with no manganese-induced morphological shift from pelleted to filamentous morphology that occurs at initial pH 2.

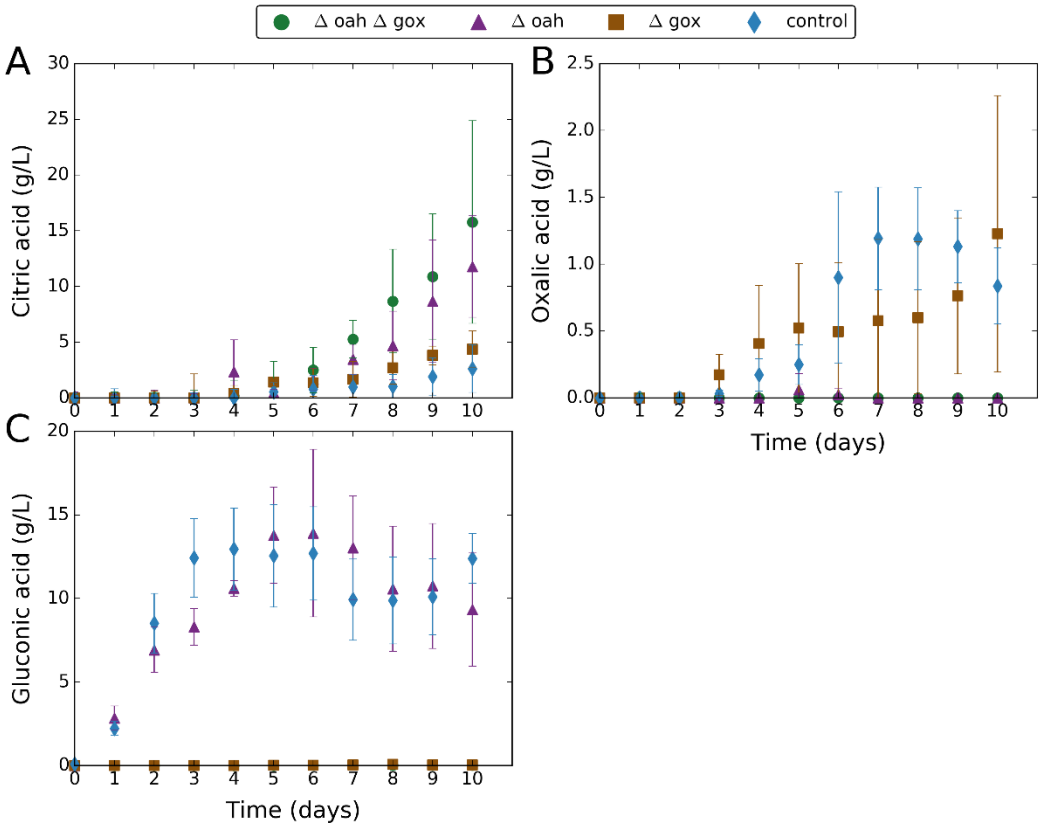

Figure 4.3. Fermentative effects of *oah* and *gox* knock-outs on citric acid production. The Δ*oah* and Δ*gox* single knock-outs, and Δ*oah* Δ*gox* double knock-out were characterised in a time-course fermentation experiment at initial pH 7. ATCC1015 Δ*pyrG* was used as the control strain. Green circles correspond to Δ*oah* Δ*gox*. Purple triangles correspond to Δ*oah*. Brown squares correspond to Δ*gox*. Blue diamonds correspond to the control strain. Each data-point is the mean average of four biological replicates and error bars represent standard deviation. Citric acid data are normalised to reflect the amount produced (subtracting the zero-point – some citric acid was initially present in the media). **(A)** Change in external citric acid concentration (g/L) over time. **(B)** Change in external oxalic acid concentration (g/L) over time. **(C)** Change in external gluconic acid concentration (g/L) over time.

4.3.2 Constitutive over-expression of a low-affinity glucose transporter

Since glucose uptake is a key step in the metabolic pipeline of citric acid production in *A. niger*, an engineering effort was made to increase the rate of glucose uptake. It is reported that *A. niger* has a low-affinity glucose transport system, that is only active at high glucose concentrations (> 15%) (Torres *et al*, 1996a; Papagianni and Mattey, 2004). The Michaelis-Menten characteristics of the low-affinity system were previously determined (Torres *et al*, 1996a; Papagianni and Mattey, 2004). The dynamic model detailed in Chapter 3 incorporated the low- and high-affinity glucose transport systems, using reported kinetic parameters. By applying this dynamic model, it was predicted that the glucose uptake rate would be significantly higher if the low-affinity system were constitutively active (Figure 4.4). Therefore, the ATCC1015 genome was searched for a low-affinity glucose transporter gene (see Methods section 4.2.5.2). A candidate gene was identified and constitutively over-expressed in this work. It was assumed that the activity of the low-affinity system is under transcriptional control and not post-translationally regulated.

Two independent transformant strains (GLU 1 and GLU 2) were characterised in a time-course fermentation experiment at initial pH 2. Dox was added at 20 µg/ml to induce constitutive over-expression of the low-affinity glucose transporter. A strain transformed with the empty vector was used as the negative control. Time series were obtained for biomass, glucose, citric acid, and phosphate (Figures 4.5 and 4.6).

Glucose uptake was increased by about 70% (from 5.7 to 9.7 mM h^{-1}) in the GLU 2 strain, however, no significant effect was observed in the GLU 1 strain. The discrepancy between the two transformant strains may arise from positional effects of genomic plasmid integration. Although the expression vector was designed for targeting to the *pyrG* locus, integration at random sites may still occur. Therefore, it may be that targeted gene expression is successful in a proportion of transformant strains, and inactive in others.

Despite the increased glucose uptake in the GLU 2 strain, no significant fermentative effects were observed, except that citric acid was consumed later in fermentation. This may be due to exhaustion of glucose at an earlier time-point.

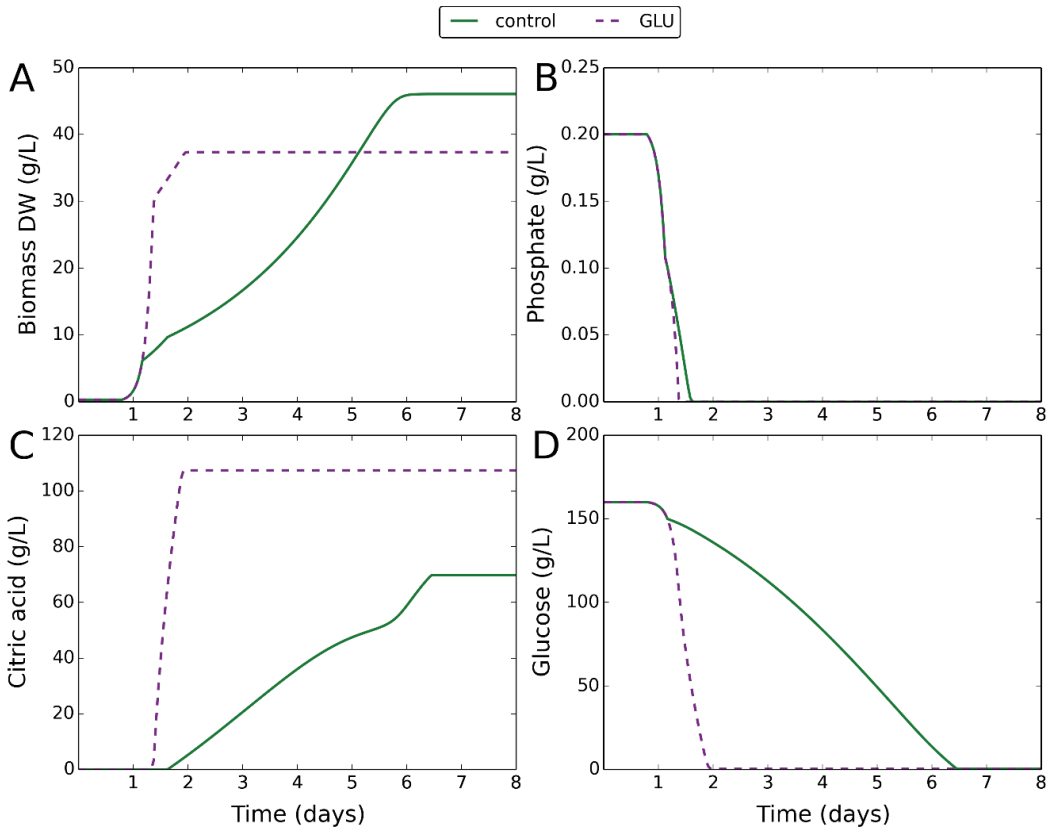

Figure 4.4. Dynamic modelling of citric acid fermentation with constitutive low-affinity glucose transport. The dynamic model described in Chapter 3 was used to predict the effects of constitutive low-affinity glucose transport. Green solid lines correspond to the control (low-affinity glucose transport only above 15% glucose). Purple dashed lines correspond to GLU (constitutive low-affinity glucose transport). **(A)** Change in biomass dry weight (g/L) over time. **(B)** Change in external phosphate concentration (g/L) over time. **(C)** Change in external citric acid concentration (g/L) over time. **(D)** Change in external glucose concentration (g/L) over time.

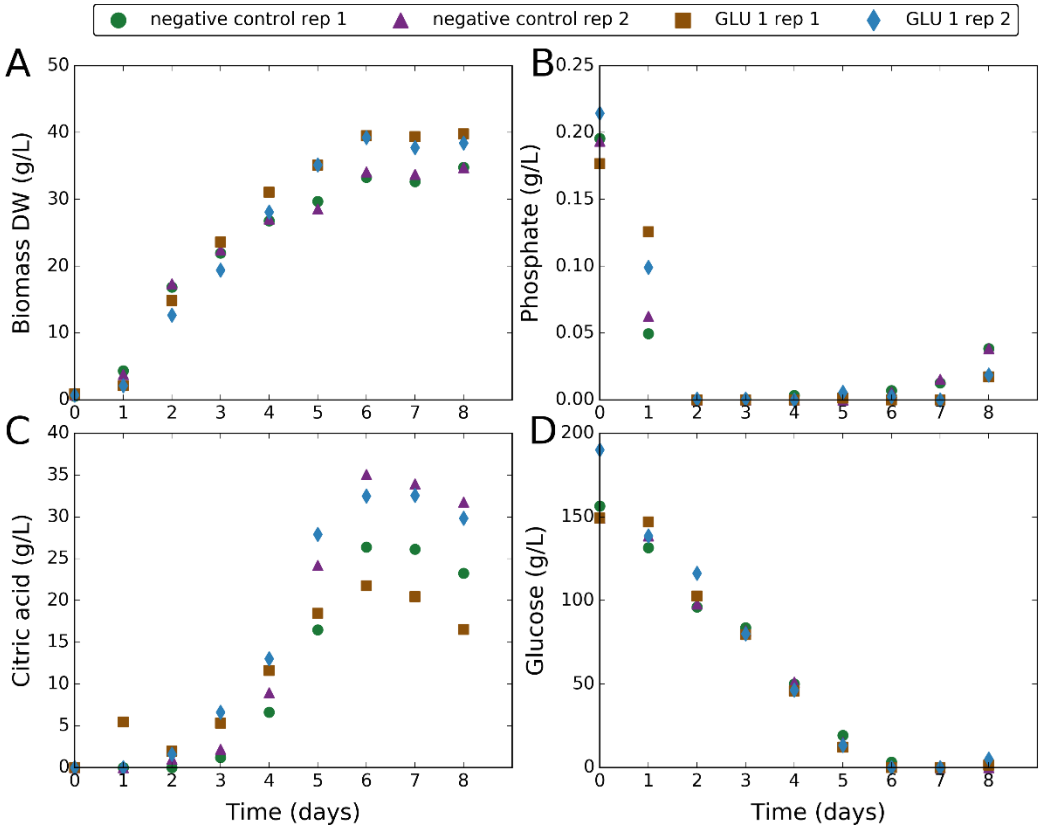

Figure 4.5. Fermentative effects of over-expression of a low-affinity glucose transporter in the GLU 1 strain with empty vector as negative control. The GLU 1 strain, engineered to over-express a low-affinity glucose transporter, was characterised in a time-course fermentation experiment at initial pH 2 with 20 µg/ml Dox. A negative control strain was created by transforming with the empty vector. Data-points represent individual biological replicates. Green circles correspond to negative control rep 1. Purple triangles correspond to negative control rep 2. Brown squares correspond to GLU 1 rep 1. Blue diamonds correspond to GLU 1 rep 2. Citric acid data are normalised to reflect the amount produced (subtracting the zero-point – some citric acid was initially present in the media). **(A)** Change in biomass dry weight (g/L) over time. **(B)** Change in external phosphate concentration (g/L) over time. **(C)** Change in external citric acid concentration (g/L) over time. **(D)** Change in external glucose concentration (g/L) over time.

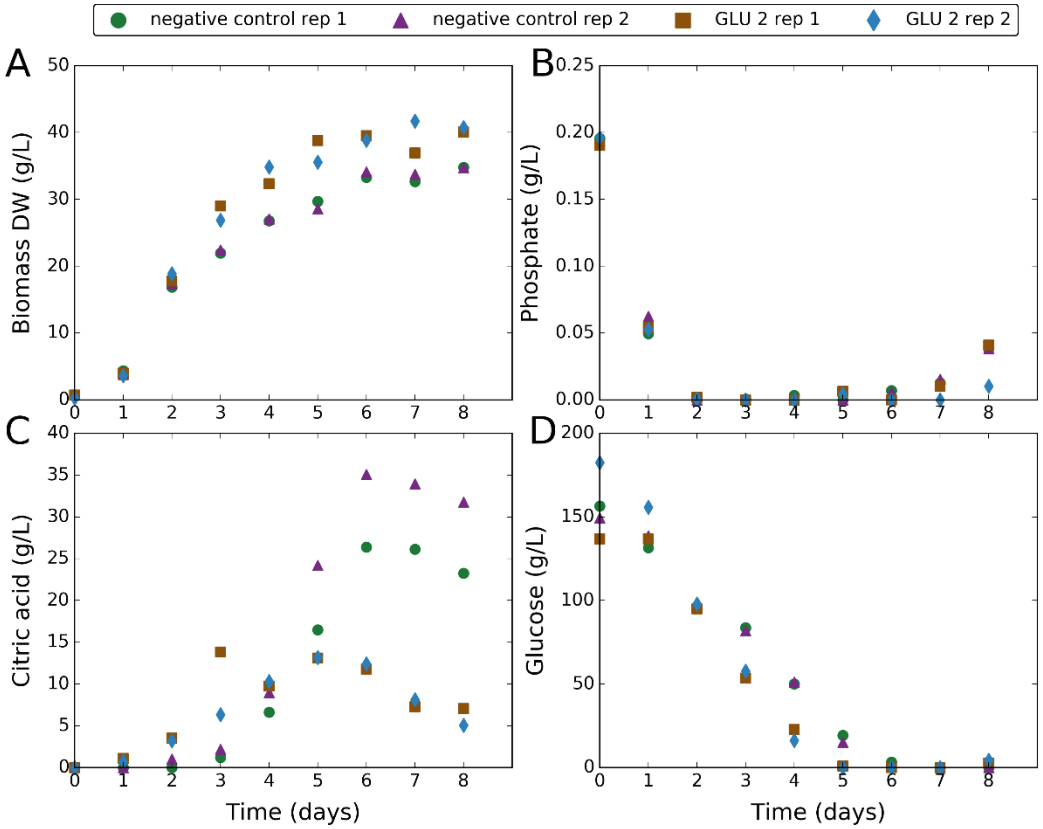

Figure 4.6. Fermentative effects of over-expression of a low-affinity glucose transporter in the GLU 2 strain with empty vector as negative control. The GLU 2 strain, engineered to over-express a low-affinity glucose transporter, was characterised in a time-course fermentation experiment at initial pH 2 with 20 µg/ml Dox. A negative control strain was created by transforming with the empty vector. Data-points represent individual biological replicates. Green circles correspond to negative control rep 1. Purple triangles correspond to negative control rep 2. Brown squares correspond to GLU 2 rep 1. Blue diamonds correspond to GLU 2 rep 2. Citric acid data are normalised to reflect the amount produced (subtracting the zero-point – some citric acid was initially present in the media). **(A)** Change in biomass dry weight (g/L) over time. **(B)** Change in external phosphate concentration (g/L) over time. **(C)** Change in external citric acid concentration (g/L) over time. **(D)** Change in external glucose concentration (g/L) over time.

To further investigate the GLU 1 and GLU 2 strains, an additional fermentation experiment was carried out at a higher Dox concentration, and testing the same strains in the absence of Dox (Figures 4.7 and 4.8). This was done to confirm phenotypic effects resulted from Dox-induced over-expression of the low-affinity glucose transporter. The concentration of Dox was increased to 50 µg/ml as an attempt to increase targeted gene expression.

The significant increase in glucose uptake in the GLU 2 strain was reproduced in this experiment (60% increase; from 6.5 to 10.4 mM h^{-1}), and did not occur in the absence of Dox, confirming the phenotypic effect was the result of over-expression of the low-affinity glucose transporter. The rate of glucose uptake was very similar to the previous experiment at 20 µg/ml Dox, suggesting this concentration was saturating.

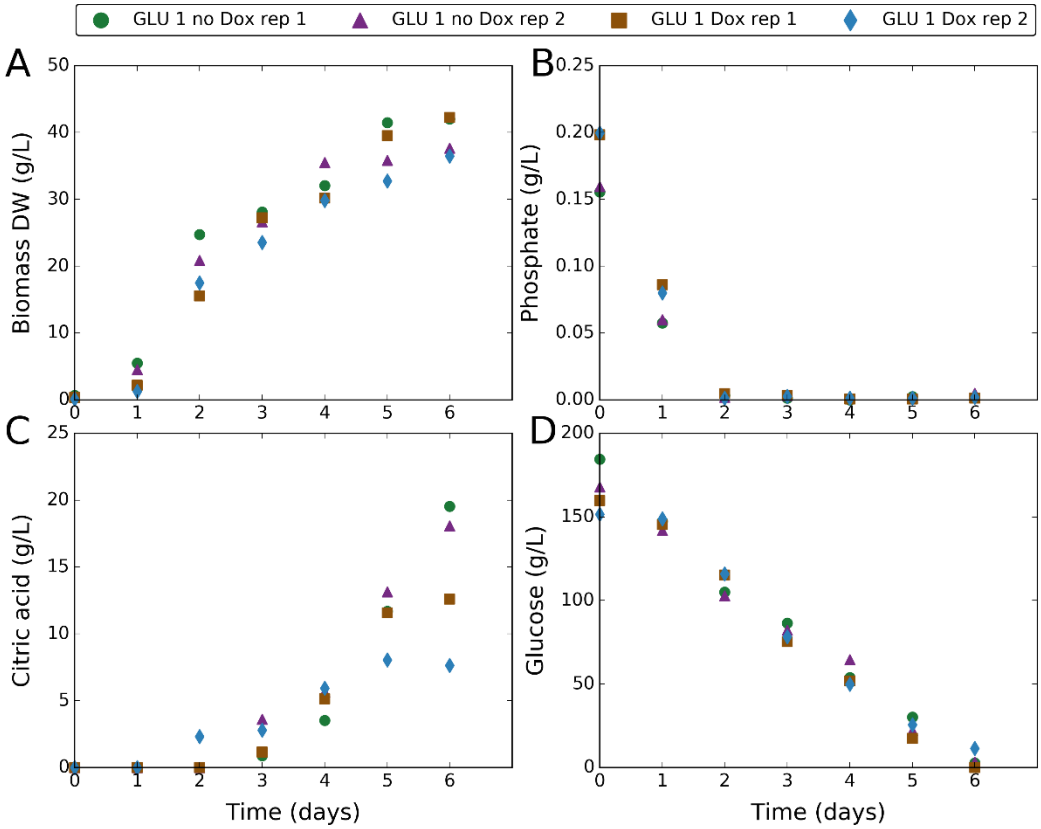

Figure 4.7. Fermentative effects of over-expression of a low-affinity glucose transporter in the GLU 1 strain with no inducer as negative control. The GLU 1 strain, engineered to over-express a low-affinity glucose transporter, was characterised in a time-course fermentation experiment at initial pH 2 with 50 µg/ml Dox. The same strain without addition of Dox was used as the negative control. Data-points represent individual biological replicates. Green circles correspond to GLU 1 without Dox rep 1. Purple triangles correspond to GLU 1 without Dox rep 2. Brown squares correspond to GLU 1 with Dox rep 1. Blue diamonds correspond to GLU 1 with Dox rep 2. Citric acid data are normalised to reflect the amount produced (subtracting the zero-point – some citric acid was initially present in the media). **(A)** Change in biomass dry weight (g/L) over time. **(B)** Change in external phosphate concentration (g/L) over time. **(C)** Change in external citric acid concentration (g/L) over time. **(D)** Change in external glucose concentration (g/L) over time.

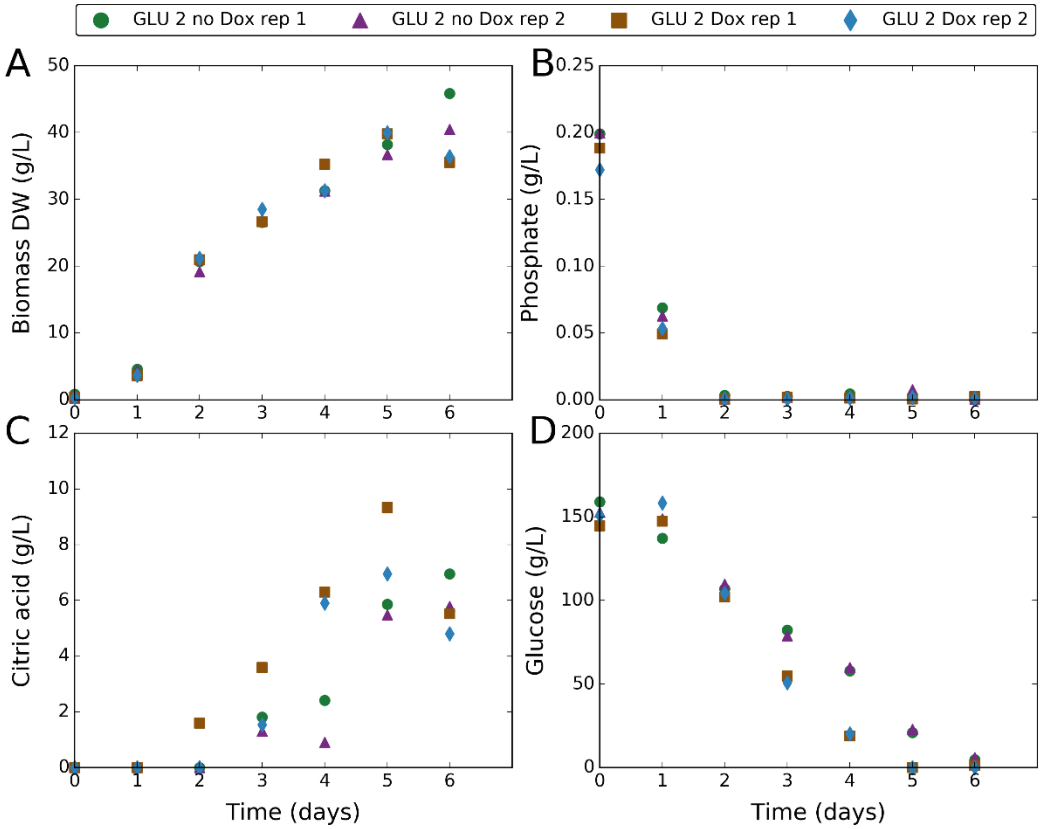

Figure 4.8. Fermentative effects of over-expression of a low-affinity glucose transporter in the GLU 2 strain with no inducer as negative control. The GLU 2 strain, engineered to over-express a low-affinity glucose transporter, was characterised in a time-course fermentation experiment at initial pH 2 with 50 µg/ml Dox. The same strain without addition of Dox was used as the negative control. Data-points represent individual biological replicates. Green circles correspond to GLU 2 without Dox rep 1. Purple triangles correspond to GLU 2 without Dox rep 2. Brown squares correspond to GLU 2 with Dox rep 1. Blue diamonds correspond to GLU 2 with Dox rep 2. Citric acid data are normalised to reflect the amount produced (subtracting the zero-point – some citric acid was initially present in the media). **(A)** Change in biomass dry weight (g/L) over time. **(B)** Change in external phosphate concentration (g/L) over time. **(C)** Change in external citric acid concentration (g/L) over time. **(D)** Change in external glucose concentration (g/L) over time.

4.3.3 Expression of cytosolic citrate synthase

It is observed that citrate synthase is exclusively localised in the mitochondria in *A. niger* (Jaklitsch *et al*, 1991), therefore requiring the mitochondrial export of citric acid for subsequent secretion. As this transport step may be limiting, the dynamic model described in Chapter 3 was used to predict the effects of addition of cytosolic citrate synthase when mitochondrial citrate export is constrained (Figure 4.9). This illustrated that a mitochondrial citrate export constraint would limit citric acid output, and that this would be bypassed by the addition cytosolic citrate synthase. Following these predictions, an attempt was made in this work to switch the site of citric acid production to the cytosol by expression of a cytosolic citrate synthase (see Methods section 4.2.5.3).

Two independent transformant strains (CIT 1 and CIT 2) were characterised in a time-course fermentation experiment at initial pH 2. Dox was added at 20 µg/ml to induce expression of cytosolic citrate synthase. A strain transformed with the empty vector was used as the negative control. Time series were obtained for biomass, glucose, citric acid, and phosphate (Figures 4.10 and 4.11).

A decrease in biomass production was observed in both strains, causing a decreased glucose uptake. This may explain the unexpected reduced citric acid production. The release of phosphate in the CIT 2 cultures at day 3 is also unexpected, and may be caused by ATP-limiting conditions that trigger an increase in polyphosphate hydrolysis.

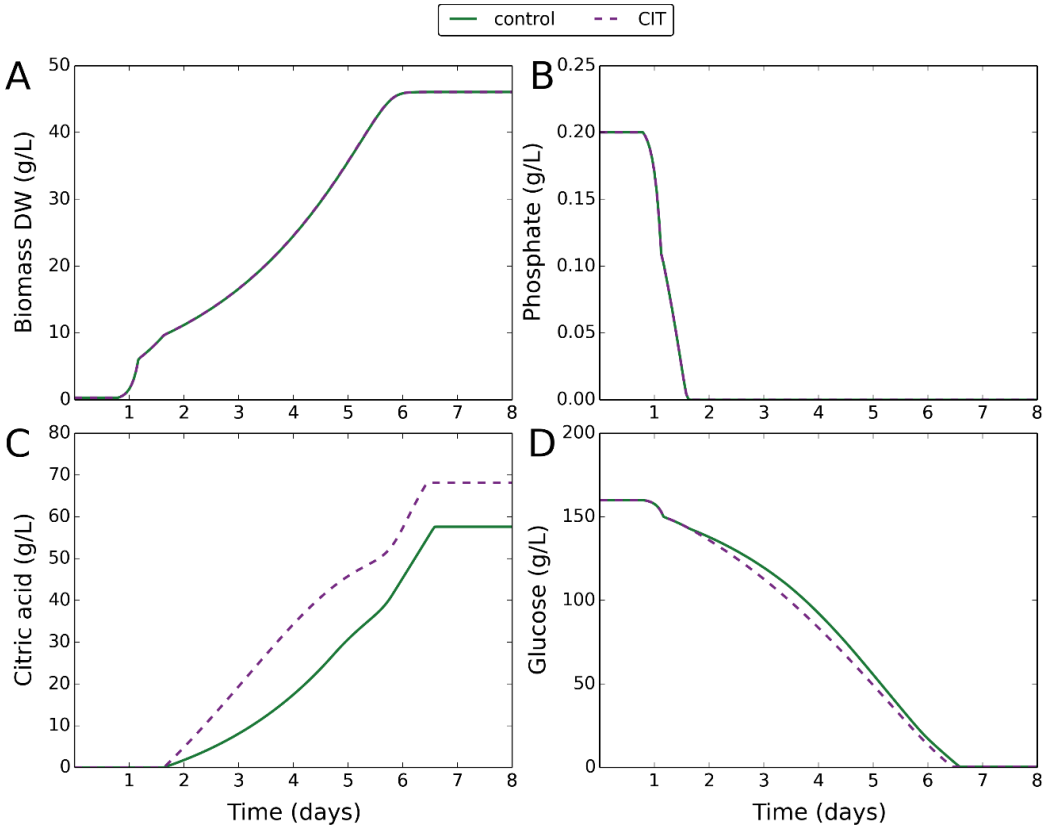

Figure 4.9. Dynamic modelling of citric acid fermentation with constrained mitochondrial citrate export and addition of cytosolic citrate synthase. The dynamic model described in Chapter 3 was used to predict the effects of addition of cytosolic citrate synthase when mitochondrial citrate export is constrained. Green solid lines correspond to the control (constrained mitochondrial citrate export and absence of cytosolic citrate synthase). Purple dashed lines correspond to CIT (constrained mitochondrial citrate export and presence of cytosolic citrate synthase). **(A)** Change in biomass dry weight (g/L) over time. **(B)** Change in external phosphate concentration (g/L) over time. **(C)** Change in external citric acid concentration (g/L) over time. **(D)** Change in external glucose concentration (g/L) over time.

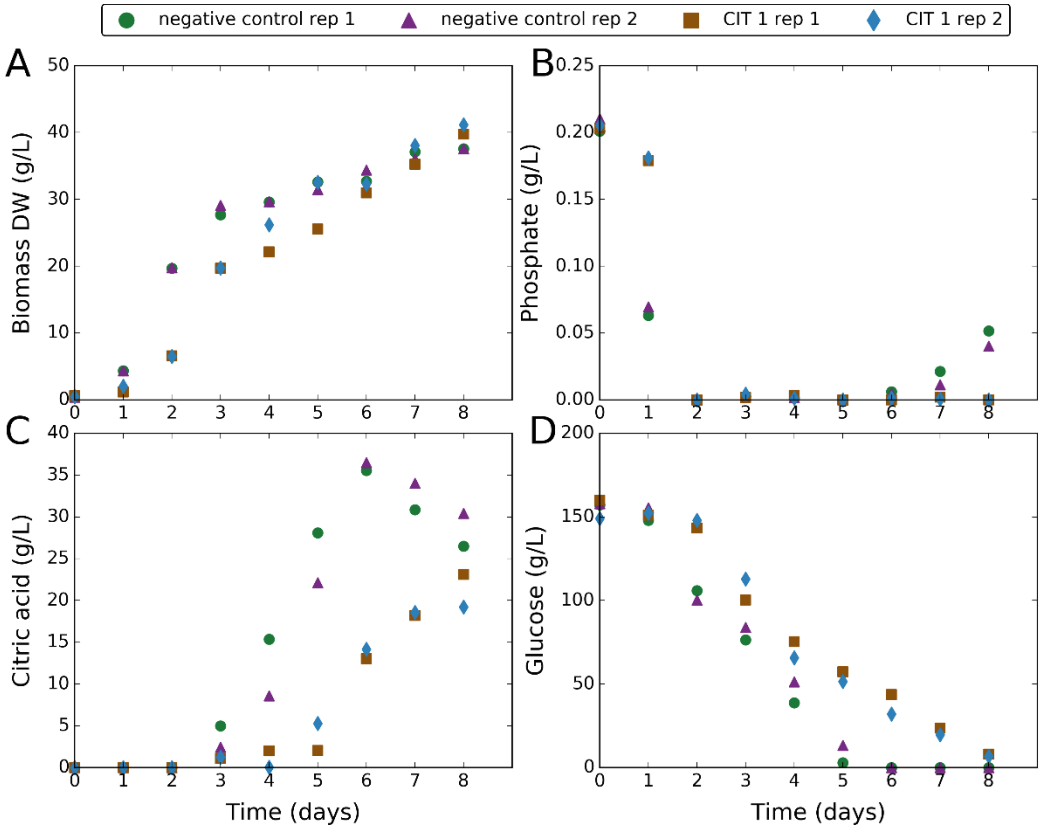

Figure 4.10. Fermentative effects of expression of cytosolic citrate synthase in the CIT 1 strain with empty vector as negative control. The CIT 1 strain, engineered to express cytosolic citrate synthase, was characterised in a time-course fermentation experiment at initial pH 2 with 20 µg/ml Dox. A negative control strain was created by transforming with the empty vector. Data-points represent individual biological replicates. Green circles correspond to negative control rep 1. Purple triangles correspond to negative control rep 2. Brown squares correspond to CIT 1 rep 1. Blue diamonds correspond to CIT 1 rep 2. Citric acid data are normalised to reflect the amount produced (subtracting the zero-point – some citric acid was initially present in the media). **(A)** Change in biomass dry weight (g/L) over time. **(B)** Change in external phosphate concentration (g/L) over time. **(C)** Change in external citric acid concentration (g/L) over time. **(D)** Change in external glucose concentration (g/L) over time.

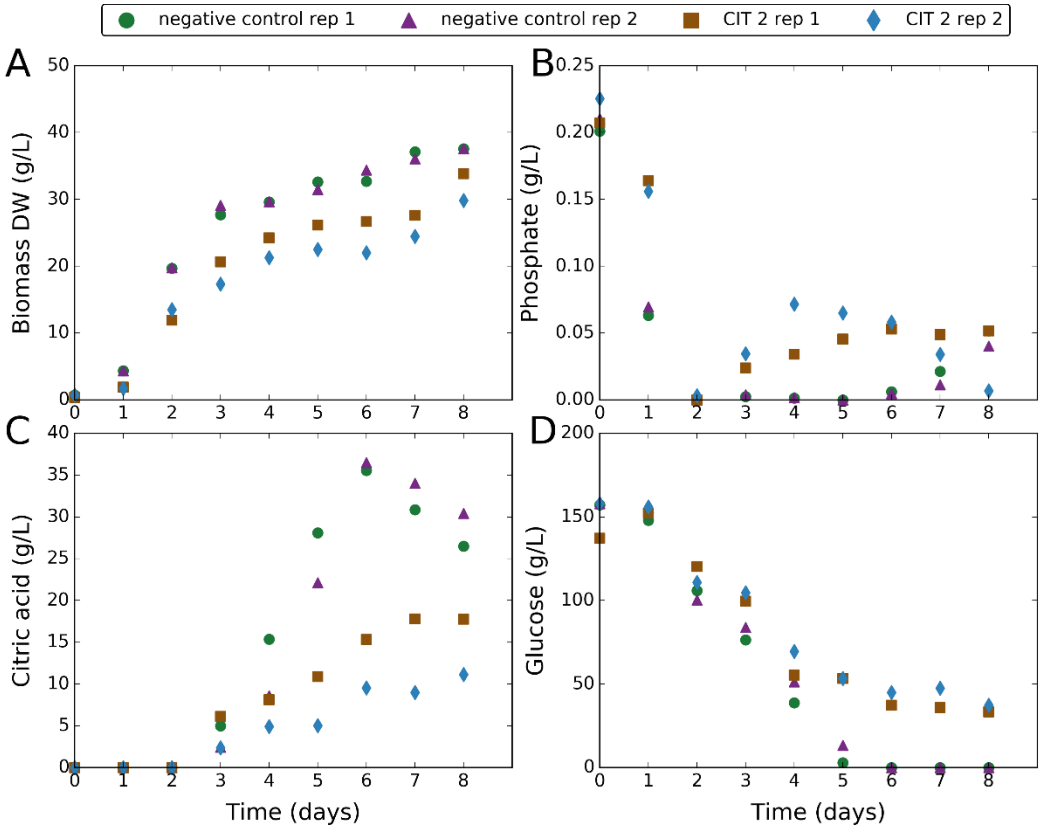

Figure 4.11. Fermentative effects of expression of cytosolic citrate synthase in the CIT 2 strain with empty vector as negative control. The CIT 2 strain, engineered to express cytosolic citrate synthase, was characterised in a time-course fermentation experiment at initial pH 2 with 20 µg/ml Dox. A negative control strain was created by transforming with the empty vector. Data-points represent individual biological replicates. Green circles correspond to negative control rep 1. Purple triangles correspond to negative control rep 2. Brown squares correspond to CIT 2 rep 1. Blue diamonds correspond to CIT 2 rep 2. Citric acid data are normalised to reflect the amount produced (subtracting the zero-point – some citric acid was initially present in the media). **(A)** Change in biomass dry weight (g/L) over time. **(B)** Change in external phosphate concentration (g/L) over time. **(C)** Change in external citric acid concentration (g/L) over time. **(D)** Change in external glucose concentration (g/L) over time.

To further investigate the CIT 1 and CIT 2 strains, an additional fermentation experiment was carried out testing the same strains in the absence of Dox (Figures 4.12 and 4.13). This was done to confirm phenotypic effects resulted from Dox-induced expression of cytosolic citrate synthase. The concentration of Dox was decreased to 5 µg/ml, sufficient to induce expression.

The CIT 1 strain behaved the same with or without Dox, and reproduced the same characteristics as in the previous experiment. This was not the case with the CIT 2 strain, however. In the absence of Dox, the CIT 2 strain showed remarkable behaviour beyond day 2. Growth stopped and did not resume until after day 4, at which point citric acid production commenced. A significant release of phosphate was observed, peaking at day 4, after which phosphate was taken back up.

On examination of glucose uptake data, it was observed that glucose consumption was unaffected up to day 4, and then stopped. This is despite the absence of growth and citric acid production between day 2 and 4, suggesting the carbon was either burned or released as extracellular compounds. The continuation of growth beyond day 4 without glucose uptake is striking, and suggests the presence of other extracellular carbon compounds, that may have been previously secreted.

It is plausible that the mitochondrial citrate synthase gene was disrupted by genomic plasmid integration, and the resulting effects were rescued by Dox-induced expression of cytosolic citrate synthase. The disruption of citrate synthase may cause ATP-limiting conditions, explaining the release of phosphate.

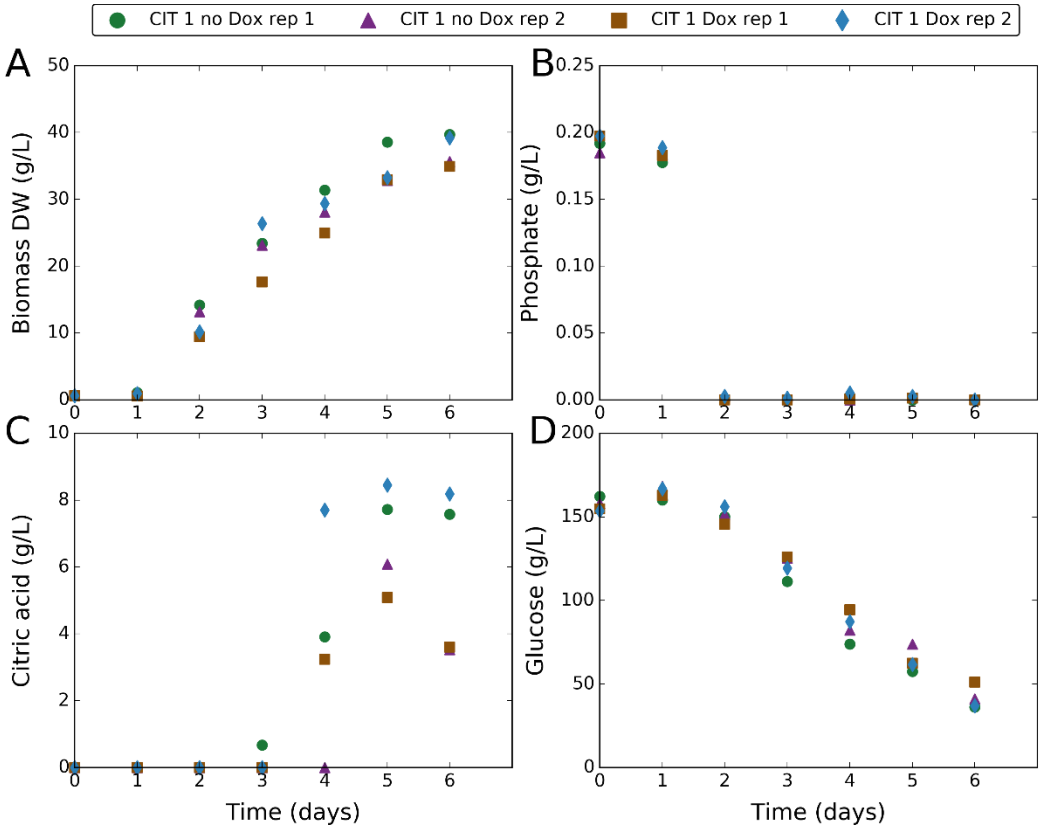

Figure 4.12. Fermentative effects of expression of cytosolic citrate synthase in the CIT 1 strain with no inducer as negative control. The CIT 1 strain, engineered to express cytosolic citrate synthase, was characterised in a time-course fermentation experiment at initial pH 2 with 5 µg/ml Dox. The same strain without addition of Dox was used as the negative control. Data-points represent individual biological replicates. Green circles correspond to CIT 1 without Dox rep 1. Purple triangles correspond to CIT 1 without Dox rep 2. Brown squares correspond to CIT 1 with Dox rep 1. Blue diamonds correspond to CIT 1 with Dox rep 2. Citric acid data are normalised to reflect the amount produced (subtracting the zero-point – some citric acid was initially present in the media). **(A)** Change in biomass dry weight (g/L) over time. **(B)** Change in external phosphate concentration (g/L) over time. **(C)** Change in external citric acid concentration (g/L) over time. **(D)** Change in external glucose concentration (g/L) over time.

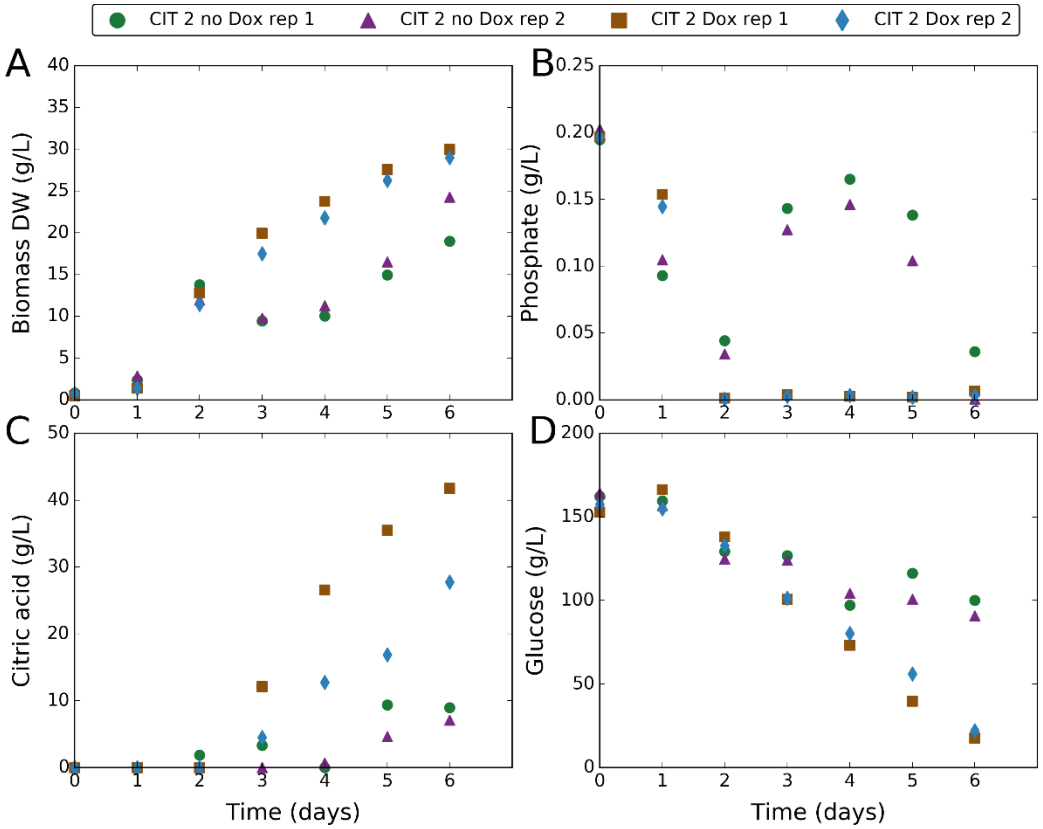

Figure 4.13. Fermentative effects of expression of cytosolic citrate synthase in the CIT 2 strain with no inducer as negative control. The CIT 2 strain, engineered to express cytosolic citrate synthase, was characterised in a time-course fermentation experiment at initial pH 2 with 5 µg/ml Dox. The same strain without addition of Dox was used as the negative control. Data-points represent individual biological replicates. Green circles correspond to CIT 2 without Dox rep 1. Purple triangles correspond to CIT 2 without Dox rep 2. Brown squares correspond to CIT 2 with Dox rep 1. Blue diamonds correspond to CIT 2 with Dox rep 2. Citric acid data are normalised to reflect the amount produced (subtracting the zero-point – some citric acid was initially present in the media). **(A)** Change in biomass dry weight (g/L) over time. **(B)** Change in external phosphate concentration (g/L) over time. **(C)** Change in external citric acid concentration (g/L) over time. **(D)** Change in external glucose concentration (g/L) over time.

4.3.4 Expression of mutated truncated 6-phosphofructo-1-kinase

An important factor in citric acid production is the glycolytic flux. A key control step in glycolysis occurs at 6-phosphofructo-1-kinase (PFK1). PFK1 is inhibited by citrate, however, a citrate-insensitive truncated form of PFK1 has been observed in *A. niger* (Capuder *et al*, 2009). This explains how *A. niger* can operate a high glycolytic flux while producing citric acid. Previous studies have expanded upon this finding, and engineered a mutated truncated form of PFK1 (mtPFK1) that is constitutively active and citrate-insensitive (Capuder *et al*, 2009). Expression of mtPFK1 in the *A. niger* A158 strain deregulated glycolysis and increased citric acid production by 70% (Capuder *et al*, 2009). In this work, the ATCC1015 strain was engineered to express mtPFK1 to investigate the reproducibility of the previous finding in a wild-type citric acid producing strain.

Two independent transformant strains (mtPFK1 1 and mtPFK1 2) were characterised in a time-course fermentation experiment at initial pH 2. Dox was added at 20 µg/ml to induce expression of mtPFK1. A strain transformed with the empty vector was used as the negative control. Time series were obtained for biomass, glucose, citric acid, and phosphate (Figures 4.14 and 4.15).

Citric acid production was increased by 60% in the mtPFK1 2 strain, consistent with previous results in the engineered A158 strain. An opposite effect, however, was observed in the mtPFK1 1 strain. The increased citric acid production in the mtPFK1 2 strain was accompanied by a decrease in biomass production. Cultures of the mtPFK1 2 strain showed a filamentous morphology and had a greater viscosity. These morphological effects did not inhibit citric acid production, and were not produced by the mtPFK1 1 strain.

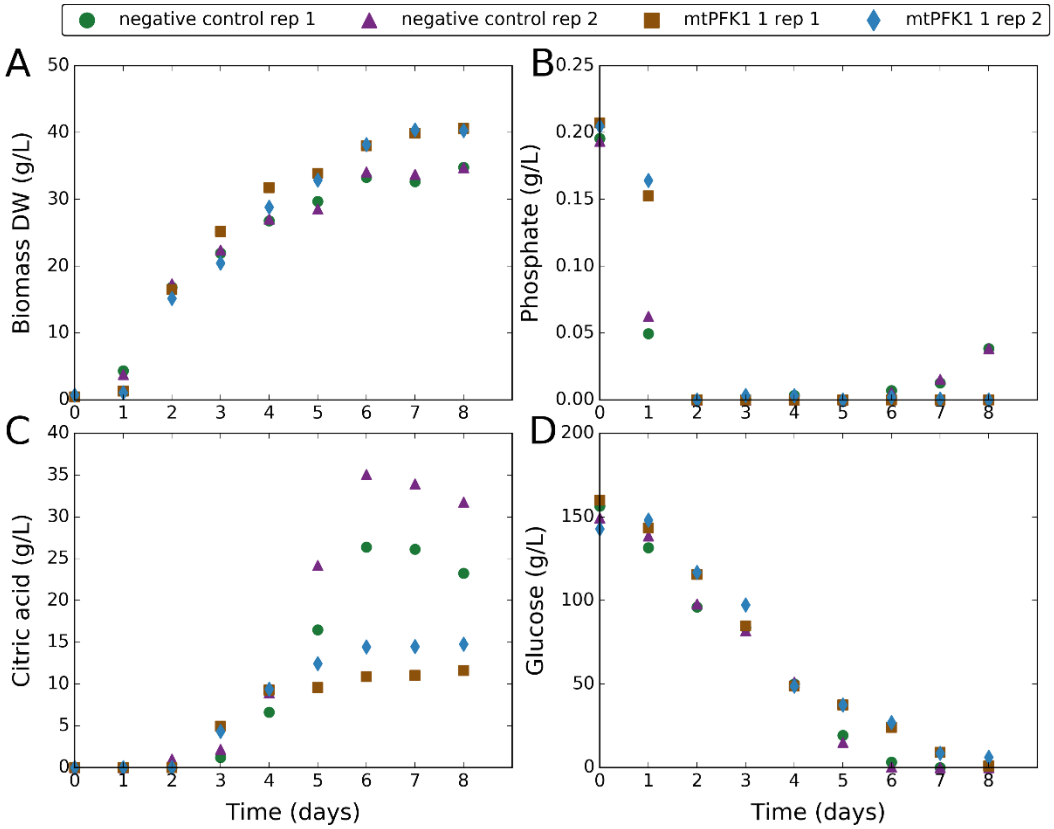

Figure 4.14. Fermentative effects of expression of mtPFK1 in the mtPFK1 1 strain with empty vector as negative control. The mtPFK1 1 strain, engineered to express mtPFK1, was characterised in a time-course fermentation experiment at initial pH 2 with 20 µg/ml Dox. A negative control strain was created by transforming with the empty vector. Data-points represent individual biological replicates. Green circles correspond to negative control rep 1. Purple triangles correspond to negative control rep 2. Brown squares correspond to mtPFK1 1 rep 1. Blue diamonds correspond to mtPFK1 1 rep 2. Citric acid data are normalised to reflect the amount produced (subtracting the zero-point – some citric acid was initially present in the media). **(A)** Change in biomass dry weight (g/L) over time. **(B)** Change in external phosphate concentration (g/L) over time. **(C)** Change in external citric acid concentration (g/L) over time. **(D)** Change in external glucose concentration (g/L) over time.

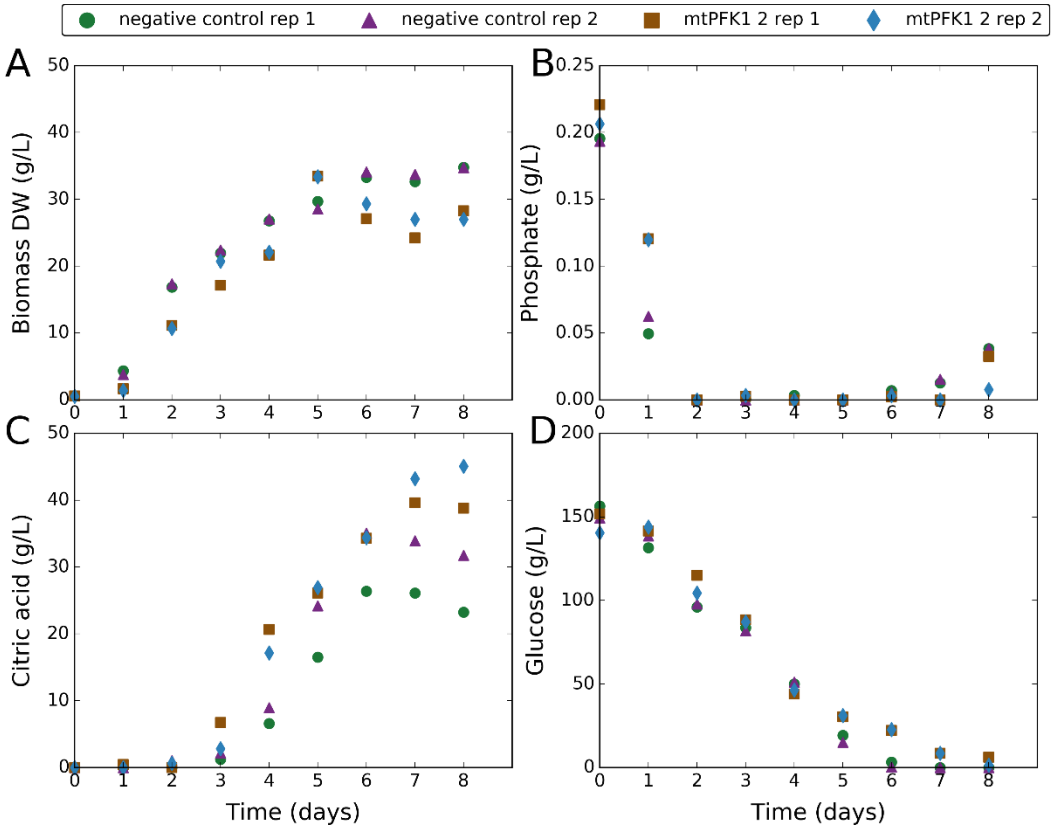

Figure 4.15. Fermentative effects of expression of mtPFK1 in the mtPFK1 2 strain with empty vector as negative control. The mtPFK1 2 strain, engineered to express mtPFK1, was characterised in a time-course fermentation experiment at initial pH 2 with 20 µg/ml Dox. A negative control strain was created by transforming with the empty vector. Data-points represent individual biological replicates. Green circles correspond to negative control rep 1. Purple triangles correspond to negative control rep 2. Brown squares correspond to mtPFK1 2 rep 1. Blue diamonds correspond to mtPFK1 2 rep 2. Citric acid data are normalised to reflect the amount produced (subtracting the zero-point – some citric acid was initially present in the media). **(A)** Change in biomass dry weight (g/L) over time. **(B)** Change in external phosphate concentration (g/L) over time. **(C)** Change in external citric acid concentration (g/L) over time. **(D)** Change in external glucose concentration (g/L) over time.

To further investigate the mtPFK1 1 and mtPFK1 2 strains, an additional fermentation experiment was carried out testing the same strains in the absence of Dox (Figures 4.16 and 4.17). This was done to confirm phenotypic effects resulted from Dox-induced expression of mtPFK1. The concentration of Dox was decreased to 5 µg/ml, sufficient to induce expression.

The mtPFK1 2 strain displayed no difference in citric acid production with or without Dox, showing that the higher citric acid yield resulted from plasmid integration at a disruptive site rather than Dox-induced mtPFK1 expression. The morphological effects were also observed in the absence of Dox, suggesting that the filamentous morphology also resulted from plasmid integration at a disruptive site.

The lower citric acid production by the mtPFK1 1 strain was reproduced in this experiment, however, did not occur in the absence of Dox. This is an unexpected result, as it suggests Dox-induced mtPFK1 expression had negative effects.

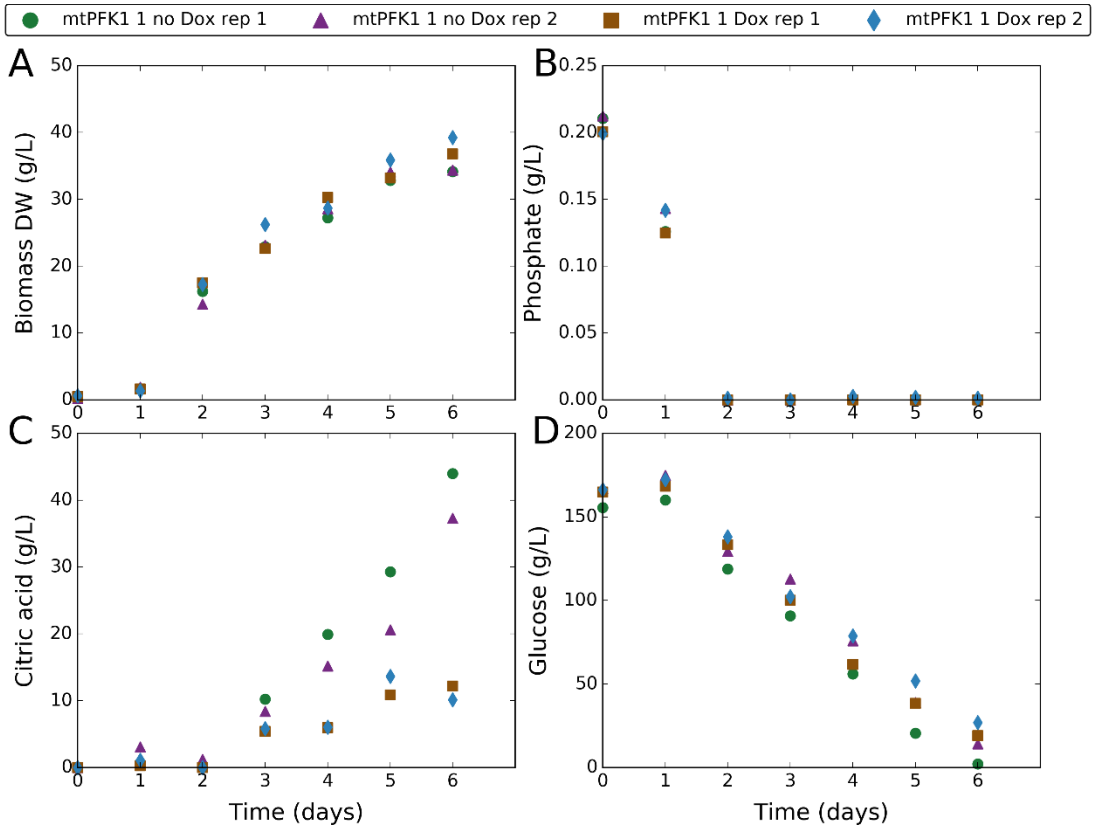

Figure 4.16. Fermentative effects of expression of mtPFK1 in the mtPFK1 1 strain with no inducer as negative control. The mtPFK1 1 strain, engineered to express mtPFK1, was characterised in a time-course fermentation experiment at initial pH 2 with 5 µg/ml Dox. The same strain without addition of Dox was used as the negative control. Data-points represent individual biological replicates. Green circles correspond to mtPFK1 1 without Dox rep 1. Purple triangles correspond to mtPFK1 1 without Dox rep 2. Brown squares correspond to mtPFK1 1 with Dox rep 1. Blue diamonds correspond to mPFK1 1 with Dox rep 2. Citric acid data are normalised to reflect the amount produced (subtracting the zero-point – some citric acid was initially present in the media). **(A)** Change in biomass dry weight (g/L) over time. **(B)** Change in external phosphate concentration (g/L) over time. **(C)** Change in external citric acid concentration (g/L) over time. **(D)** Change in external glucose concentration (g/L) over time.

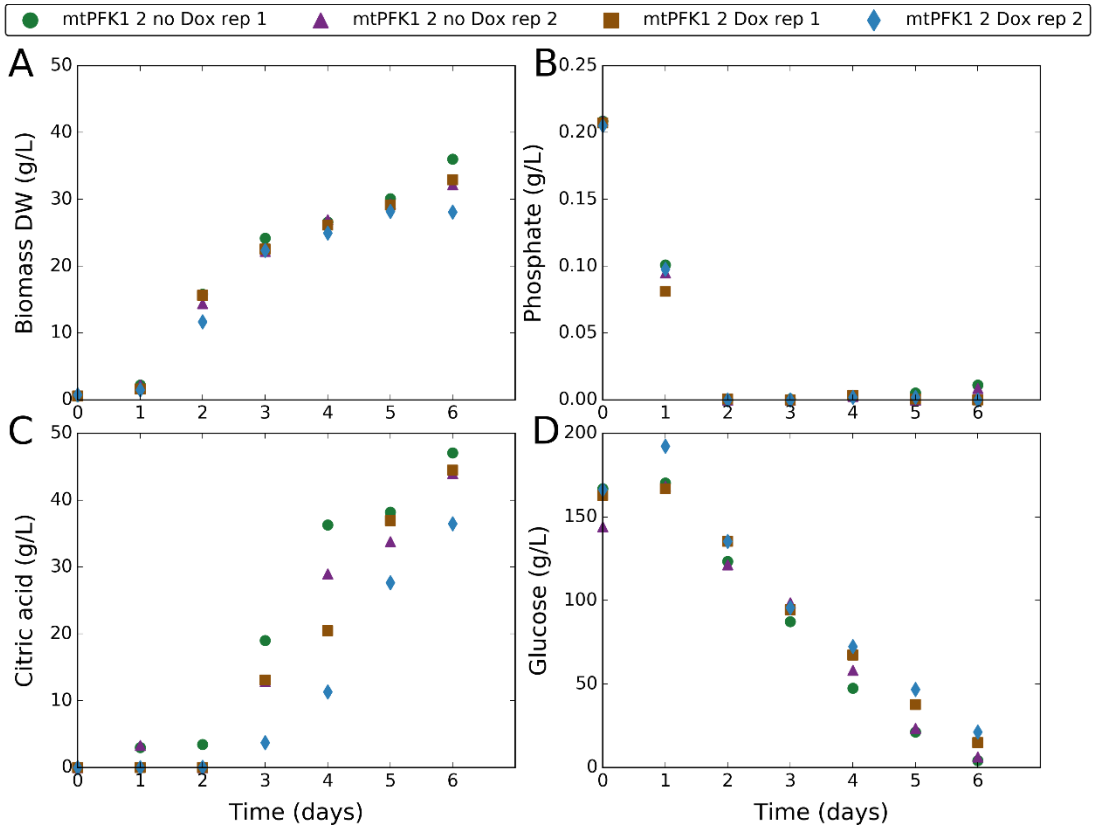

Figure 4.17. Fermentative effects of expression of mtPFK1 in the mtPFK1 2 strain with no inducer as negative control. The mtPFK1 2 strain, engineered to express mtPFK1, was characterised in a time-course fermentation experiment at initial pH 2 with 5 µg/ml Dox. The same strain without addition of Dox was used as the negative control. Data-points represent individual biological replicates. Green circles correspond to mtPFK1 2 without Dox rep 1. Purple triangles correspond to mtPFK1 2 without Dox rep 2. Brown squares correspond to mtPFK1 2 with Dox rep 1. Blue diamonds correspond to mPFK1 2 with Dox rep 2. Citric acid data are normalised to reflect the amount produced (subtracting the zero-point – some citric acid was initially present in the media). **(A)** Change in biomass dry weight (g/L) over time. **(B)** Change in external phosphate concentration (g/L) over time. **(C)** Change in external citric acid concentration (g/L) over time. **(D)** Change in external glucose concentration (g/L) over time.

4.3.5 Knock-down of exopolyphosphatase

It is observed from findings in this work that *A. niger* stores phosphate as polyphosphate, and releases it slowly causing phosphate-limited growth. The enzyme exopolyphosphatase (PPX) is responsible for the hydrolysis of polyphosphate. Using the dynamic model described in Chapter 3, it was predicted that decreased activity of PPX may further constrain growth and enhance citric acid production (Figure 4.18). To investigate this, the ATCC1015 genome was searched for a PPX gene, which returned one candidate (see Methods section 4.2.6.1). Antisense-RNA mediated knock-down was performed in this work on the candidate PPX gene.

Two independent transformant strains (PPX KD 1 and PPX KD 2) were characterised in a time-course fermentation experiment at initial pH 2. Dox was added at 20 µg/ml to induce expression of antisense-RNA and knock-down of PPX. A strain transformed with the empty vector was used as the negative control. Time series were obtained for biomass, glucose, citric acid, and phosphate (Figures 4.19 and 4.20).

Both strains had less biomass at days 2 and 3 than the negative controls, however, no significant differences in biomass were seen at other time-points. The PPX KD 1 strain had significantly reduced citric acid production, however, this was not observed in the PPX KD 2 strain.

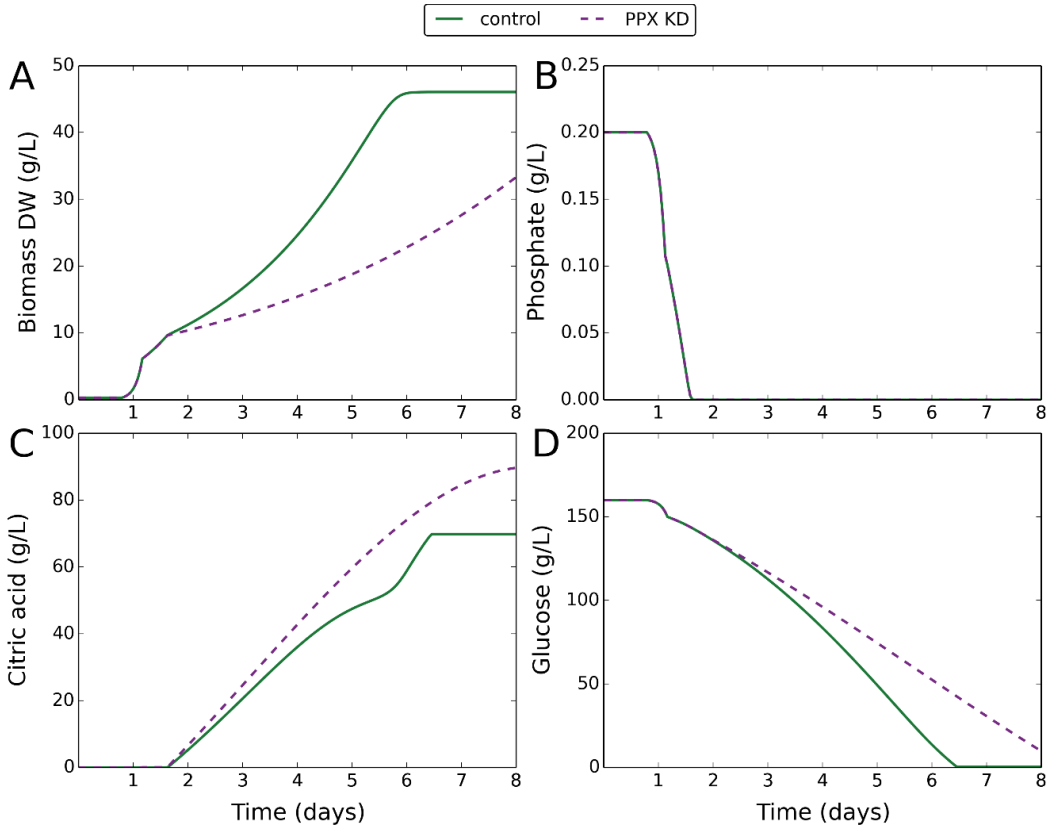

Figure 4.18. Dynamic modelling of citric acid fermentation with exopolyphosphatase knock-down (PPX KD). The dynamic model described in Chapter 3 was used to predict the effects of knock-down of PPX. Green solid lines correspond to the control. Purple dashed lines correspond to PPX KD. **(A)** Change in biomass dry weight (g/L) over time. **(B)** Change in external phosphate concentration (g/L) over time. **(C)** Change in external citric acid concentration (g/L) over time. **(D)** Change in external glucose concentration (g/L) over time.

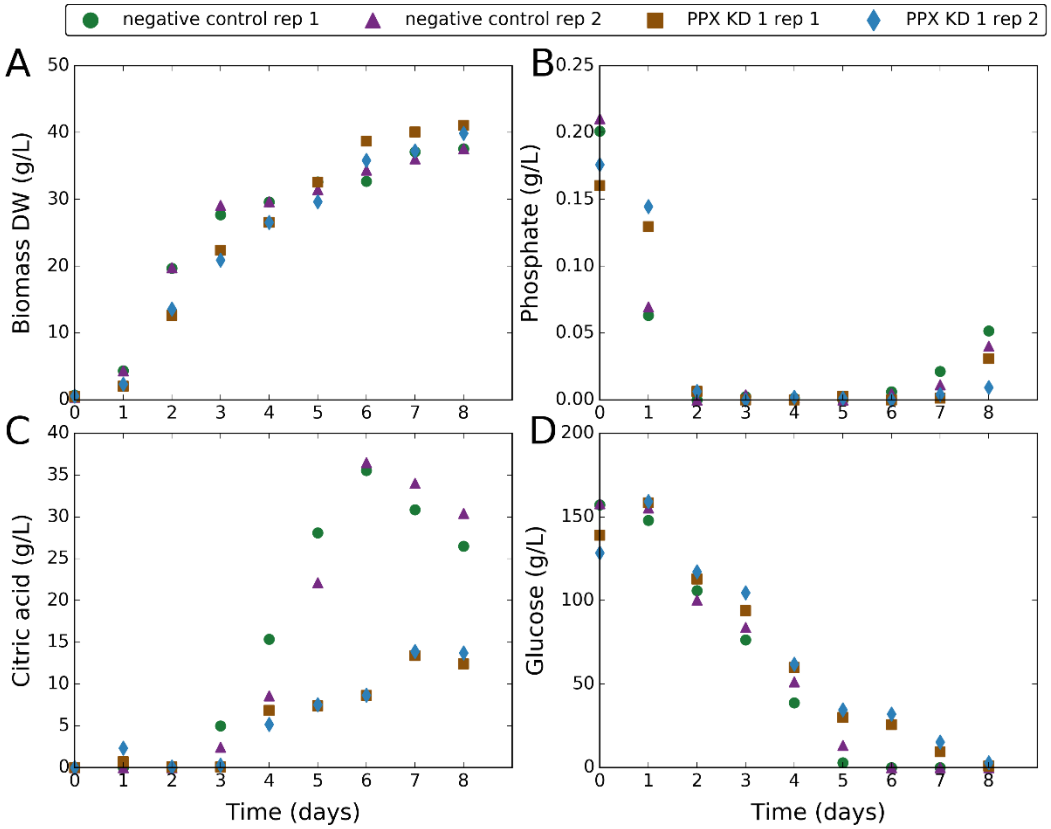

Figure 4.19. Fermentative effects of PPX knock-down in the PPX KD 1 strain with empty vector as negative control. The PPX KD 1 strain, engineered to express antisense-RNA against PPX, was characterised in a time-course fermentation experiment at initial pH 2 with 20 µg/ml Dox. A negative control strain was created by transforming with the empty vector. Data-points represent individual biological replicates. Green circles correspond to negative control rep 1. Purple triangles correspond to negative control rep 2. Brown squares correspond to PPX KD 1 rep 1. Blue diamonds correspond to PPX KD 1 rep 2. Citric acid data are normalised to reflect the amount produced (subtracting the zero-point – some citric acid was initially present in the media). **(A)** Change in biomass dry weight (g/L) over time. **(B)** Change in external phosphate concentration (g/L) over time. **(C)** Change in external citric acid concentration (g/L) over time. **(D)** Change in external glucose concentration (g/L) over time.

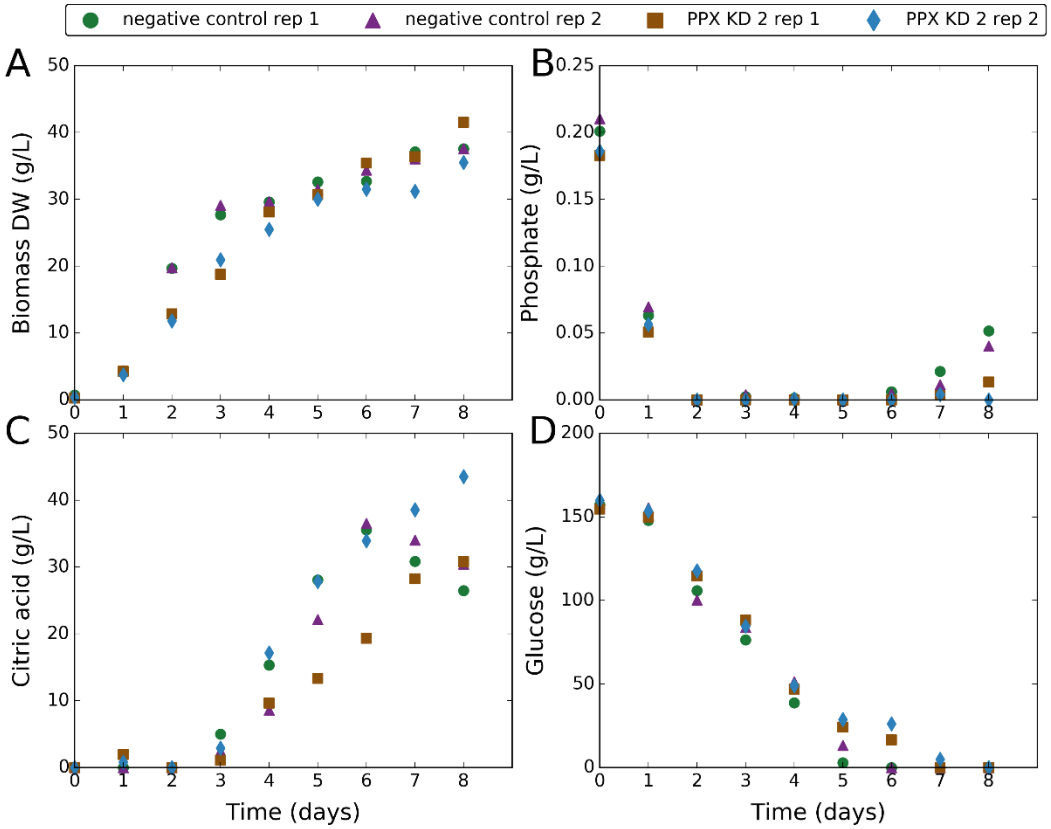

Figure 4.20. Fermentative effects of PPX knock-down in the PPX KD 2 strain with empty vector as negative control. The PPX KD 2 strain, engineered to express antisense-RNA against PPX, was characterised in a time-course fermentation experiment at initial pH 2 with 20 µg/ml Dox. A negative control strain was created by transforming with the empty vector. Data-points represent individual biological replicates. Green circles correspond to negative control rep 1. Purple triangles correspond to negative control rep 2. Brown squares correspond to PPX KD 2 rep 1. Blue diamonds correspond to PPX KD 2 rep 2. Citric acid data are normalised to reflect the amount produced (subtracting the zero-point – some citric acid was initially present in the media). **(A)** Change in biomass dry weight (g/L) over time. **(B)** Change in external phosphate concentration (g/L) over time. **(C)** Change in external citric acid concentration (g/L) over time. **(D)** Change in external glucose concentration (g/L) over time.

Since it was difficult to draw conclusions from the experiment characterising the effects of PPX knock-down, an additional experiment was carried out at a higher Dox concentration and comparing against the same engineered strains in the absence of Dox (Figures 4.21 and 4.22). This was done to determine if previous findings were the result of Dox-induced PPX knock-down or genetic differences. The concentration of Dox was increased to 50 µg/ml as an attempt to increase expression of antisense-RNA targeting PPX, therefore leading to a more effective knock-down.

Both strains had less biomass at day 2 than the same strains in the absence of Dox, suggesting this growth effect was the result of Dox-induced PPX knock-down. No significant differences in biomass were seen at other time-points. It may be that at later time-points PPX activity is naturally lower, minimising the effect of PPX knock-down. Other regulatory mechanisms controlling PPX activity are expected given the role of polyphosphate in energy storage, and these may be of a post-translational nature. Therefore, transcriptional down-regulation of PPX may have no down-stream effect due to counteracting post-translational up-regulation.

The negative effect on citric acid production in the PPX KD 1 strain was reproduced in this experiment, and did not occur in the absence of Dox. This confirmed that the phenotypic effect was related to knock-down of PPX, however, was not observed in the PPX KD 2 strain. The effect may result from the decreased ability to dissipate ATP by the continuous making and breaking of polyphosphate. Higher ATP levels would inhibit citric acid production.

As well as fermentative effects, morphological effects were observed. In the presence of Dox, morphology became more filamentous and culture viscosity increased, whereas in the absence of Dox pelleted morphology was observed. Both strains showed the same morphological effect upon Dox-induced PPX knock-down.

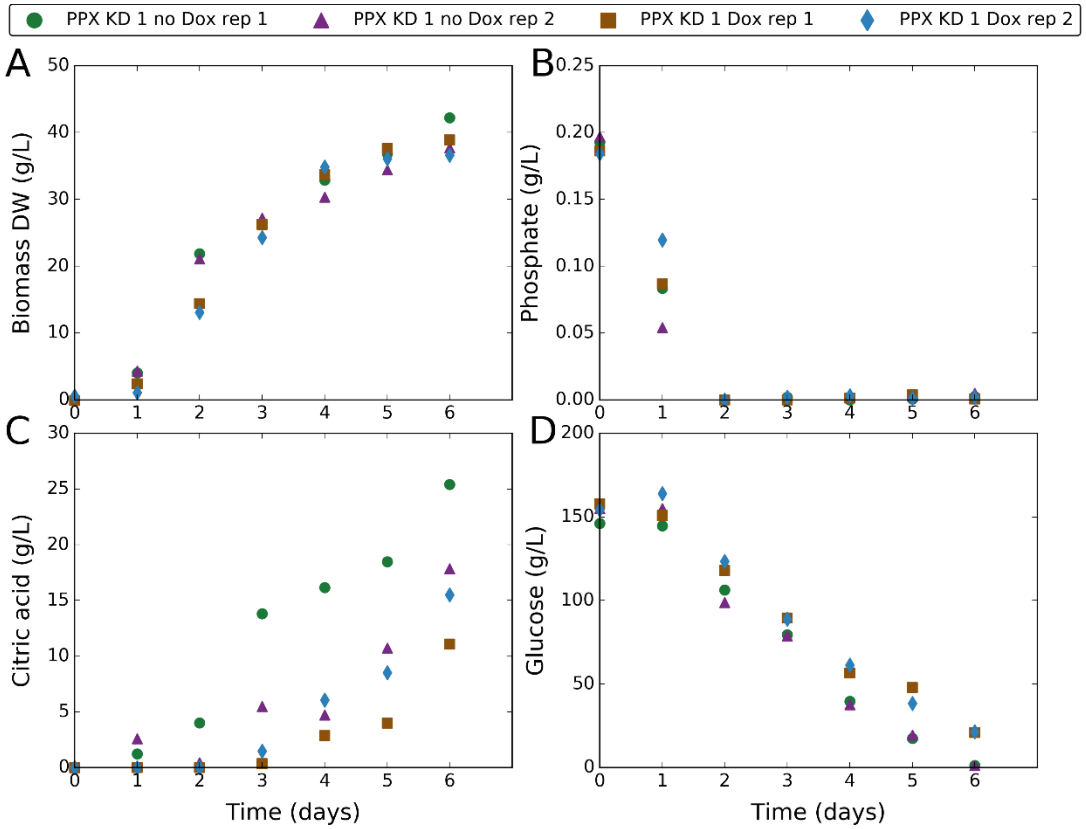

Figure 4.21. Fermentative effects of PPX knock-down in the PPX KD 1 strain with no inducer as negative control. The PPX KD 1 strain, engineered to express antisense-RNA against PPX, was characterised in a time-course fermentation experiment at initial pH 2 with 50 µg/ml Dox. The same strain without addition of Dox was used as the negative control. Data-points represent individual biological replicates. Green circles correspond to PPX KD 1 without Dox rep 1. Purple triangles correspond to PPX KD 1 without Dox rep 2. Brown squares correspond to PPX KD 1 with Dox rep 1. Blue diamonds correspond to PPX KD 1 with Dox rep 2. Citric acid data are normalised to reflect the amount produced (subtracting the zero-point – some citric acid was initially present in the media). **(A)** Change in biomass dry weight (g/L) over time. **(B)** Change in external phosphate concentration (g/L) over time. **(C)** Change in external citric acid concentration (g/L) over time. **(D)** Change in external glucose concentration (g/L) over time.

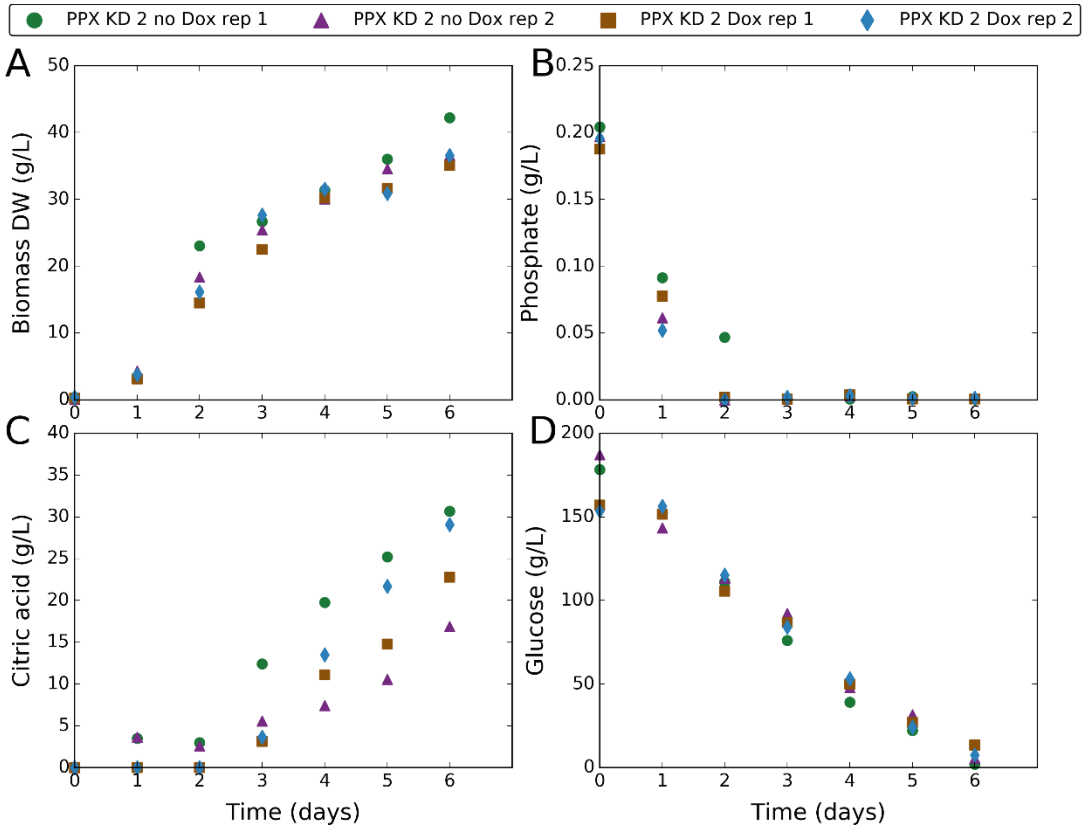

Figure 4.22. Fermentative effects of PPX knock-down in the PPX KD 2 strain with no inducer as negative control. The PPX KD 2 strain, engineered to express antisense-RNA against PPX, was characterised in a time-course fermentation experiment at initial pH 2 with 50 µg/ml Dox. The same strain without addition of Dox was used as the negative control. Data-points represent individual biological replicates. Green circles correspond to PPX KD 2 without Dox rep 1. Purple triangles correspond to PPX KD 2 without Dox rep 2. Brown squares correspond to PPX KD 2 with Dox rep 1. Blue diamonds correspond to PPX KD 2 with Dox rep 2. Citric acid data are normalised to reflect the amount produced (subtracting the zero-point – some citric acid was initially present in the media). **(A)** Change in biomass dry weight (g/L) over time. **(B)** Change in external phosphate concentration (g/L) over time. **(C)** Change in external citric acid concentration (g/L) over time. **(D)** Change in external glucose concentration (g/L) over time.

4.3.6 Knock-down of a phosphate transporter

Previous findings in this work have revealed a rapid phosphate uptake, and a synchronicity of citric acid production with a phosphate-limited growth phase. By applying the dynamic model described in Chapter 3, it was predicted that decreased phosphate uptake would delay the onset of phosphate-limited growth and citric acid production (Figure 4.23). To further probe this, an engineering effort was made in this work to decrease phosphate uptake by knock-down of a phosphate transporter. The ATCC1015 genome was searched for phosphate transporter genes, and a candidate (PHO1) was identified and subjected to antisense-RNA mediated knock-down (see Methods section 4.2.6.2).

Two independent transformant strains (PHO1 KD 1 and PHO1 KD 2) were characterised in a time-course fermentation experiment at initial pH 2. Dox was added at 20 µg/ml to induce expression of antisense-RNA and knock-down of PHO1. A strain transformed with the empty vector was used as the negative control. Time series were obtained for biomass, glucose, citric acid, and phosphate (Figures 4.24 and 4.25).

No significant effects were observed with the PHO1 KD 1 strain, however, the PHO1 KD 2 strain gave unexpected results. The PHO1 KD 2 strain behaved normally up to day 2, then released phosphate. Phosphate release continued until day 5, followed by re-uptake of phosphate. Significant reductions in biomass and citric acid production were observed. Citric acid was produced upon re-uptake of phosphate after day 5, at which point growth resumed. To investigate whether the effects were the result of Dox-induced knock-down of PHO1, the same strain was grown in the absence of Dox. Biomass was measured at day 6, and the same effect occurred without addition of Dox (Figure 4.26). This confirmed plasmid integration at a disruptive site was responsible.

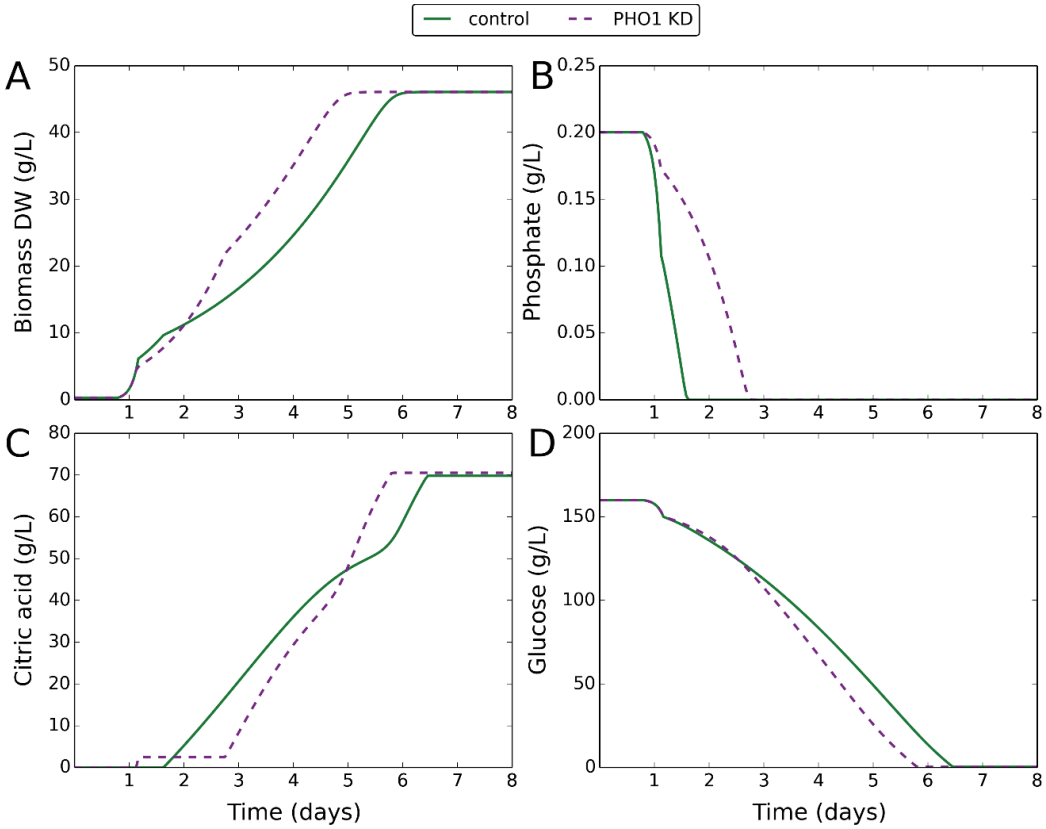

Figure 4.23. Dynamic modelling of citric acid fermentation with constrained phosphate uptake. The dynamic model described in Chapter 3 was used to predict the effects of decreased phosphate uptake to simulate the effects of a phosphate transporter knock-down (PHO1 KD). Green solid lines correspond to the control. Purple dashed lines correspond to PHO1 KD. **(A)** Change in biomass dry weight (g/L) over time. **(B)** Change in external phosphate concentration (g/L) over time. **(C)** Change in external citric acid concentration (g/L) over time. **(D)** Change in external glucose concentration (g/L) over time.

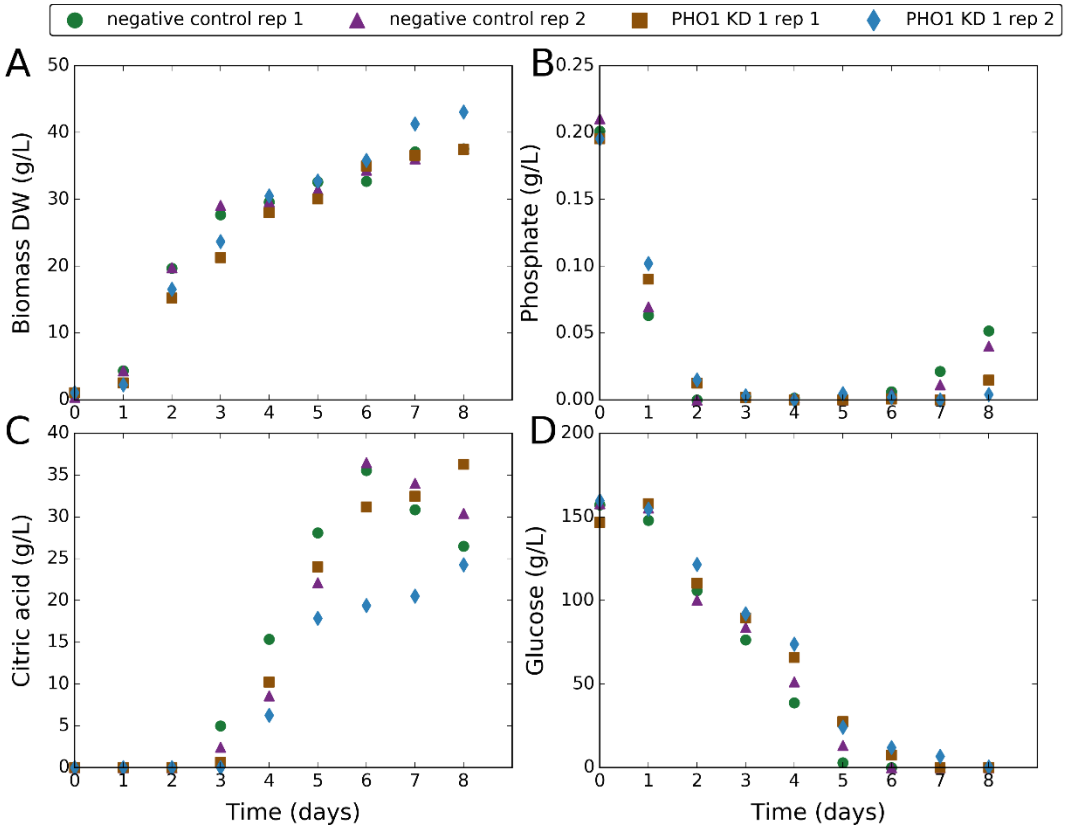

Figure 4.24. Fermentative effects of PHO1 knock-down in the PHO1 KD 1 strain with empty vector as negative control. The PHO1 KD 1 strain, engineered to express antisense-RNA against a phosphate transporter (PHO1), was characterised in a time-course fermentation experiment at initial pH 2 with 20 µg/ml Dox. A negative control strain was created by transforming with the empty vector. Data-points represent individual biological replicates. Green circles correspond to negative control rep 1. Purple triangles correspond to negative control rep 2. Brown squares correspond to PHO1 KD 1 rep 1. Blue diamonds correspond to PHO1 KD 1 rep 2. Citric acid data are normalised to reflect the amount produced (subtracting the zero-point – some citric acid was initially present in the media). **(A)** Change in biomass dry weight (g/L) over time. **(B)** Change in external phosphate concentration (g/L) over time. **(C)** Change in external citric acid concentration (g/L) over time. **(D)** Change in external glucose concentration (g/L) over time.

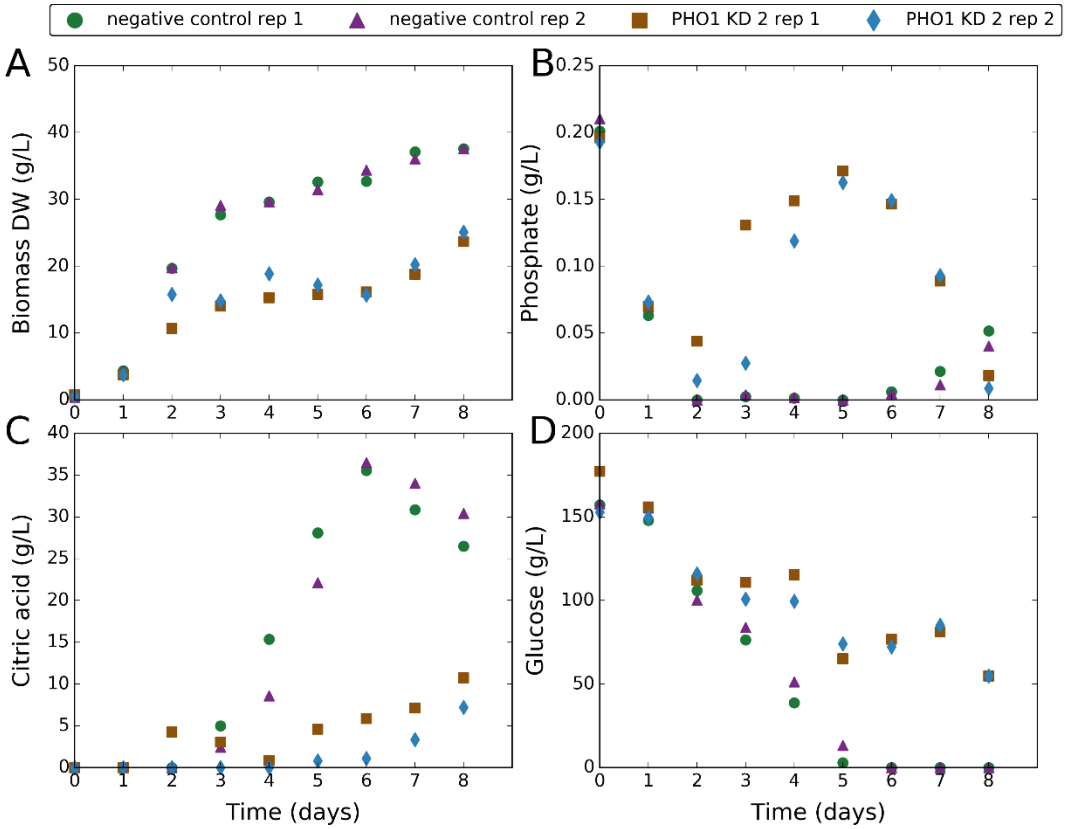

Figure 4.25. Fermentative effects of PHO1 knock-down in the PHO1 KD 2 strain with empty vector as negative control. The PHO1 KD 2 strain, engineered to express antisense-RNA against a phosphate transporter (PHO1), was characterised in a time-course fermentation experiment at initial pH 2 with 20 µg/ml Dox. A negative control strain was created by transforming with the empty vector. Data-points represent individual biological replicates. Green circles correspond to negative control rep 1. Purple triangles correspond to negative control rep 2. Brown squares correspond to PHO1 KD 2 rep 1. Blue diamonds correspond to PHO1 KD 2 rep 2. Citric acid data are normalised to reflect the amount produced (subtracting the zero-point – some citric acid was initially present in the media). **(A)** Change in biomass dry weight (g/L) over time. **(B)** Change in external phosphate concentration (g/L) over time. **(C)** Change in external citric acid concentration (g/L) over time. **(D)** Change in external glucose concentration (g/L) over time.

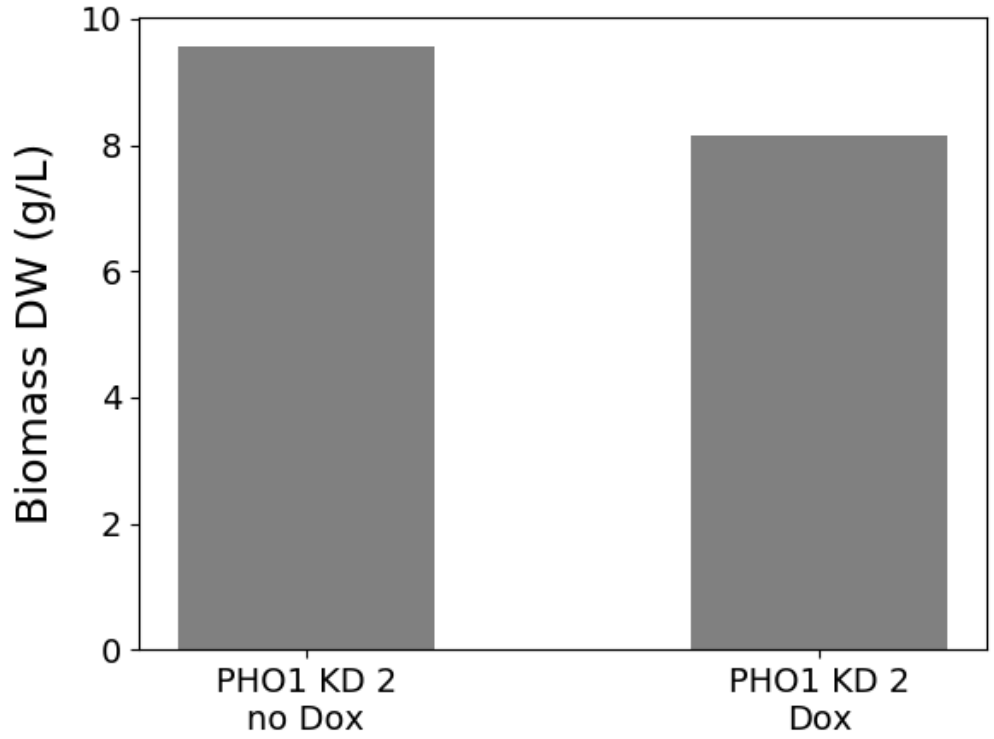

Figure 4.26. Growth phenotype of PHO1 KD 2 strain with and without Dox. The PHO1 KD 2 strain was tested with and without addition of Dox (20 µg/ml). Biomass dry weight (g/L) was measured at day 6. One biological replicate was tested for each condition.

4.4 Discussion

The purpose of this chapter was to develop new strains through targeted engineering. These were used to test model predictions, and improve mechanistic understanding of *A. niger* organic acid fermentation. A range of tools from the *A. niger* engineering tool-box were applied. These were used to switch off, up-regulate, or down-regulate the expression of target genes. New metabolic activities were also introduced. These investigations were all made using the wild-type citric acid producing ATCC1015 strain as the starting point. This was done so that the findings would closely relate to the natural acidogenic behaviour, rather than that of mutagenised strains.
The first genes to be targeted were those encoding oxaloacetate hydrolase (OAH) and glucose oxidase (GOX). These two enzymes are responsible for oxalic and gluconic acid production, respectively (Ruijter *et al*, 1999). These acids are produced at higher ambient pH (Ruijter *et al*, 1999). Organic acid fermentation at initial pH 7 was previously characterised in this project. This revealed significantly reduced citric acid production under these conditions, compared to initial pH 2. Interestingly, the timing of oxalic acid production was similar to citric, suggesting a relationship between the two acids. Meanwhile, gluconic acid was produced early in fermentation and not during the phosphate-limited growth phase, indicating it acts independently. To further investigate the production of these acids and their effect on citric, it was necessary to delete the genes responsible. It was shown that deletion of *oah* caused an oxalate-negative phenotype, and significantly increased citric acid production at initial pH 7. This was despite an excess of manganese, that would ordinarily disable citric acid production. The effect of manganese therefore seems limited to low initial pH. This finding is consistent with a previous study (Ruijter *et al*, 1999). The effects of *oah* deletion in an industrial strain were very recently reported (Yin *et al*, 2017). The knock-out had no effect on citric acid production in the industrial strain. This was not the case with the wild-type ATCC1015 strain, reported here. The discrepancy is likely due to differences in the industrial strain, resulting from its mutagenised genome. For example, expression of *oah* was shown to be down-regulated,

while a gene encoding oxalate decarboxylase was expressed at high level (Yin *et al*, 2017). Therefore, deletion of *oah* in this case has no effect, as the strain is already optimised for citric acid production. An interesting observation in this work was that the increase in citric acid produced upon *oah* deletion was considerably more than the amount of oxalic acid normally produced. This suggests the effect was regulatory, and not simply a redistribution of flux from oxalic to citric. It is possible that a cytosolic oxalate accumulation occurs in *oah* positive strains, that inhibits citric acid production. As cytosolic oxalate is absent in Δ*oah* strains, this inhibitory effect does not occur. The potential of a regulatory association between the two acids supports the idea that these acids are produced as part of the same response. Further evidence for this comes from analysis of a strain that has a mutation in the *laeA* gene. LaeA is a nuclear protein with methyltransferase activity, and acts as a global regulator of secondary metabolism (Niu *et al*, 2016). Citric and oxalic acid production no longer occurred when LaeA was disrupted, while gluconic acid was still produced (Niu *et al*, 2016). This suggests citric and oxalic acid production are under the same regulatory control. Unlike *oah*, the deletion of *gox* had no effect on citric acid production, despite causing a gluconate-negative phenotype. No effect on oxalic acid production was seen either. This provides strong evidence that gluconic acid production is decoupled from the production of oxalic and citric acid, in agreement with other observations. Although this engineering work successfully increased citric acid production at higher initial pH, the citric acid levels did not reach those obtained at initial pH 2. It is suspected that morphological differences were responsible, caused by the difference in initial pH. It is known that morphology is an important factor in citric acid fermentation, and that pH influences this (Papagianni *et al*, 1999; Papagianni and Mattey, 2006).

A key factor in citric acid production is the rate of carbon uptake, and this is a potentially limiting step (Torres *et al*, 1994). In previous work of this thesis, the effect of substrate was explored. Evidence was given that a lower carbon uptake later in fermentation is responsible for a decreased rate of citric acid production. On the other hand, an increased rate of carbon uptake earlier in

fermentation had no effect. This warranted further investigation. In this chapter, the constitutive over-expression of a low-affinity glucose transporter gene was reported. This target was chosen based on knowledge of the kinetic characteristics of *A. niger* glucose uptake (Torres *et al*, 1996a; Wayman and Mattey, 2000; Papagianni and Mattey, 2004), as well as predictions from the dynamic model. The low-affinity glucose transporter is only active at very high glucose (Torres *et al*, 1996a), and it was predicted that its constitutive activity would enable a significantly faster glucose uptake. Additionally, constitutive expression of a low-affinity glucose transporter was observed in an industrial strain, that has a much higher rate of carbon uptake (Yin *et al*, 2017). When the ATCC1015 strain was engineered to constitutively over-express a low-affinity glucose transporter, a significant increase in glucose uptake was observed. Although this was a success, the rate of glucose uptake did not reach the level predicted by the dynamic model. Post-translational regulation of the low-affinity glucose transporter cannot be ruled out. It was assumed that transcriptional control is the predominant means of regulation of this transporter. There are examples of transporter activity being controlled by post-translational regulation in other organisms. These include a nitrate transporter in *Aspergillus nidulans* (Wang *et al*, 2007), copper and zinc transporters in *Saccharomyces cerevisiae* (Radisky and Kaplan, 1999), and sucrose transporters in plants (Roblin *et al*, 1998; Krügel and Kühn, 2013). Despite the increased glucose uptake, there was no matching increase in citric acid production. This was consistent with previous observations from this work that higher carbon uptake does not enable an increased rate of citric acid production earlier in fermentation. The combined evidence indicates a rate-limiting step elsewhere, that blocks the extra carbon flux from reaching citric acid. This adds weight to the hypothesis that citric acid production is a regulated response, and not simply a consequence of overflow metabolism. It may be that a higher carbon uptake could be realised if other steps were deregulated, to accommodate the excess carbon flux and allow its passing to citric output. A blockage down-stream may trigger counteracting post-translational down-regulation of the over-expressed low-affinity glucose transporter.

Glycolytic flux is an important factor in citric acid production. There is strong evidence to suggest that its regulation at the 6-phosphofructo-1-kinase (PFK1) step plays a key role in citric acid fermentation (Schreferl *et al*, 1986; Schreferl-Kunar *et al*, 1989; Capuder *et al*, 2009). This may explain the null effect of increased carbon uptake. It was observed that PFK1 undergoes a post-translational cleavage in *A. niger*, creating a citrate-insensitive form (Mesojednik and Legiša, 2005; Mlakar and Legiša, 2006; Capuder *et al*, 2009). A modified PFK1 gene was previously expressed in the A158 strain, encoding a constitutively active PFK1 free from citrate inhibition (Capuder *et al*, 2009). This did increase citric acid production, by up to 70%. An attempt was made to reproduce the finding in this work, to see if the effect has relevance to ATCC1015 or is strain-specific. With one transformant strain, a 60% increase in citric acid production was observed, consistent with results from previous studies. When this engineered strain was further tested, it was found that the phenotypic effects resulted from plasmid integration at a disruptive site, rather than expression of the modified PFK1, as without inducer the same effects were observed. This highlighted the importance of using an inducible expression system, that allows the use of a more accurate negative control. An interesting phenotypic effect of this mutant strain was its filamentous morphology, despite its enhanced citric acid production. A pelleted morphology is usually associated with citric acid production (Papagianni and Mattey, 2006; Papagianni, 2007). This result shows that citric acid can still be produced when the morphology is in the filamentous form. An analysis of the underlying genotype of this mutant strain may provide valuable findings. With another transformant strain, a more usual behaviour was observed, with respect to the morphology. Expression of the modified PFK1 in this strain was shown to have a significant negative effect on citric acid production. This effect only occurred in the presence of inducer, confirming the targeted gene expression was responsible. Although this is contrary to previous studies, some transformants of the A158 strain also showed negative effects, though the majority were better citric acid producers (Capuder *et al*, 2009). It may be that the discrepancy is due to differences between the ATCC1015 and A158 strains. The significant effect upon expressing modified PFK1 in the ATCC1015 strain, despite being

negative, indicates that this step is an important factor. It may be that intracellular citrate production was increased, but a limitation at the step of citrate secretion prevented a corresponding increase in extracellular citrate. This bottleneck at the final step would lead to accumulation of cytosolic citrate, which may consequently trigger down-regulation of citric acid production explaining the negative effect. If so, such behaviour is unsurprising for the wild-type ATCC1015 strain. A complete and naturally evolved regulatory apparatus may be responsible for resistance to perturbations at single metabolic steps.

A potentially rate-limiting step down-stream of carbon uptake and glycolysis is mitochondrial citrate export. Since citrate synthase is exclusively localised to the mitochondria in *A. niger* (Jaklitsch *et al*, 1991), a transport step is needed to export citric acid from the mitochondria to the cytosol. It is thought that this occurs via exchange with cytosolic malate (De Jongh and Nielsen, 2008), however, the transporter is yet to be identified in *A. niger*. A recent study identified a number of candidates, and one was shown to be transcribed, but its knock-out had little effect (Kirimura *et al*, 2016). There is evidence to suggest that malate-citrate antiport is rate-limiting. When strains were engineered to increase the cytosolic malate concentration, an increase in citric acid production occurred (De Jongh and Nielsen, 2008). In this work, an attempt was made to bypass mitochondrial citrate export by introducing citrate synthase activity to the cytosol. The dynamic model was used to simulate the effect of a flux constraint on mitochondrial citrate export, and suggested the addition of cytosolic citrate synthase would override this. Engineered strains did not behave as predicted, however. Findings from an initial experiment showed a negative effect on growth, glucose uptake, and citric acid production, in comparison to strains transformed with the empty vector. In a subsequent experiment, these phenotypic effects were confirmed to be the result of genetic disruption due to the site of plasmid integration, and not cytosolic citrate synthase activity. The behaviour of one strain was significantly perturbed in the absence of inducer, with a lag phase occurring between days 2 and 4. This was coincident with a rapid release of phosphate, which was taken back up once growth resumed. Glucose uptake

continued during this lag phase, and stopped thereafter. This suggested the fungus was releasing carbon compounds, which were later consumed. Interestingly, these phenotypic effects resulting from genetic disruption were rescued by addition of inducer. This indicated a disruption of the native mitochondrial citrate synthase gene, which was without effect upon expression of compensating cytosolic citrate synthase. The observed release of phosphate is interesting. A disruption of citrate synthase may cause ATP-limiting conditions, triggering polyphosphate hydrolysis. In this work, no convincing evidence was obtained to support the hypothesis that expression of cytosolic citrate synthase increases citric acid production. This is due to positional effects of plasmid integration, and also because the effects may be cancelled out by other regulatory mechanisms. A separate study did find evidence in favour. Over-expression of a putative cytosolic citrate synthase gene in an *A. niger* strain engineered for itaconic acid production significantly increased productivity and yield (Hossain *et al*, 2016). Although the target organic acid is different, the study demonstrated that the strategy is successful in bypassing limiting mitochondrial citrate export. Further research is needed to establish whether the same success can be achieved for citric acid production in the ATCC1015 strain.

An alternative strategy to increase citric acid production is to minimise competing processes. Growth is a major competitor, diverting carbon flux away from citric acid to energise and provide resources for production of biomass. On the other hand, growth is necessary to produce the machinery required for citric acid production. Therefore, there is a fine balance between growth and citric acid production that gives the optimum productivity. The dynamic model predicts that further constraint of growth during the phosphate-limited phase is required to achieve this. The growth rate during this phase is determined by the rate of release of stored phosphate. Based on this understanding, an attempt was made in this work to decrease the activity of exopolyphosphatase (PPX). PPX is the enzyme that hydrolyses polyphosphate, allowing release of stored phosphate (Gerasimaitė and Mayer, 2017). When the expression of PPX was knocked down, an interesting phenotype emerged. A small drop in biomass production was

observed around day 2 to 3, coinciding with phosphate depletion and the onset of phosphate-limited growth. Thereafter, growth was unaffected. This result suggested that PPX knock-down had some constraining effect early in phosphate-limited growth, when PPX activity is normally high. In later stages of growth when PPX activity is lower, the effect of knock-down was too subtle to be detected, or was compensated for by up-regulatory mechanisms. It is unsurprising that PPX activity is subject to regulation, as it dissipates ATP. It is important to note that *A. niger* also has a putative endopolyphosphatase (GenBank accession number EHA17983). In *S. cerevisiae*, disruption of two polyphosphatases was required to prevent polyphosphate degradation and reduce growth rate (Gerasimaitė and Mayer, 2017). The same may be true for *A. niger*. In addition to the biomass phenotype, there was an unexpected finding. Citric acid production was negatively affected in one transformant strain, while another showed no difference. The negative effect on citric acid production was confirmed to be a result of PPX knock-down, as it was not observed in the absence of inducer. The cause of this is not clear. It indicates that there may be a more complex relationship between PPX and citric acid production. The potential function of polyphosphate in pH homeostasis (Hesse *et al*, 2002) and the possible role of PPX in reducing ATP levels could both be factors. ATP is used in formation of polyphosphate (Zhang *et al*, 2002; Gerasimaitė and Mayer, 2017), and the subsequent hydrolysis of polyphosphate by PPX may be a means to dissipate ATP. Maintenance of a low ATP level is important to citric acid production. Further investigations are needed to clarify this. A morphological effect was also linked to PPX knock-down. A shift from pelleted to filamentous morphology was observed in both transformant strains upon induction of PPX knock-down. This is also an unexpected effect, and further suggests PPX has a more complex role.

An important dynamic in citric acid fermentation is the uptake of phosphate. The kinetics of this process affect the timing of phosphate depletion and subsequent onset of phosphate-limited growth and citric acid production. To further investigate and establish more substantial evidence for this, it was necessary to disrupt the phosphate transport system in *A. niger*. An effort

was made to achieve this in the work described in this chapter. There was little research on which to base a targeting strategy. The *A. niger* phosphate transporters are yet to be characterised. A total of eight putative phosphate transporters were identified in the ATCC1015 genome, however, it was not feasible to target all of these. Therefore, phylogenetic analysis was used to identify the most convincing candidate. When the expression of this gene was knocked down, no effects could be detected. One transformant strain displayed very unusual behaviour, and this was confirmed to be due to genetic disruption caused by the site of plasmid integration rather than knock-down of the target gene. A lag phase occurred after day 2, coincident with phosphate release. This continued for three days, after which growth resumed, citric acid production commenced, and phosphate was taken back up. Interestingly, glucose uptake seemed to continue during the lag phase and stopped thereafter. This phenotype is similar to that previously described for a mutant strain engineered to express cytosolic citrate synthase. In both cases, genetic disruption was responsible for the phenotypic effects. These outcomes highlight the need for an efficient and reliable targeting system. The engineering attempt made to alter phosphate uptake characteristics was unsuccessful. A better understanding of the *A. niger* phosphate transport system is needed to inform future engineering strategies. In *S. cerevisiae*, five phosphate transporters have been identified, and disruption of all these is necessary to prevent phosphate uptake (Giots *et al*, 2003). It is likely that a similar situation exists in *A. niger*, as evidenced by its array of putative phosphate transporters and the lack of a phenotype when knocking down just one of these.

Chapter 5: Construction of the ATCC1015-specific metabolic model iDU1757

5.1 Introduction

Aspergillus niger has become an important organism exploited by industry in the production of citric acid and enzymes. These different applications of *A. niger* stem from different parent strains; the naturally evolved citric-acid-producing ATCC1015 strain and the industrial enzyme-producing CBS 513.88 strain. These two strains have both been subject to genome studies and their genomes have been sequenced and annotated (Pel *et al*, 2007; Andersen *et al*, 2011). This paved the way for genome-scale metabolic modelling of *A. niger*, and to date there are two published genome-scale metabolic models (GSMM) of *A. niger*, iMA871 (Andersen *et al*, 2008) and iHL1210 (Lu *et al*, 2017). However, these were based on the genome annotation of the enzyme-producing CBS 513.88 strain. Despite the inclusion of ATCC1015 gene assignments in iMA871, these were based on the CBS 513.88 gene-protein-reaction (GPR) associations. Therefore, the reliability of the ATCC1015 GPR associations in iMA871 is questionable.

Although the same species, the ATCC1015 and CBS 513.88 strains have significant genetic diversity, as revealed by an extensive comparative genomics study (Andersen *et al*, 2011). Each strain has around 400 to 500 unique genes, as well as regions abundant in single nucleotide polymorphisms (SNPs). This genetic diversity may underlie the different roles of the two strains, and prompts the need for an ATCC1015-specific GSMM of *A. niger* relevant to citric acid production.

The work in this chapter describes the construction of an up-to-date and ATCC1015-specific metabolic model of *A. niger*, iDU1757. An annotation process was employed that combined both Blast2GO (Conesa *et al*, 2005) and KEGG Automatic Annotation Server (KAAS) (Moriya *et al*, 2007) and used the latest and more complete version of the ATCC1015 genome. An

exhaustive list of all metabolic reactions was created based on sequence information of the ATCC1015 genome, which was used to create more accurate and reliable ATCC1015 GPR associations. Furthermore, new metabolic reactions were searched for evidence. In this chapter, the GSMM iDU1757 is presented, which has 1757 unique ORFs, 37 new metabolic reactions, and 37 new unique metabolites.

5.1.1 Aims of this Chapter

The work described in this chapter aimed to construct an up-to-date and ATCC1015-specific metabolic model of *A. niger*, to inform *in silico* guided engineering of the ATCC1015 strain.

5.2 Methods

5.2.1 Assembly of ATCC1015-specific gene-protein-reaction (GPR) associations

To assemble ATCC1015-specific GPR associations required the assignment of ATCC1015 genes to the metabolic reactions of the existing model iHL1210. One method to achieve this is by BLASTP of the CBS 513.88 gene assignments against ATCC1015 genes. This method was employed to assign ATCC1015 genes in the iMA871 model (Andersen *et al*, 2008), but was not chosen as the primary method here. This was to avoid the potential omission of metabolically relevant ATCC1015 genes that have no significant match against CBS 513.88 genes. To assemble comprehensive and reliable GPR associations specific to ATCC1015, the 11910 ATCC1015 genes of the latest ATCC1015 genome annotation from the Joint Genome Institute (v 4.0) (Andersen *et al*, 2011) were mapped to KEGG reactions. This was achieved by the use of two annotation tools; Blast2GO (Conesa *et al*, 2005), and KEGG Automatic Annotation Server (KAAS) (Moriya *et al*, 2007). Blast2GO is a Java application that assigns Gene Ontology (GO) terms to input sequences using annotation rules and BLAST. The GO terms can subsequently be mapped to EC numbers. Blast2GO version 2.7.2 was used, and BLASTP was performed using the non-redundant (nr) protein database from the NCBI. EC numbers were assigned to ATCC1015 genes, and these were mapped to KEGG reactions. KAAS is a web-based server that assigns KEGG Orthology (KO) terms to gene sequences. The ATCC1015 genes were assigned KO terms by KAAS, and these were mapped to KEGG reactions. The two lists of KEGG reactions were combined. The resulting reaction list was searched against the iHL1210 reactions to identify reactions already present in the model, and new reactions based on sequence information. Reaction matches were used to assign ATCC1015 genes. iHL1210 reactions without a match were assigned ATCC1015 genes either by matching EC numbers and KO terms or by BLASTP of the *A. niger* genes

in iHL1210. Thresholds of 90% identity and e-value 1e-20 were used for the comparison.

5.2.2 Evidence-based verification of new metabolic reactions

Reactions without a match in iHL1210 were searched for evidence in an exhaustive body of literature using a custom-built automated text search approach in Python. The body of literature contained all records with *Aspergillus niger* or *A. niger* in the title, obtained from Web of Science. The full text was searched if available through the University of York Library or open access. The abstract was searched if the full text could not be accessed, and the title was searched if the abstract was unavailable. Reactions were searched for evidence in each record by using an exhaustive list of search terms for each compound. To increase specificity, common compounds were not searched (KEGG compounds: C00001, C00002, C00003, C00004, C00005, C00006, C00007, C00008, C00009, C00010, C00011, C00013, C00014, C00016, C00027, C00080). Compound search terms were compiled from the following databases: KEGG, MMCD, HMD, PubChem, ChEBI, PDB-CCD, 3DMET, NIKKAJI, KNApSAcK, LIPIDMAPS, and LipidBank. To increase specificity, search terms less than three characters were not searched. The percentage of reaction compounds found of those searched and number of search hits were recorded and used to rank the results. Reactions with 60% or more compounds found were manually checked for evidence in records with search hits. Reactions with evidence were added to the model.

5.3 Results

5.3.1 Assembly of ATCC1015-specific gene-protein-reaction associations

The gene assignments in the latest metabolic model of *A. niger*, iHL1210 (Lu *et al*, 2017), correspond to the enzyme producing CBS 513.88 strain. The previous model, iMA871 (Andersen *et al*, 2008), included ATCC1015 gene assignments. However, these were secondary and mapped from CBS 513.88 genes using an older version of the ATCC1015 genome annotation. To create an up-to-date and ATCC1015-specific model of *A. niger*, a reconstruction process (Figure 5.1) was employed based on the latest ATCC1015 genome annotation (Andersen *et al*, 2011). Available from the Joint Genome Institute, version 4.0 has 11910 genes compared to 11197 genes in version 3.0 used in iMA871. The 713 extra genes in the latest annotation explain the missing ATCC1015 gene assignments in iMA871. In the reconstruction process, two annotation tools were used; Blast2GO (Conesa *et al*, 2005) and KEGG Automatic Annotation Server (KAAS) (Moriya *et al*, 2007). Using Blast2GO, 2372 genes were mapped to 981 EC numbers, which were mapped to 2163 KEGG reactions. Using KAAS, 3043 genes were mapped to 2624 KO (KEGG Orthology) terms. 1036 of these KO terms were mapped to 1514 KEGG reactions. From the KAAS output, 1370 genes mapped to 768 EC numbers, and 1340 genes mapped to KEGG reactions. The outputs from Blast2GO and KAAS were compared. 283 of the 1514 KEGG reactions from the KAAS output were not found in the Blast2GO output. 932 of the 2163 KEGG reactions from the Blast2GO output were not found in the KAAS output. The differences are likely due to the Blast2GO output being more exhaustive and the KAAS output being more specific. The two reaction lists were combined into 2446 KEGG reactions from a total of 2630 ATCC1015 genes. 868 of these 2446 KEGG reactions were matched to 995 reactions in iHL1210. Of the iHL1210 reactions without a match, 125 were matched to EC numbers and KO terms from the annotation process, bringing the total number of reaction matches to 1120. The corresponding

ATCC1015 genes were assigned to these 1120 reactions. The remaining reactions in iHL1210 were assigned ATCC1015 genes by BLASTP of the *A. niger* genes in iHL1210. The gene assignments for 11 of these reactions had no hits above the identity and e-value thresholds (90% and 1e-20) (Table 5.1). Two of these had hits within the e-value threshold but below the identity threshold, which were included. The other gene assignments were searched against version 3.0 of the ATCC1015 genome annotation, and the gene assignments for two reactions had hits which were included. This resulted in a total of 1730 unique ATCC1015 genes and an intermediate model. This is a significant increase of 520 ORFs over the 1210 ORFs in iHL1210. Of the 1730 genes, 689 have no match to genes in iHL1210. The reactions with no match in iHL1210 were taken as a sequence-based list of new metabolic reactions.

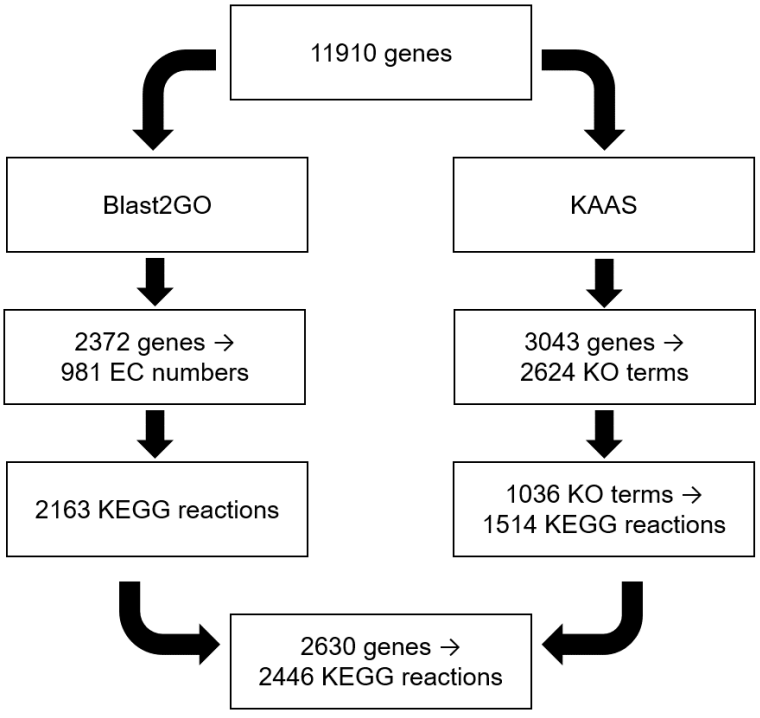

Figure 5.1. Schematic of annotation process used to map ATCC1015 genes to KEGG reactions.

Table 5.1. iHL1210 reactions for which no hits were found in version 4.0 of the ATCC1015 genome annotation.

iHL1210 reaction	Description	iHL1210 gene assignment	Top ATCC1015 hit (v 4.0)	e-value	identity (%)	Top ATCC1015 hit (v 3.0)	e-value	identity (%)
R311	2-keto-3-deoxy-L-rhamnonate aldolase	An03g00040	Aspni7_1145855	4e-75	44	ASPNIDRAFT_194527	0	96
R414	Phosphoacetylglucosamine mutase	An18g05160 or An18g05170	No hits			ASPNIDRAFT_212120	2e-153	100
R1219	Glycerol:NADP+ 2-oxidoreductase (glycerone forming)	An04g10070	Aspni7_1108731	1e-92	46	ASPNIDRAFT_183753	1e-92	46
R1332	H_2O transporter	An14g02450	Aspni7_1161552	0	84	ASPNIDRAFT_125829	0	84
R1419	D-fructose transport via PEP:Pyr PTS	An11g08360	No hits			No hits		
R1420	D-fructose transport via PEP:Pyr PTS	An11g08360	No hits			No hits		
R1468	L-arginine transport via ABC system	An13g01100	No hits			No hits		
R1479	L-lysine transport via ABC system	An13g01100	No hits			No hits		
R1483	L-proline transport via ABC system	An12g06100	No hits			No hits		

iHL1210 reaction	Description	iHL1210 gene assignment	Top ATCC1015 hit (v 4.0)	e-value	identity (%)	Top ATCC1015 hit (v 3.0)	e-value	identity (%)
R1493	Ornithine transport via ABC system	An13g01100	No hits			No hits		
R1515	Acetoacetate transport via proton symport	An08g11830	No hits			No hits		

5.3.2 Evidence-based verification of new metabolic reactions and construction of iDU1757

The reactions in the reaction list that could not be found in iHL1210 were searched in the *A. niger* literature for evidence. Evidence was found for 34 reactions (Table 5.2). Two additional reactions not present in the reaction list were added based on literature evidence. One of these (R01767) completed the amygdalin degradation pathway (Chang and Zhang, 2012). The other reaction, the interconversion of galactitol and L-sorbose, filled the missing link in the oxidoreductive galactose catabolic pathway (Mojzita *et al*, 2012a; Mojzita *et al*, 2012b). One reaction (R02396), the means of mitochondrial acetyl transfer via acetylcarnitine (Jernejc and Legiša, 1996; Jernejc *et al*, 1991), was added to both cytosolic and mitochondrial compartments. A new transport reaction that completes the mitochondrial acetyl transfer pathway via acetylcarnitine was added. These 37 new reactions were added to the model. An additional 27 unique genes corresponding to these new reactions were added, giving a total of 1757 unique ATCC1015 genes and the ATCC1015-specific model iDU1757. An additional ten transport reactions (Table 5.3) and 34 input/output reactions (Table 5.4) were added to iDU1757. The total number of reactions in iDU1757 is 1845. 47 new compounds are included in iDU1757 (Table 5.5), 37 of which are new unique metabolites, bringing the total number of unique metabolites to 939. A large number of reactions in the sequence-based list were not included in iDU1757 due to the absence of literature evidence. Corresponding to these excluded reactions, there are 1020 unique ATCC1015 genes absent from iDU1757, which have putative metabolic activities. There is therefore the potential for expansion of metabolic coverage.

Table 5.2. New reactions in iDU1757 and corresponding literature evidence.

KEGG reaction	iDU1757 reaction	Function	Evidence
R06077	CELLUe+H2Oe-->BDGLCe	Cellulose degradation	Bansal *et al*, 2014
R06101	STACe+H2Oe-->MNNTe+FRUe	Stachyose degradation	Goosen *et al*, 2007; Rubio and Maldonado, 1995
R06202	GALACTANe+H2Oe-->GLACe	Galactan degradation	Manzanares *et al*, 1998
Not found	GALOL+NAD<==>SOR+NADH	Oxidoreductive galactose catabolism	Mojzita *et al*, 2012a; Mojzita *et al*, 2012b
R00053	D345THBe+H2Oe-->345THBe	Digallate degradation	Yu *et al*, 2007; Yu and Li, 2005; Ramos *et al*, 2011; Srivastava and Kar, 2009; Lippitsch, 1961
R03372+R03394	IP6e+4*H2Oe-->IP2e+4*PIe	Phytate degradation	Tomschy *et al*, 2000; Dvořáková *et al*, 2000
R02997	CLGe+H2Oe-->CAFe+QTe	Chlorogenate degradation	Asther *et al*, 2005; Benoit *et al*, 2007
R10040	LNMe+H2Oe-->ACHe+BDGLCe	Linamarin degradation	Birk *et al*, 1996
R02156	QCTe+O2e-->2PCe+COe	Quercetin degradation	Hund *et al*, 1999
R02985	AMYDe+H2Oe-->PRNSe+DGLCe	Amygdalin degradation	Chang and Zhang, 2012

KEGG reaction	iDU1757 reaction	Function	Evidence
R02558	PRNSe+H2Oe-->MDNe+DGLCe	Amygdalin degradation	Chang and Zhang, 2012
R01767	MDNe-->HCNe+BALe	Amygdalin degradation	Chang and Zhang, 2012
R04103	PCNe+H2Oe<==>6APCNe+PHACe	Penicillin G degradation	Bashir *et al*, 2008
R03024	4NPPe+H2Oe-->4NPe+PIe	4-nitrophenyl phosphate degradation	Chelius and Wodzinski, 1994; Phillippy and Mullaney, 1997; Ashokkumar *et al*, 2004; Żyła and Gogol, 2002; Gargova *et al*, 2006
R00505	UDPGAL<==>UDPGALF	UDP-alpha-D-galactofuranose for galactoglucomannan production	Damveld *et al*, 2008
R01758	LAOL+NAD-->LARAB+NADH+H	L-arabitol oxidation	Witteveen *et al*, 1989
R09477	XOL+NAD-->XYL+NADH+H	Xylitol oxidation	Witteveen *et al*, 1989
R02396	ACCOAm+CARm<==>COAm+ALCARm	Mitochondrial acetyl transfer	Jernejc and Legiša, 1996; Jernejc *et al*, 1991
Transport reaction	CARm+ALCAR<==>CAR+ALCARm	Mitochondrial acetyl transfer	Jernejc and Legiša, 1996; Jernejc *et al*, 1991
R02396	ACCOA+CAR<==>COA+ALCAR	Mitochondrial acetyl transfer	Jernejc and Legiša, 1996; Jernejc *et al*, 1991
R00731	TYR+O2-->LDOPA+H2O	L-Dopa production	Ali and Haq, 2010

KEGG reaction	iDU1757 reaction	Function	Evidence
R00031	O2+2*TYR-->2*LDOPA	L-Dopa production	Ali and Haq, 2010
R04300	DPA+H2O+O2-->DHPHA+NH3+H2O2	Dopamine metabolism	Hoover *et al*, 1991
R02080	LDOPA-->DPA+CO2	L-Dopa metabolism	Ali and Haq, 2010
R00045	O2+2*LDOPA-->2*DQ+2*H2O	L-Dopa metabolism	Ali and Haq, 2010
R01010	T3P2+H2O-->GLYN+PI	Glycolytic reaction	R Poulsen *et al*, 2005
R07253	ACCOA+3*MALCOA+NADPH-->6MSA+4*COA+3*CO2+NADP+H2O	6-methylsalicylate production	Holm *et al*, 2014
R01408	HCN+H2O-->FMM	Cyanide degradation	Rinágelová *et al*, 2014
R02943	TRP+DMPP-->DMAT+PPI	Tryptophan prenylation	Fan *et al*, 2014
R01657	DMPP+TRP-->PPI+MBT	Tryptophan prenylation	Fan *et al*, 2014
R05655	PHN+O2+NADH+H-->PHNO+H2O+NAD	Phenanthrene degradation	Parshikov *et al*, 2015a; Cortés-Espinosa *et al*, 2011; Yogambal and Karegoudar, 1997; Sack *et al*, 1997
R00815	PHL+O2+NADPH+H-->CCL+NADP+H2O	Phenol degradation	Deng *et al*, 2015
R01372	PHPYR+O2-->2HPAC+CO2	Phenylalanine metabolism	Kishore *et al*, 1976

KEGG reaction	iDU1757 reaction	Function	Evidence
R01836	TST+NAD-->AND+NADH+H	Steroid biotransformation	Parshikov and Sutherland, 2015b
R01838	TST+NADP-->AND+NADPH+H	Steroid biotransformation	Parshikov and Sutherland, 2015b
R01837	DHAND+NAD-->AND+NADH+H	Steroid biotransformation	Parshikov and Sutherland, 2015b
R07855	PHAN+H2O-->PHAC+NH3	Phenylacetonitrile degradation	Parshikov *et al*, 2015a; Šnajdrová *et al*, 2004; Kaplan *et al*, 2006

Table 5.3. New transport reactions in iDU1757.

iDU1757 reaction	Function
BALe<==>BAL	Benzaldehyde uptake from extracellular amygdalin degradation
CPGIII-->CPGIIIm	Coproporphyrinogen III transport to mitochondria for heme biosynthesis
H2O2<==>H2O2m	Hydrogen peroxide mitochondrial transport, required in heme biosynthesis pathway
HCNe<==>HCN	Cyanide uptake, required for intracellular cyanide degradation
PHNe<==>PHN	Phenanthrene uptake, required for intracellular phenanthrene degradation
PHLe<==>PHL	Phenol uptake, required for intracellular phenol degradation
TSTe<==>TST	Testosterone uptake, required for intracellular testosterone biotransformation
ANDe<==>AND	Androstenedione export, from intracellular testosterone and dehydroepiandrosterone biotransformation
DHANDe<==>DHAND	Dehydroepiandrosterone uptake, required for intracellular dehydroepiandrosterone biotransformation
PHANe<==>PHAN	Phenylacetonitrile uptake, required for intracellular phenylacetonitrile degradation

Table 5.4. New input/output reactions in iDU1757.

iDU1757 reaction	Function
GALACTANe<==>	Galactan input for galactan degradation
D345THBe<==>	Digallate input for digallate degradation
IP6e<==>	Phytate input for phytate degradation
CLGe<==>	Chlorogenate input for chlorogenate degradation
LNMe<==>	Linamarin input for linamarin degradation
QCTe<==>	Quercetin input for quercetin degradation
AMYDe<==>	Amygdalin input for amygdalin degradation

iDU1757 reaction	Function
PRNSe<==>	Prunasin input for prunasin degradation
MDNe<==>	Mandelonitrile input for mandelonitrile degradation
PCNe<==>	Penicillin G input for penicillin G degradation
4NPPe<==>	4-nitrophenyl phosphate input for 4-nitrophenyl phosphate degradation
DIGALURe<==>	Digalacturonate input for digalacturonate degradation
6MSA<==>	6-methylsalicylate output from 6-methylsalicylate production
PHNe<==>	Phenanthrene input for phenanthrene degradation
PHLe<==>	Phenol input for phenol degradation
TSTe<==>	Testosterone input for steroid biotransformation
DHANDe<==>	Dehydroepiandrosterone input for steroid biotransformation
PHANe<==>	Phenylacetonitrile input for phenylacetonitrile degradation
CAFe<==>	Caffeate output from chlorogenate degradation
ACHe<==>	Acetone cyanohydrin output from linamarin degradation
FMM<==>	Formamide output from cyanide degradation
6APCNe<==>	6-Aminopenicillanate output from penicillin G degradation
IP2e<==>	1D-myo-Inositol 1,4-bisphosphate output from phytate degradation
4NPe<==>	4-nitrophenol output from 4-nitrophenyl phosphate degradation
MNNTe<==>	Manninotriose output from stachyose degradation
2PCe<==>	2-Protocatechoylphloroglucinolcarboxylate output from quercetin degradation
COe<==>	Carbon monoxide output from quercetin degradation
LDOPA<==>	L-Dopa output from L-Dopa production

iDU1757 reaction	Function
DHPHA<==>	3,4-dihydroxyphenylacetaldehyde output from dopamine metabolism
DQ<==>	Dopaquinone output from L-Dopa metabolism
DMAT<==>	Dimethylallyltryptophan output from tryptophan prenylation
MBT<==>	4-(3-Methylbut-2-enyl)-L-tryptophan output from tryptophan prenylation
PHNO<==>	1-Phenanthrol output from phenanthrene degradation
ANDe<==>	Androstenedione output from steroid biotransformation

Table 5.5. New compounds in iDU1757.

iDU1757 compound	KEGG compound	Compound name
MNNTe	C05404	Manninotriose (extracellular)
GALACTANe	C05796	Galactan (extracellular)
D345THBe	C01572	Digallate (extracellular)
IP6e	C01204	Phytate (extracellular)
IP2e	C01220	1D-myo-Inositol 1,4-bisphosphate (extracellular)
CLGe	C00852	Chlorogenate (extracellular)
CAFe	C01197	Caffeate (extracellular)
LNMe	C01594	Linamarin (extracellular)
ACHe	C02659	Acetone cyanohydrin (extracellular)
QCTe	C00389	Quercetin (extracellular)
2PCe	C04524	2-Protocatechoylphloroglucinolcarboxylate (extacellular)
COe	C00237	Carbon monoxide (extracellular)
AMYDe	C08325	Amygdalin (extracellular)
PRNSe	C00844	Prunasin (extracellular)
MDNe	C00561	Mandelonitrile (extracellular)
HCNe	C01326	Hydrogen cyanide (extracellular)
PCNe	C05551	Penicillin G (extracellular)
6APCNe	C02954	6-Aminopenicillanate (extracellular)
4NPPe	C03360	4-nitrophenyl phosphate (extracellular)
4NPe	C00870	4-nitrophenol (extracellular)
UDPGALF	C03733	UDP-alpha-D-galactofuranose

iDU1757 compound	KEGG compound	Compound name
ALCARm	C02571	O-Acetylcarnitine (mitochondrial)
ALCAR	C02571	O-Acetylcarnitine
LDOPA	C00355	3,4-dihydroxy-L-phenylalanine (L-Dopa)
DPA	C03758	Dopamine
DHPHA	C04043	3,4-dihydroxyphenylacetaldehyde
DQ	C00822	Dopaquinone
6MSA	C02657	6-methylsalicylate
HCN	C01326	Hydrogen cyanide
FMM	C00488	Formamide
DMAT	C06067	Dimethylallyltryptophan
MBT	C04290	4-(3-Methylbut-2-enyl)-L-tryptophan
CPGIIIm	C03263	Coproporphyrinogen III (mitochondrial)
PHNe	C11422	Phenanthrene (extracellular)
PHN	C11422	Phenanthrene
PHNO	C11432	1-Phenanthrol
PHLe	C00146	Phenol (extracellular)
PHL	C00146	Phenol
TSTe	C00535	Testosterone (extracellular)
TST	C00535	Testosterone
ANDe	C00280	Androstenedione (extracellular)
AND	C00280	Androstenedione
DHANDe	C01227	Dehydroepiandrosterone (extracellular)
DHAND	C01227	Dehydroepiandrosterone

iDU1757 compound	KEGG compound	Compound name
PHANe	C16074	Phenylacetonitrile (extracellular)
PHAN	C16074	Phenylacetonitrile
BALe	C00261	Benzaldehyde (extracellular)

5.3.3 Changes in iDU1757 to reactions from iHL1210

In constructing the iDU1757 model, some changes were made to reactions from iHL1210. The reaction that produces galactoglucomannan was altered to require UDP-alpha-D-galactofuranose based on literature evidence (Damveld *et al*, 2008). The coefficients of UDP-galactose and UDP-glucose were changed from 0.435 to 0.332 and from 0.13 to 0.1 respectively, and the coefficient of UDP-alpha-D-galactofuranose was set to 0.133. UDP-alpha-D-galactofuranose is a new compound in iDU1757 and produced by isomerisation of UDP-galactose, a new reaction in iDU1757. This new reaction is essential to biomass production, to produce the galactoglucomannan component of the cell wall, and therefore is a new growth target in iDU1757. Some errors were found in reactions from iHL1210, and corrections were made either to reaction species (Table 5.6) or compartmentalisation (Table 5.7).

Table 5.6. Reaction species corrections made to reactions from iHL1210.

iHL1210 reaction	iDU1757 reaction	KEGG reaction
GTP-->D6RP5P+PPI+FOR+H	GTP+3*H2O-->D6RP5P+PPI+FOR+3*H	R00425
CELLUe-->CELLOBe	CELLUe+H2Oe-->CELLOBe	R06200
3*O2m+2*PPPG9-->2*PPP9m+6*H2Om	3*O2m+PPPG9m-->PPP9m+3*H2O2m	R03222
SAM+UPGIII-->SAH+PRECOR	2*SAM+UPGIII-->2*SAH+PRECOR	R03194
Hm+NADPHm+ABUTm<==>NADPm+DMVATm	Hm+NADPHm+ABUTm<==>NADPm+DHMVAm	R05068
DMVATm-->H2Om+OMVALm	DHMVAm-->H2Om+OMVALm	R05070
HICITm+NADm<==>OXAm+CO2m+NADHm	HICITm+NADm<==>OXAm+NADHm	R04862
SAM-->SAH+5MCSN	SAM+CYTS-->SAH+5MCSN	Not found
APROP-->ALA+NH3	APROP+2*H2O-->ALA+NH3	R03542
ACYBUT-->GLU+NH3	ACYBUT+2*H2O-->GLU+NH3	R01887
DCTOL+3*O2+3*NADPH+3*H-->DCDOL+FOR+3*NADP+4*H2O	DCTOL+NADPH-->DCDOL+NADP	R05639

iHL1210 reaction	iDU1757 reaction	KEGG reaction
DCDOL+3*NADPH+3*O2-->DCDA+3*NADP	DCDOL+3*NADPH+3*O2-->DCDA+3*NADP+4*H2O	R07509
H2SO3+O2+H2O<==>S+H2O2	H2SO3+O2+H2O<==>SLF+H2O2	R00533
ACNL-->INAC+NH3	ACNL+2*H2O-->INAC+NH3	R03093
GL+NAD-->GLYN+NADH+H	GL+NADP-->GLYN+NADPH+H	R01039

Table 5.7. Compartmentalisation corrections made to reactions from iHL1210.

iHL1210 reaction	iDU1757 reaction
CPGIII+O2+2*H-->2*CO2+PPPG9+2*H2O	CPGIIIm+O2m+2*Hm-->2*CO2m+PPPG9m+2*H2Om
PECTIN+H2O-->METHOL+PECTATE	PECTINe+H2Oe-->METHOLe+PECTATEe
PECTATE+H2O-->GALUNT+H	PECTATEe+H2Oe-->GALUNTe+He
PECTATE+H2O-->DIGALUR+2*H	PECTATEe+H2Oe-->DIGALURe+2*He
DIGALUR+H2O-->2*GALUNT	DIGALURe+H2Oe-->2*GALUNTe
FRUCTAN+H2O-->FRU	FRUCTANe+H2Oe-->FRUe

iHL1210 reaction	**iDU1757 reaction**
XYLAN+H2O-->XYL	XYLANe+H2Oe-->XYLe
STAR+H2O-->AMYLS+GLC	STARe+H2Oe-->AMYLSe+GLCe
AMYLSe+H2O-->GLC	AMYLSe+H2Oe-->GLCe
STAR+H2O-->DEXTRIN	STARe+H2Oe-->DEXTRINe
STAR+H2O-->GLC	STARe+H2Oe-->GLCe
DEXTRIN+H2O-->GLC	DEXTRINe+H2Oe-->GLCe
13GLUCAN+H2O-->GLC	13GLUCANe+H2Oe-->GLCe
OICAPm+GLU<==>AKG+LEU	OICAP+GLU<==>AKG+LEU

5.3.4 New substrates in iDU1757

iDU1757 has nine new carbon sources (Table 5.8), one new nitrogen source (Table 5.9), and two new phosphate sources (Table 5.10). These new substrates were tested by FBA simulations of iDU1757 and confirmed to function as sole substrates. Two of these have empirical evidence; phenol as a carbon source (Sharma and Gupta, 2012a) and phytate as a phosphate source (da Silva *et al*, 2005); while the rest are hypothetical.

Table 5.8. New carbon sources in iDU1757.

iDU1757 compound	KEGG compound	Compound name	Empirical evidence
GALACTANe	C05796	Galactan (extracellular)	Hypothetical
CLGe	C00852	Chlorogenate (extracellular)	Hypothetical
LNMe	C01594	Linamarin (extracellular)	Hypothetical
AMYDe	C08325	Amygdalin (extracellular)	Hypothetical
PRNSe	C00844	Prunasin (extracellular)	Hypothetical
MDNe	C00561	Mandelonitrile (extracellular)	Hypothetical
PCNe	C05551	Penicillin G (extracellular)	Hypothetical
PHLe	C00146	Phenol (extracellular)	Sharma and Gupta, 2012a
PHANe	C16074	Phenylacetonitrile (extracellular)	Hypothetical

Table 5.9. New nitrogen sources in iDU1757.

iDU1757 compound	KEGG compound	Compound name	Empirical evidence
PHANe	C16074	Phenylacetonitrile (extracellular)	Hypothetical

Table 5.10. New phosphate sources in iDU1757.

iDU1757 compound	KEGG compound	Compound name	Empirical evidence
IP6e	C01204	Phytate (extracellular)	da Silva *et al*, 2005
4NPPe	C03360	4-nitrophenyl phosphate (extracellular)	Hypothetical

5.3.5 Input/output fluxes in iDU1757

The new model iDU1757 was applied to FBA simulations of citric acid production, using parameters from the previously described dynamic model of *A. niger* citric acid fermentation. The biomass composition used is shown in Table 5.12, which is largely the same as iHL1210 with some modifications based on previous fitting to empirical data. The non-growth associated maintenance (NGAM) was set to 1.9 mmol gDW^{-1} h^{-1}, in accordance with iMA871, as this parameter was applied in fitting of the dynamic model. Acid dissociation reactions were included in iDU1757, for modelling of organic acid production driven by proton production (Andersen *et al*, 2009b). The input/output fluxes corresponding to the two growth phases, phosphate storage and proton production, are shown in Table 5.11. These give a more accurate prediction of citric acid flux than previous models which were based on citric acid being produced as a by-product during growth or forcing citric output at a fixed value (Lu *et al*, 2017; Andersen *et al*, 2008). In this case, citric acid is produced for the objective of proton production during phosphate-limited growth.

Table 5.11. Input/output fluxes in iDU1757.

Input/output reaction	Flux during phosphate storage (mmol h^{-1} gDW^{-1})	Flux during proton production (mmol h^{-1} gDW^{-1})
Glucose (DGLCe<==>)	-0.445	-0.317
External phosphate (PIe<==>)	-0.0144	0.0
Internal phosphate (PI<==>)	0.0124	-7.43E-4
Oxygen (O2e<==>)	-0.974	-0.552
Protons (Hpe<==>)	0.0	0.0062
Citric acid (CIT-e<==>)	0.0	0.162
Biomass	0.0435	0.0159

Table 5.12. Biomass composition in iDU1757.

Component	mmol gDW^{-1}
ALA	0.285419
ARG	0.112059
ASN	0.063577
ASP	0.177634
CYS	0.021777
GLU	0.280437
GLN	0.1301
GLY	0.227706
HIS	0.055525
ILE	0.105128
LEU	0.186022
LYS	0.217713

Component	**mmol gDW^{-1}**
MET	0.027995
PHE	0.082496
PRO	0.116563
SER	0.170194
THR	0.141109
TRP	0.039378
TYR	0.059275
VAL	0.144508
AMP	0.0046740733
GMP	0.0056294467
CMP	0.0046740733
UMP	0.0037247467
DAMP	0.0006457867
DCMP	0.0006718133
DTMP	0.0006457867
DGMP	0.0006718133
GAG	0.01634
NIG	0.09652
PSNIG	0.12806
GGM	0.14478
14GLUCAN	0.14782
13GLUCAN	1.03588
CHIT	0.61674
TAGLY	0.010083
DAGLY	0.001009
MAGLY	0.008912

Component	**mmol gDW^{-1}**
C140	0.000223
C160	0.00148
C180	0.000245
C181	0.001678
C182	0.001664
C183	0.000047
ERGOST	0.034062
ERGOSE	0.010038
MGDG	0.030053
MGC181	0.012374
DGDG	0.007859
TGDMIPC	0.000005
CERB1	0.00003
CERB2	0.000031
GALCER	0.000025
GLUCER1	0.000024
GLUCER2	0.000024
CL	0.001746
PC	0.005104
PS	0.0001196667
PE	0.0116023333
ORN	0.00553
ICIT	0.00039
CIT	0.013
SUCC	0.00091
FUM	0.00007

Component	**mmol gDW^{-1}**
MAL	0.00065
NAD	0.0017
NADH	0.00018
NADP	0.00014
NADPH	0.00008
TRE	0.04
MNT	0.18
GL	0.9030928715
EOL	0.3
AOL	0.01
BT	0.0001
COA	0.0001
FOLATE	0.0001
HEMEAm	0.0001
THDP	0.0001
SIHM	0.0001
Q	0.0001
SPMD	0.0001
PTRC	0.0001
RGT	0.0001
DSAM	0.0001
RIBOFLAVIN	0.0001
PYDX	0.0001
CHOR	0.0001
CYTCCm	0.0001
ATP	71.5025735267

Component	**mmol gDW^{-1}**
H2O	69.0511151733
ADP	-71.5025795733
PI	-71.5025795733

5.4 Discussion

The work in this chapter has presented the up-to-date metabolic model iDU1757, specific to *A. niger* ATCC1015, the parent of industrial citric acid producing strains. iDU1757 is the most complete *A. niger* metabolic model to date, and with 1757 ORFs, demonstrates enormous metabolic flexibility. The exhaustive ATCC1015-specific GPR provided in iDU1757 is an invaluable resource for engineering efforts. Using the latest ATCC1015 genome information, 2446 KEGG reactions have been revealed from 2630 ATCC1015 genes, highlighting the metabolic potential of this organism. Many of these are yet to be included in the *A. niger* metabolic model, due to the lack of supporting empirical data, and give targets for future studies to further elucidate the metabolic coverage provided by *A. niger*.

Chapter 6: *In silico* evolution of organic acid production as predictive tool for engineering

6.1 Introduction

In recent years, major advances have been made in systems biology approaches (Brandl and Andersen, 2017), that lay promise for a replacement of traditional strain development methods with more efficient, *in silico* guided ones. Many decades of random mutagenesis were needed to create the strains used in industry today. Although these industrial strains are already optimised for citric acid production, they are reliant on sucrose-based feed-stocks (Dhillon *et al*, 2013a). There is an increasing need for a switch to more sustainable fermentation methods that use lower cost substrates and underused resource streams. More efficient strain development procedures are therefore indispensable. Furthermore, *A. niger* holds the metabolic potential to convert wide-ranging feed-stocks into a plethora of value-added chemicals. Genome sequencing efforts as well as improvements in targeted engineering strategies are making available the tools necessary to develop strains that release this potential.

Genome-scale metabolic modelling opens up the possibility to couple genomic and metabolomic information with computational techniques aimed at guiding metabolic engineering strategies. The mathematical method of flux balance analysis (FBA) has been used to make predictions of growth and output of metabolites in response to different conditions, and to probe the effects of gene knock-outs. The work in this thesis established a dynamic model of *A. niger* organic acid fermentation, that accurately captures physiological characteristics, providing a more accurate predictive platform to inform engineering strategies. Furthermore, an up-to-date metabolic model was constructed, iDU1757, and equipped with exhaustive gene-protein-reaction associations specific to the ATCC1015 strain. The power of FBA models has been underexploited, with most studies focused on simulating gene knock-outs (Choon *et al*, 2014; Choon *et al*, 2015; Chong *et al*, 2014;

San Chua *et al*, 2015; Patil *et al*, 2005; Rocha *et al*, 2008). The effects of forcing or constraining flux of metabolic reactions can also be predicted, informing knock-up and knock-down strategies, and not limited to gene deletion.

A metabolic engineering strategy often involves a multitude of targets. Computational approaches can be used to exhaustively evaluate combinations of a small number of targets. On increasing the complexity of combinations, the resulting combinatorial explosion leads to an enormous search space. Moreover, the incorporation of targets that force or constrain flux to differing degrees significantly expands the search space. To find optimal solutions in search spaces that are beyond the reach of exhaustive methods requires metaheuristic algorithms. These algorithms are capable of finding optimal solutions without the need for an exhaustive search, making them computationally feasible. They are typically inspired by nature. One such algorithm is the genetic algorithm (GA) or evolutionary algorithm (EA), that is designed based on natural evolutionary processes. The GA uses selection, elimination, mutation, and recombination operators to evolve a population of individuals towards increased fitness. A fitness function is needed to evaluate the fitness of individuals. An individual is represented by a genome, and the values of its genes inform the fitness function. The function applied defines the optimisation problem and the evolutionary goal. Mutation and recombination are used to create new individuals from selected parents. Mutation changes the values of genes at a frequency dependent on the mutation rate. Recombination crosses over genes from parents at a frequency dependent on the recombination rate, and is based on Mendelian inheritance. The new individuals fill a population gap created by elimination, and parents are chosen by selection. Elimination and selection are based on fitness, and the exact design of these operators can lead to significant variation in the evolutionary performance of the GA. The parameters given to the mutation and recombination rates also have to be optimised. The population is subjected to evolution until a desired fitness is reached, or for a fixed number of generations.

While many other metaheuristic algorithms exist, with examples being simulated annealing, ant colony optimisation, the bee algorithm, particle swarm optimisation, the bat algorithm, harmony search, and the firefly algorithm, each is suited to different applications. The genetic algorithm was most applicable to this work. A GA was designed for *in silico* evolution of organic acid production, to find solutions that optimise the production of a given acid. The genomes of individuals represented the flux bounds, and were composed of two chromosomes, one for the lower bounds and one for the upper bounds. Mutations forced or constrained flux by small values, with the effect strengthened by cumulative mutations. Fitness was evaluated by a function that estimated the rate of production of a target organic acid, using information from FBA simulations done with the iDU1757 model. Static FBA was parameterised based on the previously developed dynamic model, and applied to chosen time-points of fermentation. Time-course simulations would more accurately evaluate fitness, however, are computationally expensive and would significantly slow down the speed of the GA. The operators of the GA were designed and its parameters tuned to give an optimal evolutionary performance for this application.

Once developed, the algorithm was first employed to find predictive solutions that optimise citric acid production. Built into the model are a number of acid-dissociation reactions, providing different means of acidification. As well as citric, these include succinic, lactic, malic, acetic, and gluconic. The production of these other acids is not normally predicted. It should be noted that in this instance gluconic acid refers to production by intracellular reactions rather than extracellular glucose oxidase. The full power of the algorithm designed in this work was demonstrated by successfully evolving production of these acids, switching acid output from citric to the target acid. The solutions found required complex combinations of mutations, with finely tuned flux bounds, highlighting the importance and value of metaheuristic approaches to solving these problems. The results obtained by use of this algorithm have biotechnological significance, suggesting engineering strategies that could develop *A. niger* strains as production platforms for these various organic acids of commercial value. Seeing that there is

pressure to switch to alternative feed-stocks, *in silico* evolution of citric and succinic acid production were also performed on xylose.

6.1.1 Aims of this Chapter

The work described in this chapter aimed to develop a predictive computational tool based on a genetic algorithm, and to apply this in simulated evolution of organic acid production to suggest targets for engineering that optimise production of a given acid.

6.2 Methods

6.2.1 Designing of genetic algorithm for *in silico* evolution

To achieve *in silico* evolution of organic acid production, a genetic algorithm (GA) was designed. The flux bounds of the reactions in the iDU1757 model were subjected to evolution, with evolutionary pressure to maximise the rate of production of a given organic acid. Each flux bound represented a gene, with the lower bounds being on chromosome 1 and the upper bounds on chromosome 2. The wild-type genes were set as the original flux bounds. The GA was initiated with a population of 500 wild-type individuals, which were subjected to a cycle of fitness evaluation, elimination, selection, recombination, and mutation for 30,000 generations (Figure 6.1).

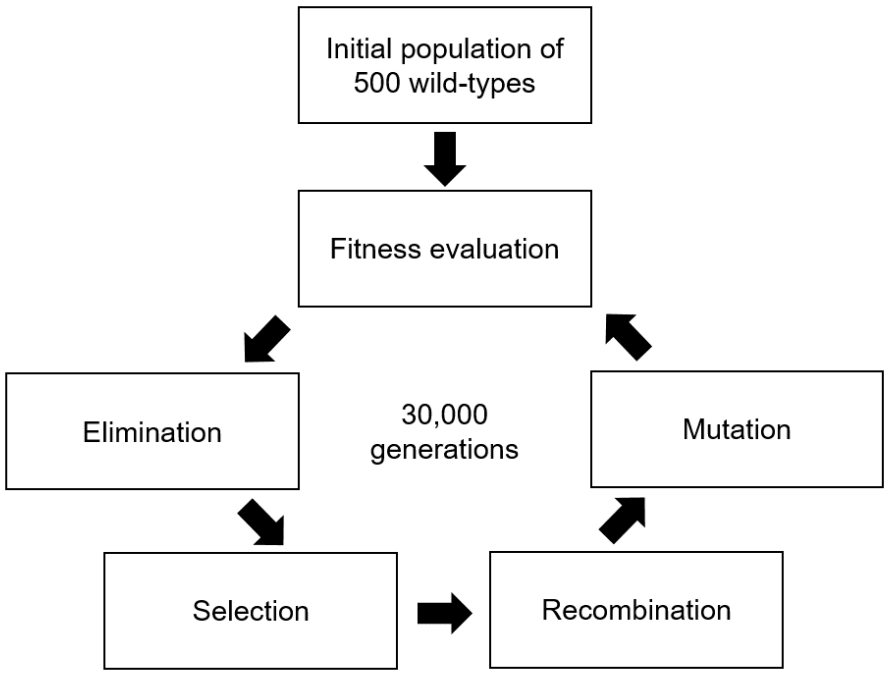

Figure 6.1. Schematic of genetic algorithm used for *in silico* evolution of organic acid production.

6.2.1.1 Fitness evaluation

The fitness of new individuals was evaluated by estimating the rate of production of the target acid based on dynamic modelling of organic acid fermentation at initial pH 2, and using the up-to-date and ATCC1015-specific iDU1757 metabolic model. Performing dFBA would evaluate fitness more accurately, however, it is computationally too expensive to be used as the means of fitness evaluation. Therefore, a fitness function was derived that uses flux values from FBA simulations of single time-points in the two growth phases (Figure 6.2), according to

$$F = \frac{c(t_f)}{t_f}, \tag{6.1}$$

where F is the fitness, t_f is the time of substrate depletion, and $c(t_f)$ is the target acid yield.

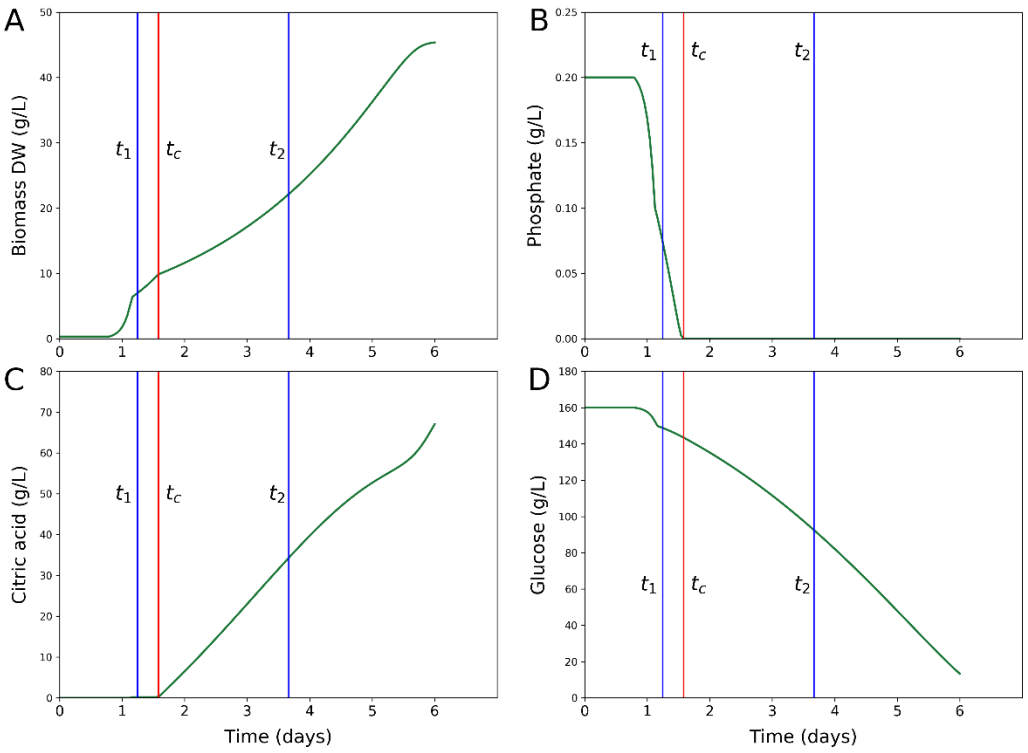

Figure 6.2. Dynamic modelling of organic acid fermentation as basis of fitness evaluation. The boundary between the two growth phases is shown by the vertical red line, annotated t_c. The time-points used for fitness evaluation are shown by the vertical blue lines, annotated t_1 and t_2.

Estimates were calculated for the target acid yield and time of substrate depletion. Growth occurs in two phases; growth phase 1 (phosphate storage), and growth phase 2 (proton production). The boundary is defined by the time t_c. The fluxes used to calculate estimates are shown in Table 6.1.

Table 6.1. Fluxes used to calculate estimates of target acid yield and time of substrate depletion for fitness evaluation.

Growth phase 1 $t_0 < t < t_c$	μ_1	specific growth rate
	f_1	substrate input flux (e.g. glucose)
	q	external phosphate input flux
Growth phase 2 $t_c < t < t_f$	μ_2	specific growth rate
	f_2	substrate input flux (e.g. glucose)
	p_2	target acid output flux

The fluxes from the time-point in growth phase 1 were used to estimate t_c, A_c, and S_c, where t_c is the time of external phosphate depletion and switch to growth phase 2, and A_c and S_c are the amounts of biomass and substrate at t_c, respectively.

The amount of biomass at time t, $x(t)$, was calculated according to

$$x(t) = \begin{cases} A_0 e^{\mu_1 t},\ t_0 < t < t_c,\ \mu_1 > 0 \\ A_0,\ t_0 < t < t_c,\ \mu_1 = 0 \\ A_c e^{\mu_2 (t - t_c)},\ t_c < t < t_f,\ \mu_2 > 0 \\ A_c,\ t_c < t < t_f,\ \mu_2 = 0 \end{cases}, \tag{6.2}$$

where A_0 is the initial biomass at t_0.

Using the equation for $x(t)$, the biomass at time t_c, A_c, was calculated according to

$$A_c = \begin{cases} A_0 e^{\mu_1 t_c},\ \mu_1 > 0 \\ A_0,\ \mu_1 = 0 \end{cases} \tag{6.3}$$

The amount of external phosphate at time t, $P_{ex}(t)$, was calculated according to

$$P_{ex}(t) = \begin{cases} P_{ex}(0) - \frac{qA_0}{\mu_1}(e^{\mu_1 t} - 1),\ t_0 < t < t_c, \mu_1 > 0 \\ P_{ex}(0) - qA_0 t,\ t_0 < t < t_c,\ \mu_1 = 0 \end{cases}, \tag{6.4}$$

where $P_{ex}(0)$ is the initial external phosphate at t_0.

The equation for $P_{ex}(t)$ was derived from the differential equation describing the rate of decrease of external phosphate, which assumed a constant external phosphate input flux

$$\frac{dP_{ex}}{dt} = -qx(t) \tag{6.5}$$

Using the equation for $P_{ex}(t)$, and knowing that external phosphate is zero at time t_c, an equation for t_c was derived

$$t_c = \begin{cases} \frac{1}{\mu_1} ln\left(1 + \frac{\mu_1 P_{ex}(0)}{qA_0}\right),\ \mu_1 > 0 \\ \frac{P_{ex}(0)}{qA_0},\ \mu_1 = 0 \end{cases} \tag{6.6}$$

The amount of substrate at time t, $S(t)$, was calculated according to

$$S(t) = \begin{cases} S_0 - \frac{f_1 A_0}{\mu_1}(e^{\mu_1 t} - 1),\ t_0 < t < t_c,\ \mu_1 > 0 \\ S_0 - f_1 A_0 t,\ t_0 < t < t_c,\ \mu_1 = 0 \\ S_c - \frac{f_2 A_c}{\mu_2}\left(e^{\mu_2 (t - t_c)} - 1\right),\ t_c < t < t_f,\ \mu_2 > 0 \\ S_c - f_2 A_c (t - t_c),\ t_c < t < t_f,\ \mu_2 = 0 \end{cases}, \quad (6.7)$$

where S_0 is the initial substrate at t_0, and S_c is the substrate at time t_c.

The equation for $S(t)$ was derived from the differential equation describing the rate of decrease of substrate, which assumed a constant substrate input flux

$$\frac{dS}{dt} = \begin{cases} -f_1 x(t),\ t_0 < t < t_c \\ -f_2 x(t),\ t_c < t < t_f \end{cases} \quad (6.8)$$

Using the equation for $S(t)$, and knowing that substrate is zero at time t_f, an equation for t_f was derived

$$t_f = \begin{cases} t_c + \frac{1}{\mu_2} ln\left(1 + \frac{S_c \mu_2}{f_2 A_c}\right),\ \mu_2 > 0 \\ t_c + \frac{S_c}{f_2 A_c},\ \mu_2 = 0 \end{cases} \quad (6.9)$$

The amount of target acid at time t, $c(t)$, was calculated according to

$$c(t) = \begin{cases} \frac{p_2 A_c}{\mu_2}\left(e^{\mu_2 (t - t_c)} - 1\right),\ t_c < t < t_f,\ \mu_2 > 0 \\ p_2 A_c (t - t_c),\ t_c < t < t_f,\ \mu_2 = 0 \end{cases} \quad (6.10)$$

The equation for $c(t)$ was derived from the differential equation describing the rate of increase of the target acid, which assumed a constant target acid output flux

$$\frac{dc}{dt} = p_2 x(t) \tag{6.11}$$

Using the equations for $c(t)$ and t_f, the target acid yield was estimated according to

$$c(t_f) = \frac{p_2 S_c}{f_2} \tag{6.12}$$

A simplification was made by only applying the mutant flux bounds to growth phase 2, and using wild-type flux bounds in growth phase 1. This assumed that mutations become active at time t_c, and are switched off during growth phase 1. This simplification was necessary to the performance of the GA, as mutations that affect growth have conflicting effects on fitness when applied to both growth phases. An FBA simulation of a time-point in growth phase 1 was no longer required, which improved the computational efficiency of fitness evaluation. A number of variables became constants by applying wild-type flux bounds to growth phase 1, including t_c, A_c, and S_c. The values for these constants were accurately determined from a dFBA simulation, avoiding the need for estimation using equations above.

To evolve production of organic acids not produced by the wild-type, adaptations to the fitness function were required. In such cases, the fitness evaluated to zero in wild-type individuals, preventing evolutionary progress. To fix this, fitness was evaluated as the sum of the estimated rates of proton production and target acid production, with different weights given to each. To ensure stronger evolutionary pressure towards production of the target acid over proton production, a higher weight was given to target acid production. The fitness function was adapted to

$$F = \frac{h(t_f)+10\ c(t_f)}{t_f}, \tag{6.13}$$

where $h(t_f)$ is the proton yield, calculated according to

$$h(t_f) = \frac{hS_c}{f_2}, \tag{6.14}$$

where h is the proton output flux.

The adapted fitness function was applied in evolution of succinic, lactic, malic, acetic, and gluconic production, since none of these organic acids are produced by the wild-type at initial pH 2. The original fitness function was applied in evolution of citric acid production, which occurs in the wild-type.

6.2.1.2 Elimination

Each generation, 5% of the population (25 individuals) were eliminated. The eliminated individuals were randomly drawn from the bottom 50% fitnesses. Therefore, individuals with fitness in the bottom 50% had an equal chance of elimination, and individuals with fitness in the top 50% were safe from elimination. This enabled individuals with more negative fitness to enter the population with some chance of reproduction, before being eliminated. This was found to be beneficial as some higher fitnesses result from mutations that individually decrease fitness, yet increase fitness when combined.

6.2.1.3 Selection

To fill the 5% population gap caused by elimination, new individuals were created. Each new individual was created from two parents, so to fill a 5% gap required a 10% selection (50 individuals). The selection was split across three sources, and did not include any individuals marked for elimination or already selected. 1% (5 individuals) were drawn randomly from across the population. 2% (10 individuals) were drawn from wild-types. The remaining 7% (35 individuals) were drawn randomly from individuals in the bottom 50% fitnesses. The percentage from across the population was set such that individuals in the top 50% fitnesses reproduced at a sufficiently low rate to prevent their otherwise rapid dominance of the gene pool. This avoided trapping the evolution on a single solution, allowing distinct solutions to evolve. The percentage from wild-types was set such that a sufficient population of wild-type genes was maintained in the gene pool, allowing the complementation of non-beneficial mutations by recombination. Although the initial population was completely wild-type, the wild-type genes were eventually lost from the gene pool unless re-introduced during the selection stage.

6.2.1.4 Recombination

A new individual was created by recombination of the genes of its two selected parents. Recombination was designed such that most genes were inherited from one parent and a few from the other parent, according to the recombination rate. The recombination rate was set to 0.04, therefore on average 96% of genes were inherited from one parent and 4% from the other parent. The dominant parent was randomly chosen from the two parents.

6.2.1.5 Mutation

Once a new individual was created through recombination of its two parents, its genes were subjected to mutation according to the mutation rate. The mutation rate was set to 0.02, and genes were mutated in a random order. Some genes were protected from mutation, including those corresponding to biomass producing reactions, the maintenance ATP reaction, and transport reactions. A gene was mutated by adding a small value to the flux bound, determined by the Laplace function. Wild-type flux values were used as starting points for mutation in the case of wild-type genes. Mutant genes were mutated from the current mutant flux bound. No flux bounds were allowed to mutate below the original lower bound or above the original upper bound, which prevented irreversible reactions from being made reversible. The location parameter of the Laplace function, μ, was set to zero. The scale parameter of the Laplace function, b, was relative to either the wild-type flux or the maximum wild-type flux, or was given the default value of 0.01 if these were zero (Figure 6.3). A mutated gene imposed a flux constraint or forced flux on the corresponding reaction. As mutations forcing flux sometimes resulted in no FBA solution, control steps were added to avoid this. If for a given gene the scale parameter of the Laplace function was set to the default value, the value of mutation was made negative for the lower bound and positive for the upper bound. This prevented mutations from forcing flux in these cases. A secondary mutation rate was added for mutations forcing flux, which was set to 0.3. Therefore, only 30% of mutations forcing flux were allowed. This increased the proportion of mutations constraining flux which

would otherwise be in equal ratio to mutations forcing flux. The final control step computed the maximum flux and capped the mutation forcing flux to 1% of the maximum flux. This 1% cap allowed multiple mutations to force flux per individual, without leading to no FBA solution. If a mutation were allowed to force 100% of the maximum flux, it would block other mutations from forcing flux in that individual.

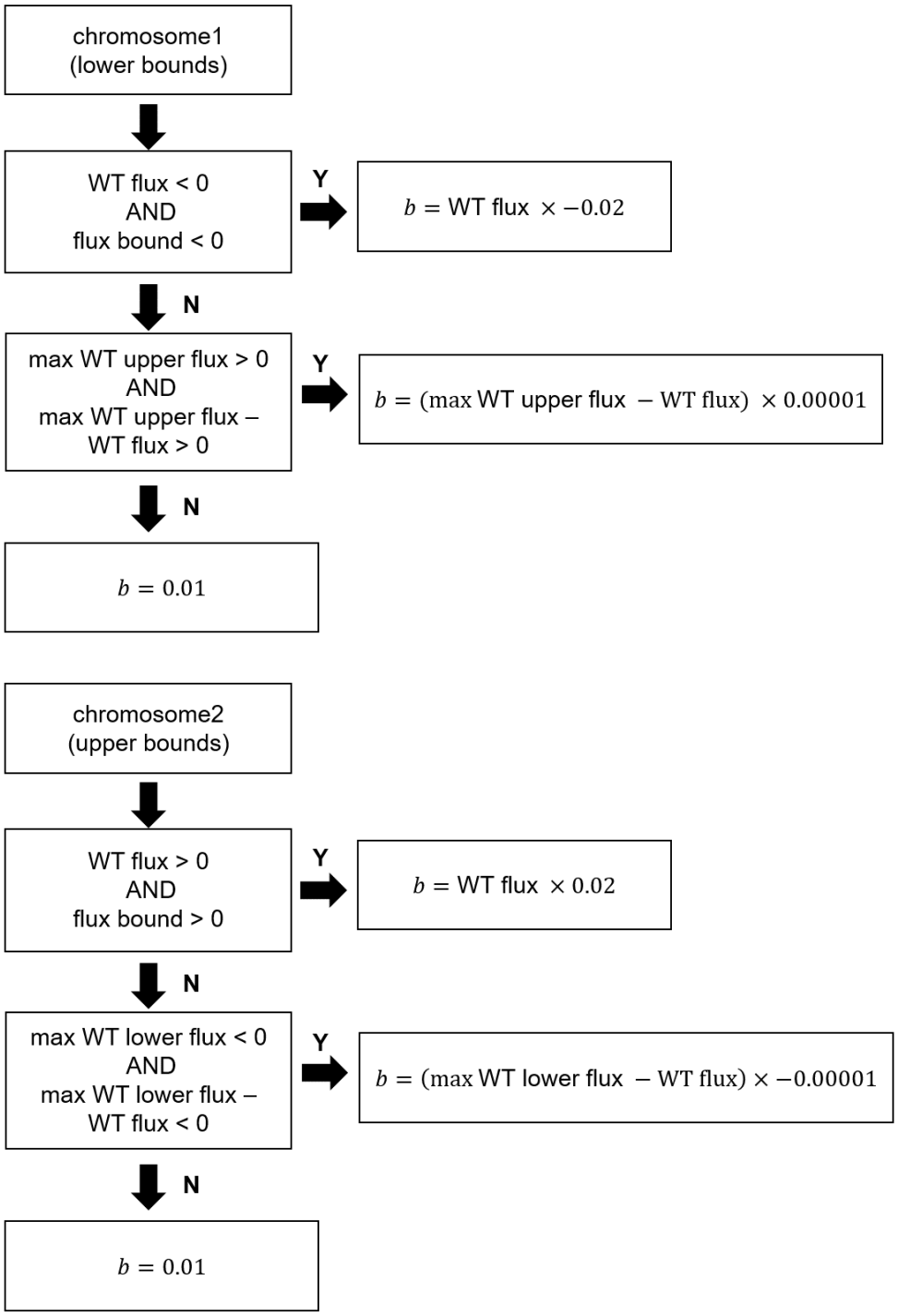

Figure 6.3. Schematic of procedure used to determine scale parameter of Laplace function.

6.2.2 Data analysis of *in silico* evolution output for target prediction

Output was generated from *in silico* evolution by logging new individuals that satisfied certain conditions upon fitness evaluation. If the target acid was not produced by the wild-type, any individual that evolved production of the target acid was recorded. In the case of evolution of citric acid production, individuals with fitness greater than the current highest fitness or with fitness greater than 110% of the wild-type fitness were recorded. The flux bounds of recorded individuals were compared with the wild-type to identify mutations. Mutations with no phenotypic effect were filtered out by only recording mutations if the mutant flux was equal to the mutant flux bound.

Solutions were obtained from the output by selecting recorded individuals with a fitness > 95% of the highest fitness. These solutions were then processed to discard mutations that have a minimal effect. The fitness was re-evaluated upon complementation of a mutation with the wild-type while retaining other mutations. If the fitness decreased by > 5% of the current solution fitness, the mutation was retained, otherwise discarded. This filtered out background from the solutions, leaving only the mutations that contribute significantly to the overall solution fitness. The frequency of each mutation was calculated from the filtered solutions, by counting the occurrences of corresponding reaction indices in the mutations of each solution, and dividing by the number of solutions. The information was used to identify mutation hotspots and inform target prediction.

6.3 Results

6.3.1 *In silico* evolution of citric acid production on glucose

The genetic algorithm was first applied to predict changes that further optimise citric acid production on glucose. 10 replicate runs were performed. The initial fitness (wild-type) was 0.1 and increased by only 20% to around 0.12 over the course of 5000 generations (Figure 6.4). Evolution was continued up to 10,000 generations, however, no further increases in fitness occurred. The variation in evolutionary speed between replicate runs was very low, and each run achieved the same maximum fitness.

The evolution output was analysed and the site and frequency of mutations are indicated in Figure 6.5. Each run only gave one or two solutions, each having a single mutation that targeted growth. The mutations across different solutions were found to be undirected and scattered across different areas of metabolism, constraining production of different biomass components. No same mutation occurred in more than one run, suggesting a large number of possible solutions resulting from multiple growth targets that are independent from the metabolic reactions required in citric acid production.

One solution was chosen (Table 6.2), and applied in dynamic modelling of organic acid fermentation with comparison to the wild-type (Figure 6.6). Mutations were induced at the point of phosphate depletion, beyond which growth was clearly constrained in the mutant. Beyond day 4, the rate of citric acid production was slightly higher, and the final yield was around 10 g/L greater than the wild-type.

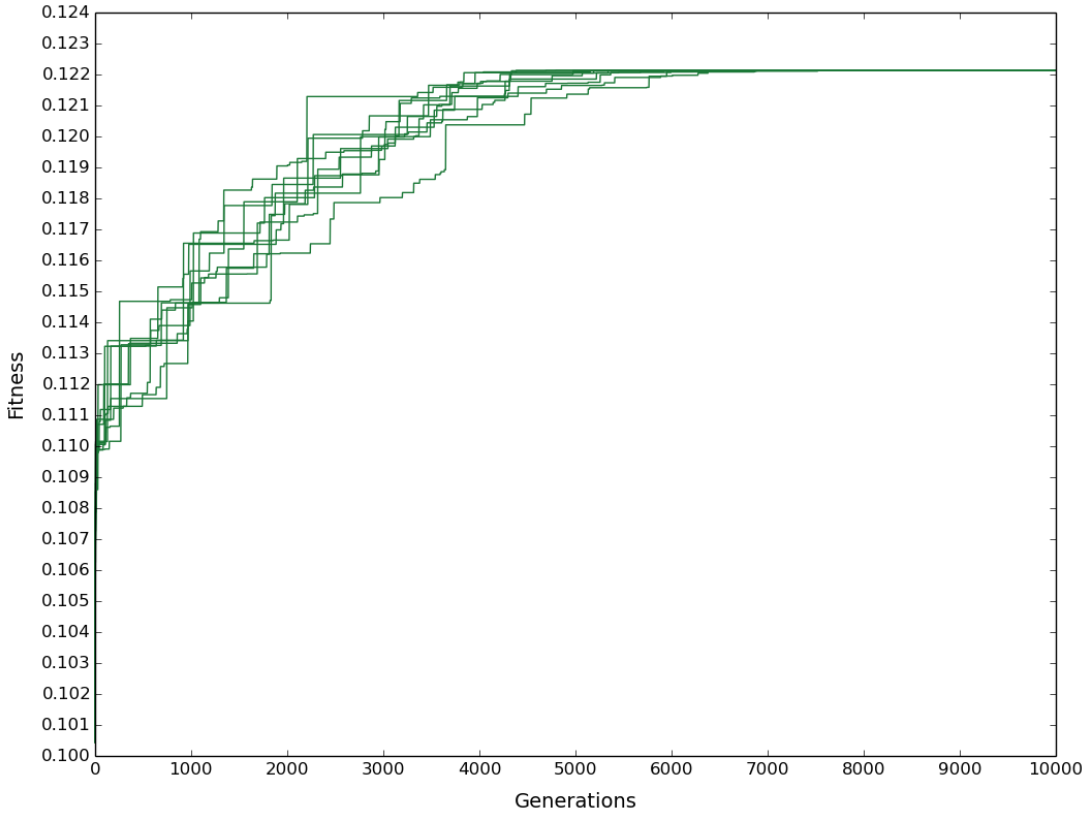

Figure 6.4. Increase in highest population fitness over generations with evolutionary pressure towards citric acid production on glucose. Each line corresponds to the evolutionary course of one replicate run.

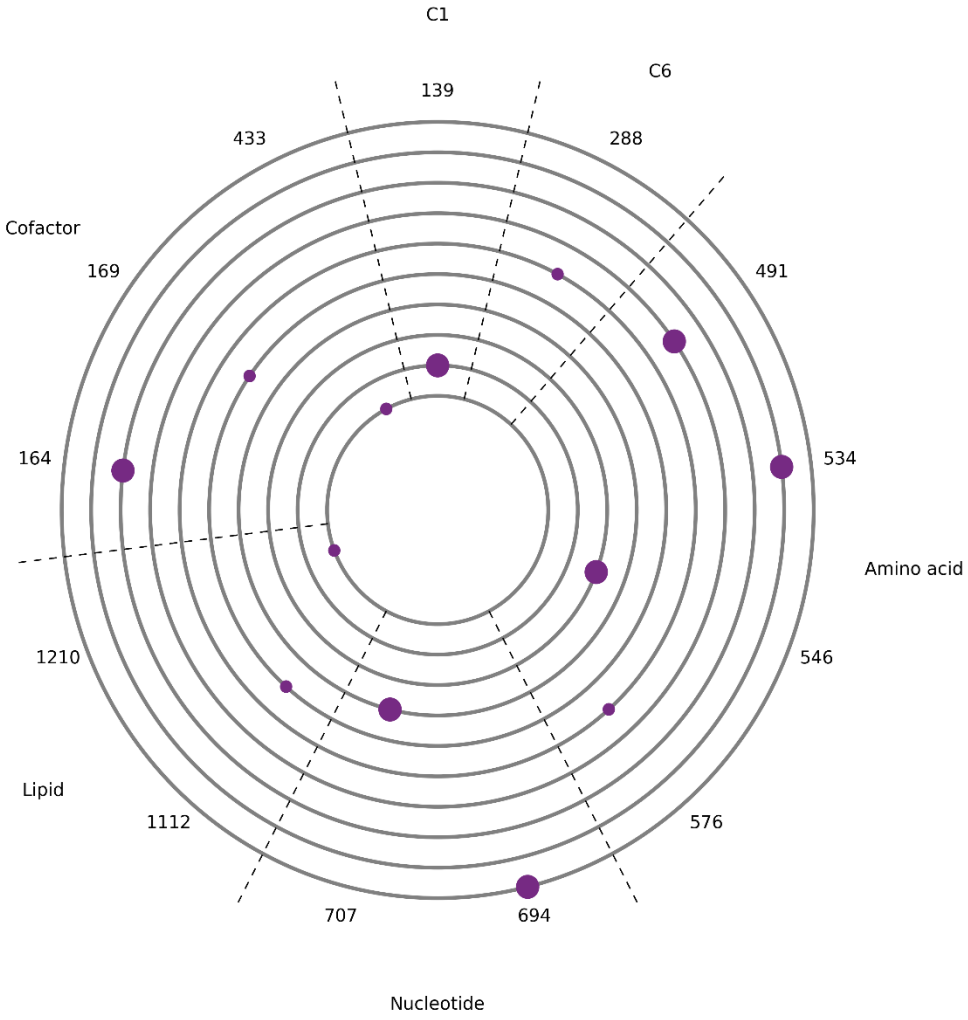

Figure 6.5. Evolution plot showing the site and frequency of mutations from 10 independent runs with evolutionary pressure towards citric acid production on glucose. Each of the ten grey circles corresponds to the results of one replicate run. The numbers on the outside are indices and refer to reactions where mutations occurred. The corresponding reactions are given in Table 6.10. Dots on the grey circles align with these indices and indicate where mutations occurred. The diameter of each dot is proportional to the frequency of the corresponding mutation across solutions from the run. The sectors indicate areas of metabolism that the mutations targeted.

Table 6.2. Example solution from evolution of citric acid production on glucose.

			Complementation results		
Index	**Reaction**	**Mutation effect**	**% Fitness decrease**	**% Acid flux decrease**	**% Growth increase**
707	DCMP+ATP+H<==>ADP+DCDP	LC	17.7	36.7	96.7

The mutation effect is given as UC or LC. UC corresponds to a mutation that imposes a flux constraint on the upper bound. LC corresponds to a mutation that imposes a flux constraint on the lower bound. Complementation results are given, showing the effect on fitness, target acid flux, and growth when the mutation is complemented with the wild-type.

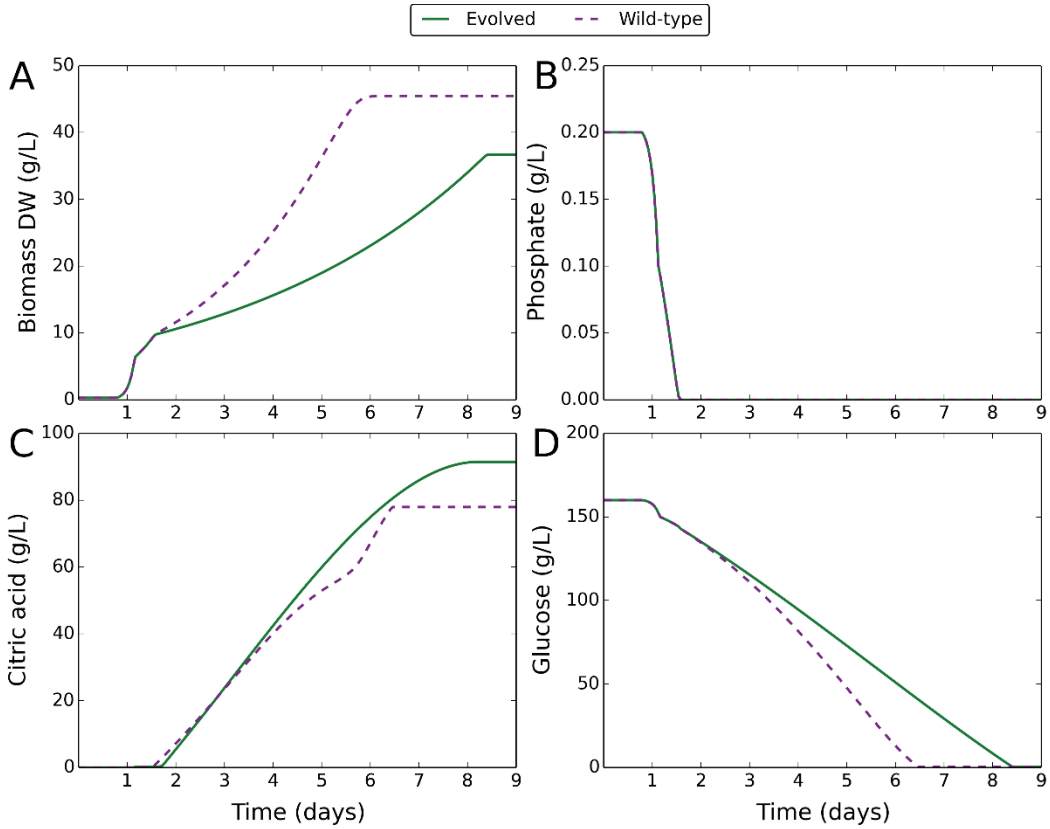

Figure 6.6. Dynamic modelling of organic acid fermentation comparing the wild-type with a solution from *in silico* evolution towards citric acid production on glucose. Green solid lines correspond to a genome evolved for citric acid production on glucose, using a chosen solution (Table 6.2). Purple dashed lines correspond to the wild-type. Mutations are induced at the point of external phosphate depletion. **(A)** Change in biomass dry weight (g/L) over time. **(B)** Change in external phosphate concentration (g/L) over time. **(C)** Change in external citric acid concentration (g/L) over time. **(D)** Change in external glucose concentration (g/L) over time.

6.3.2 *In silico* evolution of citric acid production on xylose

The genetic algorithm was applied to predict changes that optimise citric acid production on xylose. 10 replicate runs were performed. The initial fitness (wild-type) was 0.11 and increased by only 20% to around 0.13 over the course of 5000 generations (Figure 6.7). Evolution was continued up to 10,000 generations, however, no further increases in fitness occurred. The variation in evolutionary speed between replicate runs was very low, and each run achieved the same maximum fitness.

The evolution output was analysed and the site and frequency of mutations are indicated in Figure 6.8. Each run only gave one to three solutions, each having a single mutation that targeted growth. The mutations across different solutions were found to be undirected and scattered across different areas of metabolism, constraining production of different biomass components. No same mutation occurred in more than one run, suggesting a large number of possible solutions resulting from multiple growth targets that are independent from the metabolic reactions required in citric acid production.

One solution was chosen (Table 6.3), and applied in dynamic modelling of organic acid fermentation with comparison to the wild-type (Figure 6.9). Mutations were induced at the point of phosphate depletion, beyond which growth was clearly constrained in the mutant. The rate of citric acid production was slightly higher, and the final yield was around 15 g/L greater than the wild-type.

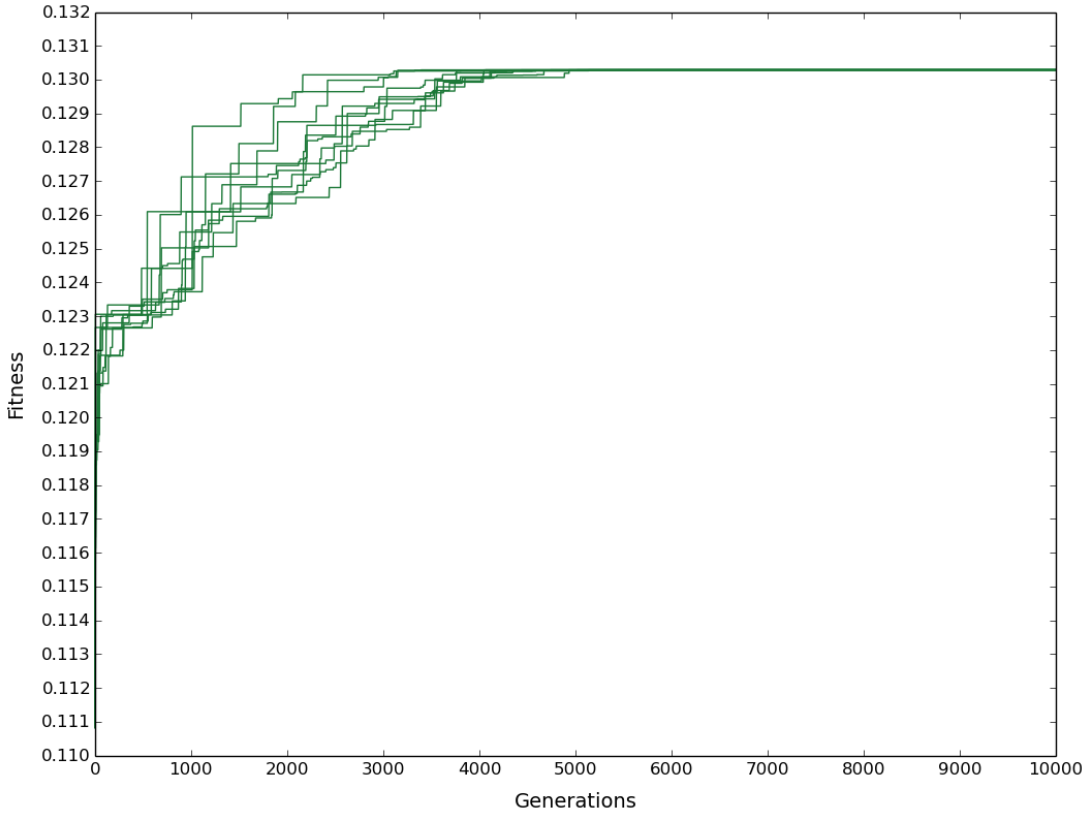

Figure 6.7. Increase in highest population fitness over generations with evolutionary pressure towards citric acid production on xylose. Each line corresponds to the evolutionary course of one replicate run.

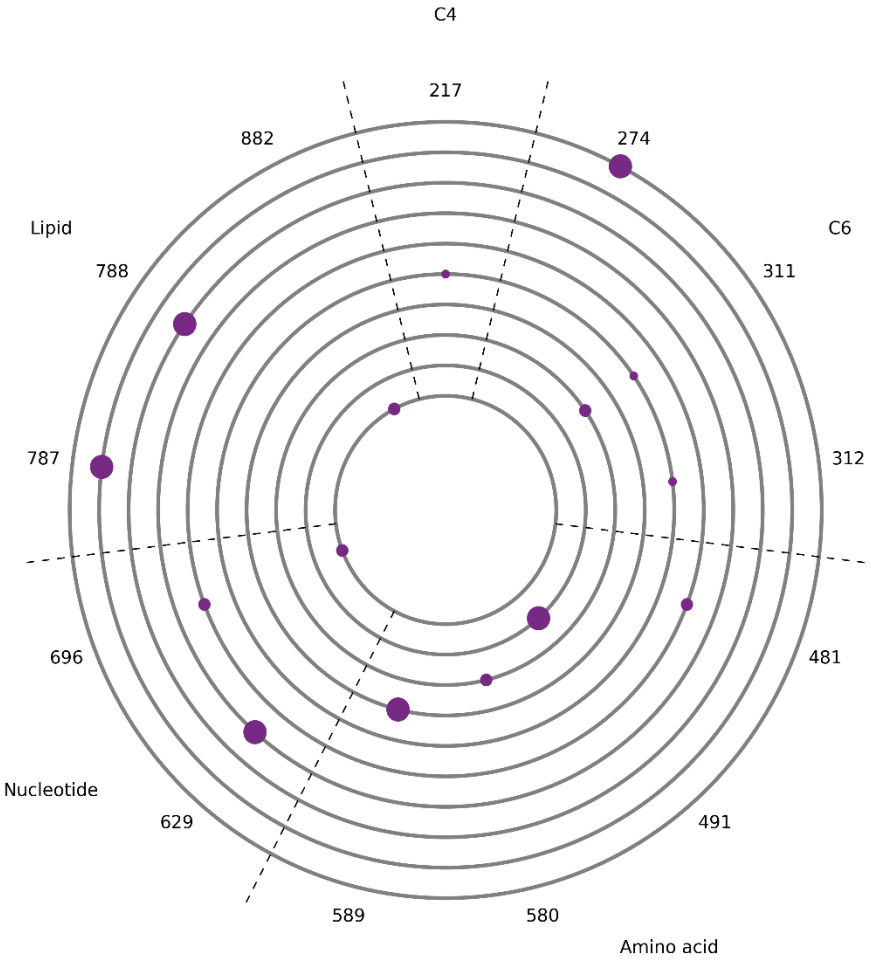

Figure 6.8. Evolution plot showing the site and frequency of mutations from 10 independent runs with evolutionary pressure towards citric acid production on xylose. Each of the ten grey circles corresponds to the results of one replicate run. The numbers on the outside are indices and refer to reactions where mutations occurred. The corresponding reactions are given in Table 6.10. Dots on the grey circles align with these indices and indicate where mutations occurred. The diameter of each dot is proportional to the frequency of the corresponding mutation across solutions from the run. The sectors indicate areas of metabolism that the mutations targeted.

Table 6.3. Example solution from evolution of citric acid production on xylose.

			Complementation results		
Index	**Reaction**	**Mutation effect**	**% Fitness decrease**	**% Acid flux decrease**	**% Growth increase**
629	H2O+GLN+PRPP -->GLU+H+PPI+PRAM	UC	11.9	24.7	54

The mutation effect is given as UC or LC. UC corresponds to a mutation that imposes a flux constraint on the upper bound. LC corresponds to a mutation that imposes a flux constraint on the lower bound. Complementation results are given, showing the effect on fitness, target acid flux, and growth when the mutation is complemented with the wild-type.

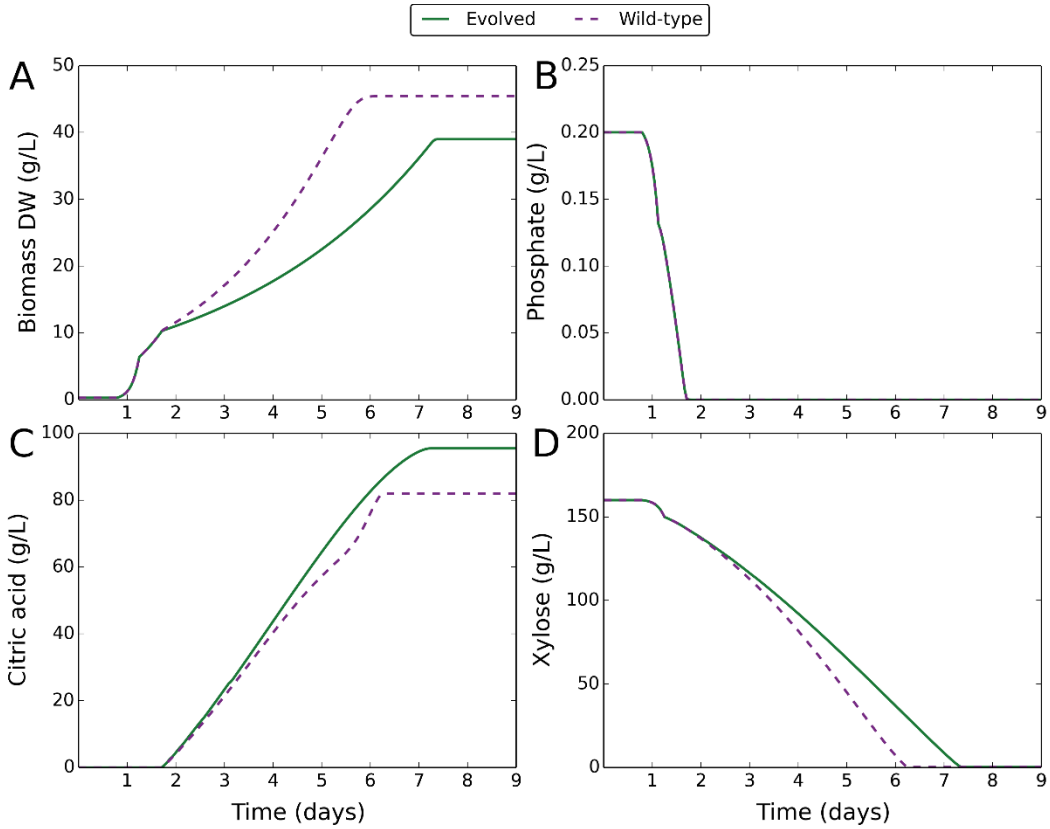

Figure 6.9. Dynamic modelling of organic acid fermentation comparing the wild-type with a solution from *in silico* evolution towards citric acid production on xylose. Green solid lines correspond to a genome evolved for citric acid production on xylose, using a chosen solution (Table 6.3). Purple dashed lines correspond to the wild-type. Mutations are induced at the point of external phosphate depletion. **(A)** Change in biomass dry weight (g/L) over time. **(B)** Change in external phosphate concentration (g/L) over time. **(C)** Change in external citric acid concentration (g/L) over time. **(D)** Change in external xylose concentration (g/L) over time.

6.3.3 *In silico* evolution of succinic acid production on glucose

The genetic algorithm was applied to predict changes that switch acid output from citric to succinic and optimise succinic acid production on glucose. 10 replicate runs were performed for a duration of 50,000 generations each. Succinic acid production successfully evolved, with a rapid increase in fitness in the first 10,000 generations followed by a more gradual increase up to 40,000 generations (Figure 6.10). The fitness was more steady beyond 40,000 generations. To be more confident that the maximum fitness was reached by 50,000 generations, one run was performed up to 100,000 generations (Figure 6.11). The fitness was constant after 40,000 generations suggesting no further increases were possible. The maximum fitness reached had some variance between replicate runs, suggesting a slower evolutionary speed in some cases or trapping at less optimal solutions. 40% of the runs achieved the same maximum fitness and were constant after 40,000 generations, suggesting these reached the global optimum.

The evolution output was analysed and the site and frequency of mutations are indicated in Figure 6.12. A number of mutations had high frequency and were repeated across replicate runs, and targeted four distinct areas of metabolism (energy, C3, TCA cycle, and gluconeogenesis). In particular, the activities of ubiquinol oxidase, succinate dehydrogenase (ubiquinone), pyruvate decarboxylase, D-lactate dehydrogenase, and pyruvate carboxylase were constrained.

The solution that best represented the average and with fitness near the maximum was chosen (Table 6.4), and applied in dynamic modelling of organic acid fermentation with comparison to the wild-type (Figure 6.13). Mutations were induced at the point of phosphate depletion, beyond which organic acids were produced. Acid output was completely switched from citric to succinic in the mutant, and the predicted yield of succinic acid was 90 g/L. Growth was also constrained, allowing a higher yield of organic acid. It was also observed that succinic acid was produced as a by-product during growth optimisation, and was not dependent on the proton production

objective function. The mutations therefore placed flux constraints that forced production of succinic acid to achieve optimal growth.

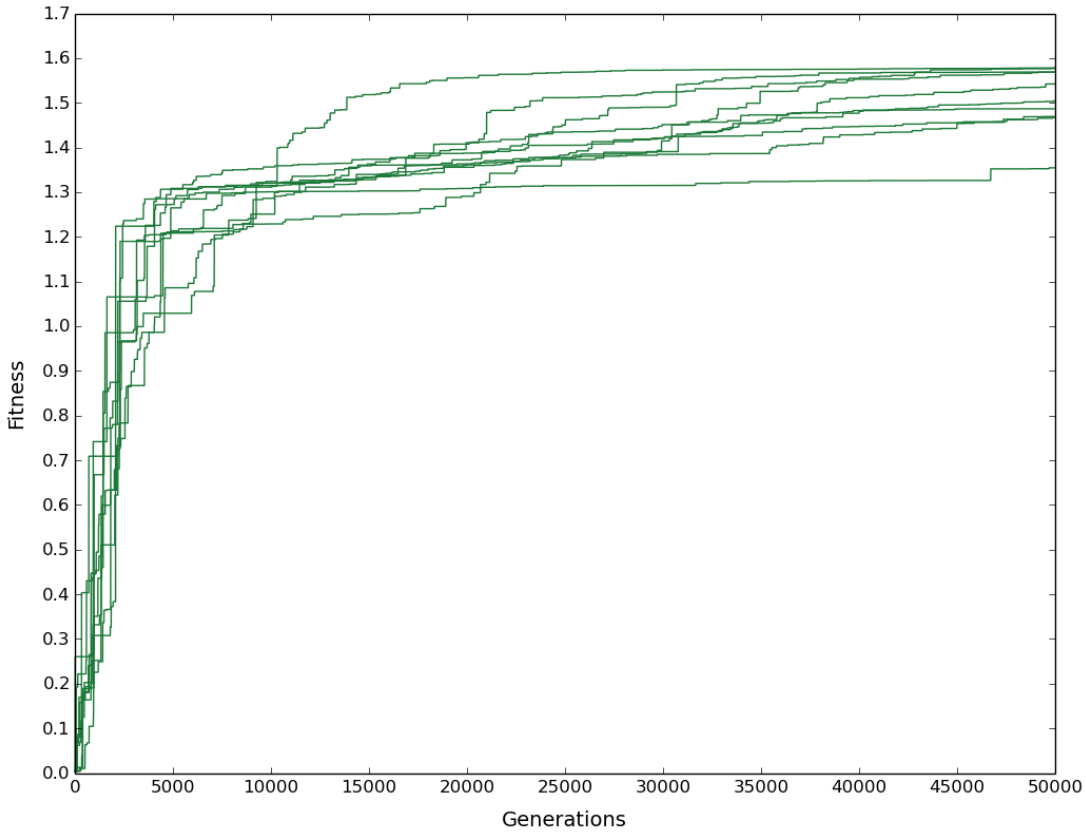

Figure 6.10. Increase in highest population fitness over generations with evolutionary pressure towards succinic acid production on glucose. Each line corresponds to the evolutionary course of one replicate run.

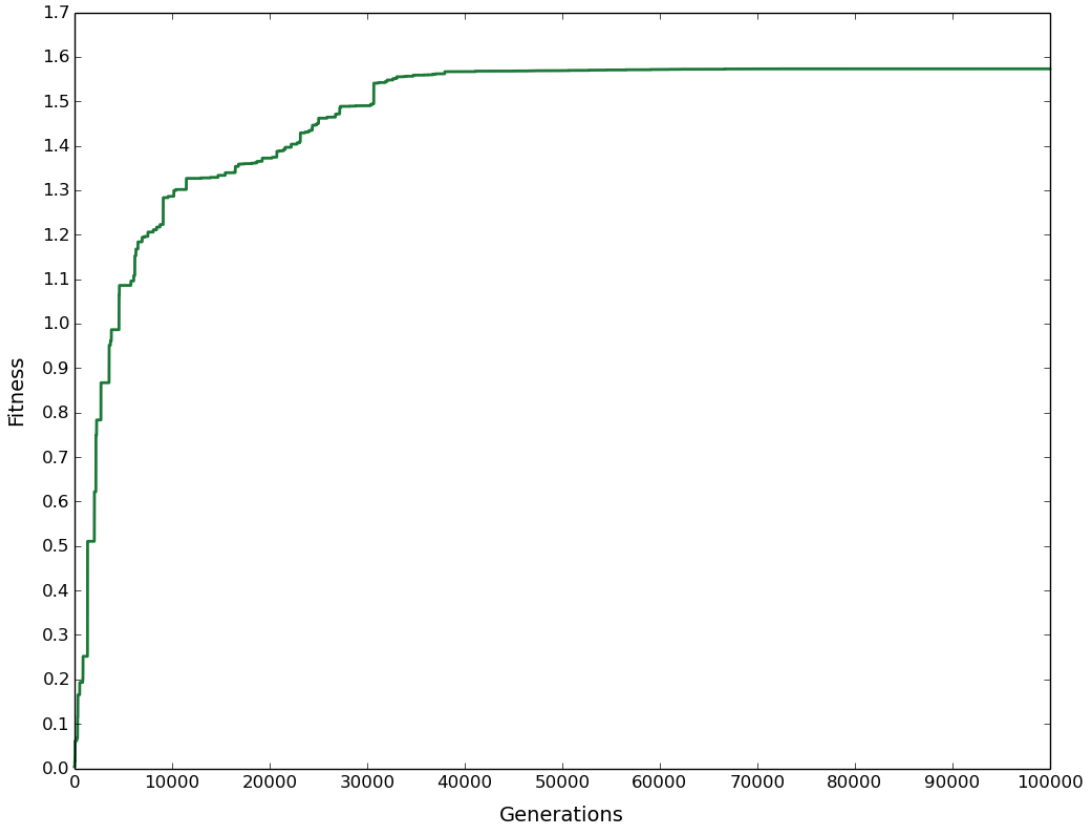

Figure 6.11. Increase in highest population fitness up to 100,000 generations with evolutionary pressure towards succinic acid production on glucose. The evolutionary course of one replicate run is shown.

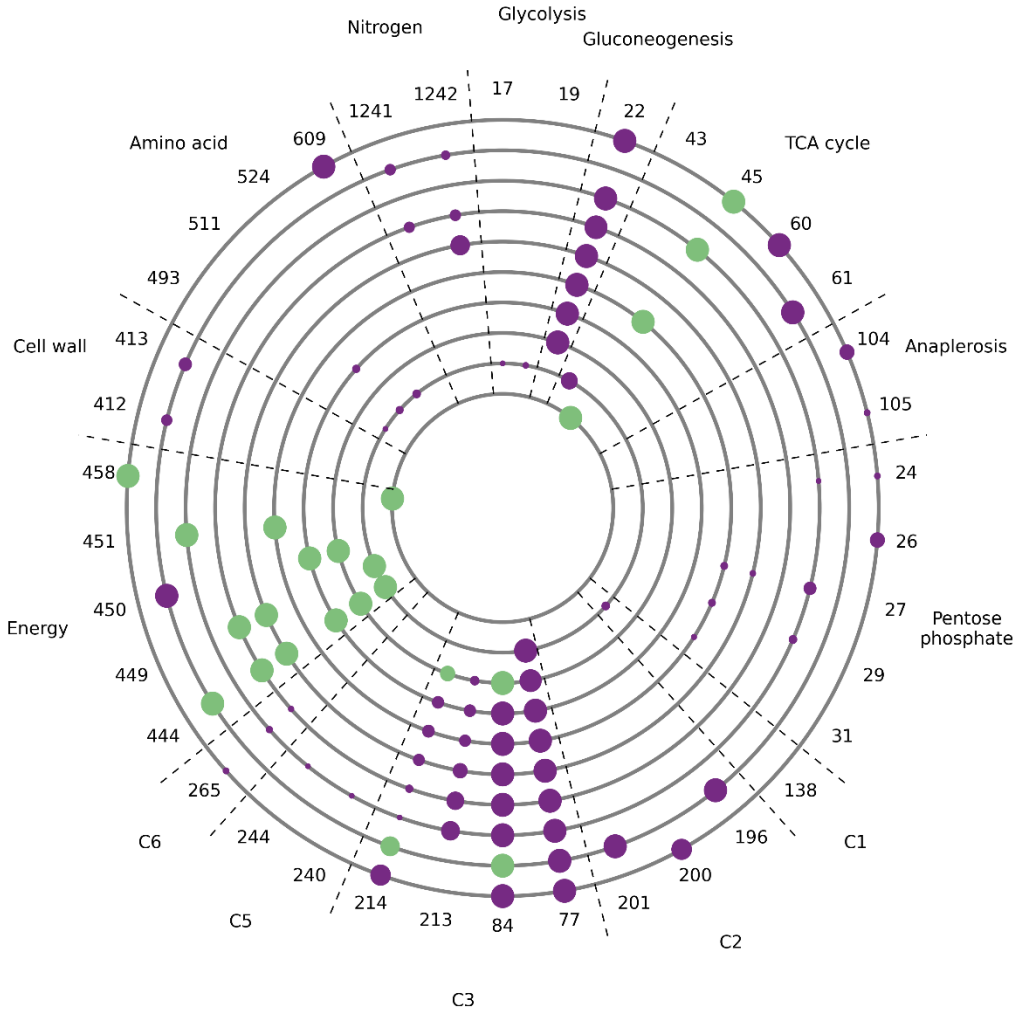

Figure 6.12. Evolution plot showing the site and frequency of mutations from 10 independent runs with evolutionary pressure towards succinic acid production on glucose. Each of the ten grey circles corresponds to the results of one replicate run. The numbers on the outside are indices and refer to reactions where mutations occurred. The corresponding reactions are given in Table 6.10. Dots on the grey circles align with these indices and indicate where mutations occurred. The diameter of each dot is proportional to the frequency of the corresponding mutation across solutions from the run. A frequency cut-off of 0.2 was applied. Mutations with a frequency lower than the cut-off are not represented. Green dots indicate mutations that when complemented decrease target acid flux by > 95%. Purple dots indicate mutations that when complemented decrease target acid flux by < 95%. The sectors indicate areas of metabolism that the mutations targeted.

Table 6.4. Example solution from evolution of succinic acid production on glucose.

			Complementation results		
Index	**Reaction**	**Mutation effect**	**% Fitness decrease**	**% Acid flux decrease**	**% Growth increase**
444	QH2m+0.5*O2m-->Qm+H2Om	UC	99.8	100	98.2
449	QH2m+2*FERIm+2*Hm -->Qm+2*FEROm+4*Ho	UC	99.8	100	98.2
213	PYR+NADH+H-->LLAC+NAD	UC	85.3	86.2	19.3
84	LAC+NAD<==>PYR+NADH+H	LC	85.2	86.2	19.3
77	H+PYR-->ACAL+CO2	UC	77.1	77.8	9.6
265	GLCNT+ATP-->D6PGC+ADP+H	UC	52.4	54.4	12.5
24	G6P+NADP-->D6PGL+NADPH+H	UC	49.7	51.8	12.3
22	ATPm+PYRm+H2Om+CO2m -->ADPm+PIm+OAm+2*Hm	UC	18.9	22.5	14
1242	NH4OH<==>NH3+H2O	UC	12.8	13.8	3.5

The example solution is chosen as the best representative of the average solution and based on fitness. The mutation effect is given as UC or LC. UC corresponds to a mutation that imposes a flux constraint on the upper bound. LC corresponds to a mutation that imposes a flux constraint on the lower bound. Complementation results are given for each mutation, showing the effect on fitness, target acid flux, and growth when the mutation is complemented with the wild-type while retaining the other mutations.

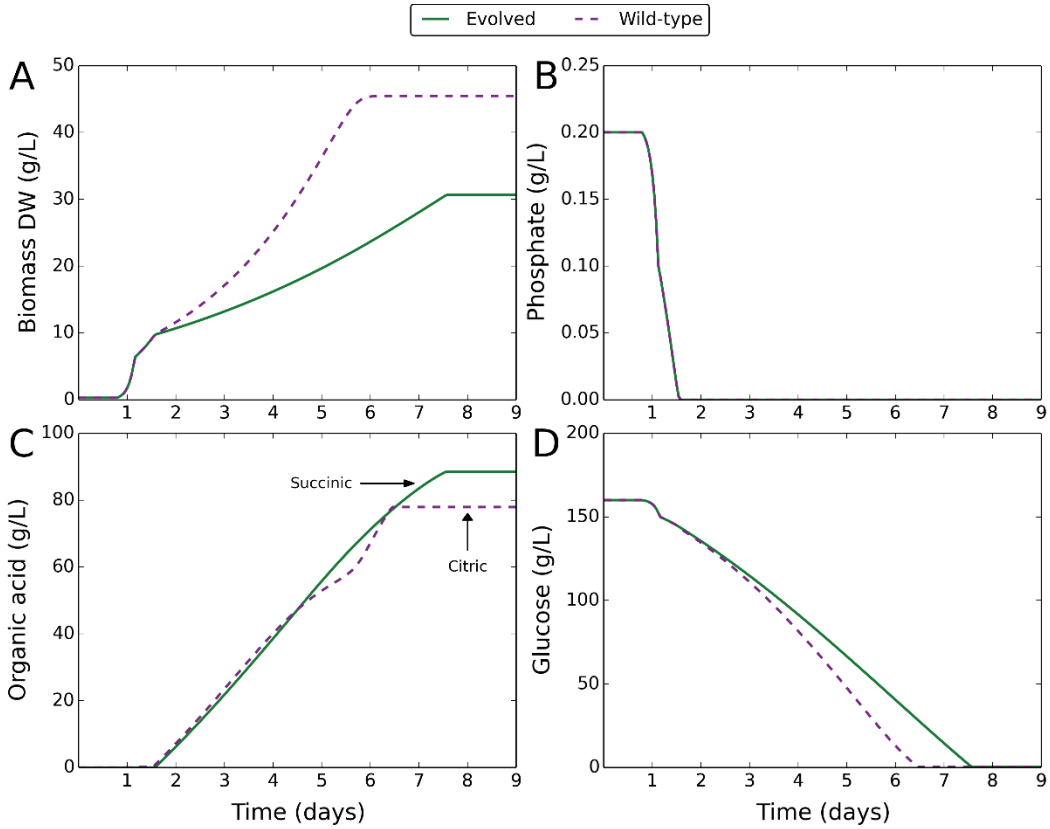

Figure 6.13. Dynamic modelling of organic acid fermentation comparing the wild-type with a solution from *in silico* evolution towards succinic acid production on glucose. Green solid lines correspond to a genome evolved for succinic acid production on glucose, using a solution that best represents the average evolved genome and based on fitness (Table 6.4). Purple dashed lines correspond to the wild-type. Mutations are induced at the point of external phosphate depletion. **(A)** Change in biomass dry weight (g/L) over time. **(B)** Change in external phosphate concentration (g/L) over time. **(C)** Change in external organic acid concentration (g/L) over time. Lines are annotated to indicate the organic acid produced. **(D)** Change in external glucose concentration (g/L) over time.

6.3.4 *In silico* evolution of succinic acid production on xylose

The genetic algorithm was applied to predict changes that switch acid output from citric to succinic and optimise succinic acid production on xylose. 10 replicate runs were performed for a duration of 50,000 generations each. Succinic acid production successfully evolved, with a rapid increase in fitness in the first 5,000 generations followed by a more gradual increase up to 20,000 generations (Figure 6.14). The fitness was more steady beyond 20,000 generations. The maximum fitness reached had some variance between replicate runs, suggesting a slower evolutionary speed in some cases or trapping at less optimal solutions. 60% of the runs achieved the same maximum fitness and were constant after 20,000 generations, suggesting these reached the global optimum.

The evolution output was analysed and the site and frequency of mutations are indicated in Figure 6.15. A number of mutations had high frequency and were repeated across replicate runs, and targeted four distinct areas of metabolism (energy, C3, TCA cycle, and gluconeogenesis). In particular, the activities of ubiquinol oxidase, ubiquinol-cytochrome c reductase, succinate dehydrogenase (ubiquinone), pyruvate decarboxylase, lactate dehydrogenase, and pyruvate carboxylase were constrained.

The solution that best represented the average and with fitness near the maximum was chosen (Table 6.5), and applied in dynamic modelling of organic acid fermentation with comparison to the wild-type (Figure 6.16). Mutations were induced at the point of phosphate depletion, beyond which organic acids were produced. Acid output was completely switched from citric to succinic in the mutant, and the predicted yield of succinic acid was 80 g/L. Growth was also constrained, allowing a higher yield of organic acid. It was also observed that succinic acid was produced as a by-product during growth optimisation, and was not dependent on the proton production objective function. The mutations therefore placed flux constraints that forced production of succinic acid to achieve optimal growth.

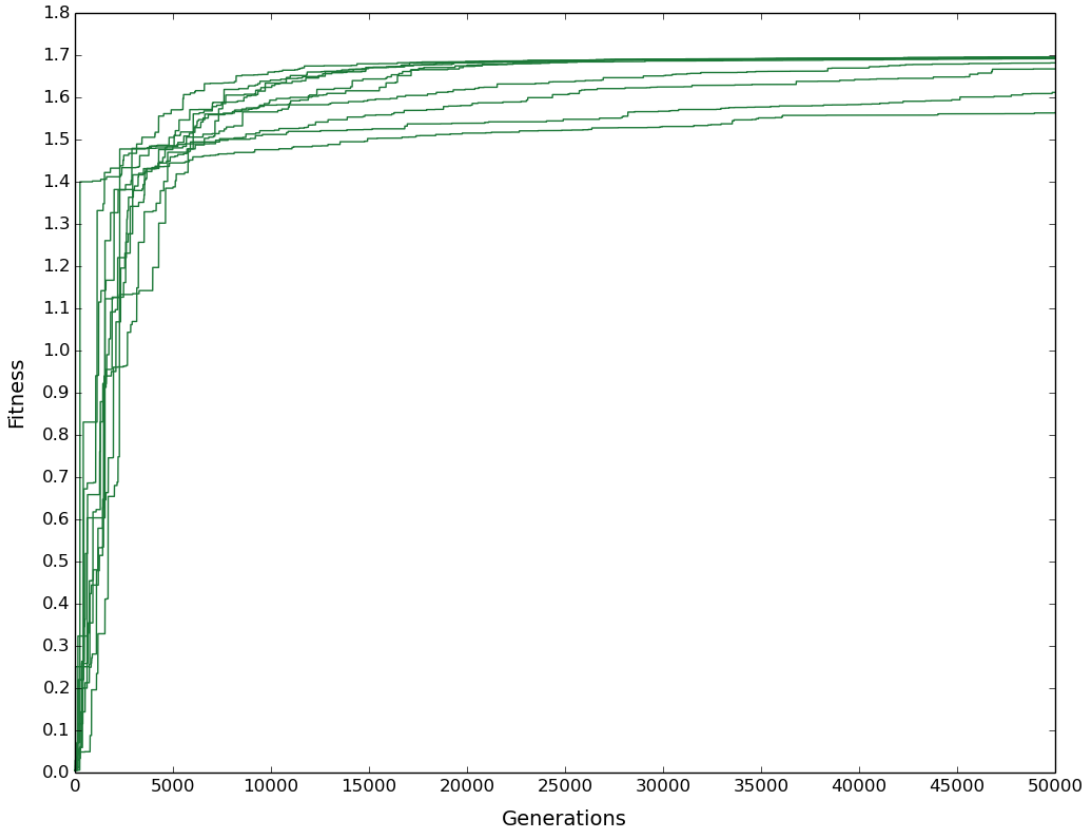

Figure 6.14. Increase in highest population fitness over generations with evolutionary pressure towards succinic acid production on xylose. Each line corresponds to the evolutionary course of one replicate run.

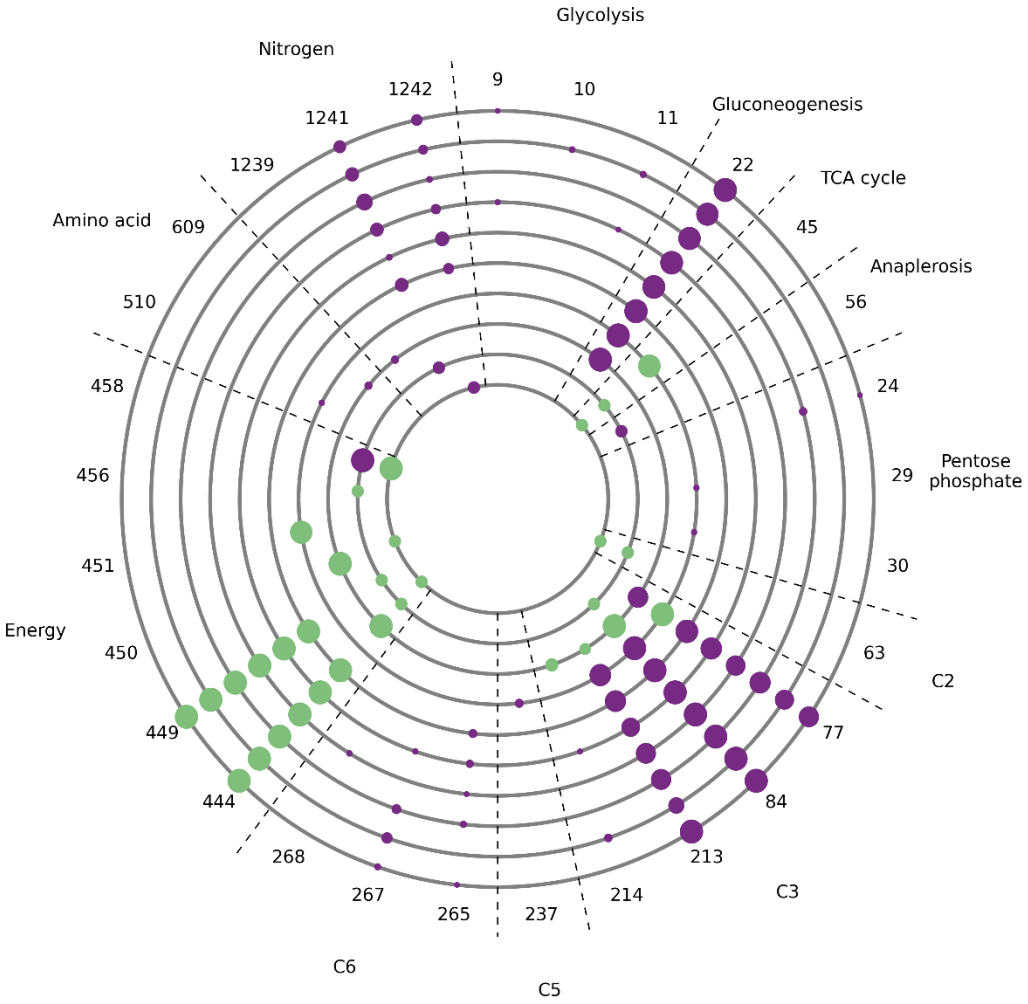

Figure 6.15. Evolution plot showing the site and frequency of mutations from 10 independent runs with evolutionary pressure towards succinic acid production on xylose. Each of the ten grey circles corresponds to the results of one replicate run. The numbers on the outside are indices and refer to reactions where mutations occurred. The corresponding reactions are given in Table 6.10. Dots on the grey circles align with these indices and indicate where mutations occurred. The diameter of each dot is proportional to the frequency of the corresponding mutation across solutions from the run. A frequency cut-off of 0.2 was applied. Mutations with a frequency lower than the cut-off are not represented. Green dots indicate mutations that when complemented decrease target acid flux by > 95%. Purple dots indicate mutations that when complemented decrease target acid flux by < 95%. The sectors indicate areas of metabolism that the mutations targeted.

Table 6.5. Example solution from evolution of succinic acid production on xylose.

			Complementation results		
Index	**Reaction**	**Mutation effect**	**% Fitness decrease**	**% Acid flux decrease**	**% Growth increase**
444	QH2m+0.5*O2m-->Qm+H2Om	UC	99.8	100	99.8
449	QH2m+2*FERIm+2*Hm -->Qm+2*FEROm+4*Ho	UC	99.8	100	99.8
84	LAC+NAD<==>PYR+NADH+H	LC	88.3	89.2	22.5
213	PYR+NADH+H-->LLAC+NAD	UC	88.3	89.1	22.4
77	H+PYR-->ACAL+CO2	UC	72	72.8	9.8
267	GLCNT<==>KDDGC+H2O	LC	51.4	53.2	12.2
24	G6P+NADP-->D6PGL+NADPH+H	UC	40.8	42.8	11
22	ATPm+PYRm+H2Om+CO2m -->ADPm+PIm+OAm+2*Hm	UC	20.6	24.4	16.3
1241	HNO2+3*NADH+5*H -->NH4OH+3*NAD+H2O	UC	11.1	12.1	3.6

The example solution is chosen as the best representative of the average solution and based on fitness. The mutation effect is given as UC or LC. UC corresponds to a mutation that imposes a flux constraint on the upper bound. LC corresponds to a mutation that imposes a flux constraint on the lower bound. Complementation results are given for each mutation, showing the effect on fitness, target acid flux, and growth when the mutation is complemented with the wild-type while retaining the other mutations.

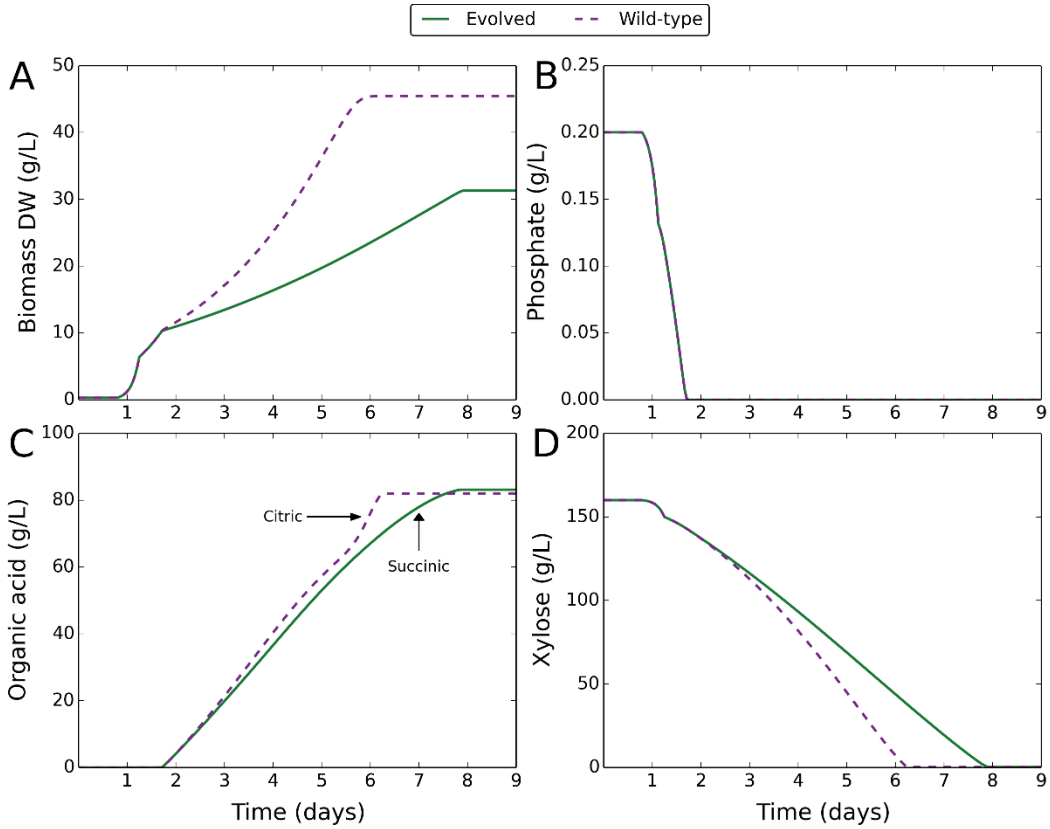

Figure 6.16. Dynamic modelling of organic acid fermentation comparing the wild-type with a solution from *in silico* evolution towards succinic acid production on xylose. Green solid lines correspond to a genome evolved for succinic acid production on xylose, using a solution that best represents the average evolved genome and based on fitness (Table 6.5). Purple dashed lines correspond to the wild-type. Mutations are induced at the point of external phosphate depletion. **(A)** Change in biomass dry weight (g/L) over time. **(B)** Change in external phosphate concentration (g/L) over time. **(C)** Change in external organic acid concentration (g/L) over time. Lines are annotated to indicate the organic acid produced. **(D)** Change in external xylose concentration (g/L) over time.

6.3.5 *In silico* evolution of lactic acid production on glucose

The genetic algorithm was applied to predict changes that switch acid output from citric to lactic and optimise lactic acid production on glucose. 10 replicate runs were performed for a duration of 30,000 generations each. Lactic acid production successfully evolved, with a very rapid fitness increase in the first 3000 generations, followed by a more gradual increase to 12,000 generations (Figure 6.17). All but two runs reached the same maximum fitness at this point and remained steady up to 30,000 generations. The other two runs had a prolonged lag lasting around 10,000 generations, followed by further increases in fitness and reaching the maximum by 20,000 generations. The uniformity in the maximum fitness achieved suggests each run successfully found the global optimum.

The evolution output was analysed and the site and frequency of mutations are indicated in Figure 6.18. One key mutation was observed in all solutions from all runs, and was found to be essential to lactic acid production. The mutation occurred at the heart of energy metabolism, constraining the flux of ATP synthase. Another essential mutation that occurred across multiple runs but at lower frequency acted to constrain the activity of malate synthase, reducing flux through the glyoxylate cycle.

The solution that best represented the average and with fitness near the maximum was chosen (Table 6.6), and applied in dynamic modelling of organic acid fermentation with comparison to the wild-type (Figure 6.19). Mutations were induced at the point of phosphate depletion, beyond which organic acids were produced. Acid output was completely switched from citric to lactic in the mutant, and the predicted yield of lactic acid was 90 g/L. Growth was also constrained, allowing a higher yield of organic acid.

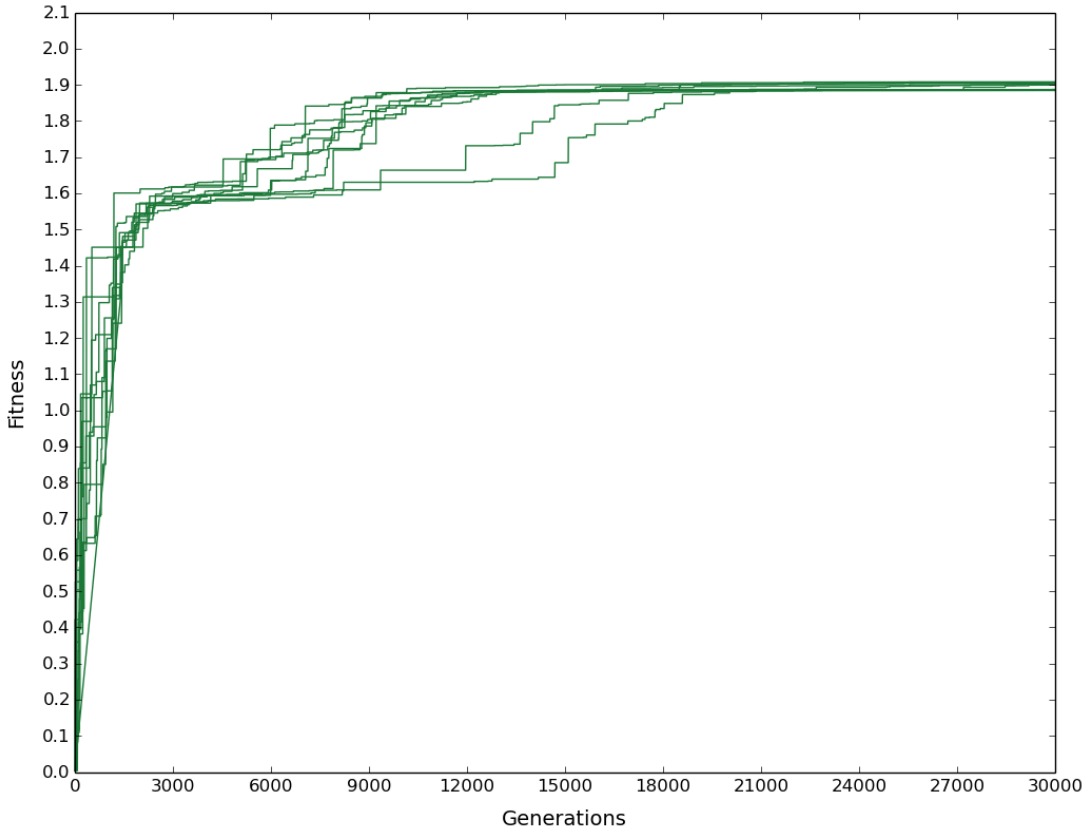

Figure 6.17. Increase in highest population fitness over generations with evolutionary pressure towards lactic acid production on glucose. Each line corresponds to the evolutionary course of one replicate run.

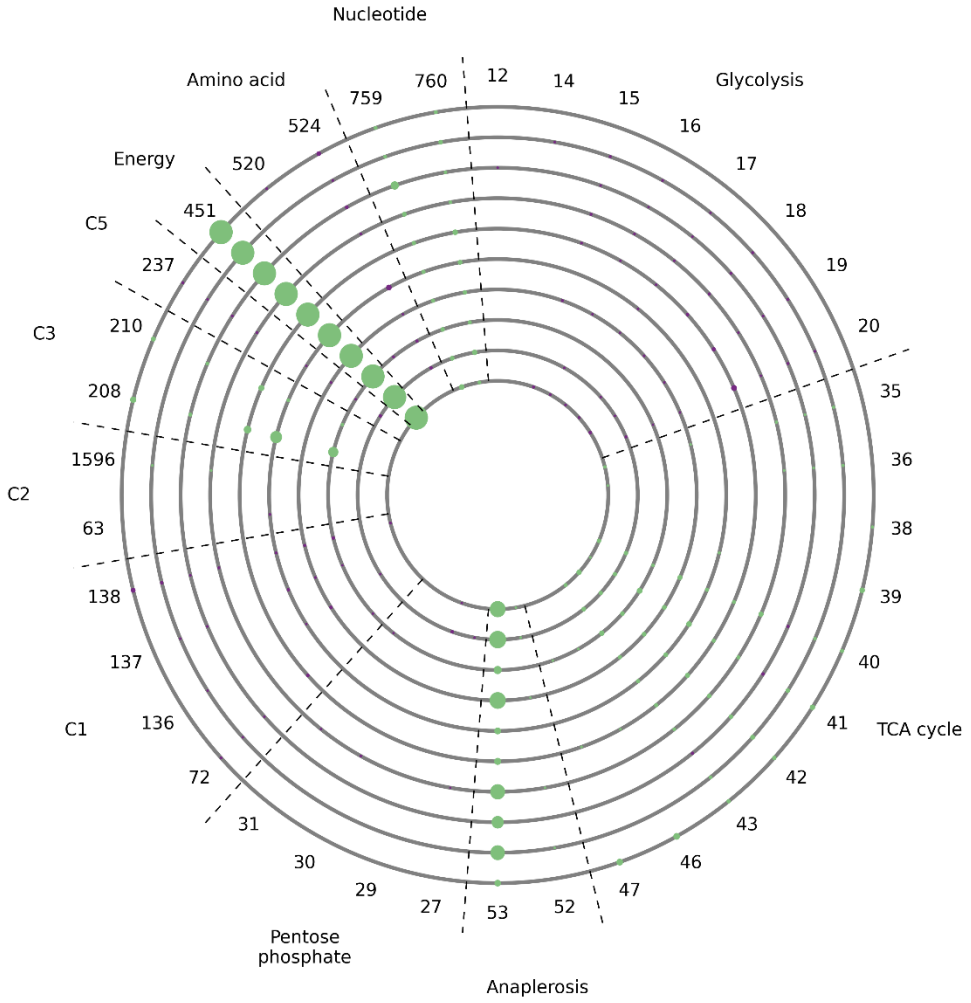

Figure 6.18. Evolution plot showing the site and frequency of mutations from 10 independent runs with evolutionary pressure towards lactic acid production on glucose. Each of the ten grey circles corresponds to the results of one replicate run. The numbers on the outside are indices and refer to reactions where mutations occurred. The corresponding reactions are given in Table 6.10. Dots on the grey circles align with these indices and indicate where mutations occurred. The diameter of each dot is proportional to the frequency of the corresponding mutation across solutions from the run. A frequency cut-off of 0.05 was applied. Mutations with a frequency lower than the cut-off are not represented. Green dots indicate mutations that when complemented decrease target acid flux by > 95%. Purple dots indicate mutations that when complemented decrease target acid flux by < 95%. The sectors indicate areas of metabolism that the mutations targeted.

Table 6.6. Example solution from evolution of lactic acid production on glucose.

			Complementation results		
Index	**Reaction**	**Mutation effect**	**% Fitness decrease**	**% Acid flux decrease**	**% Growth increase**
759	ATPm+AMPm+H<==>2*ADPm	LC	100	100	56.1
53	ACCOAp+H2Op+GLXp -->MALp+COAp+Hp	UC	100	100	12.9
451	ADPm+PIm+4.5454*Ho -->ATPm+H2Om+4.5454*Hm	UC	99.8	100	113.5
524	ALA+GLX<==>PYR+GLY	UC	68.4	70.6	22.2

The example solution is chosen as the best representative of the average solution and based on fitness. The mutation effect is given as UC or LC. UC corresponds to a mutation that imposes a flux constraint on the upper bound. LC corresponds to a mutation that imposes a flux constraint on the lower bound. Complementation results are given for each mutation, showing the effect on fitness, target acid flux, and growth when the mutation is complemented with the wild-type while retaining the other mutations.

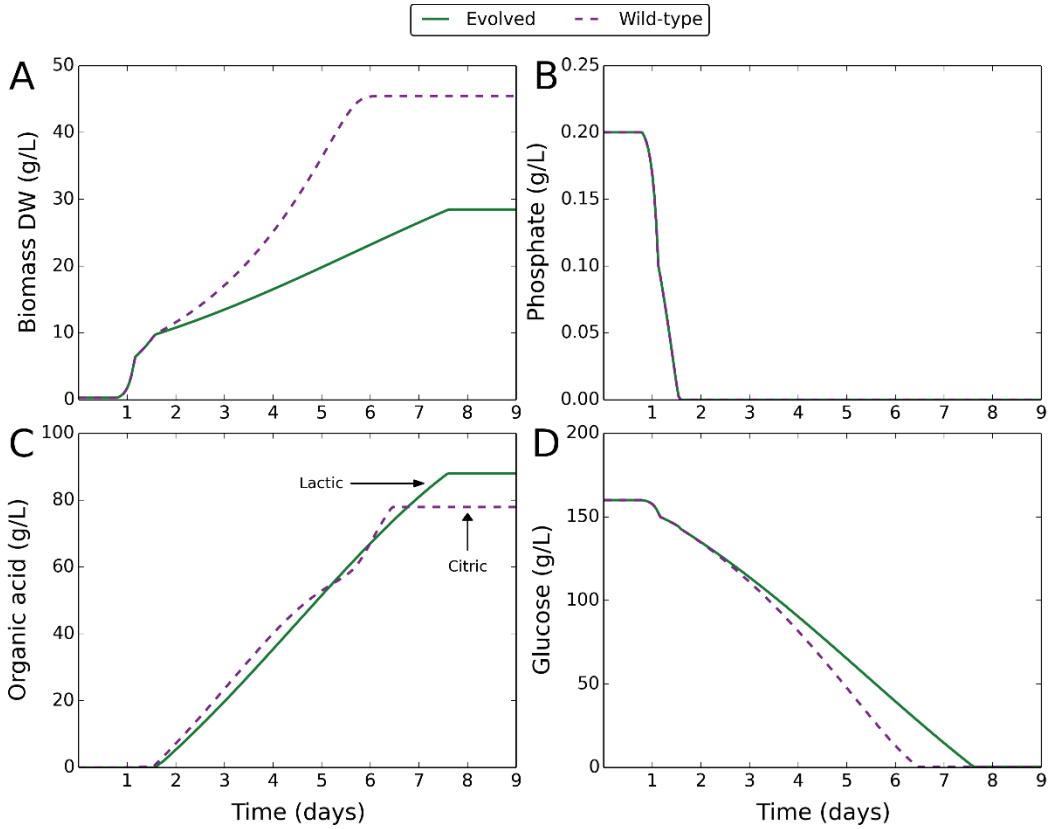

Figure 6.19. Dynamic modelling of organic acid fermentation comparing the wild-type with a solution from *in silico* evolution towards lactic acid production on glucose. Green solid lines correspond to a genome evolved for lactic acid production on glucose, using a solution that best represents the average evolved genome and based on fitness (Table 6.6). Purple dashed lines correspond to the wild-type. Mutations are induced at the point of external phosphate depletion. **(A)** Change in biomass dry weight (g/L) over time. **(B)** Change in external phosphate concentration (g/L) over time. **(C)** Change in external organic acid concentration (g/L) over time. Lines are annotated to indicate the organic acid produced. **(D)** Change in external glucose concentration (g/L) over time.

6.3.6 *In silico* evolution of malic acid production on glucose

The genetic algorithm was applied to predict changes that switch acid output from citric to malic and optimise malic acid production on glucose. 10 replicate runs were performed for a duration of 50,000 generations each. Malic acid production successfully evolved, with a rapid increase in fitness for the first 5000 generations, followed by a very gradual increase up to 30,000 generations (Figure 6.20). To be confident that the maximum fitness was reached, the duration was increased to 50,000 generations. The fitness was constant beyond 30,000 generations, with all runs achieving the same maximum fitness, suggesting the global optimum was reached. Variation in evolutionary speed was very low.

The evolution output was analysed and the site and frequency of mutations are indicated in Figure 6.21. One key mutation, that constrained citrate synthase, was observed in all solutions from all runs, and was found to be essential to malic acid production. Another mutation that occurred in all runs but at lower frequency targeted formyltetrahydrofolate deformylase.

The solution that best represented the average and with fitness near the maximum was chosen (Table 6.7), and applied in dynamic modelling of organic acid fermentation with comparison to the wild-type (Figure 6.22). Mutations were induced at the point of phosphate depletion, beyond which organic acids were produced. Acid output was completely switched from citric to malic in the mutant, and the predicted yield of malic acid was 100 g/L. Growth was also constrained, allowing a higher yield of organic acid.

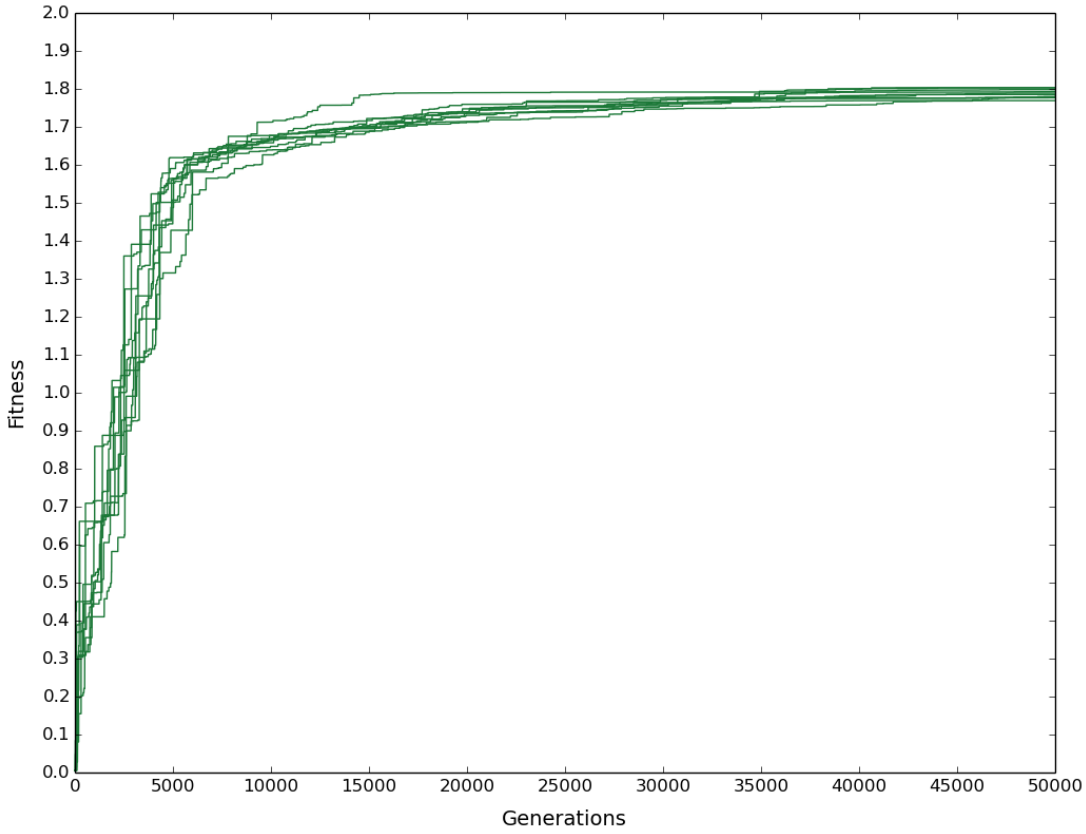

Figure 6.20. Increase in highest population fitness over generations with evolutionary pressure towards malic acid production on glucose. Each line corresponds to the evolutionary course of one replicate run.

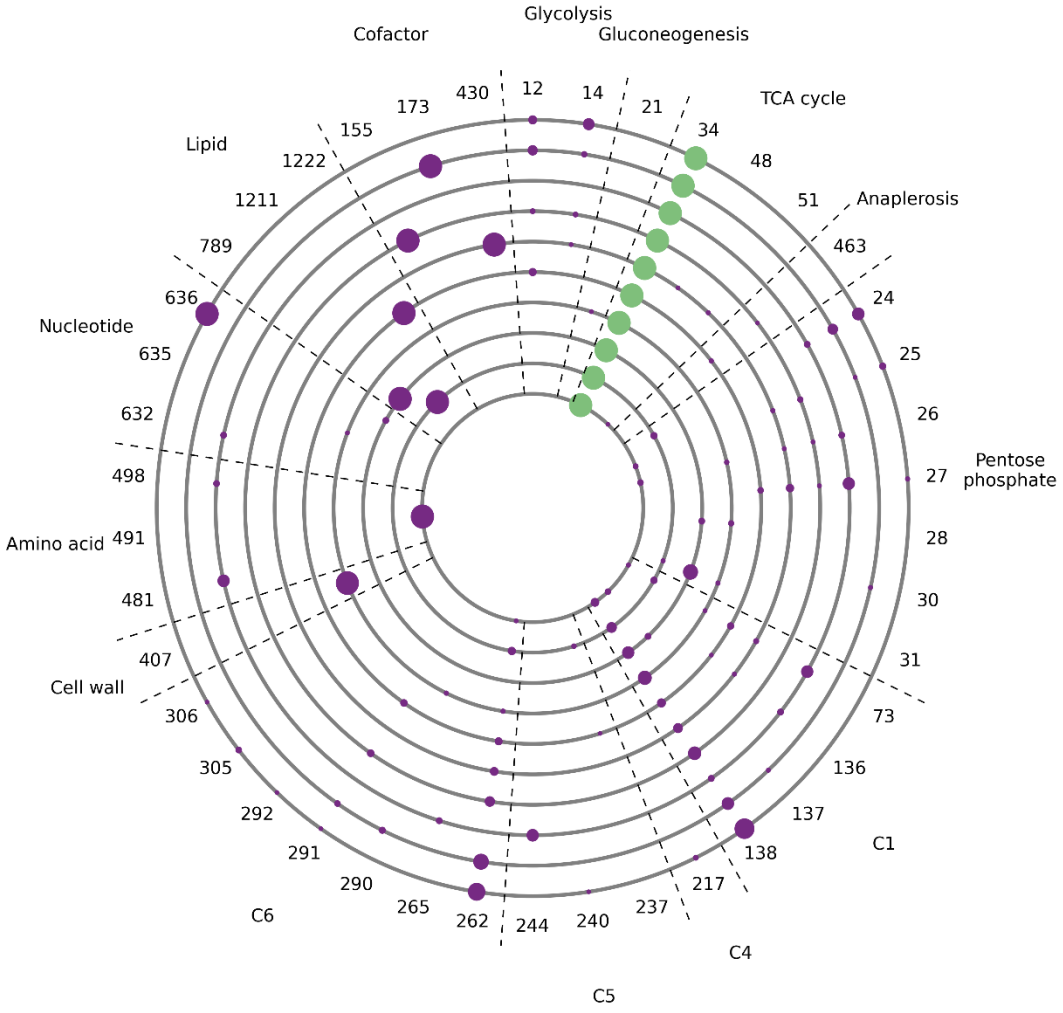

Figure 6.21. Evolution plot showing the site and frequency of mutations from 10 independent runs with evolutionary pressure towards malic acid production on glucose. Each of the ten grey circles corresponds to the results of one replicate run. The numbers on the outside are indices and refer to reactions where mutations occurred. The corresponding reactions are given in Table 6.10. Dots on the grey circles align with these indices and indicate where mutations occurred. The diameter of each dot is proportional to the frequency of the corresponding mutation across solutions from the run. A frequency cut-off of 0.15 was applied. Mutations with a frequency lower than the cut-off are not represented. Green dots indicate mutations that when complemented decrease target acid flux by > 95%. Purple dots indicate mutations that when complemented decrease target acid flux by < 95%. The sectors indicate areas of metabolism that the mutations targeted.

Table 6.7. Example solution from evolution of malic acid production on glucose.

			Complementation results		
Index	**Reaction**	**Mutation effect**	**% Fitness decrease**	**% Acid flux decrease**	**% Growth increase**
34	ACCOAm+H2Om+OAm <==>CITm+COAm+Hm	UC	99.7	100	0
138	FTHF+H2O-->FOR+THF+H	UC	70.5	70.7	0
26	D6PGC+NADP-->RL5P+CO2+NADPH	UC	62.2	62.4	0
636	SAICAR<==>FUM+AICAR	UC	27.9	41.1	66.7

The example solution is chosen as the best representative of the average solution and based on fitness. The mutation effect is given as UC or LC. UC corresponds to a mutation that imposes a flux constraint on the upper bound. LC corresponds to a mutation that imposes a flux constraint on the lower bound. Complementation results are given for each mutation, showing the effect on fitness, target acid flux, and growth when the mutation is complemented with the wild-type while retaining the other mutations.

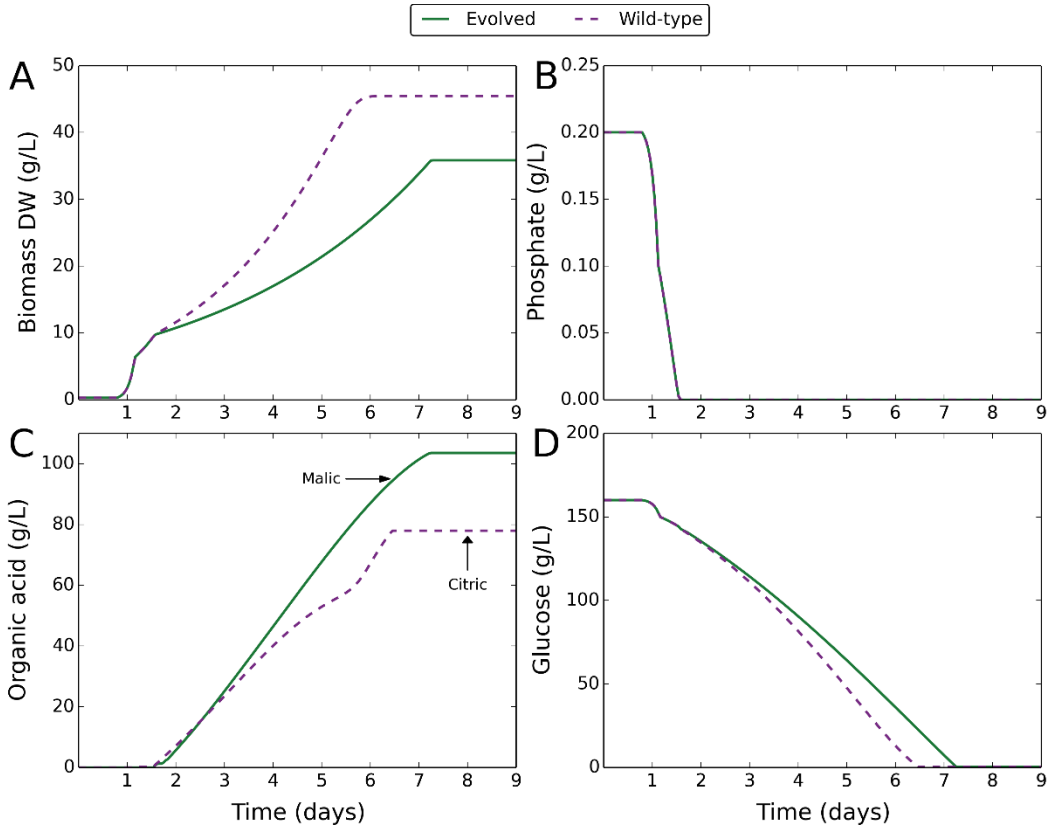

Figure 6.22. Dynamic modelling of organic acid fermentation comparing the wild-type with a solution from *in silico* evolution towards malic acid production on glucose. Green solid lines correspond to a genome evolved for malic acid production on glucose, using a solution that best represents the average evolved genome and based on fitness (Table 6.7). Purple dashed lines correspond to the wild-type. Mutations are induced at the point of external phosphate depletion. **(A)** Change in biomass dry weight (g/L) over time. **(B)** Change in external phosphate concentration (g/L) over time. **(C)** Change in external organic acid concentration (g/L) over time. Lines are annotated to indicate the organic acid produced. **(D)** Change in external glucose concentration (g/L) over time.

6.3.7 *In silico* evolution of acetic acid production on glucose

The genetic algorithm was applied to predict changes that switch acid output from citric to acetic and optimise acetic acid production on glucose. 10 replicate runs were performed for a duration of 30,000 generations each. Acetic acid production successfully evolved, with a very rapid increase in fitness in the first 3000 generations, followed by a more gradual increase until maximum fitness was achieved (Figure 6.23). The generations taken to reach a constant fitness showed variation between replicate runs, with some very fast and others experiencing a lag period. Most runs had a near constant fitness after 15,000 generations, however, some variation was observed in the maximum fitness reached. This suggests that not all runs reached the global optimum due to trapping at less optimal solutions.

The evolution output was analysed and the site and frequency of mutations are indicated in Figure 6.24. The mutations were found to be mainly directed at energy metabolism, constraining activities of ubiquinol oxidase, ubiquinol-cytochrome c reductase, ADP/ATP translocase or cytochrome c oxidase. These mutations were essential to acetic acid production, and were often accompanied by mutations aimed at C3 metabolism, constraining the activities of D-lactate dehydrogenase, glycerol-3-phosphate dehydrogenase, L-lactate dehydrogenase, or lactate-2-monooxygenase. A mutation constraining aconitate hydratase occurred in one run and was essential.

The solution that best represented the average and with fitness near the maximum was chosen (Table 6.8), and applied in dynamic modelling of organic acid fermentation with comparison to the wild-type (Figure 6.25). Mutations were induced at the point of phosphate depletion, beyond which organic acids were produced. Acid output was completely switched from citric to acetic in the mutant, and the predicted yield of acetic acid was 85 g/L. Growth was also constrained, allowing a higher yield of organic acid. It was also observed that acetic acid was produced as a by-product during growth optimisation, and was not dependent on the proton production

objective function. The mutations therefore placed flux constraints that forced production of acetic acid to achieve optimal growth.

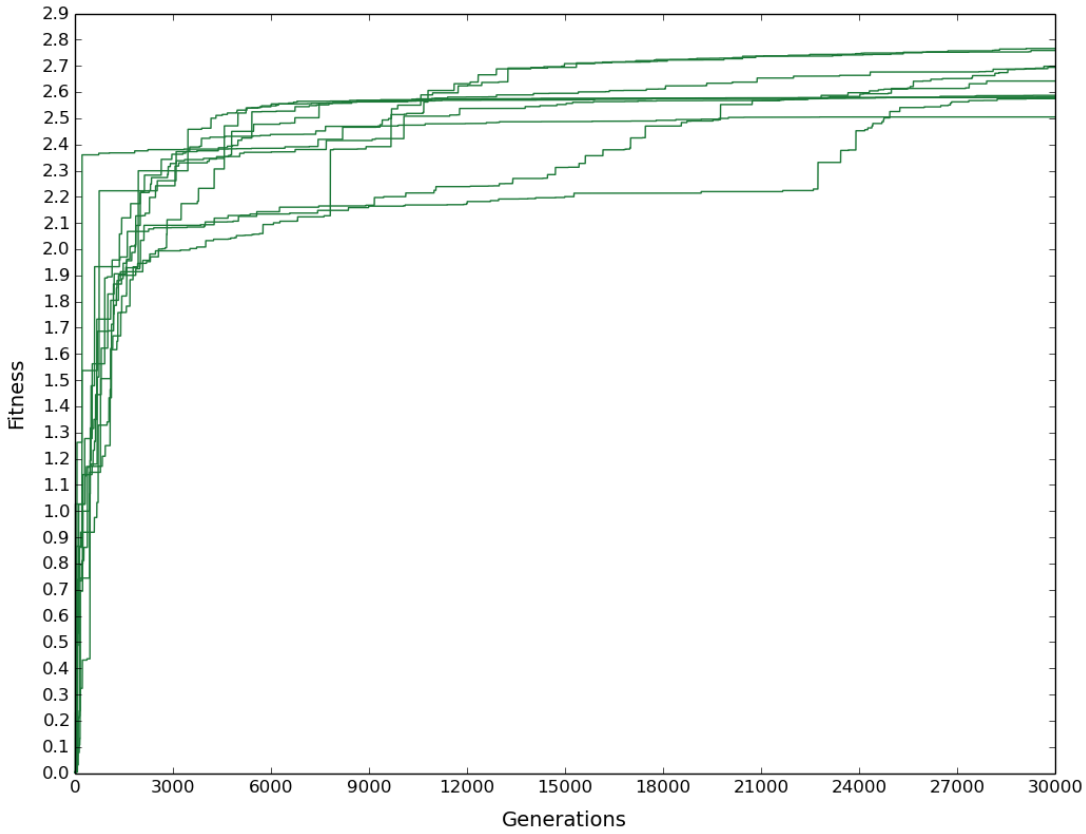

Figure 6.23. Increase in highest population fitness over generations with evolutionary pressure towards acetic acid production on glucose. Each line corresponds to the evolutionary course of one replicate run.

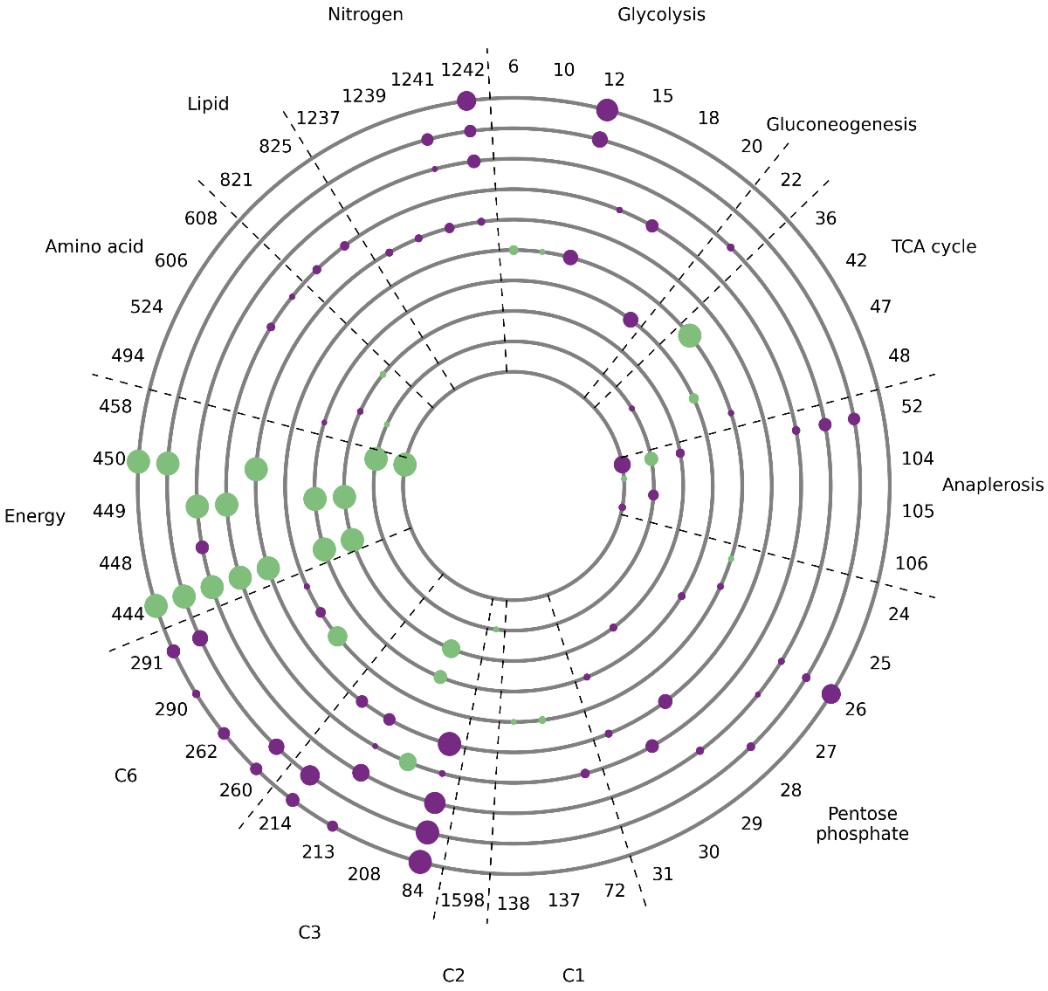

Figure 6.24. Evolution plot showing the site and frequency of mutations from 10 independent runs with evolutionary pressure towards acetic acid production on glucose. Each of the ten grey circles corresponds to the results of one replicate run. The numbers on the outside are indices and refer to reactions where mutations occurred. The corresponding reactions are given in Table 6.10. Dots on the grey circles align with these indices and indicate where mutations occurred. The diameter of each dot is proportional to the frequency of the corresponding mutation across solutions from the run. A frequency cut-off of 0.2 was applied. Mutations with a frequency lower than the cut-off are not represented. Green dots indicate mutations that when complemented decrease target acid flux by > 95%. Purple dots indicate mutations that when complemented decrease target acid flux by < 95%. The sectors indicate areas of metabolism that the mutations targeted.

Table 6.8. Example solution from evolution of acetic acid production on glucose.

			Complementation results		
Index	**Reaction**	**Mutation effect**	**% Fitness decrease**	**% Acid flux decrease**	**% Growth increase**
458	ADP+PI+ATPm+H2Om -->ADPm+PIm+ATP+H2O	UC	99.9	100	97.4
36	ACOm+H2Om<==>ICITm	UC	99.9	100	8.8

The example solution is chosen as the best representative of the average solution and based on fitness. The mutation effect is given as UC or LC. UC corresponds to a mutation that imposes a flux constraint on the upper bound. LC corresponds to a mutation that imposes a flux constraint on the lower bound. Complementation results are given for each mutation, showing the effect on fitness, target acid flux, and growth when the mutation is complemented with the wild-type while retaining the other mutations.

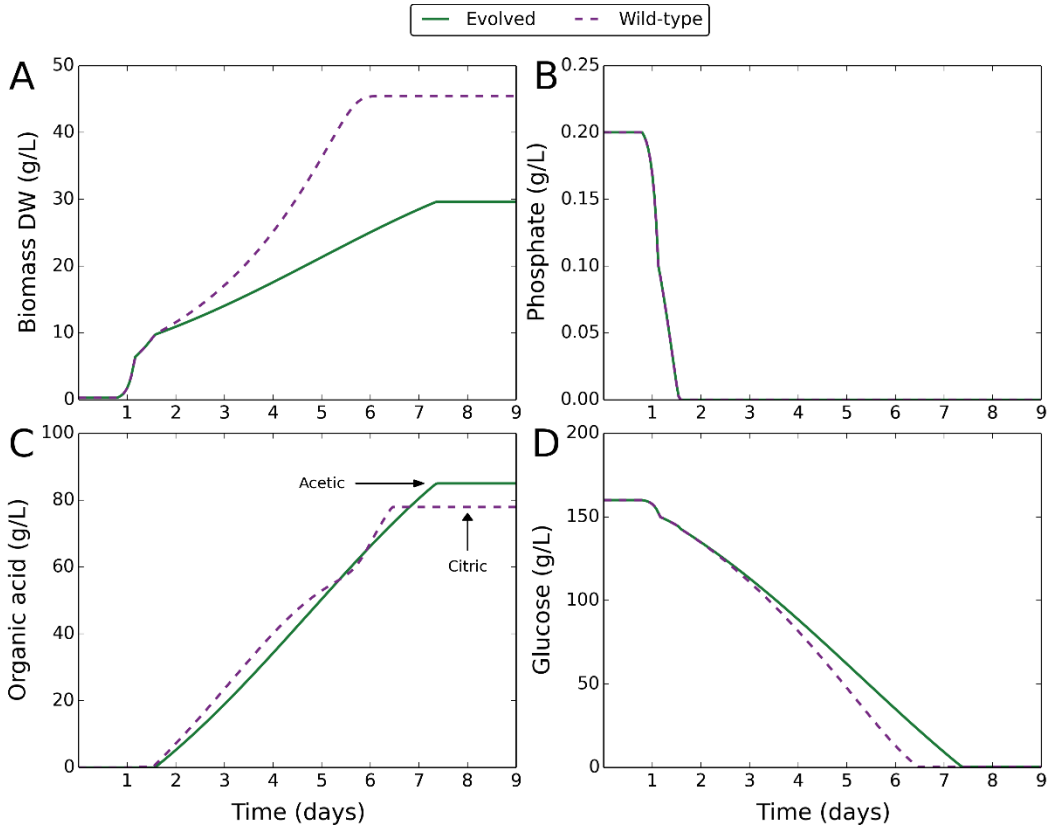

Figure 6.25. Dynamic modelling of organic acid fermentation comparing the wild-type with a solution from *in silico* evolution towards acetic acid production on glucose. Green solid lines correspond to a genome evolved for acetic acid production on glucose, using a solution that best represents the average evolved genome and based on fitness (Table 6.8). Purple dashed lines correspond to the wild-type. Mutations are induced at the point of external phosphate depletion. **(A)** Change in biomass dry weight (g/L) over time. **(B)** Change in external phosphate concentration (g/L) over time. **(C)** Change in external organic acid concentration (g/L) over time. Lines are annotated to indicate the organic acid produced. **(D)** Change in external glucose concentration (g/L) over time.

6.3.8 *In silico* evolution of gluconic acid production on glucose

The genetic algorithm was applied to predict changes that switch acid output from citric to gluconic and optimise gluconic acid production on glucose. 10 replicate runs were performed for a duration of 30,000 generations each. Gluconic acid production successfully evolved, with increasing fitness up to 10,000 generations, beyond which fitness was constant (Figure 6.26). All replicate runs achieved the same maximum fitness, suggesting the global optimum was reached in all cases. Evolutionary speed was consistent across the runs, with little variation.

The evolution output was analysed and the site and frequency of mutations are indicated in Figure 6.27. The mutations were mainly directed at glycolysis and C6 metabolism. Activities of glucose-6-phosphate isomerase and fructose-bisphosphate aldolase were frequently constrained, decreasing flux through glycolysis. Mutations also targeted the activities of gluconate dehydratase and 2-keto-3-deoxygluconate aldolase, reducing flux down the gluconate catabolic pathway. Mutations affecting the pentose-phosphate pathway frequently occurred, most commonly targeting ribulose-phosphate 3-epimerase. In all these cases, the mutations were essential to gluconic acid production.

The solution that best represented the average and with fitness near the maximum was chosen (Table 6.9), and applied in dynamic modelling of organic acid fermentation with comparison to the wild-type (Figure 6.28). Mutations were induced at the point of phosphate depletion, beyond which organic acids were produced. Acid output was completely switched from citric to gluconic in the mutant, and the predicted yield of gluconic acid was 100 g/L. Growth was also constrained, allowing a higher yield of organic acid. It was also observed that gluconic acid was produced as a by-product during growth optimisation, and was not dependent on the proton production objective function. The mutations therefore placed flux constraints that forced production of gluconic acid to achieve optimal growth.

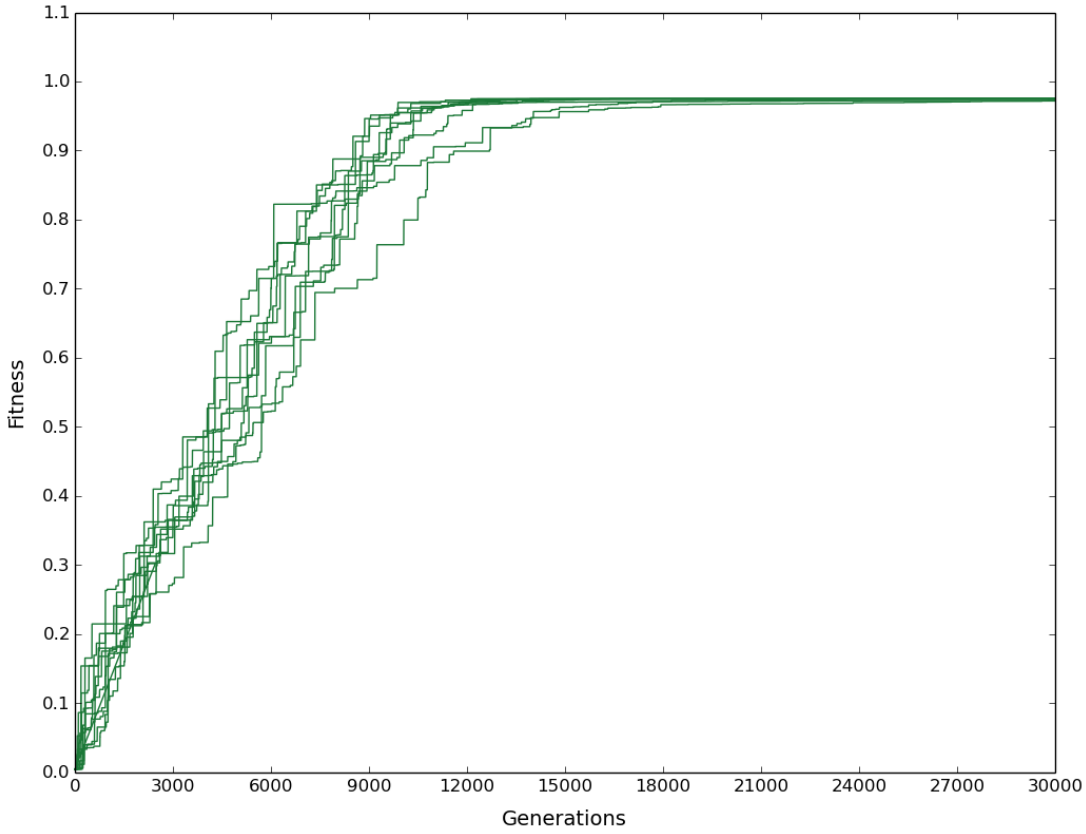

Figure 6.26. Increase in highest population fitness over generations with evolutionary pressure towards gluconic acid production on glucose. Each line corresponds to the evolutionary course of one replicate run.

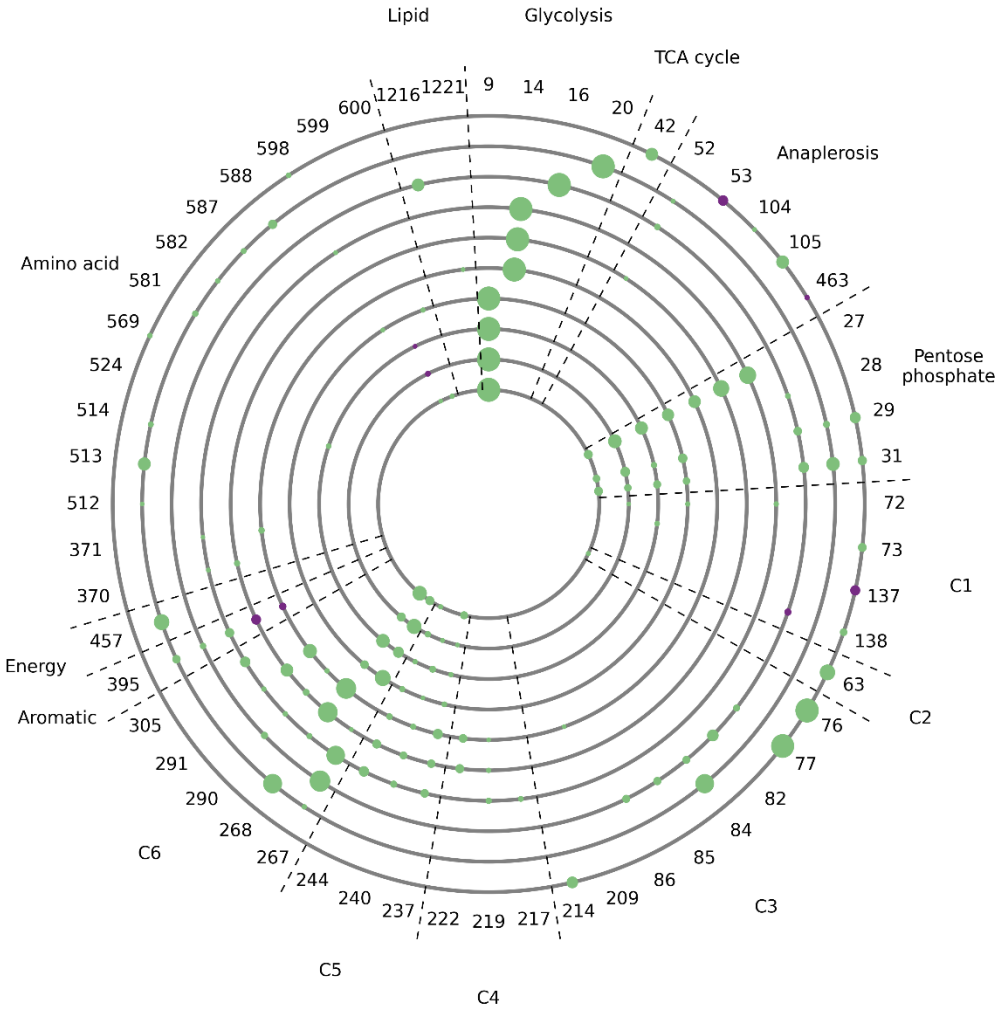

Figure 6.27. Evolution plot showing the site and frequency of mutations from 10 independent runs with evolutionary pressure towards gluconic acid production on glucose. Each of the ten grey circles corresponds to the results of one replicate run. The numbers on the outside are indices and refer to reactions where mutations occurred. The corresponding reactions are given in Table 6.10. Dots on the grey circles align with these indices and indicate where mutations occurred. The diameter of each dot is proportional to the frequency of the corresponding mutation across solutions from the run. A frequency cut-off of 0.15 was applied. Mutations with a frequency lower than the cut-off are not represented. Green dots indicate mutations that when complemented decrease target acid flux by > 95%. Purple dots indicate mutations that when complemented decrease target acid flux by < 95%. The sectors indicate areas of metabolism that the mutations targeted.

Table 6.9. Example solution from evolution of gluconic acid production on glucose.

			Complementation results		
Index	**Reaction**	**Mutation effect**	**% Fitness decrease**	**% Acid flux decrease**	**% Growth increase**
28	R5P<==>RL5P	LC	99.6	100	117.2
268	KDDGC<==>PYR+GLYAL	UC	99.6	100	117.2
27	RL5P<==>XUL5P	UC	99.6	100	117.2
9	BDG6P<==>F6P	UC	99.6	100	117.2

The example solution is chosen as the best representative of the average solution and based on fitness. The mutation effect is given as UC or LC. UC corresponds to a mutation that imposes a flux constraint on the upper bound. LC corresponds to a mutation that imposes a flux constraint on the lower bound. Complementation results are given for each mutation, showing the effect on fitness, target acid flux, and growth when the mutation is complemented with the wild-type while retaining the other mutations.

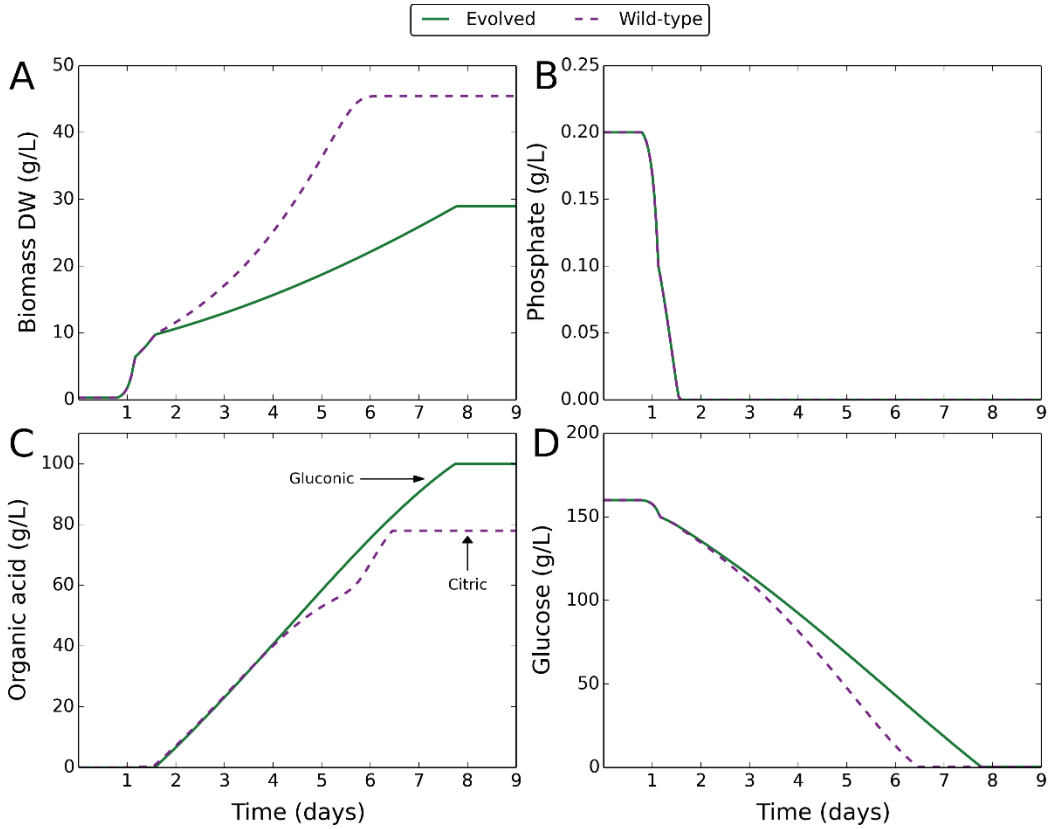

Figure 6.28. Dynamic modelling of organic acid fermentation comparing the wild-type with a solution from *in silico* evolution towards gluconic acid production on glucose. Green solid lines correspond to a genome evolved for gluconic acid production on glucose, using a solution that best represents the average evolved genome and based on fitness (Table 6.9). Purple dashed lines correspond to the wild-type. Mutations are induced at the point of external phosphate depletion. **(A)** Change in biomass dry weight (g/L) over time. **(B)** Change in external phosphate concentration (g/L) over time. **(C)** Change in external organic acid concentration (g/L) over time. Lines are annotated to indicate the organic acid produced. **(D)** Change in external glucose concentration (g/L) over time.

Table 6.10. Index numbers of mutations and corresponding reactions and mutation effects.

			Mutation effect					
Index	**Reaction**	**Description**	**Succinic**	**Lactic**	**Malic**	**Citric**	**Acetic**	**Gluconic**
6	ATP+GLC-->ADP+G6P+H	Hexokinase	N	N	N	N	**UC**	N
9	BDG6P<==>F6P	Glucose-6-phosphate isomerase	N	N	N	N	N	**UC**
10	G6P<==>ADG6P	Glucose-6-phosphate isomerase	N	N	N	N	**LC**	N
11	ADG6P<==>BDG6P	Glucose-6-phosphate 1-epimerase	**LC**	N	N	N	N	N
12	ATP+F6P-->ADP+FDP+H	6-phosphofructo-1-kinase	N	**UC**	**UC**	N	**UC**	N
14	FDP<==>T3P2+T3P1	Fructose-bisphosphate aldolase	N	**UC**	**UC**	N	N	**UC**
15	T3P2<==>T3P1	Triosephosphate isomerase	N	**UC**	N	N	**UC**	N
16	T3P1+PI+NAD<==>13PDG+NADH+H	Glyceraldehyde 3-phosphate dehydrogenase	N	**UC**	N	N	N	**UC**
17	ADP+13PDG<==>ATP+3PG	Phosphoglycerate kinase	**UC**	**UC**	N	N	N	N
18	3PG<==>2PG	Phosphoglycerate mutase	N	**UC**	N	N	**UC**	N
19	2PG<==>PEP+H2O	Phosphopyruvate hydratase	**UC**	**UC**	N	N	N	N
20	ADP+PEP+H-->ATP+PYR	Pyruvate kinase	N	**UC**	N	N	**UC**	**UC**

			Mutation effect					
Index	**Reaction**	**Description**	**Succinic**	**Lactic**	**Malic**	**Citric**	**Acetic**	**Gluconic**
21	ATP+PYR+H2O+CO2-->ADP+PI+OA+2*H	Pyruvate carboxylase	N	N	**UC**	N	N	N
22	ATPm+PYRm+H2Om+CO2m-->ADPm+PIm+OAm+2*Hm	Pyruvate carboxylase	**UC**	N	N	N	**UC**	N
24	G6P+NADP-->D6PGL+NADPH+H	Glucose 6-phosphate 1-dehydrogenase	**UC**	N	**UC**	N	**UC**	N
25	D6PGL+H2O-->D6PGC+H	6-Phospho-gluconolactonase	N	N	**UC**	N	**UC**	N
26	D6PGC+NADP-->RL5P+CO2+NADPH	Phosphogluconate dehydrogenase	**UC**	N	**UC**	N	**UC**	N
27	RL5P<==>XUL5P	Ribulose-phosphate 3-epimerase	**UC**	**UC**	**UC**	N	**UC**	**UC**
28	R5P<==>RL5P	Ribose-5-phosphate isomerase	N	N	**LC**	N	**LC**	**LC**
29	R5P+XUL5P<==>S7P+T3P1	Transketolase	**UC**	**LC**	N	N	**UC**	**UC**
30	E4P+XUL5P<==>F6P+T3P1	Transketolase	N	**UC**	**LC**	N	**LC**	N
31	S7P+T3P1<==>E4P+F6P	Transaldolase	**UC**	**LC**	**UC**	N	**UC**	**UC**
34	ACCOAm+H2Om+OAm<==>CITm+COAm+Hm	Citrate synthase	N	N	**UC**	N	N	N
35	CITm<==>ACOm+H2Om	Aconitate hydratase	N	**UC**	N	N	N	N
36	ACOm+H2Om<==>ICITm	Aconitate hydratase	N	**UC**	N	N	**UC**	N
38	ICITm+NADm-->AKGm+CO2m+NADHm	Isocitrate dehydrogenase (NAD+)	N	**UC**	N	N	N	N
39	ICIT+NADP-->AKG+CO2+NADPH	Isocitrate dehydrogenase (NADP+)	N	**UC**	N	N	N	N

			Mutation effect					
Index	**Reaction**	**Description**	**Succinic**	**Lactic**	**Malic**	**Citric**	**Acetic**	**Gluconic**
40	AKGm+TDPE1m-->AKGE1m+CO2m	alpha-ketoglutarate dehydrogenase	N	**UC**	N	N	N	N
41	AKGE1m+LPSE2m-->AKGE2m+TDPE1m	Dihydrolipoamide S-succinyl transferase	N	**UC**	N	N	N	N
42	AKGE2m+COAm+NADm<==>LPSE2m+SUCCOAm+NADHm	Dihydrolipoamide dehydrogenase	N	**UC**	N	N	**UC**	**UC**
43	GDPm+PIm+SUCCOAm<==>GTPm+SUCCm+COAm	Succinate CoA ligase (GDP forming)	**UC**	**UC**	N	N	N	N
45	SUCCm+Qm<==>FUMm+QH2m	Succinate dehydrogenase (ubiquinone)	**UC**	N	N	N	N	N
46	FUMm+FADH2m-->SUCCm+FADm+Hm	Succinate dehydrogenase	N	**UC**	N	N	N	N
47	FUM+FADH2m-->SUCC+FADm+Hm	Succinate dehydrogenase	N	**UC**	N	N	**UC**	N
48	FUMm+H2Om<==>MALm	Fumarate hydratase	N	N	**UC**	N	**UC**	N
51	MAL+NAD<==>OA+NADH+H	Malate dehydrogenase	N	N	**LC**	N	N	N
52	ICITp-->SUCCp+GLXp	Isocitrate lyase	N	**UC**	N	N	**UC**	**UC**
53	ACCOAp+H2Op+GLXp-->MALp+COAp+Hp	Malate synthase	N	**UC**	N	N	N	**UC**
56	MAL+NADP-->PYR+CO2+NADPH	Malate dehydrogenase (NADP-specific)	**UC**	N	N	N	N	N
60	ATPm+CITm+COAm-->ADPm+PIm+ACCOAm+OAm	Mitochondrial ATP:citrate lyase	**UC**	N	N	N	N	N
61	CITm-->OAm+ACm	Mitochondrial citrate lyase	**UC**	N	N	N	N	N
63	OA+H2O-->OXAL+AC+H	Oxaloacetate hydrolase	N	**UC**	N	N	N	**UC**

			Mutation effect					
Index	**Reaction**	**Description**	**Succinic**	**Lactic**	**Malic**	**Citric**	**Acetic**	**Gluconic**
72	FALD+NAD+H2O<==>FOR+NADH+2*H	Formaldehyde dehydrogenase	N	**LC**	N	N	**LC**	**LC**
73	FOR+O2+H-->H2O2+CO2	Formate oxidase	N	N	**UC**	N	N	**UC**
76	COAm+ADHLIPOm+NADm<==>ACCOAm+LIPOm+ NADHm+Hm	Dihydrolipoamide S-acetyltransferase and lipoamide dehydrogenase	N	N	N	N	N	**UC**
77	H+PYR-->ACAL+CO2	Pyruvate decarboxylase	**UC**	N	N	N	N	**UC**
82	H+MTHGXL+NADPH<==>LACAL+NADP	D-Lactaldehyde dehydrogenase (Methylglyoxal reductase)	N	N	N	N	N	**UC**
84	LAC+NAD<==>PYR+NADH+H	D-lactate dehydrogenase	**LC**	N	N	N	**LC**	**UC**
85	RGT+MTHGXL<==>LGT	Lactoylglutathione lyase (glyoxylase I)	N	N	N	N	N	**UC**
86	LGT+H2O-->LAC+RGT+H	Hydroxyacylglutathione hydrolase (glyoxylase II)	N	N	N	N	N	**UC**
104	GLUm+Hm-->GABAm+CO2m	Glutamate decarboxylase	**UC**	N	N	N	**UC**	**UC**
105	GABAm+AKGm-->SUCCSALm+GLUm	4-Aminobutyrate transaminase	**UC**	N	N	N	**UC**	**UC**
106	SUCCSALm+NADm+H2Om-->SUCCm+NADHm+2*Hm	Succinate-semialdehyde dehydrogenase (NAD(P)+)	N	N	N	N	**UC**	N
136	METTHF+NAD-->METHF+NADH	Methylenetetrahydrofolate dehydrogenase (NAD+)	N	**UC**	**UC**	N	N	N

			Mutation effect					
Index	**Reaction**	**Description**	**Succinic**	**Lactic**	**Malic**	**Citric**	**Acetic**	**Gluconic**
137	METHF+H2O<==>FTHF+H	Methenyltetrahydrofolate cyclohydrolase	N	**UC**	**UC**	N	**UC**	**UC**
138	FTHF+H2O-->FOR+THF+H	5-formyltetrahydrofolate deformylase	**UC**	**UC**	**UC**	N	**UC**	**UC**
139	METTHF+NADPH+H-->MTHF+NADP	Methylenetetrahydrofolate reductase (NADPH)	N	N	N	**UC**	N	N
155	T3P1+RL5P+GLN-->PYDX5P+GLU+PI+3*H2O+H	5'-phosphate synthase pdxT subunit	N	N	**UC**	N	N	N
164	PD+4HBA-->4HP+PPI	polyisopentenylpyrolinate: 4-hydroxybenzoate nonaprenyltransferase	N	N	N	**UC**	N	N
169	2PMB+SAM-->2PMMB+SAH+H	ubiquinone biosynthesis methyltransferase	N	N	N	**UC**	N	N
173	D6RP5P+H2O+H-->A6RP5P+NH3	2,5-diamino-6-hydroxy-4-(5-phosphoribosylamino)-pyrimidine 2-aminohydrolase	N	N	**UC**	N	N	N
196	ACCOA+H2O-->COA+AC+H	Acetyl-CoA hydrolase	**UC**	N	N	N	N	N
200	ACm+COAm+ATPm-->AMPm+PPIm+ACCOAm+Hm	Acetyl-CoA synthase	**UC**	N	N	N	N	N
201	ACCOAm+H2Om-->COAm+ACm+Hm	Acetyl-CoA hydrolase	**UC**	N	N	N	N	N
208	GL3P+FADm-->T3P2+FADH2m	Glycerol 3-phosphate dehydrogenase (FAD dependent)	N	**UC**	N	N	**UC**	N

			Mutation effect					
Index	**Reaction**	**Description**	**Succinic**	**Lactic**	**Malic**	**Citric**	**Acetic**	**Gluconic**
209	GLYN+ATP-->T3P2+ADP+H	Glycerone kinase	N	N	N	N	N	**UC**
210	H+T3P2+NADH-->GL3P+NAD	Glycerol 3-phosphate dehydrogenase (NAD+ dependent)	N	**UC**	N	N	N	N
213	PYR+NADH+H-->LLAC+NAD	L-Lactate dehydrogenase	**UC**	N	N	N	**UC**	N
214	LLAC+O2-->AC+CO2+H2O	Lactate 2-monooxygenase	**UC**	N	N	N	**UC**	**UC**
217	E+NADPH+H-->EOL+NADP	Glycerol dehydrogenase	N	N	**UC**	N	N	**UC**
219	E4P+H2O-->PI+E	Erythrose 4-phosphate phosphatase	N	N	N	N	N	**UC**
222	EU+ATP-->EU1P+ADP+H	Erythrulose kinase	N	N	N	N	N	**UC**
237	XUL5P+FALD<==>T3P1+GLYN	Dihydroxyacetone synthase	N	**UC**	**UC**	N	N	**UC**
240	RIB+NADPH+H<==>RIBOL+NADP	D-Ribose reductase	**UC**	N	**UC**	N	N	**UC**
244	RL+NADPH+H-->AOL+NADP	ribulose reductase	**UC**	N	**UC**	N	N	**UC**
260	BDGLC+NADP-->GLCN15LAC+NADPH+H	beta-D-Glucose:NADP+ 1-oxoreductase	N	N	N	N	**UC**	N
262	GLCN15LAC+H2O-->GLCNT	Non enzymatic reaction	N	N	**UC**	N	**UC**	N
265	GLCNT+ATP-->D6PGC+ADP+H	Gluconokinase	**UC**	N	**UC**	N	N	N
267	GLCNT<==>KDDGC+H2O	Gluconate dehydratase	N	N	N	N	N	**UC**
268	KDDGC<==>PYR+GLYAL	2-keto-3-deoxygluconate aldolase	N	N	N	N	N	**UC**

			Mutation effect					
Index	**Reaction**	**Description**	**Succinic**	**Lactic**	**Malic**	**Citric**	**Acetic**	**Gluconic**
274	G6P<==>G1P	Phosphoglucomutase	N	N	N	**UC**	N	N
288	MAN6P<==>F6P	Mannose-6-phosphate isomerase	N	N	N	**LC**	N	N
290	F6P+NADH+H<==>MNT1P+NAD	Mannitol-1-phosphate 5-dehydrogenase	N	N	**UC**	N	**UC**	**UC**
291	MNT1P+H2O-->MNT+PI	Mannitol-1-phosphatase	N	N	**UC**	N	**UC**	**UC**
292	MNT+NADP-->FRU+NADPH+H	Mannitol 2-dehydrogenase (NADP+)	N	N	**UC**	N	N	N
305	ATP+FRU-->ADP+F1P+H	ketohexokinase	N	N	**UC**	N	N	**UC**
306	F1P<==>T3P2+GLYAL	fructose-bisphosphate aldolase, class II	N	N	**UC**	N	N	N
311	UDPG+G6P-->UDP+TRE6P	Trehalose-6-phosphate synthase	N	N	N	**UC**	N	N
312	TRE6P+H2O-->TRE+PI	Trehalose-phosphatase	N	N	N	**UC**	N	N
370	FKYN+H2O-->FOR+KYN+H	Kynurenine formamidase	N	N	N	N	N	**UC**
371	KYN+H2O-->ALA+AN+H	Kynureninase	N	N	N	N	N	**UC**
395	DHSK<==>PCC+H2O	5-dehydroshikimate dehydrase	N	N	N	N	N	**UC**
407	UDPG-->UDP+14GLUCAN	1,4-alpha-Glucan branching enzyme	N	N	**UC**	N	N	N
412	ACCOA+GA6P<==>COA+NAGA6P+H	Glucosamine-phosphate N-acetyltransferase	**UC**	N	N	N	N	N

			Mutation effect					
Index	**Reaction**	**Description**	**Succinic**	**Lactic**	**Malic**	**Citric**	**Acetic**	**Gluconic**
413	NAGA6P+H2O-->GA6P+AC	N-acetylglucosamine-6-phosphate deacetylase	**UC**	N	N	N	N	N
430	PPP9m-->HEMEBm	protoheme ferro-lyase (protoporphyrin-forming)	N	N	**UC**	N	N	N
433	HEMEBm-->HEMEOm	heme A farnesyltransferase	N	N	N	**UC**	N	N
444	QH2m+0.5*O2m-->Qm+H2Om	Ubiquinol oxidase (mitochondrial alternative oxidase)	**UC**	N	N	N	**UC**	N
448	NADPH+2*FERIm-->NADP+2*FEROm	NADPH-ferrihemoprotein reductase	N	N	N	N	**UC**	N
449	QH2m+2*FERIm+2*Hm-->Qm+2*FEROm+4*Ho	Ubiquinol-cytochrome c reductase	**UC**	N	N	N	**UC**	N
450	2*FEROm+0.5*O2m+6*Hm-->2*FERIm+H2Om+4*Ho	Cytochrome c oxidase subunit I	**UC**	N	N	N	**UC**	N
451	ADPm+PIm+4.5454*Ho-->ATPm+H2Om+4.5454*Hm	F1F0-ATPase complex	**UC**	**UC**	N	N	N	N
456	2*FERIm+LLACm-->PYRm+2*FEROm	Lactic acid dehydrogenase	**UC**	N	N	N	N	N
457	2*FERIm+LACm-->PYRm+2*FEROm	Mitochondrial enzyme D-lactate ferricytochrome c oxidoreductase	N	N	N	N	N	**UC**
458	ADP+PI+ATPm+H2Om-->ADPm+PIm+ATP+H2O	ADP/ATP translocase	**UC**	N	N	N	**UC**	N
463	2*H2O2p-->2*H2Op+O2p	Catalase	N	N	**UC**	N	N	**UC**

			Mutation effect					
Index	**Reaction**	**Description**	**Succinic**	**Lactic**	**Malic**	**Citric**	**Acetic**	**Gluconic**
481	H+SAM<==>CO2+DSAM	S-adenosylmethionine decarboxylase	N	N	**UC**	N	N	N
491	NAGLUm+ATPm-->NAGLUPm+ADPm	Acetylglutamate kinase	N	N	**UC**	**UC**	N	N
493	NAGLUSm+GLUm-->AKGm+NAORNm	Acetylornithine aminotransferase	**UC**	N	N	N	N	N
494	GLUm+NAORNm-->ORNm+NAGLUm	Glutamate N-acetyltransferase	N	N	N	N	**UC**	N
498	MTA+HSER+H-->SAM+H2O	S-Adenosyl-L-methionine hydrolase	N	N	**UC**	N	N	N
510	H2Om+NADPm+GLUGSALm-->GLUm+2*Hm+NADPHm	Delta-1-pyrroline-5-carboxylate dehydrogenase	**UC**	N	N	N	N	N
511	2*H2Om+NADm+P5Cm-->GLUm+Hm+NADHm	Delta-1-pyrroline-5-carboxylate dehydrogenase	**UC**	N	N	N	N	N
512	NAD+3PG<==>H+NADH+PHP	Phosphoglycerate dehydrogenase	N	N	N	N	N	**UC**
513	PHP+GLU-->AKG+3PSER	Phosphoserine transaminase	N	N	N	N	N	**UC**
514	H2O+3PSER-->PI+SER	Phosphoserine phosphatase	N	N	N	N	N	**UC**
520	GLY+THF+NAD-->METTHF+NADH+CO2+NH3	Aminomethyltransferase	N	**UC**	N	N	N	N

			Mutation effect					
Index	**Reaction**	**Description**	**Succinic**	**Lactic**	**Malic**	**Citric**	**Acetic**	**Gluconic**
524	ALA+GLX<==>PYR+GLY	Alanine-glyoxylate transaminase	**UC**	**UC**	N	N	**UC**	**UC**
534	H2O+PRBAMP-->PRFP	phosphoribosyl-AMP cyclohydrolase	N	N	N	**UC**	N	N
546	GLUm+OIVALm<==>AKGm+VALm	Branched chain amino acid aminotransferase	N	N	N	**UC**	N	N
569	ACCOA+HSER<==>COA+OAHSER	homoserine O-acetyltransferase	N	N	N	N	N	**LC**
576	HCYS+MTHF-->MET+THF	Methionine synthase	N	N	N	**UC**	N	N
580	H2O+PEP+E4P-->PI+3DDAH7P	3-deoxy-7-phosphoheptulonate synthase	N	N	N	**UC**	N	N
581	3DDAH7P-->PI+DQT	Pentafunctional arom polypeptide	N	N	N	N	N	**UC**
582	DQT-->H2O+DHSK	3-dehydroquinase	N	N	N	N	N	**UC**
587	PEP+SME3P-->PI+3PSME	3-phosphoshikimate-1-carboxyvinyltransferase	N	N	N	N	N	**UC**
588	3PSME-->PI+CHOR	Chorismate synthase	N	N	N	N	N	**UC**
589	CHOR-->PHEN	Chorismate mutase	N	N	N	**UC**	N	N
598	PRPP+AN-->H+PPI+NPRAN	Anthranilate phosphoribosyl transferase	N	N	N	N	N	**UC**

			Mutation effect					
Index	**Reaction**	**Description**	**Succinic**	**Lactic**	**Malic**	**Citric**	**Acetic**	**Gluconic**
599	NPRAN-->CPAD5P	N-(5'-phosphoribosyl)-anthranilate isomerase	N	N	N	N	N	**UC**
600	H+CPAD5P-->H2O+CO2+IGP	Indoleglycerol phosphate synthase	N	N	N	N	N	**UC**
606	2*H+NADPH+P5C<==>PRO+NADP	Pyrroline-5-carboxylate reductase	N	N	N	N	**UC**	N
608	NADm+PROm-->2*Hm+NADHm+P5Cm	Proline dehydrogenase	N	N	N	N	**UC**	N
609	GLUGSALm<==>P5Cm+H2O+H	Non enzymatic reaction	**LC**	N	N	N	N	N
629	H2O+GLN+PRPP-->GLU+H+PPI+PRAM	Phosphoribosyl-pyrophosphate amidotransferase	N	N	N	**UC**	N	N
632	H2O+GLN+ATP+FGAR-->GLU+H+PI+ADP+FGAM	5'-phosphoribosylformyl glycinamidine synthetase	N	N	**UC**	N	N	N
635	ASP+ATP+CAIR<==>2*H+PI+ADP+SAICAR	Phosphoribosyl amino imidazole-succinocarbozamide synthetase	N	N	**UC**	N	N	N
636	SAICAR<==>FUM+AICAR	5'-phosphoribosyl-4-(N-succinocarboxamide)-5-aminoimidazole lyase	N	N	**UC**	N	N	N
694	ADP+UDP<==>ATP+UMP+H	Cytidylate kinase	N	N	N	**LC**	N	N
696	UDP+ATP<==>UTP+ADP	Nucleoside-diphosphate kinase	N	N	N	**UC**	N	N

			Mutation effect					
Index	**Reaction**	**Description**	**Succinic**	**Lactic**	**Malic**	**Citric**	**Acetic**	**Gluconic**
707	DCMP+ATP+H<==>ADP+DCDP	Cytidylate kinase	N	N	N	**LC**	N	N
759	ATPm+AMPm+H<==>2*ADPm	Adenylate kinase	N	**LC**	N	N	N	N
760	GTPm+AMPm+H<==>ADPm+GDPm	Adenylate kinase	N	**UC**	N	N	N	N
787	CBCCP+ACCOA<==>BCCP+MALCOA	Biotin carboxylase	N	N	N	**UC**	N	N
788	ATP+BCCP+CO2+H2O<==>ADP+PI+CBCCP+2*H	Biotin carboxylase	N	N	N	**UC**	N	N
789	MALCOA+ACP<==>MALACP+COA	Malonyl transferase	N	N	**UC**	N	N	N
821	C140ACP+MALACP-->C16OACP+CO2+ACP	3-oxoacyl-[acyl-carrier-protein] synthase	N	N	N	N	**UC**	N
825	2*H+C140ACP+MALACP+2*NADPH-->C160ACP+ACP+2*NADP+H2O+CO2	Fatty-acid synthase	N	N	N	N	**UC**	N
882	H+C170ACP+NADPH+O2<==>C171ACP+NADP+2*H2O	C170-CoA 9-desaturase	N	N	N	**UC**	N	N
1112	CLCDPDG+PG-->CMP+CL	Cardiolipin synthase	N	N	N	**UC**	N	N
1210	DAGLYP+H2O-->DAGLY+PI	phosphatidate phosphatase	N	N	N	**UC**	N	N
1211	0.024*C120ACP+0.013*C140ACP+0.012*C141ACP+0.002*C150ACP+0.154*C160ACP+0.02*C161ACP+0.008*C162ACP+0.002*C170ACP+0.026*C180ACP+0.374*C181ACP+0.327*C182ACP+0.032*C183ACP+0.006*C200ACP+DAGLY-->TAGLY+ACP	1-acylglycerol-3-phosphate acyltransferase	N	N	**UC**	N	N	N
1216	G+NADH+2*H<==>GLYAL+NAD+H2O	D-Glyceraldehyde:NAD+ oxidoreductase	N	N	N	N	N	**LC**
1221	ATP+GLYN-->ADP+T3P2+H	ATP:glycerone phosphotransferase	N	N	N	N	N	**UC**

			Mutation effect					
Index	**Reaction**	**Description**	**Succinic**	**Lactic**	**Malic**	**Citric**	**Acetic**	**Gluconic**
1222	DAGLY+UDPGAL<==>UDP+MGDG	UDP-galactose:1,2-diacylglycerol 3-beta-D-galactosyltransferase	N	N	**UC**	N	N	N
1237	HNO3+NADPH+H-->HNO2+NADP+H2O	Nitrate reductase	N	N	N	N	**UC**	N
1239	HNO3+NADH+H-->HNO2+NAD+H2O	Nitrate reductase	N	N	N	N	**UC**	N
1241	HNO2+3*NADH+5*H-->NH4OH+3*NAD+H2O	Nitrite reductase	**UC**	N	N	N	**UC**	N
1242	NH4OH<==>NH3+H2O	Non enzymatic reaction	**UC**	N	N	N	**UC**	N
1596	ACCOAm+CARm<==>COAm+ALCARm	Mitochondrial acetyl transfer	N	**UC**	N	N	N	N
1598	ACCOA+CAR<==>COA+ALCAR	Mitochondrial acetyl transfer	N	N	N	N	**LC**	N

The mutation effect is given as LC, UC or N. LC corresponds to a mutation that imposes a flux constraint on the lower bound. UC corresponds to a mutation that imposes a flux constraint on the upper bound. N signifies no mutation.

6.4 Discussion

To establish a picture of the underlying flux changes in solutions from *in silico* evolution, the flux patterns were examined for each of the evolved target acids. In the case of evolution of citric acid production on glucose or xylose, the solutions are simply single growth targets. The flux constraints applied to these result in a growth rate that gives optimum citric acid productivity. Switching acid output requires more complex solutions. As well as inducing a re-distribution of flux that brings about a complete switch of acid output to the target acid, these solutions also constrain growth to give optimum productivity.

When investigating the flux patterns of succinic, lactic, and acetic acid solutions, a relationship was observed. All shared a common feature. The primary mutations targeted aerobic respiration, most commonly a combined disruption of ubiquinol-cytochrome c reductase and alternative oxidase. These reaction steps are necessary for the recycling of NADH to NAD, to maintain a high glycolytic flux. Other mutations frequently occurred that also caused a decreased flux through the electron transport chain. In all lactic acid solutions, ATP synthase was disrupted, and this same mutation was present in some succinic acid solutions. Mutations targeting ADP/ATP translocase and cytochrome c oxidase were found in both acetic and succinic acid solutions. Mutations that disrupted oxidative phosphorylation, and thereby forcing an alternative means of NADH recycling, were found to be essential to production of these acids. On further examination, it was realised that the production of each of these acids provided a different solution to the recycling of NADH to NAD. Therefore, a competition between the three acids resulted, and solutions for optimum production of one acid frequently incorporated mutations to block production of the other two acids.

The simplest case is lactic acid production. The conversion of pyruvate to lactate by lactate dehydrogenase converts NADH to NAD. This reaction provides the sole source of lactic acid output. This is common of anaerobic

respiration, where accumulation of lactic acid enables maintenance of glycolytic flux to yield energy in oxygen-limiting conditions (Zehnder and Svensson, 1986; Mat-Jan *et al*, 1989). Lactate dehydrogenase was frequently disrupted in succinic acid solutions and in some acetic acid solutions, therefore blocking this reaction as the means of NADH recycling.

The production of acetic acid is associated with a more complex flux pattern. The acetate is sourced from the conversion of citrate to oxaloacetate and acetate by citrate lyase, followed by the hydrolysis of oxaloacetate to oxalate and acetate. The oxalate is recycled by oxalate decarboxylase, producing formate. This reaction loses one carbon as carbon dioxide. The subsequent conversion of formate to formaldehyde by formaldehyde dehydrogenase provides the means of NADH recycling. The recycling of formaldehyde into glycolytic intermediates requires the supply of xylulose-5-phosphate from the pentose phosphate pathway. Interestingly, mutations targeting the pentose phosphate pathway were common in succinic acid solutions, and these constrained the supply of xylulose-5-phosphate, thereby blocking the formaldehyde dehydrogenase reaction and shutting down a competing process of NADH recycling. Such mutations were required to disrupt acetic acid production resulting from constrained aerobic respiration. It was observed in evolution of acetic acid production that some runs converged on solutions with lower fitness. When these were examined, a different flux pattern and simpler means of acetic acid production were found. In these solutions, acetate is produced by the decarboxylation of pyruvate to acetaldehyde followed by conversion to acetate. This route of acetic acid production is less preferable, as for every six carbons two carbons are lost, whereas only one carbon is lost in the previously described process. This explains the difference in fitness. The more complex route allows a higher flux of carbon to acetic acid. The pyruvate decarboxylase reaction that produces acetaldehyde, a precursor to acetate, was frequently constrained in succinic acid solutions. Both routes of acetic acid production had to be disrupted to channel flux to succinic. In terms of NADH recycling, flux patterns revealed that malate dehydrogenase was responsible when the simpler route was used.

The solutions that optimise succinic acid productivity appeared to be more complex than those for the other acids, and this is resembled by the more elaborate re-distribution of flux observed in evolved succinic acid producers. This is illustrated in Figure 6.29. The evolution of succinic acid production was performed on both glucose and xylose, which gave very similar solutions and flux patterns. The flux patterns reveal that succinic output is sourced from two reactions. Isocitrate lyase provides 56%, while fumarate reductase provides the remaining 44%. The glyoxylate shunt is key. Citrate is catabolised to isocitrate via the action of aconitase, and isocitrate serves as the substrate for the glyoxylate shunt. Isocitrate is converted to succinate and glyoxylate by isocitrate lyase, and the glyoxylate is combined with acetyl-CoA by malate synthase to form malate. This malate is then converted to fumarate by fumarase, providing the substrate for fumarate reductase, which in turn produces succinate. Fumarate reductase plays an important role, as it recycles FADH2 to FAD, which is used to recycle NADH to NAD. Therefore, as well as lactic and acetic acid production, succinic acid production is a means of NADH recycling. This only occurs if mutations are present that block NADH recycling via the production of lactic and acetic acid, including disruptions of lactate dehydrogenase, pyruvate decarboxylase, and the pentose phosphate pathway. Interestingly, some lactic and acetic acid solutions have mutations that constrain the glyoxylate shunt, thereby blocking this route of succinic acid production. It is important to note that the glyoxylate shunt occurs in the peroxisome compartment, and that its operation is dependent on the provision of acetyl-CoA to this compartment. This requires a means to transfer acetyl-CoA from the mitochondria where it is produced, to the cytosol where it can enter the peroxisome. In the iDU1757 model, new reactions were added that enable the transfer of mitochondrial acetyl-CoA via acetyl-carnitine. A flux change in these reactions was observed in succinic acid producers. When these reactions were switched off, succinic production via the glyoxylate shunt was abolished. The flux through the fumarate reductase reaction increased in response, and this became the sole source of the succinic acid output. Overall, there was a small negative effect on succinic production, with a drop

in output flux from 0.33 to 0.29 mmol gDW^{-1} h^{-1}. The optimum solution therefore required operation of the glyoxylate shunt. This case highlighted the value in updating metabolic models to include new and relevant reactions, that have an effect when applying *in silico* tools.

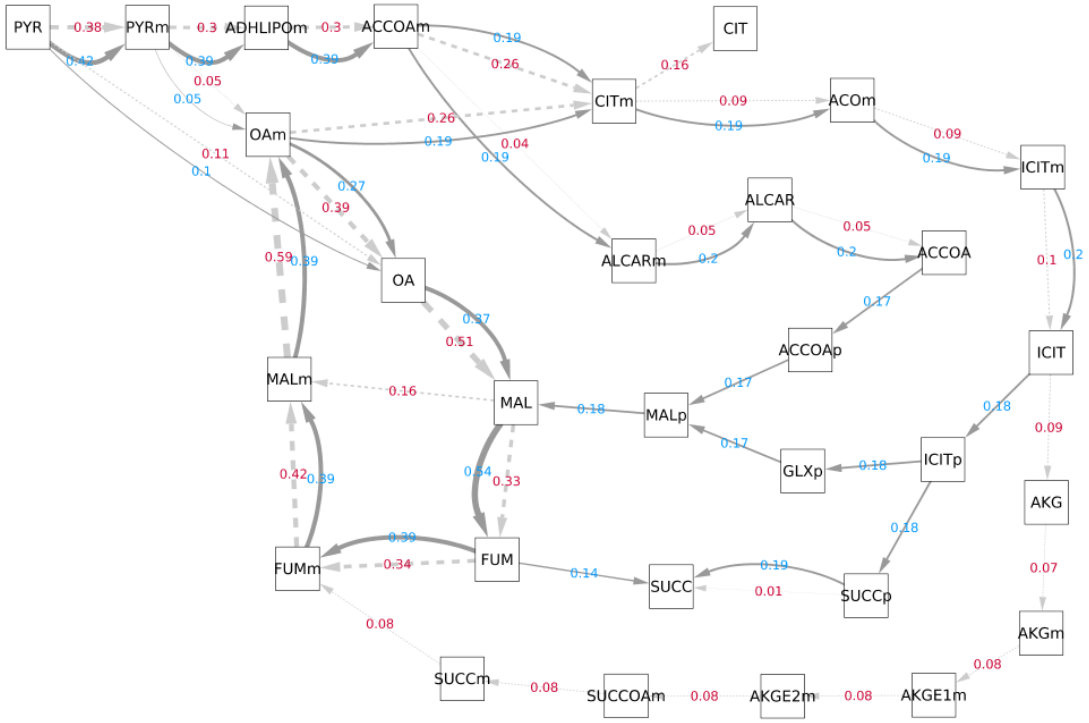

Figure 6.29. Flux diagram illustrating re-distribution of flux in evolved succinic acid producer compared to wild-type. The chosen solution from evolution of succinic acid production on glucose was applied in FBA simulations to determine the re-distribution of flux relative to the wild-type. Flux values are given to two decimal places. Dark grey and solid arrows with light blue flux labels correspond to the evolved succinic acid producer. Light grey and dashed arrows with red flux labels correspond to the wild-type. The thickness of arrows is proportional to the corresponding flux.

It is worthy to raise awareness of attempts reported in the literature to engineer *A. niger* for increased succinic acid production. One study investigated the effect of over-expressed isocitrate lyase and inhibition of succinate dehydrogenase by addition of malonate (Meijer *et al*, 2009b). It was hypothesised that these changes would increase flux down the glyoxylate shunt and increase succinic acid production. This was not the outcome, however. It became clear that tampering of single metabolic steps is unsuccessful due to the compensating regulatory apparatus. When isocitrate lyase was over-expressed, fumarate production significantly increased rather than succinic acid, and this was not due to increased activity of the glyoxylate shunt. Upon inhibition of succinate dehydrogenase by malonate, the production of fumarate shifted to malate. Inhibition of succinate dehydrogenase alone resulted in heightened citric and oxalic acid production. These targets drew parallels with solutions from *in silico* evolution of succinic acid production performed in this work. In these solutions, succinate dehydrogenase was frequently disrupted, and in combination with other alterations, an increased flux down the glyoxylate shunt was induced. In a different study, ATP-citrate lyase was knocked out, which resulted in production of acetate and a small increase in succinic acid production (Meijer *et al*, 2009a). It was suggested that pyruvate decarboxylase would also need to be disrupted, and that limiting succinic acid transport steps may be responsible. There was a general increase in acidogenesis. Based on empirical observations, it was proposed that fumarate reductase has low activity in *A. niger* (Meijer *et al*, 2009a). Therefore, this is an important target in strategies to increase succinic acid production in *A. niger*.

Efforts to improve succinic acid production have also been made in other organisms, and these have similarities with strategies suggested in this work for increasing succinic acid production in *A. niger*. The organism *Corynebacterium glutamicum* secretes lactic and succinic acid under anaerobic conditions, and was subjected to engineering (Zhu *et al*, 2014). The disruption of lactate dehydrogenase in this organism increased succinic acid production, and but also induced acetate production. Succinic acid

production was further increased by the disruption of pathways involved in acetate production. Additional beneficial effects were achieved by over-expression of the enzymes involved in the glyoxylate shunt, and a succinic acid exporter. It was demonstrated that succinic acid transport is a key target for over-expression. Succinic acid production has also been investigated in *Saccharomyces cerevisiae,* which produces succinic acid during dough fermentation (Rezaei *et al*, 2015). It was shown that the glyoxylate shunt contributes significantly to succinic acid production in this organism, as deletion of aconitase and isocitrate lyase reduced production by 77%. A two-fold increase in production was observed upon knock-out of succinate dehydrogenase, while deletion of fumarate reductase had no effect.

Succinic acid production is an emerging topic. This organic acid is currently produced by chemical synthesis from petroleum-derived maleic anhydride, however, there is an increasing shift to fermentative production as this could realise cheaper and more sustainable manufacture (Zhu *et al*, 2014). There are currently two companies operating in this market, BioAmber and DSM-Roquette, and these use engineered *E. coli* and *S. cerevisiae*, respectively (Zhu *et al*, 2014). Succinic acid has significant potential as a building block chemical, and can be used to derive chemicals such as 1,4-butanediol and tetrahydrofuran, for application in synthesis of biobased polymers (Sauer *et al*, 2008). This potential can only be realised if a more cost-effective means of succinic acid production becomes available, and microbial production may provide the answer. It is intuitive to think that *A. niger* fermentation can help deliver this goal, and the strategies suggested in this work for engineering *A. niger* for optimum succinic acid productivity may guide steps forward.

As well as succinic acid, malic acid is a potential platform chemical that is currently produced by petrochemical methods from maleic anhydride (Brown *et al*, 2013). *In silico* evolution of *A. niger* malic acid production was performed in this work. An examination of the output revealed that citrate synthase is the primary target. A disruption of citrate synthase prevents citric acid production as a means of acidification, and malic acid production is the next most efficient means of proton production based on modelling

predictions. When the mutation constraining the citrate synthase step is applied individually, a mixture of citric and malic acid results, corresponding to the flux constraint on citrate synthase. Other mutations are necessary for a complete switch of acid output from citric to malic. Flux patterns were investigated to understand the effect of these. With citrate synthase constrained in the absence of these mutations, a complex cycle is induced that consumes excess ATP. This maintains flux through the electron transport chain, recycling NADH to NAD. It was observed that the mutations disrupt this cycle, blocking this pathway of excess ATP consumption. As a result, flux through the electron transport chain decreases in the presence of these mutations, necessitating an alternative means of NADH recycling. This is provided by the conversion of oxaloacetate to malate catalysed by malate dehydrogenase, with the subsequent production of malic acid. The oxaloacetate is formed by carboxylation of pyruvate. The importance of these two steps was demonstrated by the engineering of *A. oryzae* for increased malic acid production (Brown *et al*, 2013). Over-expression of pyruvate carboxylase and malate dehydrogenase enhanced malic acid production. It was also shown that over-expression of a native C4-dicarboxylate transporter gave a two-fold increase, highlighting the need to consider organic acid transport steps to achieve optimum productivity.

The final organic acid that was subjected to *in silico* evolution in this work was gluconic acid. *A. niger* is already used in commercial production of gluconic acid, however, this process is dependent on the action of extracellular glucose oxidase and requires the maintenance of a suitable pH (Ramachandran *et al*, 2006). As the *in silico* evolution work was performed at initial pH 2, gluconic acid production by the extracellular route was prevented. Intracellular production was therefore evolved, that can still operate at low pH. When the solutions and flux patterns were analysed, some key aspects were observed. Some mutations disrupt glycolysis, causing a re-distribution of flux via gluconate to bypass this. *A. niger* has two catabolic routes for gluconate, and other mutations constrain both of these. The result of the set of flux constraints is forced gluconate accumulation, and its subsequent secretion.

The methodologies presented in this chapter demonstrate the feasibility of rational *in silico* strain design. Genome-scale metabolic models provide a conduit between the genome and the metabolome, however, their complexity results in a combinatorial explosion when considering engineering strategies. The computational techniques described here show that optimal solutions can be found in an exhaustive search space for a range of metabolic engineering goals. This is an important advance, and will help to realise the metabolic potential of industrial organisms such as *A. niger*.

Chapter 7: Final Discussion

This project was born of the quest to establish computational tools that guide rational engineering strategies. The fungus *A. niger* has within it a metabolic treasure trove that could be the source of solutions for coming world challenges. To release this potential requires the targeted creation of new strains and conditions. Metabolic engineering is a complex field, and necessitates a holistic and systems-level view. The principal current service of *A. niger* is in organic acid production, with both citric and gluconic acid produced commercially (Max *et al* 2010; Ramachandran, 2006). *A. niger* has the potential to produce other acids of commercial value, but this is yet to be realised. Industrial processes of *A. niger* fermentation continue to depend on sucrose-based feed-stocks (Dhillon *et al*, 2013a), but rising costs in energy and resources are prompting a switch to more sustainable methods. This project made steps towards solving these challenges. A number of contributions were made. A dynamic genome-scale metabolic model of *A. niger* organic acid fermentation was developed, and shown to accurately capture physiological characteristics. The model is relevant to the industrial setting of batch or fed-batch fermentation. To inform this model, empirical work was done to characterise organic acid fermentation by the wild-type citric acid producing ATCC1015 strain. The model therefore reflects the naturally evolved acidogenic behaviour. A mechanistic understanding of this baseline is critical. Empirical observations made in this project contributed new findings. In particular, citric acid production was shown to coincide with phosphate-limited growth, caused by rapid phosphate uptake and phosphate storage as polyphosphate. The rate of polyphosphate hydrolysis correlated with the rates of growth and citric acid production. With a predictive platform established, targets for engineering could be suggested. The *A. niger* engineering tool-box was explored, and a number of tools were deployed in this project. A total of seven targets were investigated. These were either subject to knock-out, knock-down, knock-up, or knock-in. An overview of these and their effects on citric acid production is given in Figure 7.1. Once the full iterative cycle was established – fermentation experiments,

modelling, engineering – further attention was given to the *in silico* engineering tool-kit. The genome-scale metabolic network was updated and made specific to the ATCC1015 strain, with particular regard to the gene-protein-reaction associations. This stands as another contribution from the project, and was necessary to suggest further engineering strategies relevant to ATCC1015. Genome-scale metabolic networks contain large numbers of reactions, and this leads to a combinatorial explosion when searching for solutions to engineering goals. Such optimisation problems are tackled using meta-heuristic algorithms, as previously demonstrated (Choon *et al*, 2014; Choon *et al*, 2015; Chong *et al*, 2014; San Chua *et al*, 2015; Patil *et al*, 2005; Rocha *et al*, 2008; Gonçalves *et al*, 2012). The final contribution of this project was an algorithm for *in silico* evolution of *A. niger* organic acid production. This was based on a genetic algorithm, and developed from the previous modelling work. Similar approaches have been used for applications in other organisms, but usually limited to suggesting knock-out strategies (Patil *et al*, 2005; Rocha *et al*, 2008). The algorithm developed in this work was designed to be robust, able to find complex solutions that combine knock-out, knock-down, and knock-up. This significantly widened the search space to be inclusive of many optimal solutions that would otherwise not be found. The full power of this algorithm was demonstrated by its ability to find solutions that switch acid output from citric to other acids not normally produced. Production of succinic, lactic, malic, acetic, and gluconic acids were individually evolved and optimised. The results of this work suggest engineering strategies that could create new strains of industrial value.

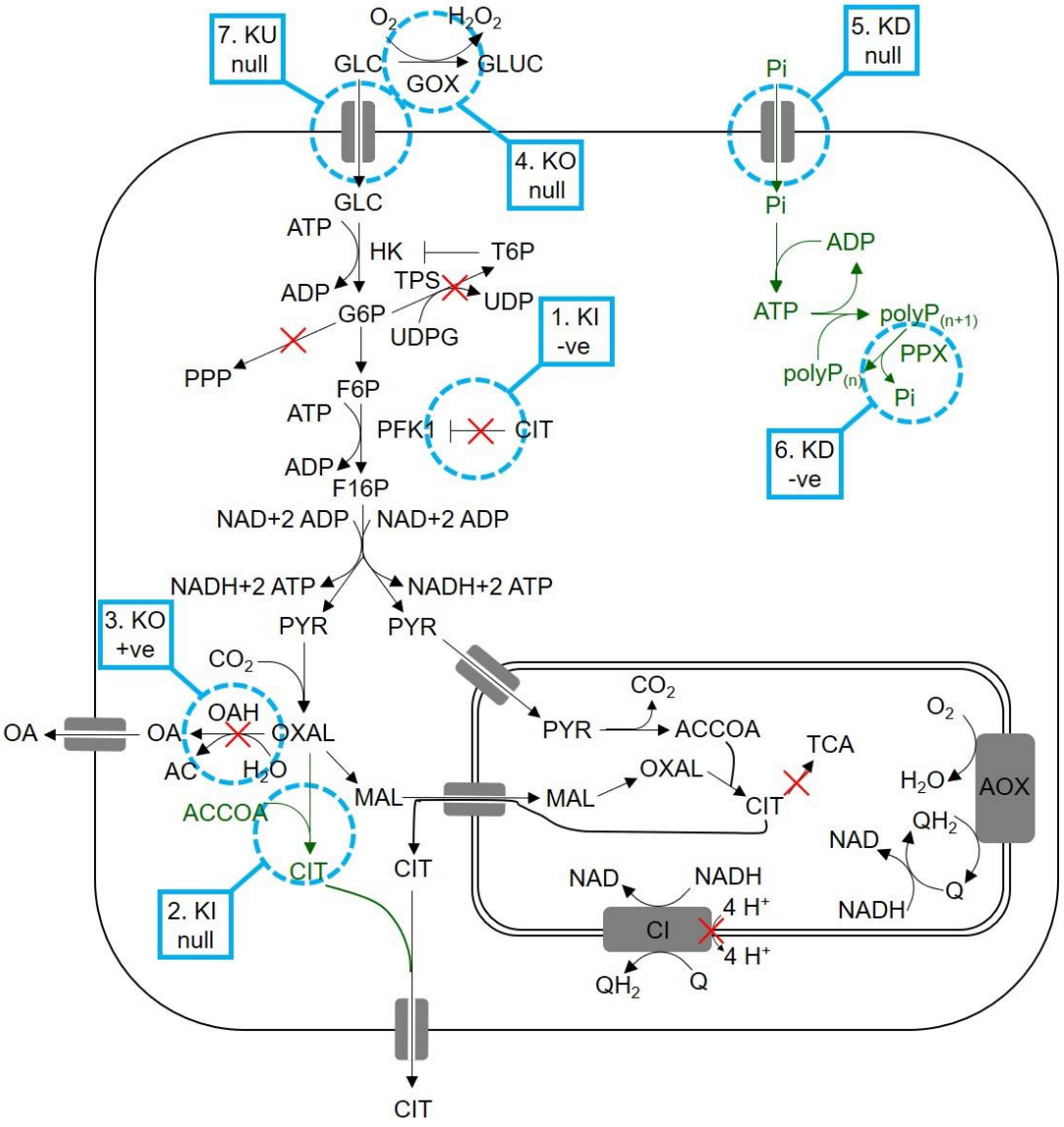

Figure 7.1. Schematic overview of metabolic and transport reactions relevant to *A. niger* organic acid production highlighting contributions from this work. The intracellular compartment reflects the mitochondria. Red crosses indicate reactions that when disrupted lead to improvements in citric acid production. New reactions that were investigated in this work are shown in green. These include phosphate uptake and ATP-dependent storage as polyphosphate and subsequent release by PPX, as well as cytosolic citrate synthase normally absent in *A. niger*. The storage and release of phosphate affects rates of growth and citric acid production, and the formation and hydrolysis of polyphosphate may be an extra means to dissipate ATP, beneficial to citric acid production. Blue dashed circles indicate reactions that were targeted for engineering in this work. These are

annotated as KI (knock-in), KO (knock-out), KD (knock-down) and KU (knock-up), and their effects on citric acid production are given as “-ve” (negative effect), “null” (no effect) and “+ve” (positive effect). These are numbered and are as follows: 1. Expression of citrate-insensitive 6-phosphofructo-1-kinase. 2. Expression of cytosolic citrate synthase. 3. Knock-out of oxaloacetate hydrolase. 4. Knock-out of glucose oxidase. 5. Knock-down of a phosphate transporter. 6. Knock-down of exopolyphosphatase. 7. Over-expression of a low-affinity gluose transporter. Abbreviations are as follows: GLC, glucose; GLUC, gluconic acid; GOX, glucose oxidase; HK, hexokinase; G6P, glucose-6-phosphate; T6P, trehalose-6-phosphate; UDPG, UDP-glucose; TPS, trehalose-6-phosphate synthase; PPP, pentose phosphate pathway; F6P, fructose-6-phosphate; F16P, fructose-1,6-bisphosphate; PFK1, 6-phosphofructo-1-kinase; CIT, citric acid; PYR, pyruvate; OXAL, oxaloacetate; OA, oxalic acid; OAH, oxaloacetate hydrolase; AC, acetic acid; MAL, malic acid; ACCOA, acetyl-CoA; TCA, tricarboxylic acid cycle; CI, complex I; AOX, alternative oxidase; Q, ubiquinone; QH2, ubiquinol; Pi, phosphate; polyP, polyphosphate; PPX, exopolyphosphatase.

Although a century of research has brought understanding of *A. niger* organic acid fermentation a long way, there remain outstanding questions. As these are the goal posts of future research, this final chapter shall discuss these and make recommendations for future experimental directions.

There remains debate concerning the underlying cause and trigger of *A. niger* organic acid production. Early researchers thought that uncontrolled overflow metabolism was responsible (Prömper *et al*, 1993; Arisan-Atac and Kubicek, 1996b). It was known that specific conditions were required – excess carbon combined with a limitation of phosphate or trace metals (Shu and Johnson, 1948). It was proposed that a catabolic overflow resulted from the growth-limiting conditions and the abundance of carbon (Prömper *et al*, 1993; Arisan-Atac and Kubicek, 1996b). As metal ions serve as enzyme cofactors, it was suggested that deficiencies of certain metals favour citrate formation by reducing the activity of enzymes involved in citrate breakdown (La Nauze, 1966; Kubicek and Röhr, 1977; Kubicek and Röhr, 1978; Legiša and Kidrič, 1989). The picture became increasingly complex, however. Interdependencies were found. One metal could be in excess if another were limiting, and vice versa (Shu and Johnson, 1948). Manganese deficiency was widely regarded as essential to citric acid production (Kubicek and Röhr, 1977; Mirminachi *et al*, 2002), but excess manganese had no effect at higher initial pH in oxalate-negative strains (Ruijter *et al*, 1999). Phosphate limitation was necessary only if metals were abundant (Shu and Johnson, 1948). The observation that different strains behave in different ways further complicated the picture (Bowes and Mattey, 1980; Jernejc and Legiša, 2004). Biochemical investigations surfaced many arguments as to what triggered citric acid production, and no sound answer was found (Ramakrishnan *et al*, 1955; Kubicek and Röhr, 1978; Legiša and Mattey, 1986; Wallrath *et al*, 1991; Rugsaseel *et al*, 1996; Gradisnik-Grapulin and Legisa, 1997; Mesojednik and Legiša, 2005). Lack of uniformity between different studies in conditions and the strain used may have been responsible. It is possible that different strains evolved different mechanisms of acidogenesis, resulting in a murky picture that is a conglomerate of many individual ones. The discovery that citric acid production could be induced in otherwise non-

producing conditions by precultivation in producing conditions was striking (Xu *et al*, 1989a). This suggested a regulatory response rather than uncontrolled overflow metabolism. The possibility that *A. niger* has evolved to deliberately produce organic acids in response to its environment started gathering evidence. Transcriptomic analysis at different ambient pH values revealed many pH-regulated genes relevant to organic acid production (Andersen *et al*, 2009b). This correlated with the knowledge that the *A. niger* organic acid production profile is dependent on the environmental pH (Andersen *et al*, 2009b). It was hypothesised that *A. niger* has evolved efficient and pH-responsive acidification strategies. The study revealed a number of candidate transcription factors that may play a role. When one of these was knocked out, oxalic acid production increased significantly (Poulsen *et al*, 2012). The idea that the acidogenic behaviour of *A. niger* is regulated was further strengthened by the finding that knock-out of LaeA, a global regulator of secondary metabolism, eliminates citric acid production (Niu *et al*, 2016). Research into the transcriptional control of citric acid production is still in its infancy, and this area warrants further investigation. If *A. niger* organic acid production is a coordinated and regulated response, one may question the evolutionary drive behind this. It makes sense to relate this to the causative conditions that trigger the behaviour. A deficiency of phosphate or one of a number of metals is paramount (Shu and Johnson, 1948). It is known that production of organic acids can mobilise phosphate and metals from the environment (Schneider *et al*, 2010; Odoni *et al*, 2017). The resulting acidification also helps to kill off rival microorganisms, which would otherwise benefit from the mobilised nutrients. The acidified environment can furthermore assist in the degradation of plant biomass, which the saprotrophic *A. niger* thrives on. It is understandable that the response is only induced when carbon and energy are in excess, as organic acid production is a costly process for the fungus. Further research can aim to identify and unravel the sensory systems, and the transcription factors that initiate acidogenesis.

One outstanding question that this work tried to answer is what limits citric acid production in the wild-type ATCC1015 strain. This question was

motivated by predictions of the dynamic model, which over-estimated citric acid production despite giving close fits for biomass production and glucose consumption. This indicated a rate-limiting step not reflected in the model. Experiments in this work aimed at increasing carbon uptake also raised the same question. Increases in carbon uptake early in citric acid production had no effect. Despite the extra carbon input flux, there was no corresponding increase in citric acid output flux. The findings highlighted a constraint at another step that blocked the extra flux from getting through to citric acid. The project sought to identify this rate-limiting step. Based on existing literature (Mesojednik and Legiša, 2005; Mlakar and Legiša, 2006; Capuder *et al*, 2009), the first candidate under the spotlight was 6-phosphofructo-1-kinase (PFK1). PFK1 is a key regulatory point in glycolysis, and glycolytic flux is an important factor in citric acid production. PFK1 is inhibited by physiological concentrations of intracellular citrate, and a citrate-insensitive cleaved form was identified in *A. niger* (Mlakar and Legiša, 2006). Expression of a constitutively active and citrate-insensitive PFK1 increased citric acid production in the A158 strain (Capuder *et al*, 2009). When this was performed with the ATCC1015 strain in this work, a negative effect was observed. To be confident of this finding, reproducibility in other transformant strains is needed. The negative effect suggested another rate-limiting factor, and the inhibition of citric acid production by the triggering of down-regulatory mechanisms. This project also explored a means to bypass mitochondrial citrate export. There is some evidence to suggest this could be a rate-limiting step (De Jongh and Nielsen, 2008). It is proposed that this occurs via an antiport mechanism by exchange with cytosolic malate (De Jongh and Nielsen, 2008), although the transporter in *A. niger* is yet to be identified. Candidates were found, and one was shown to be transcribed, but its knock-out had little effect (Kirimura *et al*, 2016). This either suggests redundancy or the wrong transporter. There are currently ongoing efforts by researchers to identify the transporter responsible (Kirimura *et al*, 2016). Engineering of strains to increase cytosolic malate concentration caused increased citric acid production, possibly by enhancing mitochondrial citrate export (De Jongh and Nielsen, 2008). In this project, a different strategy was undertaken. Seeing that *A. niger* lacks cytosolic citrate synthase (Ruijter *et*

al, 2000), this activity was introduced into the ATCC1015 strain. This was hypothesised to divert citrate formation from the mitochondria to the cytosol, thereby avoiding the need for mitochondrial citrate export. No convincing evidence was found that this benefited citric acid production. The null effect may be due to limitation at the citrate secretion step. The same strategy was applied in an *A. niger* strain engineered for itaconic acid production, and successfully increased productivity and yield (Hossain *et al*, 2016). This approach therefore warrants further research, and it may be that the same success can be realised for citric acid production in the ATCC1015 strain, once other rate-limiting steps are overcome. The final step in citric acid production is citrate secretion, and as transport steps often pose bottlenecks, this may be the limiting factor. Although this is an important research direction, this project did not seek to investigate citrate export as there was little research basis from which to proceed. There is a possibility, however, that this is the step that constrains citric acid production in the ATCC1015 strain. Studies have often reported increased intracellular citrate accumulation in engineered strains, without a corresponding increase in extracellular citrate (Legiša and Kidrič, 1989; Prömper *et al*, 1993). This strongly suggests a flux constraint at the step of citrate secretion. A blockage at this step explains the null effects observed when targeting steps up-stream. It is known that citrate secretion is mediated by an active proton symport mechanism (Netik *et al*, 1997). The transporter responsible was very recently identified (GenBank accession number EHA22412) (Odoni *et al*, 2018). Expression of this transporter in *Saccharomyces cerevisiae* led to citrate secretion, while its knock-out in *A. niger* abolished citric acid production (Odoni *et al*, 2018). Over-expression of the identified transporter in the ATCC1015 strain is a valuable pursuit and may lead to increased citric acid production. There are a number of other factors which may also restrict citric acid production in ATCC1015. The activities of enzymes involved in citrate breakdown (aconitase, isocitrate dehydrogenase, and α-ketoglutarate dehydrogenase) may be too high. Oxidative phosphorylation may be too active, increasing ATP to inhibitory levels. Recycling of NADH may be insufficient due to low activity of alternative oxidase, and thereby causing reduced glycolytic flux. The activity of pyruvate carboxylase may be too low,

leading to insufficient supply of oxaloacetate to citrate synthase. All these factors need to be assessed to establish a better picture. Seeing that ATCC1015 has an intact and naturally evolved regulatory apparatus, it may be that perturbations at single steps are compensated for. An understanding of the transcriptional regulation of organic acid production in ATCC1015 therefore becomes important.

Much work in this project was undertaken to characterise citric acid fermentation by the ATCC1015 strain on different substrates. It was promising that fermentative performance on xylose was similar to glucose, with little difference in sugar consumption and growth. The pentose sugar xylose is abundant in waste plant biomass, and poorly assimilated by many organisms. The ability to convert it to chemicals of commercial value is therefore beneficial. An interesting observation with fermentation on xylose compared to glucose was the two-fold lower rate of citric acid production, despite the same rate of carbon uptake. This was not consistent with modelling predictions. This again highlighted limiting factors present in the ATCC1015 strain that constrain citric acid production. In this case, a difference in morphology was observed, which affected culture viscosity. The more viscous xylose cultures may have been less aerated than the glucose cultures. It is known that aeration is important to citric acid production (Kubicek *et al*, 1980a; Dawson *et al*, 1986; McIntyre and McNeil, 1997). Further investigations could study the rheology (flow of liquids) of cultures and quantify morphological differences such as pellet diameter, hyphal diameter, hyphal length, and hyphal branching frequency. The ability to do this has been previously demonstrated (Olsvik *et al*, 1993). It has been shown that morphological parameters influence the culture viscosity (Olsvik *et al*, 1993). Morphological effects are typically influenced by the germination conditions and early stages of fermentation (Papagianni *et al*, 1999; Papagianni and Mattey, 2006). To avoid morphological differences, the fungus can be precultivated under the same conditions and then transferred to the experimental conditions. Precultivation experiments have been done in the past. It was discovered that citric acid production can be induced on otherwise non-producing substrates by precultivation in producing conditions

(Xu *et al*, 1989a). While morphological effects may be responsible, it seems more likely that a regulatory response is induced that stimulates citric acid production. The lower citric acid levels observed with xylose as substrate may be due to down-regulation of citric acid production rather than morphological differences. This further establishes the need to aim research at the transcriptional control mechanisms that govern the acidogenic behaviour. Other substrates tested in this project were arabinose, glycerol, and cellobiose. These performed poorly due to very slow carbon uptake relative to glucose. No citric acid was produced on these substrates and growth was constrained. These findings are in agreement with previous ones that showed no citric acid production on these carbon sources (Xu *et al*, 1989a). These substrates were chosen due to their presence in underused resource streams – arabinose and cellobiose from lignocellulosic wastes, and glycerol from bio-diesel production. The limiting carbon uptake is a clear target in the creation of strains for sustainable fermentation processes. A better understanding of the carbon uptake systems in *A. niger* is needed. Post-translational regulation of these should not be ruled out, and this may counteract over-expression of transporter genes. It is unsurprising if the fungus limits carbon uptake in response to flux constraints in down-stream catabolic steps. These should be investigated, especially for arabinose, glycerol, and cellobiose that have slow uptake. The arabinose catabolic pathway has been previously studied in *A. niger*, and it was suggested that the expression levels of the first three enzymes need to be increased to achieve greater flux down the pathway (de Groot *et al*, 2005). Precultivation experiments are a worthwhile pursuit, and may induce increased uptake of substrates that otherwise have limited uptake. The goal behind the work testing different carbon sources was to assess the applicability of lignocellulose-based feed-stocks to citric acid fermentation by *A. niger*, and the problems that may occur when attempting to shift to these feed-stocks from sucrose-based ones. Data on arabinose and cellobiose revealed limiting uptake of these substrates, and this is a problem that needs to be solved to achieve optimal citric acid production on feed-stocks containing these sugars. Data on xylose revealed an unknown factor that limits citric acid production from this sugar, and this needs to be investigated and

overcome in order to use lignocellulose-based feed-stocks effectively. When using a mixture of glucose and xylose, it became clear that the presence of glucose interferes with the assimilation of other sugars. This is suspected to be due to carbon catabolite repression, which is known to occur in *A. niger* and is mediated by CreA (de Vries *et al*, 1999). Solving this problem is a necessity as lignocellulose-based feed-stocks contain mixtures of sugars including glucose. This may be achieved by knock-out of CreA. *A. niger* strains with a deletion of CreA have been previously created (van den Brink *et al*, 2014). Characterisation of such strains on sugar mixtures revealed that factors other than CreA play a role (Mäkelä *et al*, 2018). Sugar uptake was shown to be sequential, even when CreA was deleted, and transcriptome analysis showed this to be due to regulation at the level of sugar transport rather than sugar catabolism (Mäkelä *et al*, 2018). Although there are clearly difficulties to be overcome in the realisation of optimal citric acid production on lignocellulose-based feed-stocks, there have been promising examples of citric acid production on such feed-stocks (Table 1.1), although this is yet to be realised at the industrial level.

Another question raised in this project that remains to be answered came from the characterisation of the ATCC1015 Δ*oah* Δ*gox* strain. Although citric acid production was increased four-fold at initial pH 7, the yield was three-fold lower than observed at initial pH 2. This revealed extra limiting factors present at the higher initial pH. These may be of a regulatory nature, or may be due to morphological differences. Pellet diameter was greater and more variable at higher initial pH, which could limit gas exchange and transport processes due to reduced surface area to volume ratio. A better awareness of the factors that influence morphology and the subsequent consequences is needed. Precultivation at initial pH 2 may be required to give the desired morphology. Transfer to conditions of higher pH could then be performed, to see if this has any negative effect on citric acid production by the Δ*oah* Δ*gox* strain.

One of the contributions from this project was the observation of a rapid phosphate uptake coupled with phosphate storage via polyphosphate. This

leads to a phase of phosphate-limited growth synchronous with citric acid production. An effort was undertaken to further probe this behaviour, to establish more substantial evidence. It was hypothesised, and predicted by the dynamic model, that a slower phosphate uptake would delay the onset of phosphate-limited growth and citric acid production. The phosphate transport system of *A. niger* ATCC1015 was therefore investigated. Despite insubstantial research on which to base an engineering strategy, an attempt was made to disrupt phosphate uptake. By phylogenetic analysis, a candidate was chosen from a list of eight putative phosphate transporters, and targeted. Knock-down of this transporter was unable to produce any phenotypic effect. A more substantial effort is needed to achieve results, and this research direction is still worth pursuing. A greater number of transformant strains need to be screened, and a more efficient phenotyping procedure would assist in this. The use of a multiwell plate system as a primary screen, before shake flask culture as a secondary screen, is one option. The null effect of targeting a single phosphate transporter is unsurprising. *A. niger* may have a well-armed and regulated phosphate transport system, as suggested by its extensive collection of putative phosphate transporters. Some of these may be phosphate sensors rather than transporters, and targeting the phosphate sensory system may produce interesting phenotypes. In *S. cerevisiae*, five phosphate transporters have been identified, and knock-out of all of these is necessary to abolish phosphate uptake (Giots *et al*, 2003). Two of these have also been shown to act as phosphate sensors (Giots *et al*, 2003). To go forward, the expression profiles of the candidate phosphate transporter genes in *A. niger* need to be examined. This would narrow down targeting efforts onto those which are most abundantly expressed. It is worthy to note that recent transcriptomic analysis of the industrial H915-1 strain (Yin *et al*, 2017) revealed the increasing expression of a putative phosphate transporter during citric acid production. The ATCC1015 homologue of this has GenBank accession number EHA20181, not found in our bioinformatics based search. Although most closely related to a glycerophosphoinositol permease, this transporter shares homology with a phosphate uptake domain (e-value 8e-20). This extends the collection to nine putative phosphate transporters, and more

may exist. Broader engineering efforts may be warranted. Knock-down should be applied rather than knock-out, otherwise lethal phenotypes may result. To overcome potential redundancy, an experiment worth considering is the tandem knock-down of the candidate transporters. One strategy to achieve this may be the expression of multiple antisense RNAs from a single construct, separated by self-cleaving ribozymes. Multiple knock-down has been demonstrated previously in mammalian cells by expression of several short-hairpin RNAs from a single vector (Stove *et al*, 2006).

While phosphate uptake determines the rate at which phosphate is stored as polyphosphate, the activity of exopolyphosphatase (PPX) determines its rate of release. A correlation between PPX activity and growth is therefore expected. An analysis of polyphosphate levels during citric acid fermentation supported this. The growth rate is a key factor affecting citric acid productivity. Biomass production is a competing process, but is needed to create the machinery that produces citric acid. This leads to a delicate balance between growth and citric acid production that determines the productivity and yield. An alteration of PPX activity is one means by which to shift this balance towards the optimum. The dynamic model suggested a further constraint of PPX activity was needed, and so in this project knock-down was performed against PPX expression. A small inhibitory effect on growth shortly after phosphate depletion indicated some success, however, the effect did not carry through to later time-points. An unexpected finding was also produced. A negative effect on citric acid production suggested a more complex role of polyphosphate. To be confident of this finding, reproducibility in other transformant strains is needed. As well as phosphate storage, polyphosphate has functions in energy storage and pH homeostasis (Hesse *et al*, 2002). Its connection with citric acid production certainly warrants further research. A new hypothesis is that the formation and hydrolysis of polyphosphate may be a means to reduce ATP levels, which would otherwise inhibit citric acid production. The mechanisms of synthesis and degradation of polyphosphate in *A. niger* is a poorly trodden area, and this project made the first steps. A better understanding is available for *S. cerevisiae*, which has seen considerably more research on this topic. A

complex system of polyphosphate degradation exists in *S. cerevisiae*, involving three enzymes with polyphosphatase activity (Gerasimaitė and Mayer, 2017). One of these, localised to the cytosol, is exo-acting and releases phosphate. The other two are localised to the vacuole where polyphosphate is predominantly stored in yeast. Of these, one has exo- and endo-activities, while the other is solely endo-acting (Gerasimaitė and Mayer, 2017). Deletion of both vacuolar polyphosphatases was required to prevent polyphosphate degradation and reduce growth rate in low phosphate medium (Gerasimaitė and Mayer, 2017). Polyphosphate formation is usually attributed to polyphosphate kinase (PPK). PPK has been identified in several species of bacteria and is highly conserved (Zhang *et al*, 2002), however, it has been rarely reported in eukaryotes. It is found in the yeast *Candida humicola* with homology to bacterial PPK (McGrath *et al*, 2005), but efforts to identify its activity in *S. cerevisiae* have failed (McGrath *et al*, 2005). No putative polyphosphate kinases exist in *S. cerevisiae*, and likewise for *A. niger*. Instead, the vacuolar transporter chaperone complex is responsible for polyphosphate synthesis in *S. cerevisiae* (Gerasimaitė and Mayer, 2017). This uses ATP to form polyphosphate that is concomitantly transferred to the vacuole. Loss of this complex in *S. cerevisiae* results in an absence of polyphosphate (Gerasimaitė and Mayer, 2017). It is possible that the same mechanism for polyphosphate formation occurs in *A. niger*, which has putative genes that encode subunits of this complex (GenBank accession numbers EHA17790, EHA24341 and EHA25246). The gene with GenBank accession number EHA25246 encodes the catalytic subunit, and deletion of this in *S. cerevisiae* prevents synthesis of polyphosphate (Desfougères *et al*, 2016). Investigating the effects of knock-out of this gene in *A. niger* is worthwhile, and may result in slower phosphate uptake due to the inability to store phosphate as polyphosphate. The effect of this on citric acid production would be interesting. In terms of polyphosphate breakdown in *A. niger*, further exploration should seek to establish the transcriptional profile of PPX expression, and probe the effect of PPX over-expression. PPX is likely to be subject to regulation, and compensating regulatory mechanisms are expected. An elucidation of the factors affecting PPX activity is of value. It is important to note that *A. niger* also have a putative endopolyphosphatase

(GenBank accession number EHA17983). This would also be a valuable target for further research. As is the case for *S. cerevisiae*, disruption of a single polyphosphatase may have little effect due to redundancy. This explains the observations in this work when knocking down PPX in *A. niger*. It may be necessary to target all putative polyphosphatases simultaneously to obtain a clear phenotype. Many times in this project a rapid phosphate release was observed under energy-limiting conditions. This indicates that *A. niger* has mechanisms to quickly release the energy stored in polyphosphate to form ATP when it becomes limited. Future work could attempt to elucidate these. PPK could be a mediator, as it can produce ATP from polyphosphate hydrolysis when ADP levels are high. That said, its scarcity among eukaryotes and the absence of a putative PPK in *A. niger* suggest an alternative mechanism. It is striking that the phosphate-limited growth behaviour of *A. niger* is self-imposed. Sufficient phosphate is available for growth and can be released, but is deliberately retained.

The final contribution of this project was an algorithm for *in silico* evolution of *A. niger* organic acid production. This was first applied to suggest targets that optimise citric acid productivity. The outcome of this was a number of single growth targets, that when given a particular flux constraint bring about the optimum growth rate for maximising citric acid productivity. These targets may be more effective than PPX. A word of caution is needed here, however. The model assumes a constant biomass equation, and that each component is required for growth. In actuality, the biomass composition is likely to be dynamic, changing in response to environmental and genetic perturbations. Constraining the production of components such as the cell wall and lipids may result in a shift in biomass composition with no effect on growth. These targets may also bring about morphological effects. Deletion of genes involved in cell wall biosynthesis in *A. niger* has been done previously, and while one of these had a strong negative effect on growth, another had no growth phenotype (Damveld *et al*, 2008). The most effective growth targets may be those that constrain DNA synthesis. The use of inhibitors may be more appropriate here (Table 7.1), rather than knocking down expression of growth-related genes. The *in silico* evolution methodology was also applied

to suggest strategies for switching acid output and optimising the productivity of the target acid. The output of this was complex solutions requiring knock-down of multiple targets. It is possible to follow up on these by considering tandem knock-down approaches, such as the expression of several antisense RNAs from a single construct separated by self-cleaving ribozymes. The use of specific inhibitors of the target metabolic reactions should be considered (Table 7.1), as this would be a simpler and faster method to probe the model predictions. In both cases, the flux constraints can be induced at the onset of phosphate-limited growth, either by inducible knock-down or the addition of inhibitors at the respective time-point. Experiments using inhibitors of metabolic reactions have been performed previously in *A. niger*. When malonate (inhibitor of succinate dehydrogenase) was applied, an increase in citrate and oxalate production was observed (Meijer *et al*, 2009b). When malonate was added in addition to over-expression of isocitrate lyase, organic production shifted to malate (Meijer *et al*, 2009b). Although such experiments are important steps forward, there is a cautionary note. Attempts to switch acid output may be futile without knowledge of the acid transporters required to secrete the intracellular accumulating acid. This point is illustrated by previous attempts to engineer non-citric acid producing strains to produce citric acid, which caused an intracellular citrate accumulation without a corresponding rise in extracellular citrate (Legiša and Kidrič, 1989; Prömper *et al*, 1993). Consideration should be given to introducing foreign transporters for the target organic acid, alongside other changes that cause the intracellular accumulation. The importance of transport steps was illustrated by the engineering of *Corynebacterium glutamicum* for increased succinate production. Over-expression of a succinate exporter resulted in a higher succinate yield (Zhu *et al*, 2014). Although *A. niger* is an attractive organism for organic acid production due to its usage in industrial citric acid production, efforts to produce different organic acids using *A. niger* may prove troublesome. This is suggested by the complex solutions from *in silico* evolution. *A. niger* is also evolutionarily optimised for citric acid production, and so engineering it to produce different organic acids may involve combatting an evolved regulatory apparatus that favours citric acid

production. Alternative efforts could be focused on increasing the value of citric acid produced from *A. niger* fermentation, using it to make other products of value. Examples of these include biodegradable polymers made by esterification of citric acid and glycerol (Halpern *et al*, 2014), biodegradable elastic polyesters such as polyoctanediol citrate (Yang *et al*, 2004), and dendrimers made from citric acid and polyethylene glycol (Namazi and Adeli, 2005).

Table 7.1. Inhibitors of metabolic processes.

Inhibitor	**Target**
Hydroxyurea	DNA synthesis (ribonucleotide reductase)
Actinomycin D	RNA synthesis (transcription)
Cycloheximide	Protein synthesis (translation)
Antimycin A	Ubiquinol-cytochrome c reductase
Salicylhydroxamic acid	Ubiquinol oxidase (alternative oxidase)
Oligomycin	ATP synthase
Bongkrekic acid	ADP/ATP translocase
Cyanide	Cytochrome c oxidase
Malonate	Succinate dehydrogenase (ubiquinone)
Carboxin	Succinate dehydrogenase (ubiquinone)
Oxamate	Lactate dehydrogenase
Fluoroacetate	Aconitase

The project described by this thesis has fulfilled another window of research into the acidogenic behaviour of *A. niger*. This project has made significant and original contributions to the field, and provides many directions for future research endeavours. Progress has been made in realising the goal of *in silico* guided metabolic engineering of *A. niger* for sustainable organic acid fermentation. This project has established a set of tools to this end. In chapter 2, an empirical system was developed that gave the physiological basis to construct the dynamic flux model presented in chapter 3. In chapter 4, predictions of this dynamic model were probed by a range of targeted engineering strategies, including knock-out, knock-down, knock-up, and knock-in. In chapters 5 and 6, the modelling work from chapter 3 was extended to develop a more powerful target finding tool, to guide further rational engineering by methods described in chapter 4.

Abbreviations

AMM	*Aspergillus* minimal medium
AOX	alternative oxidase
ARP	autonomously replicating plasmid
ARS	autonomously replicating sequence
BSA	bovine serum albumin
CN	cyanide
CRISPR	clustered regularly interspaced short palindromic repeats
dFBA	dynamic flux balance analysis
DMAB	3-(dimethylamino)-benzoic acid
DMSO	dimethylsulphoxide
Dox	doxycycline
dsRNA	double-stranded RNA
EA	evolutionary algorithm
FBA	flux balance analysis
FGSC	Fungal Genetics Stock Center
FOA	fluoroorotic acid
GA	genetic algorithm
GABA	gamma-aminobutyric acid
GAM	growth-associated maintenance
gDNA	genomic DNA
GO	gene ontology
GOX	glucose oxidase
GPR	gene-protein-reaction
GSMM	genome-scale metabolic model
GUS	β-glururonidase
HR	homologous recombination
ICDH	isocitrate dehydrogenase
ICP-MS	ion coupled plasma mass spectrometry
IPTG	isopropyl-β-thiogalactopyranoside
JGI	Joint Genome Institute
KAAS	KEGG automatic annotation server

KO	KEGG orthology
LB	Luria-Bertani broth
MBTH	3-methyl-2-benzothiazolinone hydrazine
mRNA	messenger RNA
mtPFK1	mutated truncated PFK1
NGAM	non-growth associated maintenance
NHEJ	non-homologous end joining
OAH	oxaloacetate hydrolase
ORF	open-reading frame
PCR	polymerase chain reaction
PDA	potato dextrose agar
PEG	polyethylene glycol
PFK1	6-phosphofructo-1-kinase
PPK	polyphosphate kinase
PPX	exopolyphosphatase
RISC	RNA-induced silencing complex
RNAi	RNA interference
sgRNA	single guide-RNA
SHAM	salicylhydroxamic acid
siRNA	silencing RNA
SNP	single nucleotide polymorphism
TBE	Tris-Borate-EDTA buffer
TCA cycle	tricarboxylic acid cycle
Tet	tetracycline resistance operon
*tet*O	Tet operator element
UV	ultraviolet
X-Gal	5-bromo-4-chloro-3-indolyl β-D-galactopyranoside

References

Acourene S, Ammouche A (2012) Optimization of ethanol, citric acid, and α-amylase production from date wastes by strains of *Saccharomyces cerevisiae*, *Aspergillus niger*, and *Candida guilliermondii*. ***J Ind Microbiol Biot* 39**: 759-66

Agrawal PK, Bhatt CS, Viswanathan L (1983) Studies on some enzymes relevant to citric acid accumulation by *Aspergillus niger*. ***Enzyme Microb Tech* 5**: 369-72

Ahmed SA, Smith JE, Anderson JG (1972) Mitochondrial activity during citric acid production by *Aspergillus niger*. ***T Brit Mycol Soc* 59**: 51-61

Al Obaidi ZS, Berry DR (1980) cAMP concentration, morphological differentiation and citric acid production in *Aspergillus niger*. ***Biotechnol Lett* 2**: 5-10

Alam MZ, Jamal P, Nadzir MM (2008) Bioconversion of palm oil mill effluent for citric acid production: statistical optimization of fermentation media and time by central composite design. ***World J Microb Biot* 24**: 1177-85

Ali S, Haq I (2010) Production of 3, 4-dihydroxy L-phenylalanine by a newly isolated *Aspergillus niger* and parameter significance analysis by Plackett-Burman design. ***BMC Biotechnol* 10**: 86

Ali HK, Daud MZ, Al-Azzawi Z (2012) Economic benefit from the optimization of citric acid production from rice straw through Plackett-Burman design and central composite design. ***Turk J Eng Environ Sci* 36**: 81-93

Alvarez-Vasquez F, González-Alcón C, Torres NV (2000) Metabolism of citric acid production by *Aspergillus niger*: Model definition, steady-state analysis and constrained optimization of citric acid production rate. ***Biotechnol Bioeng* 70**: 82-108

Amaike S, Keller NP (2011) *Aspergillus flavus*. ***Annu Rev Phytopathol* 49**: 107-33

Andersen MR, Nielsen ML, Nielsen J (2008) Metabolic model integration of the bibliome, genome, metabolome and reactome of *Aspergillus niger*. ***Mol Syst Biol* 4**: 178

Andersen MR, Nielsen J (2009a) Current status of systems biology in *Aspergilli*. ***Fungal Genet Biol* 46**: S180-90

Andersen MR, Lehmann L, Nielsen J (2009b) Systemic analysis of the response of *Aspergillus niger* to ambient pH. ***Genome Biol* 10**: R47

Andersen MR, Salazar MP, Schaap PJ, van de Vondervoort PJ, Culley D, Thykaer J, Frisvad JC, Nielsen KF, Albang R, Albermann K, Berka RM (2011) Comparative genomics of citric-acid-producing *Aspergillus niger* ATCC 1015 versus enzyme-producing CBS 513.88. ***Genome Res* 21**: 885-97

Antunes MS, Hodges TK, Carpita NC (2016) A benzoate-activated promoter from *Aspergillus niger* and regulation of its activity. ***Appl Microbiol Biot* 100**: 5479-89

Aoshima M (2007) Novel enzyme reactions related to the tricarboxylic acid cycle: phylogenetic/functional implications and biotechnological applications. ***Appl Microbiol Biot* 75**: 249-55

Aravantinos-Zafiris G, Tzia C, Oreopoulou V, Thomopoulos CD (1994) Fermentation of orange processing wastes for citric acid production. ***J Sci Food Agr*** **65**: 117-20

Arentshorst M, Niu J, Ram AF (2015) Efficient generation of *Aspergillus niger* knock out strains by combining NHEJ mutants and a split marker approach. In: ***Genetic Transformation Systems in Fungi***, Vol. 1. pp. 263-72, Springer International Publishing

Arisan-Atac I, Wolschek MF, Kubicek CP (1996a) Trehalose-6-phosphate synthase A affects citrate accumulation by *Aspergillus niger* under conditions of high glycolytic flux. ***FEMS Microbiol Lett*** **140**: 77-83

Arisan-Atac I, Kubicek CP (1996b) Glycerol is not an inhibitor of mitochondrial citrate oxidation by *Aspergillus niger*. ***Microbiology+*** **142**: 2937-42

Arts E, Kubicek CP, Röhr M (1987) Regulation of phosphofructokinase from *Aspergillus niger*: effect of fructose 2, 6-bisphosphate on the action of citrate, ammonium ions and AMP. ***Microbiology+*** **133**: 1195-9

Ashokkumar B, Senthilkumar SR, Gunasekaran P (2004) Derepressed 2-deoxyglucose-resistant mutants of *Aspergillus niger* with altered hexokinase and acid phosphatase activity in hyperproduction of β-fructofuranosidase. ***Appl Biochem Biotech*** **118**: 89-96

Assadi MM, Nikkhah M (2002) Production of citric acid from date pulp by solid state fermentation. ***J Agric Sci Technol*** **4**: 119

Asther M, Alvarado MI, Haon M, Navarro D, Asther M, Lesage-Meessen L, Record E (2005) Purification and characterization of a chlorogenic acid hydrolase from *Aspergillus niger* catalysing the hydrolysis of chlorogenic acid. ***J Biotechnol*** **115**: 47-56

Awakawa T, Yang XL, Wakimoto T, Abe I (2013) Pyranonigrin E: A PKS-NRPS Hybrid Metabolite from *Aspergillus niger* Identified by Genome Mining. ***ChemBioChem* 14**: 2095-9

Awan MS, Tabbasam N, Ayub N, Babar ME, Rana SM, Rajoka MI (2011) Gamma radiation induced mutagenesis in *Aspergillus niger* to enhance its microbial fermentation activity for industrial enzyme production. ***Mol Biol Rep* 38**: 1367-74

Baker SE (2006) *Aspergillus niger* genomics: past, present and into the future. ***Med Mycol* 44**: S17-21

Bansal N, Janveja C, Tewari R, Soni R, Soni SK (2014) Highly thermostable and pH-stable cellulases from *Aspergillus niger* NS-2: properties and application for cellulose hydrolysis. ***Appl Biochem Biotech* 172**: 141-56

Bari N, Alam Z, Muyibi SA, Jamal P, Al-Mamun A (2010) Statistical optimization of process parameters for the production of citric acid from oil palm empty fruit bunches. ***Afr J Biotechnol* 9**

Barnes SE, Alcocer MJ, Archer DB (2008) siRNA as a molecular tool for use in *Aspergillus niger*. ***Biotechnol Lett* 30**: 885-90

Bashir N, Syed Q, Kashmiri MA (2008) Shake flask studies for the production of penicillin G acylase from *Aspergillus niger*. ***Micol Aplicada Int* 20**: 55-61

Benoit I, Asther M, Bourne Y, Navarro D, Canaan S, Lesage-Meessen L, Herweijer M, Coutinho PM, Asther M, Record E (2007) Gene overexpression and biochemical characterization of the biotechnologically relevant chlorogenic acid hydrolase from *Aspergillus niger*. ***Appl Environ Microb* 73**: 5624-32

Bercovitz A, Peleg Y, Battat E, Rokem JS, Goldberg I (1990) Localization of pyruvate carboxylase in organic acid-producing *Aspergillus* strains. ***Appl Environ Microb* 56**: 1594-7

Bindumole VR, Sasikiran K, Balagopalan C, Nambisan B (2005) Cassava starch factory waste as an alternative substrate for citric acid production by *Aspergillus niger* MTCC 282. ***Indian J Microbiol* 45**: 235

Birk R, Bravdo B, Shoseyov O (1996) Detoxification of cassava by *Aspergillus niger* B-1. ***Appl Microbiol Biot* 45**: 411-4

Bizukojc M, Ledakowicz S (2003) Morphologically structured model for growth and citric acid accumulation by *Aspergillus niger*. ***Enzyme Microb Tech* 32**: 268-81

Bizukojc M, Ledakowicz S (2004) The kinetics of simultaneous glucose and fructose uptake and product formation by *Aspergillus niger i*n citric acid fermentation. ***Process Biochem* 39**: 2261-8

Bloom SJ, Johnson MJ (1962) The pyruvate carboxylase of *Aspergillus niger*. ***J Biol Chem* 237**: 2718-20

Blumhoff M, Steiger MG, Marx H, Mattanovich D, Sauer M (2013) Six novel constitutive promoters for metabolic engineering of *Aspergillus niger*. ***Appl Microbiol Biot* 97**: 259-67

Bowes I, Mattey M (1980) A study of mitochondrial NADP+-specific isocitrate dehydrogenase from selected strains of *Aspergillus niger*. ***FEMS Microbiol Lett* 7**: 323-5

Brandl J, Andersen MR (2017) *Aspergilli*: Models for systems biology in filamentous fungi. ***Curr Opin Syst Biol***

Brown SH, Bashkirova L, Berka R, Chandler T, Doty T, McCall K, McCulloch M, McFarland S, Thompson S, Yaver D, Berry A (2013) Metabolic engineering of *Aspergillus oryzae* NRRL 3488 for increased production of L-malic acid. ***Appl Microbiol Biot*** **97**: 8903-12

Burgard AP, Pharkya P, Maranas CD (2003) Optknock: a bilevel programming framework for identifying gene knockout strategies for microbial strain optimization. ***Biotechnol Bioeng*** **84**: 647-57

Buxton FP, Gwynne DI, Davies RW (1985) Transformation of *Aspergillus niger* using the argB gene of *Aspergillus nidulans*. ***Gene*** **37**: 207-14

Campbell EI, Unkles SE, Macro JA, van den Hondel C, Contreras R, Kinghorn JR (1989) Improved transformation efficiency of *Aspergillus niger* using the homologous niaD gene for nitrate reductase. ***Curr Genet*** **16**: 53-6

Capuder M, Šolar T, Benčina M, Legiša M (2009) Highly active, citrate inhibition resistant form of *Aspergillus niger* 6-phosphofructo-1-kinase encoded by a modified pfkA gene. ***J Biotechnol*** **144**: 51-7

Chang J, Zhang Y (2012) Catalytic degradation of amygdalin by extracellular enzymes from *Aspergillus niger*. ***Process Biochem*** **47**: 195-200

Chelius MK, Wodzinski RJ (1994) Strain improvement of *Aspergillus niger* for phytase production. ***Appl Microbiol Biot*** **41**: 79-83

Chen H, He X, Geng H, Liu H (2014) Physiological characterization of ATP-citrate lyase in *Aspergillus niger*. ***J Ind Microbiol Biot*** **41**: 721-31

Chesters CG, Rolinson GN (1951) Zinc in the metabolism of a strain of *Aspergillus niger*. ***Microbiology+*** **5**: 553-8

Chinese citric acid industry begins to consolidate. In: Analysis. F.O. Licht Renewable Chemicals. 2011. http://stage.renewablechemicals.agra-net.com/chinese-citric-acid-industry-begins-to-consolidate/. Accessed 6 July 2017.

Chong SK, Mohamad MS, Salleh AH, Choon YW, Chong CK, Deris S (2014) A hybrid of ant colony optimization and minimization of metabolic adjustment to improve the production of succinic acid in *Escherichia coli*. ***Comput Biol Med*** **49**: 74-82

Choon YW, Mohamad MS, Deris S, Illias RM (2014) A hybrid of bees algorithm and flux balance analysis (BAFBA) for the optimisation of microbial strains. ***Int J Data Min Bioin*** **10**: 225-38

Choon YW, Mohamad MS, Deris S, Chong CK, Omatu S, Corchado JM (2015) Gene knockout identification using an extension of Bees Hill Flux Balance Analysis. ***BioMed Res Int*** **2015**

Citric Acid. In: Chemical Economics Handbook. IHS. 2015. https://www.ihs.com/products/citric-acid-chemical-economics-handbook.html. Accessed 6 July 2017.

Cleland WW, Johnson MJ (1954) Tracer experiments on the mechanism of citric acid formation by *Aspergillus niger*. ***J Biol Chem*** **208**: 679-90

Conesa A, Götz S, García-Gómez JM, Terol J, Talón M, Robles M (2005) Blast2GO: a universal tool for annotation, visualization and analysis in functional genomics research. ***Bioinformatics*** **21**: 3674-6

Cortés-Espinosa DV, Absalón ÁE, Sánchez N, Loera O, Rodríguez-Vázquez R, Fernández FJ (2011) Heterologous expression of manganese peroxidase in *Aspergillus niger* and its effect on phenanthrene removal from soil. ***J Mol Microb Biotech*** **21**: 120-9

Currie JN (1917) The citric acid fermentation of *Aspergillus niger*. ***J Biol Chem*** **31**: 15-37

da Silva LG, Trugo LC, da Costa Terzi S, Couri S (2005) Low phytate lupin flour based biomass obtained by fermentation with a mutant of *Aspergillus niger*. ***Process Biochem*** **40**: 951-4

Dagenais TR, Keller NP (2009) Pathogenesis of *Aspergillus fumigatus* in invasive aspergillosis. ***Clin Microbiol Rev*** **22**: 447-65

Dai Z, Aryal UK, Shukla A, Qian WJ, Smith RD, Magnuson JK, Adney WS, Beckham GT, Brunecky R, Himmel ME, Decker SR (2013) Impact of *alg3* gene deletion on growth, development, pigment production, protein secretion, and functions of recombinant *Trichoderma reesei* cellobiohydrolases in *Aspergillus niger*. ***Fungal Genet Biol*** **61**: 120-32

Damveld RA, Franken A, Arentshorst M, Punt PJ, Klis FM, van den Hondel CA, Ram AF (2008) A novel screening method for cell wall mutants in *Aspergillus niger* identifies UDP-galactopyranose mutase as an important protein in fungal cell wall biosynthesis. ***Genetics*** **178**: 873-81

Dave K, Punekar NS (2011) Utility of *Aspergillus niger* citrate synthase promoter for heterologous expression. ***J Biotechnol*** **155**: 173-7

Dave KK, Punekar NS (2015) Expression of lactate dehydrogenase in *Aspergillus niger* for L-lactic acid production. ***PloS One*** **10**: e0145459

David H, Åkesson M, Nielsen J (2003) Reconstruction of the central carbon metabolism of *Aspergillus niger*. ***FEBS J*** **270**: 4243-53

David H, Özçelik İŞ, Hofmann G, Nielsen J (2008) Analysis of *Aspergillus nidulans* metabolism at the genome-scale. ***BMC Genomics*** **9**: 163

Dawson MW, Maddox IS, Brooks JD (1986) Effect of interruptions to the air supply on citric acid production by *Aspergillus niger*. ***Enzyme Microb Tech*** **8**: 37-40

de Bekker C, Wiebenga A, Aguilar G, Wösten HA (2009) An enzyme cocktail for efficient protoplast formation in *Aspergillus niger*. ***J Microbiol Meth*** **76**: 305-6

de Groot MJ, Prathumpai W, Visser J, Ruijter GJ (2005) Metabolic control analysis of *Aspergillus niger* L-arabinose catabolism. ***Biotechnol Progr*** **21**: 1610-6

De Jongh WA, Nielsen J (2008) Enhanced citrate production through gene insertion in *Aspergillus niger*. ***Metab Eng*** **10**: 87-96

de Vries RP, Visser J, de Graaff LH (1999) CreA modulates the XlnR-induced expression on xylose of *Aspergillus niger* genes involved in xylan degradation. ***Res Microbiol*** **150**: 281-5

Delmas S, Llanos A, Parrou JL, Kokolski M, Pullan ST, Shunburne L, Archer DB (2014) Development of an unmarked gene deletion system for the filamentous fungi *Aspergillus niger* and *Talaromyces versatilis*. ***Appl Environ Microb*** **80**: 3484-7

Deng W, Lin D, Yao K, Yuan H, Wang Z, Li J, Zou L, Han X, Zhou K, He L, Hu X (2015) Characterization of a novel β-cypermethrin-degrading *Aspergillus niger* YAT strain and the biochemical degradation pathway of β-cypermethrin. ***Appl Microbiol Biot*** **99**: 8187-98

Desfougères Y, Gerasimaite R, Jessen HJ, Mayer A (2016) Vtc5, a novel subunit of the vacuolar transporter chaperone complex, regulates polyphosphate synthesis and phosphate homeostasis in yeast. ***J Biol Chem*** jbc-M116.

Dhillon GS, Brar SK, Verma M, Tyagi RD (2011) Utilization of different agro-industrial wastes for sustainable bioproduction of citric acid by *Aspergillus niger*. ***Biochem Eng J*** **54**: 83-92

Dhillon GS, Brar SK, Verma M (2012) Biotechnological potential of industrial wastes for economical citric acid bioproduction by *Aspergillus niger* through submerged fermentation. ***Int J Food Sci Tech*** **47**: 542-8

Dhillon GS, Brar SK, Kaur S, Verma M (2013a) Screening of agro-industrial wastes for citric acid bioproduction by *Aspergillus niger* NRRL 2001 through solid state fermentation. ***J Sci Food Agr*** **93**: 1560-7

Dhillon GS, Kaur S, Sarma SJ, Brar SK (2013b) Integrated process for fungal citric acid fermentation using apple processing wastes and sequential extraction of chitosan from waste stream. ***Ind Crop Prod*** **50**: 346-51

Dvořáková J, Kopecký J, Havlíček V, Křen V (2000) Formation of myo-inositol phosphates by *Aspergillus niger* 3-phytase. ***Folia Microbiol*** **45**: 128-32

Edgar RC (2004) MUSCLE: multiple sequence alignment with high accuracy and high throughput. ***Nucleic Acids Res*** **32**: 1792-7

Elimer E (1998) Citric acid production from rape seed oil by *Aspergillus niger*. ***Food Technol Biotech*** **36**: 189-92

Fan A, Chen H, Wu R, Xu H, Li SM (2014) A new member of the DMATS superfamily from *Aspergillus niger* catalyzes prenylations of both tyrosine and tryptophan derivatives. ***Appl Microbiol Biot*** **98**: 10119-29

Feir HA, Suzuki I (1969) Pyruvate carboxylase of *Aspergillus niger*: kinetic study of a biotin-containing carboxylase. ***Can J Biochem*** **47**: 697-710

Fiedler MR, Gensheimer T, Kubisch C, Meyer V (2017) HisB as novel selection marker for gene targeting approaches in *Aspergillus niger*. ***BMC Microbiol*** **17**: 57

Fisch KM, Gillaspy AF, Gipson M, Henrikson JC, Hoover AR, Jackson L, Najar FZ, Wägele H, Cichewicz RH (2009) Chemical induction of silent biosynthetic pathway transcription in *Aspergillus niger*. ***J Ind Microbiol Biot*** **36**: 1199-213

Forment JV, Flipphi M, Ramón D, Ventura L, MacCabe AP (2006) Identification of the mstE gene encoding a glucose-inducible, low affinity glucose transporter in *Aspergillus nidulans*. ***J Biol Chem*** **281**: 8339-46

Ganzlin M, Rinas U (2008) In-depth analysis of the *Aspergillus niger* glucoamylase (*glaA*) promoter performance using high-throughput screening and controlled bioreactor cultivation techniques. ***J Biotechnol*** **135**: 266-71

Garg N, Hang YD (1995) Microbial production of organic acids from carrot processing waste. ***J Food Sci Tech Mys*** **32**: 119-21

Gargova S, Sariyska M, Angelov A, Stoilova I (2006) *Aspergillus niger* pH 2.1 optimum acid phosphatase with high affinity for phytate. ***Folia Microbiol*** **51**: 541-5

Gawryluk RM, Eme L, Roger AJ (2015) Gene fusion, fission, lateral transfer, and loss: Not-so-rare events in the evolution of eukaryotic ATP citrate lyase. ***Mol Phylogenet Evol*** **91**: 12-6

Gems D, Johnstone IL, Clutterbuck AJ (1991) An autonomously replicating plasmid transforms *Aspergillus nidulans* at high frequency. ***Gene*** **98**: 61-7

Gerasimaitė R, Mayer A (2017) Ppn2, a novel Zn2+-dependent polyphosphatase in the acidocalcisome-like yeast vacuole. ***J Cell Sci*** jcs-201061

Giots F, Donaton MC, Thevelein JM (2003) Inorganic phosphate is sensed by specific phosphate carriers and acts in concert with glucose as a nutrient signal for activation of the protein kinase A pathway in the yeast *Saccharomyces cerevisiae*. ***Mol Microbiol* 47**: 1163-81

Gonçalves E, Pereira R, Rocha I, Rocha M (2012) Optimization approaches for the *in silico* discovery of optimal targets for gene over/underexpression. ***J Comput Biol* 19:** 102-14

Goosen C, Yuan XL, van Munster JM, Ram AF, van der Maarel MJ, Dijkhuizen L (2007) Molecular and biochemical characterization of a novel intracellular invertase from *Aspergillus niger* with transfructosylating activity. ***Eukaryot Cell* 6**: 674-81

Gradisnik-Grapulin M, Legisa M (1997) A spontaneous change in the intracellular cyclic AMP level in *Aspergillus niger* is influenced by the sucrose concentration in the medium and by light. ***Appl Environ Microb* 63**: 2844-9

Grimoux E, Adams P (1880) Synthèse de l'ácide citrique. ***C R Hebd Seances Acad Sci* 90**: 1252

Gupta S, Sharma CB (1995) Citric acid fermentation by the mutant strain of the *Aspergillus niger* resistant to manganese ions inhibition. ***Biotechnol Lett* 17**: 269-74

Gupta S, Sharma CB (2002) Biochemical studies of citric acid production and accumulation by *Aspergillus niger* mutants. ***World J Microb Biot* 18**: 379-83

Guynn RW, Gelberg HJ, Veech RL (1973) Equilibrium constants of the malate dehydrogenase, citrate synthase, citrate lyase, and acetyl coenzyme A hydrolysis reactions under physiological conditions. ***J Biol Chem* 248**: 6957-65

Habison A, Kubicek CP, Röhr M (1979) Phosphofructokinase as a regulatory enzyme in citric acid producing *Aspergillus niger*. ***FEMS Microbiol Lett*** **5**: 39-42

Habison A, Kubicek CP, Röhr M (1983) Partial purification and regulatory properties of phosphofructokinase from *Aspergillus niger*. ***Biochem J*** **209**: 669-76

Halpern JM, Urbanski R, Weinstock AK, Iwig DF, Mathers RT, Von Recum HA (2014) A biodegradable thermoset polymer made by esterification of citric acid and glycerol. ***J Biomed Mater Res A*** **102**: 1467-77

Hamdy HS (2013) Citric acid production by *Aspergillus niger* grown on orange peel medium fortified with cane molasses. ***Ann Microbiol*** **63**: 267-78

Hang YD, Woodams EE (1985) Grape pomace: A novel substrate for microbial production of citric acid. ***Biotechnol Lett*** **7**: 253-4

Hang YD, Woodams EE (2000) Corn husks: a potential substrate for production of citric acid by *Aspergillus niger*. ***LWT-Food Sci Technol*** **33**: 520-1

Harmsen HJ, Kubicek-Pranz EM, Röhr M, Visser J, Kubicek CP (1992) Regulation of 6-phosphofructo-2-kinase from the citric-acid-accumulating fungus *Aspergillus niger*. ***Appl Microbiol Biot*** **37**: 784-8

Hattori T, Honda Y, Kino K, Kirimura K (2008) Expression of alternative oxidase gene (aox1) at the stage of single-cell conidium in citric acid-producing *Aspergillus niger*. ***J Biosci Bioeng*** **105**: 55-7

Hattori T, Kino K, Kirimura K (2009) Regulation of alternative oxidase at the transcription stage in *Aspergillus niger* under the conditions of citric acid production. ***Curr Microbiol*** **58**: 321-5

Hayer K, Stratford M, Archer DB (2013) Structural features of sugars that trigger or support conidial germination in the filamentous fungus *Aspergillus niger*. ***Appl Environ Microb*** AEM-02061

Hellmuth K, Pluschkell S, Jung JK, Ruttkowski E, Rinas U (1995) Optimization of glucose oxidase production by *Aspergillus niger* using genetic-and process-engineering techniques. ***Appl Microbiol Biot*** **43**: 978-84

Hesse SJ, Ruijter GJ, Dijkema C, Visser J (2002) Intracellular pH homeostasis in the filamentous fungus *Aspergillus niger*. ***Eur J Biochem*** **269**: 3485-94

Higgins DG, Sharp PM (1988) CLUSTAL: a package for performing multiple sequence alignment on a microcomputer. ***Gene*** **73**: 237-44

Hockertz S, Plönzig J, Auling G (1987) Impairment of DNA formation is an early event in *Aspergillus niger* under manganese starvation. ***Appl Microbiol Biot*** **25**: 590-3

Holda A, Kisielowska E, Niedoba T (2011) Bioaccumulation of Cr (VI) ions from aqueous solutions by *Aspergilus niger*. ***Polish J Environ Stud*** **20**: 345-9

Holm DK, Petersen LM, Klitgaard A, Knudsen PB, Jarczynska ZD, Nielsen KF, Gotfredsen CH, Larsen TO, Mortensen UH (2014) Molecular and chemical characterization of the biosynthesis of the 6-MSA-derived meroterpenoid yanuthone D in *Aspergillus niger*. ***Chem Biol*** **21**: 519-29

Hoover LK, Moo-Young M, Legge RL (1991) Biotransformation of dopamine to norlaudanosoline by *Aspergillus niger*. ***Biotechnol Bioeng*** **38**: 1029-33

Hossain M, Brooks JD, Maddox IS (1984) The effect of the sugar source on citric acid production by *Aspergillus niger*. ***Appl Microbiol Biot*** **19**: 393-7

Hossain M, Ahmed S (1992) The effect of trace elements on citric acid production from whey permeate by fermentation using *Aspergillus niger*. ***Bangl J Microbiol*** **9**: 1-9

Hossain AH, Li A, Brickwedde A, Wilms L, Caspers M, Overkamp K, Punt PJ (2016) Rewiring a secondary metabolite pathway towards itaconic acid production in *Aspergillus niger*. ***Microb Cell Fact*** **15**: 130

Hu W, Liu J, Chen JH, Wang SY, Lu D, Wu QH, Li WJ (2014) A mutation of *Aspergillus niger* for hyper-production of citric acid from corn meal hydrolysate in a bioreactor. ***J Zhejiang Univ SC-B*** **15**: 1006-10

Hund HK, Breuer J, Lingens F, Hüttermann J, Kappl R, Fetzner S (1999) Flavonol 2, 4-dioxygenase from *Aspergillus niger* DSM 821, a type 2 CuII-containing glycoprotein. ***Eur J Biochem*** **263**: 871-8

Inglis DO, Binkley J, Skrzypek MS, Arnaud MB, Cerqueira GC, Shah P, Wymore F, Wortman JR, Sherlock G (2013) Comprehensive annotation of secondary metabolite biosynthetic genes and gene clusters of *Aspergillus nidulans*, *A. fumigatus*, *A. niger* and *A. oryzae*. ***BMC Microbiol*** **13**: 91

Jaklitsch WM, Kubicek CP, Scrutton MC (1991) Intracellular location of enzymes involved in citrate production by *Aspergillus niger*. ***Can J Microbiol*** **37**: 823-7

Javed S, Asgher M, Sheikh MA, Nawaz H, Jamil A (2011) Enhanced citric acid production by *Aspergillus niger* EB-3 mutant using an inert solid support in molasses medium. ***Afr J Biotechnol*** **10**: 11784

Jernejc K, Vendramin M, Cimerman A (1989) Lipid composition of *Aspergillus niger* in citric acid accumulating and nonaccumulating conditions. ***Enzyme Microb Tech*** **11**: 452-6

Jernejc K, Perdih A, Cimerman A (1991) ATP: citrate lyase and carnitine acetyltransferase activity in a citric-acid-producing *Aspergillus niger* strain. ***Appl Microbiol Biot*** **36**: 92-5

Jernejc K, Perdih A, Cimerman A (1992) Biochemical composition of *Aspergillus niger* mycelium grown in citric acid productive and nonproductive conditions. ***J Biotechnol*** **25**:341-8

Jernejc K, Legiša M (1996) Purification and properties of carnitine acetyltransferase from citric acid producing *Aspergillus niger*. ***Appl Biochem Biotech*** **60**: 151-8

Jernejc K, Legiša M (2004) A drop of intracellular pH stimulates citric acid accumulation by some strains of *Aspergillus niger*. ***J Biotechnol*** **112**: 289-97

Jianlong W, Ping L (1998) Phytate as a stimulator of citric acid production by *Aspergillus niger*. ***Process Biochem*** **33**: 313-6

Jianlong W (2000) Enhancement of citric acid production by *Aspergillus niger* using *n*-dodecane as an oxygen-vector. ***Process Biochem*** **35**: 1079-83

Jianlong W, Xinmin Z, Decai D, Ding Z (2001) Bioadsorption of lead (II) from aqueous solution by fungal biomass of *Aspergillus niger*. ***J Biotechnol*** **87**: 273-7

Kaplan O, Vejvoda V, Plíhal O, Pompach P, Kavan D, Bojarová P, Bezouška K, Macková M, Cantarella M, Jirků V, Křen V (2006) Purification and characterization of a nitrilase from *Aspergillus niger* K10. ***Appl Microbiol Biot*** **73**: 567-75

Kartal SN, Kakitani T, Imamura Y (2004) Bioremediation of CCA-C treated wood by *Aspergillus niger* fermentation. ***Holz Roh Werkst* 62**: 64-8

Kelly JM, Hynes MJ (1985) Transformation of *Aspergillus niger* by the *amdS* gene of *Aspergillus nidulans*. ***EMBO J* 4**: 475-9

Khosravi-Darani K, Zoghi A (2008) Comparison of pretreatment strategies of sugarcane baggase: Experimental design for citric acid production. ***Bioresource Technol* 99**: 6986-93

Kirimura K, Kumagai K, Morisada S, Kawabe S, Usami S (1984) The changes in enzyme activities during citric acid fermentation by *Aspergillus niger* in solid culture. ***Hakkokogaku* 62**: 127-33

Kirimura K, Hirowatari Y, Usami S (1987) Alterations of respiratory systems in *Aspergillus niger* under the conditions of citric acid fermentation. ***Agr Biol Chem Tokyo* 51**: 1299-303

Kirimura K, Matsui T, Sugano S, Usami S (1996) Enhancement and repression of cyanide-insensitive respiration in *Aspergillus niger*. ***FEMS Microbiol Lett* 141**: 251-4

Kirimura K, Watanabe T, Sunagawa T, Usami S (1999a) Citric acid production from xylan and xylan hydrolysate by semi-solid culture of *Aspergillus niger*. ***Biosci Biotechnol Biochem* 63**: 226-8

Kirimura K, Yoda M, Usami S (1999b) Cloning and expression of the cDNA encoding an alternative oxidase gene from *Aspergillus niger* WU-2223L. ***Curr Genet* 34**: 472-7

Kirimura K, Yoda M, Ko I, Oshida Y, Miyake K, Usami S (1999c) Cloning and sequencing of the chromosomal DNA and cDNA encoding the mitochondrial citrate synthase of *Aspergillus niger* WU-2223L. ***J Biosci Bioeng* 88**: 237-43

Kirimura K, Yoda M, Shimizu H, Sugano S, Mizuno M, Kino K, Usami S (2000) Contribution of cyanide-insensitive respiratory pathway, catalyzed by the alternative oxidase, to citric acid production in *Aspergillus niger*. ***Biosci Biotechnol Biochem*** **64**: 2034-9

Kirimura K, Ogawa S, Hattori T, Kino K (2006) Expression analysis of alternative oxidase gene (*aox1*) with enhanced green fluorescent protein as marker in citric acid-producing *Aspergillus niger*. ***J Biosci Bioeng*** **102**: 210-4

Kirimura K, Kobayashi K, Ueda Y, Hattori T (2016) Phenotypes of gene disruptants in relation to a putative mitochondrial malate–citrate shuttle protein in citric acid-producing *Aspergillus niger*. ***Biosci Biotechnol Biochem*** **80**: 1737-46

Kishore G, Sugumaran M, Vaidyanathan CS (1976) Metabolism of DL-(+/-)-phenylalanine by *Aspergillus niger*. ***J Bacteriol*** **128**: 182-91

Kisser M, Kubicek CP, Röhr M (1980) Influence of manganese on morphology and cell wall composition of *Aspergillus niger* during citric acid fermentation. ***Arch Microbiol*** **128**: 26-33

Kobayashi K, Hattori T, Hayashi R, Kirimura K (2014) Overexpression of the NADP+-specific isocitrate dehydrogenase gene (*icdA*) in citric acid-producing *Aspergillus niger* WU-2223L. ***Biosci Biotechol Biochem*** **78**: 1246-53

Kontopidis G, Mattey M, Kristiansen B (1995) Citrate transport during the citric acid fermentation by *Aspergillus niger*. ***Biotechnol Lett*** **17**: 1101-6

Kristiansen B, Linden J, Mattey M (2014) Citric acid biotechnology. ***CRC Press***

Krügel U, Kühn C (2013) Post-translational regulation of sucrose transporters by direct protein–protein interactions. ***Front Plant Sci*** **4**: 237

Krzystek L, Gluszcz P, Ledakowicz S (1996) Determination of yield and maintenance coefficients in citric acid production by *Aspergillus niger*. ***Chem Eng J* 62**: 215-22

Kubicek CP, Röhr M (1977) Influence of manganese on enzyme synthesis and citric acid accumulation in *Aspergillus niger*. ***Appl Microbiol Biot* 4**: 167-75

Kubicek CP, Röhr M (1978) The role of the tricarboxylic acid cycle in citric acid accumulation by *Aspergillus niger*. ***Appl Microbiol Biot* 5**: 263-71

Kubicek CP, Zehentgruber O, El-Kalak H, Röhr M (1980a) Regulation of citric acid production by oxygen: effect of dissolved oxygen tension on adenylate levels and respiration in *Aspergillus niger*. ***Eur J Appl Microbiol* 9**: 101-15

Kubicek CP, Röhr M (1980b) Regulation of citrate synthase from the citric acid-accumulating fungus, *Aspergillus niger*. ***Biochim Biophys Acta* 615**: 449-57

Kubicek CP, Röhr M (1985) Aconitase and citric acid fermentation by *Aspergillus niger*. ***Appl Environ Microb* 50**: 1336-8

Kubicek CP, Schreferl-Kunar G, Wöhrer W, Röhr M (1988) Evidence for a cytoplasmic pathway of oxalate biosynthesis in *Aspergillus niger*. ***Appl Environ Microb* 54**: 633-7

Kubicek-Pranz EM, Mozelt M, Rōhr M, Kubicek CP (1990) Changes in the concentration of fructose 2, 6-bisphosphate in *Aspergillus niger* during stimulation of acidogenesis by elevated sucrose concentration. ***BBA-Gen Subjects* 1033**: 250-5

Kuforiji OO, Kuboye AO, Odunfa SA (2010) Solid state fermentation process for citric acid production using corn and cassava wastes. ***Adv Food Sci* 32**: 71-4

Kuivanen J, Wang YM, Richard P (2016) Engineering *Aspergillus niger* for galactaric acid production: elimination of galactaric acid catabolism by using RNA sequencing and CRISPR/Cas9. ***Microb Cell Fact* 15**: 210

Kumar S, Punekar NS, SatyaNarayan V, Venkatesh KV (2000) Metabolic fate of glutamate and evaluation of flux through the 4-aminobutyrate (GABA) shunt in *Aspergillus niger*. ***Biotechnol Bioeng* 67**: 575-84

Kumar D, Jain VK, Shanker G, Srivastava A (2003) Utilisation of fruits waste for citric acid production by solid state fermentation. ***Process Biochem* 38**: 1725-9

Kusters-van Someren M, Flipphi M, de Graaff L, van den Broeck H, Kester H, Hinnen A, Visser J (1992) Characterization of the *Aspergillus niger pelB* gene: structure and regulation of expression. ***Mol Gen Genet* 234**: 113-20

Kwon MJ, Arentshorst M, Roos ED, van den Hondel CA, Meyer V, Ram AF (2011) Functional characterization of Rho GTPases in *Aspergillus niger* uncovers conserved and diverged roles of Rho proteins within filamentous fungi. ***Mol Microbiol* 79**: 1151-67

La Nauze JM (1966) Aconitase and isocitric dehydrogenases of *Aspergillus niger* in relation to citric acid production. ***Microbiology+* 44**: 73-81

Lee YH, Suh MG, Chung KT (2006) Kinetics for Citric Acid Production from the Concentrated Milk Factory Waste Water by *Aspergillus niger* ATCC 9142. ***J Life Sci* 16**: 6-11

Legiša M, Mattey M (1986) Glycerol as an initiator of citric acid accumulation in *Aspergillus niger*. ***Enzyme Microb Tech* 8**: 258-9

Legiša M, Mattey M (1988) Citrate regulation of the change in carbohydrate degradation during the initial phase of the citric acid production by *Aspergillus niger*. ***Enzyme Microb Tech*** **10**: 33-6

Legiša M, Kidrič J (1989) Initiation of citric acid accumulation in the early stages of *Aspergillus niger* growth. ***Appl Microbiol Biot*** **31**: 453-7

Legiša M, Benčina M (1994) Evidence for the activation of 6-phosphofructo-1-kinase by cAMP-dependent protein kinase in *Aspergillus niger*. ***FEMS Microbiol Lett*** **118**: 327-33

Li CH, Yan TR (2014) Use of *Aspergillus niger* β-glucosidase II gene (*bglII*) promoter elements to construct an efficient expression vector. ***J Taiwan Inst Chem E*** **45**: 749-54

Lin Y, Tanaka S (2006) Ethanol fermentation from biomass resources: current state and prospects. ***Appl Microbiol Biot*** **69**: 627-42

Lippitsch M (1961) Untersuchungen über Tannase bei *Aspergillus niger*. ***Arch Microbiol*** **39**: 209-20

Liu JZ, Zhang QL, Weng LP, Ji LN (2003) Screening and mutagenesis of *Aspergillus niger* for the improvement of Glucose-6-phosphate dehydrogenase production. ***Appl Biochem Micro+*** **39**: 493-6

Liu J, Gao Q, Xu N, Liu L (2013) Genome-scale reconstruction and *in silico* analysis of *Aspergillus terreus* metabolism. ***Mol Biosyst*** **9**: 1939-48

Lotfy WA, Ghanem KM, El-Helow ER (2007) Citric acid production by a novel *Aspergillus niger* isolate: I. Mutagenesis and cost reduction studies. ***Bioresource Technol*** **98**: 3464-9

Lu H, Cao W, Ouyang L, Xia J, Huang M, Chu J, Zhuang Y, Zhang S, Noorman H (2017) Comprehensive reconstruction and *in silico* analysis of *Aspergillus niger* genome-scale metabolic network model that accounts for 1210 ORFs. ***Biotechnol Bioeng*** **114**: 685-95

Ma H, Kubicek CP, Röhr M (1985) Metabolic effects of manganese deficiency in *Aspergillus niger*: evidence for increased protein degradation. ***Arch Microbiol*** **141**: 266-8

Machida M, Yamada O, Gomi K (2008) Genomics of *Aspergillus oryzae*: learning from the history of Koji mold and exploration of its future. ***DNA Res*** **15**: 173-83

Magaña-Ortíz D, Coconi-Linares N, Ortiz-Vazquez E, Fernández F, Loske AM, Gómez-Lim MA (2013) A novel and highly efficient method for genetic transformation of fungi employing shock waves. ***Fungal Genet Biol*** **56**: 9-16

Mahadevan R, Edwards JS, Doyle FJ (2002) Dynamic flux balance analysis of diauxic growth in *Escherichia coli*. ***Biophys J*** **83**: 1331-40

Mahmoud MS, Mostafa MK, Mohamed SA, Sobhy NA, Nasr M (2017) Bioremediation of red azo dye from aqueous solutions by *Aspergillus niger* strain isolated from textile wastewater. ***J Environ Chem Eng*** **5**: 547-54

Mäkelä MR, Aguilar-Pontes MV, van Rossen-Uffink D, Peng M, de Vries RP (2018) The fungus *Aspergillus niger* consumes sugars in a sequential manner that is not mediated by the carbon catabolite repressor CreA. ***Sci Rep-UK*** **8**

Manzanares P, de Graaff LH, Visser J (1998) Characterization of galactosidases from *Aspergillus niger*: purification of a novel α-galactosidase activity. ***Enzyme Microb Tech*** **22**: 383-90

Markwell J, Frakes LG, Brott EC, Osterman J, Wagner FW (1989) *Aspergillus niger* mutants with increased glucose oxidase production. ***Appl Microbiol Biot* 30**: 166-9

Mat-Jan F, Alam KY, Clark DP (1989) Mutants of *Escherichia coli* deficient in the fermentative lactate dehydrogenase. ***J Bacteriol* 171**: 342-8

Mattern IE, van Noort JM, van den Berg P, Archer DB, Roberts IN, van den Hondel CA (1992) Isolation and characterization of mutants of *Aspergillus niger* deficient in extracellular proteases. ***Mol Gen Genet* 234**: 332-6

Mattey M (1977) Citrate regulation of citric acid production in *Aspergillus niger*. ***FEMS Microbiol Lett* 2**: 71-4

Mattey M, Bowes I (1978) Citrate regulation of NADP+-specific isocitrate dehydrogenase of *Aspergillus niger* ***Biochem Soc T* 6**: 1224-6

Mattey M. Biochemistry of citric acid production by yeasts. In: Citric acid biotechnology. Taylor and Francis. 1999. London. pp. 33–54

Max B, Salgado JM, Rodríguez N, Cortés S, Converti A, Domínguez JM (2010) Biotechnological production of citric acid. ***Braz J Microbiol* 41**: 862-75

McGrath JW, Kulakova AN, Kulakov LA, Quinn JP (2005) *In vitro* detection and characterisation of a polyphosphate synthesising activity in the yeast *Candida humicola* G-1. ***Res Microbiol* 156**: 485-91

McIntyre M, McNeil B (1997) Dissolved carbon dioxide effects on morphology, growth, and citrate production in *Aspergillus niger* A60. ***Enzyme Microb Tech* 20**: 135-42

Meijer S, Nielsen ML, Olsson L, Nielsen J (2009a) Gene deletion of cytosolic ATP: citrate lyase leads to altered organic acid production in *Aspergillus niger*. ***J Ind Microbiol Biot*** **36**: 1275-80

Meijer S, Otero J, Olivares R, Andersen MR, Olsson L, Nielsen J (2009b) Overexpression of isocitrate lyase—glyoxylate bypass influence on metabolism in *Aspergillus niger*. ***Metab Eng*** **11**: 107-16

Meixner-Monori B, Kubicek CP, Röhr M (1984) Pyruvate kinase from *Aspergillus niger*: a regulatory enzyme in glycolysis?. ***Can J Microbiol*** **30**: 16-22

Meixner-Monori BI, Kubicek CP, Habison AY, Kubicek-Pranz EM, Röhr M (1985) Presence and regulation of the alpha-ketoglutarate dehydrogenase multienzyme complex in the filamentous fungus *Aspergillus niger*. ***J Bacteriol*** **161**: 265-71

Meixner-Monori B, Kubicek CP, Harrer W, Schreferl G, Rohr M (1986) NADP-specific isocitrate dehydrogenase from the citric acid-accumulating fungus *Aspergillus niger*. ***Biochem J*** **236**: 549-57

Mesojednik S, Legiša M (2005) Posttranslational modification of 6-phosphofructo-1-kinase in *Aspergillus niger*. ***Appl Environ Microb*** **71**: 1425-32

Meyer V, Arentshorst M, El-Ghezal A, Drews AC, Kooistra R, van den Hondel CA, Ram AF (2007) Highly efficient gene targeting in the *Aspergillus niger kusA* mutant. ***J Biotechnol*** **128**: 770-5

Meyer V (2008) Genetic engineering of filamentous fungi—progress, obstacles and future trends. ***Biotechnol Adv*** **26**: 177-85

Meyer V, Wu B, Ram AF (2011a) *Aspergillus* as a multi-purpose cell factory: current status and perspectives. ***Biotechnol Lett*** **33**: 469-76

Meyer V, Wanka F, van Gent J, Arentshorst M, van den Hondel CA, Ram AF (2011b) Fungal gene expression on demand: an inducible, tunable, and metabolism-independent expression system for *Aspergillus niger*. ***Appl Environ Microb* 77**: 2975-83

Micheli PA (1729) Nova Plantarum Genera. Florentiae

Mirminachi F, Zhang A, Roehr M (2002) Citric Acid Fermentation and Heavy Metal Ions–I. Effects of Iron, Manganese and Copper. ***Eng Life Sci* 22**: 363-73

Mischak H, Kubicek CP, Röhr M (1984) Citrate inhibition of glucose uptake in *Aspergillus niger*. ***Biotechnol Lett* 6**: 425-30

Mischak H, Kubicek CP, Röhr M (1985) Formation and location of glucose oxidase in citric acid producing mycelia of *Aspergillus niger*. ***Appl Microbiol Biot* 21**: 27-31

Mlakar T, Legiša M (2006) Citrate inhibition-resistant form of 6-phosphofructo-1-kinase from *Aspergillus niger*. ***Appl Environ Microb* 72**: 4515-21

Mojzita D, Koivistoinen OM, Maaheimo H, Penttilä M, Ruohonen L, Richard P (2012a) Identification of the galactitol dehydrogenase, LadB, that is part of the oxido-reductive D-galactose catabolic pathway in *Aspergillus niger*. ***Fungal Genet Biol* 49**: 152-9

Mojzita D, Herold S, Metz B, Seiboth B, Richard P (2012b) L-xylo-3-hexulose reductase is the missing link in the oxidoreductive pathway for D-galactose catabolism in filamentous fungi. ***J Biol Chem* 287**: 26010-8

Moriya Y, Itoh M, Okuda S, Yoshizawa AC, Kanehisa M (2007) KAAS: an automatic genome annotation and pathway reconstruction server. ***Nucleic Acids Res* 35**: W182-5

Moyer AJ (1953) Effect of Alcohols on the Mycological Production of Citric Acid in Surface and Submerged Culture: I. Nature of the Alcohol Effect. ***Appl Microbiol* 1**: 1

Namazi H, Adeli M (2005) Dendrimers of citric acid and poly (ethylene glycol) as the new drug-delivery agents. ***Biomaterials* 26**: 1175-83

Netik A, Torres NV, Riol JM, Kubicek CP (1997) Uptake and export of citric acid by *Aspergillus niger* is reciprocally regulated by manganese ions. ***BBA-Biomembranes* 1326**: 287-94

Ngiam C, Jeenes DJ, Punt PJ, Van Den Hondel CA, Archer DB (2000) Characterization of a foldase, protein disulfide isomerase A, in the protein secretory pathway of *Aspergillus niger*. ***Appl Environ Microb* 66**: 775-82

Nishi A (1961) Role of polyphosphate and phospholipid in germinating spores of *Aspergillus niger*. ***J Bacteriol* 81**: 10

Niu J, Arentshorst M, Nair PD, Dai Z, Baker SE, Frisvad JC, Nielsen KF, Punt PJ, Ram AF (2016) Identification of a classical mutant in the industrial host *Aspergillus niger* by systems genetics: LaeA is required for citric acid production and regulates the formation of some secondary metabolites. ***G3-Genes Genom Genet* 6**: 193-204

Nødvig CS, Nielsen JB, Kogle ME, Mortensen UH (2015) A CRISPR-Cas9 system for genetic engineering of filamentous fungi. ***PLoS One* 10**

Odoni DI, van Gaal MP, Schonewille T, Tamayo-Ramos JA, dos Santos VA, Suarez-Diez M, Schaap PJ (2017) *Aspergillus niger* secretes citrate to increase iron bioavailability. ***Front Microbiol* 8**

Odoni DI, Laothanachareon T, Vazquez-Vilar M, van Gaal MP, Schonewille T, Bruinsma L, dos Santos VA, Tamayo-Ramos JA, Suarez-Diez M, Schaap PJ (2018). *Aspergillus niger* citrate exporter revealed by comparison of two alternative citrate producing conditions. ***bioRxiv*** 259051

Oliveira JM, van der Veen D, de Graaff LH, Qin L (2008) Efficient cloning system for construction of gene silencing vectors in *Aspergillus niger*. ***Appl Microbiol Biot*** **80**: 917-24

Olsvik E, Tucker KG, Thomas CR, Kristiansen B (1993) Correlation of *Aspergillus niger* broth rheological properties with biomass concentration and the shape of mycelial aggregates. ***Biotechnol Bioeng*** **42**: 1046-52

Orth JD, Thiele I, Palsson BØ (2010) What is flux balance analysis? ***Nat Biotechnol*** **28**: 245-8

Orthofer R, Kubicek CP, Röhr M (1979) Lipid levels and manganese deficiency in citric acid producing strains of *Aspergillus niger*. ***FEMS Microbiol Lett*** **5**: 403-6

Ozeki K, Kyoya FF, Hizume K, Kanda A, Hamachi M (1994) Transformation of intact *Aspergillus niger* by electroporation. ***Biosci Biotechnol Biochem*** **58**: 2224-7

Panneman H, Ruijter GJ, Broeck HC, Driever E, Visser J (1996) Cloning and biochemical characterisation of an *Aspergillus niger* glucokinase. ***FEBS J*** **240**: 518-25

Panneman H, Ruijter GJ, van den Broeck HC, Visser J (1998) Cloning and biochemical characterisation of *Aspergillus niger* hexokinase. ***FEBS J*** **258**: 223-32

Papagianni M, Mattey M, Kristiansen B (1999) The influence of glucose concentration on citric acid production and morphology of *Aspergillus niger* in batch and culture. ***Enzyme Microb Tech* 25**: 710-7

Papagianni M, Mattey M (2004) Modeling the mechanisms of glucose transport through the cell membrane of *Aspergillus niger* in submerged citric acid fermentation processes. ***Biochem Eng J* 20**: 7-12

Papagianni M, Wayman F, Mattey M (2005) Fate and role of ammonium ions during fermentation of citric acid by *Aspergillus niger*. ***Appl Environ Microb* 71**: 7178-86

Papagianni M, Mattey M (2006) Morphological development of *Aspergillus niger* in submerged citric acid fermentation as a function of the spore inoculum level. Application of neural network and cluster analysis for characterization of mycelial morphology. ***Microb Cell Fact* 5**: 3

Papagianni M (2007) Advances in citric acid fermentation by *Aspergillus niger*: biochemical aspects, membrane transport and modeling. ***Biotechnol Adv* 25**: 244-63

Parshikov IA, Sutherland JB (2014) The use of *Aspergillus niger* cultures for biotransformation of terpenoids. ***Process Biochem* 49**: 2086-100

Parshikov IA, Woodling KA, Sutherland JB (2015a) Biotransformations of organic compounds mediated by cultures of *Aspergillus niger*. ***Appl Microbiol Biot* 99**: 6971-86

Parshikov IA, Sutherland JB (2015b) Biotransformation of steroids and flavonoids by cultures of *Aspergillus niger*. ***Appl Biochem Biotech* 176**: 903-23

Patagundi BI, Kaliwal BB (2008) Biotechnological Production of Citric Acid Using Different Substrates by *Aspergillus niger* ATCC 26550. ***Res J Biotechnol*** **1**:196-206

Patil KR, Rocha I, Förster J, Nielsen J (2005) Evolutionary programming as a platform for *in silico* metabolic engineering. ***BMC Bioinformatics*** **6**: 308

Peksel A, Torres N, Liu J, Juneau G, Kubicek C (2002) 13C-NMR analysis of glucose metabolism during citric acid production by *Aspergillus niger*. ***Appl Microbiol Biot*** **58**: 157

Pel HJ, de Winde JH, Archer DB, Dyer PS, Hofmann G, Schaap PJ, Turner G, de Vries RP, Albang R, Albermann K, Andersen MR, Bendtsen JD, Benen JAE, van den Berg M, Breestraat S, Caddick MX, Contreras R, Cornell M, Coutinho PM, Danchin EGJ, Debets AJM, Dekker P, van Dijck PWM, van Dijk A, Dijkhuizen L, Driessen AJM, d'Enfert C, Geysens S, Goosen C, Groot GSP, de Groot PWJ, Guillemette T, Henrissat B, Herweijer M, van den Hombergh JPTW, van den Hondel CAMJJ, van der Heijden RTJM, van der Kaaij RM, Klis FM, Kools HJ, Kubicek CP, van Kuyk PA, Lauber J, Lu X, van der Maarel MJEC, Meulenberg R, Menke H, Mortimer MA, Nielsen J, Oliver SG, Olsthoorn M, Pal K, van Peij NNME, Ram AFJ, Rinas U, Roubos JA, Sagt CMJ, Schmoll M, Sun J, Ussery D, Varga J, Vervecken W, van de Vondervoort PJJ, Wedler H, Wösten HAB, Zeng AP , van Ooyen AJJ, Visser J, Stam H (2007) Genome sequencing and analysis of the versatile cell factory *Aspergillus niger* CBS 513.88. ***Nat Biotechnol*** **25**: 221-231

Petersen LM, Holm DK, Knudsen PB, Nielsen KF, Gotfredsen CH, Mortensen UH, Larsen TO (2015) Characterization of four new antifungal yanuthones from *Aspergillus niger*. ***J Antibiot*** **68**: 201

Phillippy BQ, Mullaney EJ (1997) Expression of an *Aspergillus niger* phytase (phyA) in *Escherichia coli*. ***J Agr Food Chem*** **45**: 3337-42

Poulsen L, Andersen MR, Lantz AE, Thykaer J (2012) Identification of a transcription factor controlling pH-dependent organic acid response in *Aspergillus niger*. ***PLoS One* 7**: e50596

Price MS, Classen JJ, Payne GA (2001) *Aspergillus niger* absorbs copper and zinc from swine wastewater. ***Bioresource Technol* 77**: 41-9

Prömper C, Schneider R, Weiss H (1993) The role of the proton-pumping and alternative respiratory chain NADH: ubiquinone oxidoreductases in overflow catabolism of *Aspergillus niger*. ***FEBS J* 216**: 223-30

Punt PJ, Schuren FH, Lehmbeck J, Christensen T, Hjort C, van den Hondel CA (2008) Characterization of the *Aspergillus niger* prtT, a unique regulator of extracellular protease encoding genes. ***Fungal Genet Biol* 45**: 1591-9

Purohit HJ, Ratledge C (1988) Mitochondrial location of pyruvate carboxylase in *Aspergillus niger*. ***FEMS Microbiol Lett* 55**: 129-32

R Poulsen B, Nøhr J, Douthwaite S, Hansen LV, Iversen JJ, Visser J, Ruijter GJ (2005) Increased NADPH concentration obtained by metabolic engineering of the pentose phosphate pathway in *Aspergillus niger*. ***Febs J* 272**: 1313-25

Radisky D, Kaplan J (1999) Regulation of transition metal transport across the yeast plasma membrane. ***J Biol Chem* 274**: 4481-4

Ramachandran S, Fontanille P, Pandey A, Larroche C (2006) Gluconic acid: properties, applications and microbial production. ***Food Technol Biotech* 44**: 185-95

Ramakrishnan CV, Steel R, Lentz CP (1955) Mechanism of citric acid formation and accumulation in *Aspergillus niger*. ***Arch Biochem Biophys* 55**: 270-3

Ramos EL, Mata-Gómez MA, Rodríguez-Durán LV, Belmares RE, Rodríguez-Herrera R, Aguilar CN (2011) Catalytic and thermodynamic properties of a tannase produced by *Aspergillus niger* GH1 grown on polyurethane foam. ***Appl Biochem Biotech*** **165**: 1141-51

Rezaei MN, Aslankoohi E, Verstrepen KJ, Courtin CM (2015) Contribution of the tricarboxylic acid (TCA) cycle and the glyoxylate shunt in *Saccharomyces cerevisiae* to succinic acid production during dough fermentation. ***Int J Food Microbiol*** **204**: 24-32

Rinágelová A, Kaplan O, Veselá AB, Chmátal M, Křenková A, Plíhal O, Pasquarelli F, Cantarella M, Martínková L (2014) Cyanide hydratase from *Aspergillus niger K*10: overproduction in *Escherichia coli*, purification, characterization and use in continuous cyanide degradation. ***Process Biochem*** **49**: 445-50

Rivas B, Torrado A, Torre P, Converti A, Domínguez JM (2008) Submerged citric acid fermentation on orange peel autohydrolysate. ***J Agr Food Chem*** **56**: 2380-7

Rivera AL, Magana-Ortiz D, Gomez-Lim M, Fernández F, Loske AM (2014) Physical methods for genetic transformation of fungi and yeast. ***Phys Life Rev*** **11**: 184-203

Roblin G, Sakr S, Bonmort J, Delrot S (1998) Regulation of a plant plasma membrane sucrose transporter by phosphorylation. ***FEBS Lett*** **424**: 165-8

Rocha M, Maia P, Mendes R, Pinto JP, Ferreira EC, Nielsen J, Patil KR, Rocha I (2008) Natural computation meta-heuristics for the *in silico* optimization of microbial strains. ***BMC Bioinformatics*** **9**: 499

Roehr M, Zehentgruber O, Kubicek CP (1981) Kinetics of biomass formation and citric acid production by *Aspergillus niger* on pilot plant scale. ***Biotechnol Bioeng*** **23**: 2433-45

Röhr M, Kubicek CP, Zehentgruber O, Orthofer R (1987) Accumulation and partial re-consumption of polyols during citric acid fermentation by *Aspergillus niger*. ***Appl Microbiol Biot* 27**: 235-9

Roth AH, Dersch P (2010) A novel expression system for intracellular production and purification of recombinant affinity-tagged proteins in *Aspergillus niger*. ***Appl Microbiol Biot* 86**: 659-70

Roukas T (1998) Carob pod: A new substrate for citric acid production by *Aspergillus niger*. ***Applied Biochem Biotech* 74**: 43-53

Rubio MC, Maldonado MC (1995) Purification and characterization of invertase from *Aspergillus niger*. ***Curr Microbiol* 31**: 80-3

Rugsaseel S, Kirimura K, Usami S (1996) Citric acid accumulation by cycloheximide-sensitive mutant strains of *Aspergillus niger*. ***Appl Microbiol Biot* 45**: 28-35

Ruijter GJ, Panneman H, Visser J (1997) Overexpression of phosphofructokinase and pyruvate kinase in citric acid-producing *Aspergillus niger*. ***BBA-Gen Subjects* 1334**: 317-26

Ruijter GJ, van de Vondervoort PJ, Visser J (1999) Oxalic acid production by *Aspergillus niger*: an oxalate-non-producing mutant produces citric acid at pH 5 and in the presence of manganese. ***Microbiology+* 145**: 2569-76

Ruijter GJ, Panneman H, Xu DB, Visser J (2000) Properties of *Aspergillus niger* citrate synthase and effects of citA overexpression on citric acid production. ***FEMS Microbiol Lett* 184**: 35-40

Sack U, Heinze TM, Deck J, Cerniglia CE, Cazau MC, Fritsche W (1997) Novel metabolites in phenanthrene and pyrene transformation by *Aspergillus niger*. ***Appl Environ Microb* 63**: 2906-9

Samson RA, Visagie CM, Houbraken J, Hong SB, Hubka V, Klaassen CH, Perrone G, Seifert KA, Susca A, Tanney JB, Varga J (2014) Phylogeny, identification and nomenclature of the genus *Aspergillus*. ***Stud Mycol*** **78**: 141-73

San Chua P, Salleh AH, Mohamad MS, Deris S, Omatu S, Yoshioka M (2015) Identifying a gene knockout strategy using a hybrid of the bat algorithm and flux balance analysis to enhance the production of succinate and lactate in *Escherichia coli*. ***Biotechnol Bioproc E*** **20**: 349-57

Sassi G, Ruggeri B, Specchia V, Gianetto A (1991) Citric acid production by *A. niger* with banana extract. ***Bioresource Technol*** **37**: 259-69

Sauer M, Porro D, Mattanovich D, Branduardi P (2008) Microbial production of organic acids: expanding the markets. ***Trends Biotechnol*** **26**: 100-8

Saunders G, Picknett TM, Tuite MF, Ward M (1989) Heterologous gene expression in filamentous fungi. ***Trends Biotechnol*** **7**: 283-7

Schink B, Zeikus JG (1980) Microbial methanol formation: a major end product of pectin metabolism. ***Curr Microbiol*** **4**: 387-9

Schmidt M, Wallrath J, Dörner A, Weiss H (1992) Disturbed assembly of the respiratory chain NADH: ubiquinone reductase (complex I) in citric-acid-accumulating *Aspergillus niger* strain B60. ***Appl Microbiol Biot*** **36**: 667-72

Schneider KD, Van Straaten P, Orduña D, Mira R, Glasauer S, Trevors J, Fallow D, Smith PS (2010) Comparing phosphorus mobilization strategies using *Aspergillus niger* for the mineral dissolution of three phosphate rocks. ***J Appl Microbiol*** **108**: 366-74

Schneider M, Zimmer GF, Cremonese EB, de C de S Schneider R, Corbellini VA (2014) By-products from the biodiesel chain as a substrate to citric acid production by solid-state fermentation. ***Waste Manage Res* 32**: 653-60

Schreferl GE, Kubicek CP, Röhr M (1986) Inhibition of citric acid accumulation by manganese ions in *Aspergillus niger* mutants with reduced citrate control of phosphofructokinase. ***J Bacteriol* 165**: 1019-22

Schreferl-Kunar G, Grotz M, Röhr M, Kubicek CP (1989) Increased citric acid production by mutants of *Aspergillus niger* with increased glycolytic capacity. ***FEMS Microbiol Lett* 59**: 297-300

Shankaranand VS, Lonsane BK (1994) Coffee husk: an inexpensive substrate for production of citric acid by *Aspergillus niger* in a solid-state fermentation system. ***World J Microb Biot* 10**: 165-8

Sharma N, Gupta VC (2012a) Batch biodegradation of phenol of paper and pulp effluent by *Aspergillus niger*. ***Int J Chem Eng Appl* 3**: 182

Sharma R, Katoch M, Govindappa N, Srivastava PS, Sastry KN, Qazi GN (2012b) Evaluation of the catalase promoter for expressing the alkaline xylanase gene (*alx*) in *Aspergillus niger*. ***FEMS Microbiol Lett* 327**: 33-40

Shu P, Johnson MJ (1948) The interdependence of medium constituents in citric acid production by submerged fermentation. ***J Bacteriol* 56**: 577

Singh R, Kumar M, Mittal A, Mehta PK (2016) Microbial enzymes: industrial progress in 21st century. ***3 Biotech* 6**: 174

Šnajdrová R, Kristová-Mylerová V, Crestia D, Nikolaou K, Kuzma M, Lemaire M, Gallienne E, Bolte J, Bezouška K, Křen V, Martínková L (2004) Nitrile biotransformation by *Aspergillus niger*. ***J Mol Catal B-Enzym* 29**: 227-32

Šolar T, Turšič J, Legiša M (2008) The role of glucosamine-6-phosphate deaminase at the early stages of *Aspergillus niger* growth in a high-citric-acid-yielding medium. ***Appl Microbiol Biot* 78**: 613-9

Song W, Liang J, Wen T, Wang X, Hu J, Hayat T, Alsaedi A, Wang X (2016) Accumulation of Co (II) and Eu (III) by the mycelia of *Aspergillus niger* isolated from radionuclide-contaminated soils. ***Chem Eng J* 304**: 186-93

Srivastava A, Kar R (2009) Characterization and application of tannase produced by *Aspergillus niger* ITCC 6514.07 on pomegranate rind. ***Braz J Microbiol* 40**: 782-9

Steinböck F, Choojun S, Held I, Roehr M, Kubicek CP (1994) Characterization and regulatory properties of a single hexokinase from the citric acid accumulating fungus *Aspergillus niger*. ***BBA-Gen Subjects* 1200**: 215-23

Stove V, Smits K, Naessens E, Plum J, Verhasselt B (2006) Multiple gene knock-down by a single lentiviral vector expressing an array of short hairpin RNAs. ***Electron J Biotechn* 9**: 0

Subramanian S, Sivaraman C (1984) Bacterial citrate lyase. ***J Bioscience* 6**: 379-401

Sun J, Lu X, Rinas U, Zeng AP (2007) Metabolic peculiarities of *Aspergillus niger* disclosed by comparative metabolic genomics. ***Genome Biol* 8**: R182

Szczodrak J (1981) Biosynthesis of citric acid in relation to the activity of selected enzymes of the Krebs cycle in *Aspergillus niger* mycelium. ***Appl Microbiol Biot* 13**: 107-12

Thom C, Raper KB (1945) A Manual of the *Aspergilli*. The Williams and Wilkins Company, Baltimore

Tomlinson N, Campbell JJ, Trussell PC (1950) The influence of zinc, iron, copper, and manganese on the production of citric acid by *Aspergillus niger*. ***J Bacteriol* 59**: 217

Tomschy A, Wyss M, Kostrewa D, Vogel K, Tessier M, Höfer S, Bürgin H, Kronenberger A, Rémy R, van Loon AP, Pasamontes L (2000) Active site residue 297 of *Aspergillus niger* phytase critically affects the catalytic properties. ***FEBS Lett* 472**: 169-72

Torrado AM, Cortés S, Salgado JM, Max B, Rodríguez N, Bibbins BP, Converti A, Domínguez JM (2011) Citric acid production from orange peel wastes by solid-state fermentation. ***Braz J Microbiol* 42**: 394-409

Torres NV (1994) Modeling approach to control of carbohydrate metabolism during citric acid accumulation by *Aspergillus niger*: II. Sensitivity analysis. ***Biotechnol Bioeng* 44**: 112-8

Torres NV, Riol-Cimas JM, Wolschek M, Kubicek CP (1996a) Glucose transport by *Aspergillus niger*: the low-affinity carrier is only formed during growth on high glucose concentrations. ***Appl Microbiol Biot* 44**: 790-4

Torres NV, Voit EO, González-Alcón C (1996b) Optimization of nonlinear biotechnological processes with linear programming: application to citric acid production by *Aspergillus niger*. ***Biotechnol Bioeng* 49**: 247-58

Tran CT, Sly LI, Mitchell DA (1998) Selection of a strain of *Aspergillus* for the production of citric acid from pineapple waste in solid-state fermentation. ***World J Microb Biot* 14**: 399-404

Upton DJ, McQueen-Mason SJ, Wood AJ (2017) An accurate description of *Aspergillus niger* organic acid batch fermentation through dynamic metabolic modelling. ***Biotechnol Biofuels* 10**: 258

van den Hombergh JP, van de Vondervoort PJ, Fraissinet-Tachet L, Visser J (1997) *Aspergillus* as a host for heterologous protein production: the problem of proteases. ***Trends Biotechnol*** **15**: 256-63

van den Brink J, Maitan-Alfenas GP, Zou G, Wang C, Zhou Z, Guimarães VM, de Vries RP (2014) Synergistic effect of *Aspergillus niger* and *Trichoderma reesei* enzyme sets on the saccharification of wheat straw and sugarcane bagasse. ***Biotechnol J*** **9**: 1329-38

Vongsangnak W, Olsen P, Hansen K, Krogsgaard S, Nielsen J (2008) Improved annotation through genome-scale metabolic modeling of *Aspergillus oryzae*. ***BMC Genomics*** **9**: 1

Wallrath J, Schmidt M, Weiss H (1991) Concomitant loss of respiratory chain NADH: ubiquinone reductase (complex I) and citric acid accumulation in *Aspergillus niger*. ***Appl Microbiol Biot*** **36**: 76-81

Wallrath J, Schmidt M, Weiss H (1992) Correlation between manganese-deficiency, loss of respiratory chain complex I activity and citric acid production in *Aspergillus niger*. ***Arch Microbiol*** **158**: 435-8

Wang H, Ward M (2000) Molecular characterization of a PDI-related gene *prpA* in *Aspergillus niger var. awamori*. ***Curr Genet*** **37**: 57-64

Wang Y, Li W, Siddiqi Y, Kinghorn JR, Unkles SE, Glass AD (2007) Evidence for post-translational regulation of NrtA, the *Aspergillus nidulans* high-affinity nitrate transporter. ***New Phytol*** **175**: 699-706

Wang L, Zhang J, Cao Z, Wang Y, Gao Q, Zhang J, Wang D (2015) Inhibition of oxidative phosphorylation for enhancing citric acid production by *Aspergillus niger*. ***Microb Cell Fact*** **14**: 7

Ward M, Wilson LJ, Carmona CL, Turner G (1988) The *oliC3* gene of *Aspergillus niger*: isolation, sequence and use as a selectable marker for transformation. ***Curr Genet* 14**: 37-42

Watanabe T, Suzuki A, Nakagawa H, Kirimura K, Usami S (1998) Citric acid production from cellulose hydrolysate by a 2-deoxyglucose-resistant mutant strain of *Aspergillus niger*. ***Bioresource Technol* 66**: 271-4

Wayman FM, Mattey M (2000) Simple diffusion is the primary mechanism for glucose uptake during the production phase of the *Aspergillus niger* citric acid process. ***Biotechnol Bioeng* 67**: 451-6

Wehmer C (1893) Note sur la fermentation citrique. ***Bull Soc Chem Fr* 9**: 728

Wilson CP (1921) The Manufacture of Citric Acid from Lemons. ***Ind Eng Chem* 13**: 554-8

Wilson R, Turner APF (1992) Glucose oxidase: an ideal enzyme. ***Biosens Bioelectron* 7**: 165-85

Witteveen CF, Busink R, Van de Vondervoort P, Dijkema C, Swart K, Visser J (1989) L-Arabinose and D-xylose catabolism in *Aspergillus niger*. ***Microbiology+* 135**: 2163-71

Wold WS, Suzuki I (1973) Cyclic AMP and citric acid accumulation by *Aspergillus niger*. ***Biochem Bioph Res Co* 50**: 237-44

Wolschek MF, Kubicek CP (1997) The filamentous fungus *Aspergillus niger* contains two “differentially regulated” trehalose-6-phosphate synthase-encoding genes, *tpsA* and *tpsB*. ***J Biol Chem* 272**: 2729-35

Wurst H, Shiba T, Kornberg A (1995) The gene for a major exopolyphosphatase of *Saccharomyces cerevisiae*. ***J Bacteriol*** **177**: 898-906

Van Hartingsveldt W, Mattern IE, van Zeijl CM, Pouwels PH, van den Hondel CA (1987) Development of a homologous transformation system for *Aspergillus niger* based on the *pyrG* gene. ***Mol Gen Genet*** **206**: 71-5

Xie G, West TP (2006) Citric acid production by *Aspergillus niger* on wet corn distillers grains. ***Lett Appl Microbiol*** **43**: 269-73

Xu DB, Madrid CP, Röhr M, Kubicek CP (1989a) The influence of type and concentration of the carbon source on production of citric acid by *Aspergillus niger*. ***Appl Microbiol Biot*** **30**: 553-8

Xu DB, Röhr M, Kubicek CP (1989b) *Aspergillus niger* cyclic AMP levels are not influenced by manganese deficiency and do not correlate with citric acid accumulation. ***Appl Microbiol Biot*** **32**: 124-8

Yang J, Webb AR, Ameer GA (2004) Novel citric acid-based biodegradable elastomers for tissue engineering. ***Adv Mater*** **16**: 511-6

Yin X, Shin HD, Li J, Du G, Liu L, Chen J (2017) Comparative genomics and transcriptome analysis of *Aspergillus niger* and metabolic engineering for citrate production. ***Sci Rep*** **7**: 41040

Yogambal RK, Karegoudar TB (1997) Metabolism of polycyclic aromatic hydrocarbons by *Aspergillus niger*. ***Indian J Exp Biol*** **35**: 1021-3

Yongquan LI (2001) Study on the Screening High Yield Xylanase Producing Strain *Aspergillus Niger* by Microwave Mutagenesis [J]. ***J Microw*** **1**: 010

Yu XW, Li YQ (2005) Microencapsulated mycelium-bound tannase from *Aspergillus niger*. ***Appl Biochem Biotech*** **126**: 177-87

Yu XW, Li YQ, Zhou SM, Zheng YY (2007) Synthesis of propyl gallate by mycelium-bound tannase from *Aspergillus niger* in organic solvent. ***World J Microbiol Biotechnol* 23**: 1091-8

Zabala AO, Xu W, Chooi YH, Tang Y (2012) Characterization of a silent azaphilone gene cluster from *Aspergillus niger* ATCC 1015 reveals a hydroxylation-mediated pyran-ring formation. ***Chem Biol* 19**: 1049-59

Zehentgruber O, Kubicek CP, Röhr M (1980) Alternative respiration of *Aspergillus niger*. ***FEMS Microbiol Lett* 8**: 71-4

Zehnder AJ, Svensson BH (1986) Life without oxygen: what can and what cannot? ***Experientia* 42**: 1197-205

Zhang H, Ishige K, Kornberg A (2002) A polyphosphate kinase (PPK2) widely conserved in bacteria. ***Proc Natl Acad Sci* 99**: 16678-83

Zhou PP, Meng J, Bao J (2017) Fermentative production of high titer citric acid from corn stover feedstock after dry dilute acid pretreatment and biodetoxification. ***Bioresource Technol* 224**: 563-72

Zhu N, Xia H, Yang J, Zhao X, Chen T (2014) Improved succinate production in *Corynebacterium glutamicum* by engineering glyoxylate pathway and succinate export system. ***Biotechnol Lett* 36**: 553-60

Żyła K, Gogol D (2002) *In vitro* efficacies of phosphorolytic enzymes synthesized in mycelial cells of *Aspergillus niger* AbZ4 grown by a liquid surface fermentation. ***J Agr Food Chem* 50**: 899-905